Effect of a penetration enhancer on lipid membranes : a molecular dynamics study.

Wahab, Habibah Bin

The Effect of A Penetration Enhancer on Lipid Membrane - A Molecular Dynamics Study

A thesis submitted by

Habibah Bt A. Wahab

For the degree of Doctor of Philosophy

in the Faculty of Medicine

of the University of London

Department of Pharmacy
King's College London

January 1999

ABSTRACT

The success of transdermal drug delivery to date is still limited to only a few drugs e.g. glyceryltrinitrate, nicotine and estradiol. Many other drugs have been precluded from this means of delivery due to the barrier property of the skin. In most cases, it is necessary to incorporate a chemical penetration enhancer in the transdermal drug delivery device to reduce this barrier.

The object of this study is to investigate the molecular interactions of a penetration enhancer, namely Azone, with a model lipid membrane. This penetration enhancer is thought to exert its penetration effects by interacting with the intercellular lipid of the *stratum corneum* and causing an increase in 'fluidity' i.e. acyl chain disorder. The disorder, consequently, facilitates the diffusion of molecules through the hydrocarbon region of the bilayer.

Molecular dynamics (MD) simulations of three different pure DPPC bilayers, Lβ', Lα-AMBER, Lα-CHARMm as well as two DPPC bilayers containing two and four molecules of Azone have been carried out. In addition, MD of pure liquid Azone, a single molecule of Azone in water and a single Azone and DPPC in water are also simulated. The choice of Lα-AMBER as the model for Azone incorporation was justified by its success in reproducing the experimentally measured parameters. Incorporation of Azone into the lipid bilayer results in increased disorder of both hydrocarbon and headgroup regions of the bilayer as well as increased DPPC and water diffusion. All of these indicate that Azone increases the fluidity of the lipid membrane. Increasing concentration of Azone results in an increase in the disorder of the bilayer. Thus, based on these results an Azone-enhancement model is proposed to illustrate the mechanism of drug-penetration enhancement of Azone on a lipid membrane. This model, where the lipid bilayer is divided into four diffusion regions (hydrophilic and lipophilic regions), proposes that Azone perturbs all of the diffusion zones within the lipid bilayer and reduces the permeability resistance in these regions. This thus explains the ability of Azone in enhancing both lipophilic and hydrophilic drug molecules.

To Ahmad, Vivek, Aeishah and Ajay

ACKNOWLEDGEMENT

"And We have enjoined on man (to be good) to his parents: in travail upon travail did his mother bear him, and in years twain was his weaning: (hear the command), "Be thankful to Me and to thy parents: to Me is (thy final) Goal.".
(Holy Quran, 31:14)

First of all, I would like to express my praise and gratitude to God Almighty for His mercy and countless blessings to me and my family throughout all of our lives. And to my parents, thank you for the unconditional love and continuous support both of you have shown to me and thank you also for constantly praying for my success. I thank my mother-in-law too for her immense help and support especially during the final year of my PhD.

To Dr. Jamshed Anwar and Dr. David Barlow, both of whom I am fortunate to have as my supervisors, thank you both very much for your help and support, and also for making this thesis a reality.

My thanks are also due to Professor Kenneth Merz Jr and Dr K. V. Damodaran at the Pennsylvania State University for their invaluable contributions towards the completion of this project. I must also thank Dam, Mini, Sam, Jalani and Shahida for their hospitality during my stay in America.

There will never be another place like King's College London in Chelsea for me. There are a lot of people connected to this great place who have helped me either directly or indirectly with this project. They include Professor C.M. Marriott, Professor R. C. Hider and Professor David Cowan, Dr. Jayne Lawrence, Dr. Chris Richardson, Dr Gary Ma, Dr. Peter Quinn, Dr. Patrick William, Dr. Gary Martin, Mark George and also my colleagues (especially *Papa* and Chan) working in Lab 64 and 6. I would also like to thank Dr J. Baum (Imperial College) Dr. L. Cruzario-Hanson (Birkbeck College) and Dr R Wilson (QMW College) for comforting me (with their advice) when the experiments were not working.

My gratitude also goes to the University of Science, Malaysia, for funding this project via it's Academic Staff Training Scheme. I would also like to thank Puan Fazia Ali, Dato' Ishak, Dato' Maznah, Prof. Ahmad Pauzi, Drs. Tan Soo Choon, Saringat, Aishah, Nur Hayati, Munavvar, Shukri and Mohd Ibrahim for their support especially during the last year of my PhD.

Being a mother of two small babies, I am particularly indebted to Mrs Sarwar A. Waris for looking after my children patiently and kindly all the time I was struggling in front of the computer in the college. I would also like to acknowledge my aunt Aminah and her family in Queens Park, Dato' Hassan, Mr A. Waris, Br. Abdul Mueed, Srs. Aishah, Ghazala, Nur Azlin and Maimon and also R.G.C. Manzetti and J. Steven for their helps all the time throughout my stay in London.

To Dr. Christina Hadgigeorgio, my friend in laughter and tears, I can never thank you enough for your help and support throughout the first three years in my PhD.

And finally and most of all, to the most special and important persons in my life, my husband *Anuar Shamsudin* and our children (who were born during my PhD), *Ahmad Danial Azhar* and *Aeishah Ameera*, no words can ever express my gratitude and love for all of them. To Anuar thank you for supporting and persevering with me all these years and to Ahmad and Aeishah I hope both of you would find forgiveness in your hearts for me for having to compromise the time I should be spending with you with this project.

CONTENTS

Lists of Figures

Lists of Tables

1. INTRODUCTION

1.1 Statement of the problem

Transdermal drug delivery is the delivery of drugs through the skin and provides a promising alternative to oral and intravenous administration of drugs. It offers several advantages over the more conventional forms of drug delivery, including the avoidance of hepatic first pass effects and the reduction of unwanted systemic side effects of drugs. However, there are currently very few drugs administered via this route and the major reason for this is that the skin itself constitutes a significant barrier to drug penetration.

The main barrier of the skin is its outermost layer, the *stratum corneum*, which consists of cells known as corneocytes embedded in an intercellular matrix of lamellar lipids and it is the lipid bilayers of the *stratum corneum* that provide the rate limiting barrier to percutaneous penetration of drugs (Scheuplein & Blank, 1971, Behl *et al.*, 1982, Elias, 1983). One way to reduce this barrier is through the incorporation of chemical penetration enhancers in a transdermal formulation. Many chemicals such as Azone, alkyl methyl sulfoxide and various forms of surfactants have been screened for penetration enhancement (Barry, 1987). Most of these compounds, however, are still not widely used in transdermal formulation, in part because of their associated toxicity and allergenicity (Weichers, 1989), and also probably due to a general lack understanding of the mechanism of their penetration enhancement effects (Sugibayashi et al., 1992).

The present study aims to use computer simulations of model membrane/enhancer systems in order to determine how one particular enhancer, Azone, might work. These studies involve full molecular dynamics (MD) simulations of phospholipid assemblies in the presence and absence of Azone. Obtaining an understanding of the mechanism of Azone penetration enhancement from the observations made in these studies at a

molecular level might, in turn, shed some light on the broader question of how penetration enhancers work. An increased understanding of how enhancers exert their effect should also provide a basis for the development of safer and more effective penetration enhancers.

1.2 TRANSDERMAL DRUG DELIVERY

1.2.1 Overview

For many years, considerable attention has been focused on the development of alternative forms of drug delivery to replace the conventional oral dosage forms and one such alternative involves the delivery of drugs across the skin. Currently, few drugs have been marketed for transdermal application. These include glyceryltrinitrate, nicotine, hyoscine oestradiol (Guy *et al.*, 1987) as well as testosterone and fentanyl. Several other compounds such as timolol has also been considered as candidates for this form of drug delivery as too have the new generation of peptide and protein drugs (because of their instability in gastro-intestinal environment and their large size of which makes it difficult to develop these agents for oral administration).

It is suggested that transdermal drug delivery can offer several advantages over the more conventional forms of drug delivery. Barry (1983) stated that, provided that the transdermally administered drug can be absorbed in sufficient quantity to exert a systemic effect, it is possible:

i. to eliminate the variables which influence gut absorption, such as changes in pH along the gastrointestinal tract, food and fluid intake, stomach emptying rate, intestinal motility and transit time
ii. to avoid the hepatic "first-pass" metabolism
iii. to provide for controlled and sustained drug release
iv. to allow utilisation of drugs with short biological half-lives and low therapeutic index
v. to enhance therapeutic efficacy
vi. to reduce frequency of dosing
vii. to improve patient compliance

viii. to permit relatively abrupt termination of drug effect by removal of the delivery device from the skin

ix. to reduce inter and intra-patient variability, and

x. to avoid pulse entry into the circulation, i.e. peak and trough blood concentration associated with conventional oral administration (peak level often producing undesirable effects and troughs leading to subtherapeutic activity).

However, as with any method of drug delivery, transdermal drug delivery is not without limitations. It has been recognised that the skin produces enzymes, which are capable of metabolising certain drugs (Guy *et al.*, 1987). In addition to this, there have been many reports of toxicological responses to transdermally administered drugs such as irritation, contact allergy and hyperpigmentation (Weichers, 1989). The main limitation to transdermal drug delivery, however, lies in the fact that the skin represents a barrier to drug absorption.

1.2.2 The structure and function of the skin

The skin, one of the most extensive and readily accessible organs of the human body, is a complex multi-layered structure with a variety of functions. Its major functions are to separate the underlying blood circulation network from the outside environment and to provide a barrier against physical, chemical and microbial attack. In addition, the skin is responsible for helping to maintain body temperature and to regulate blood pressure, as well as protecting the body against the penetration of ultra violet rays.

In general, the skin can be described in terms of two important tissue layers, the epidermis and dermis (Figure 1.1). The hypodermis, the innermost layer, is considered of little importance as far as percutaneous absorption is concerned because it mainly consists of adipose tissue, serving only as an insulating, shock absorbing and energy-reserve layer.

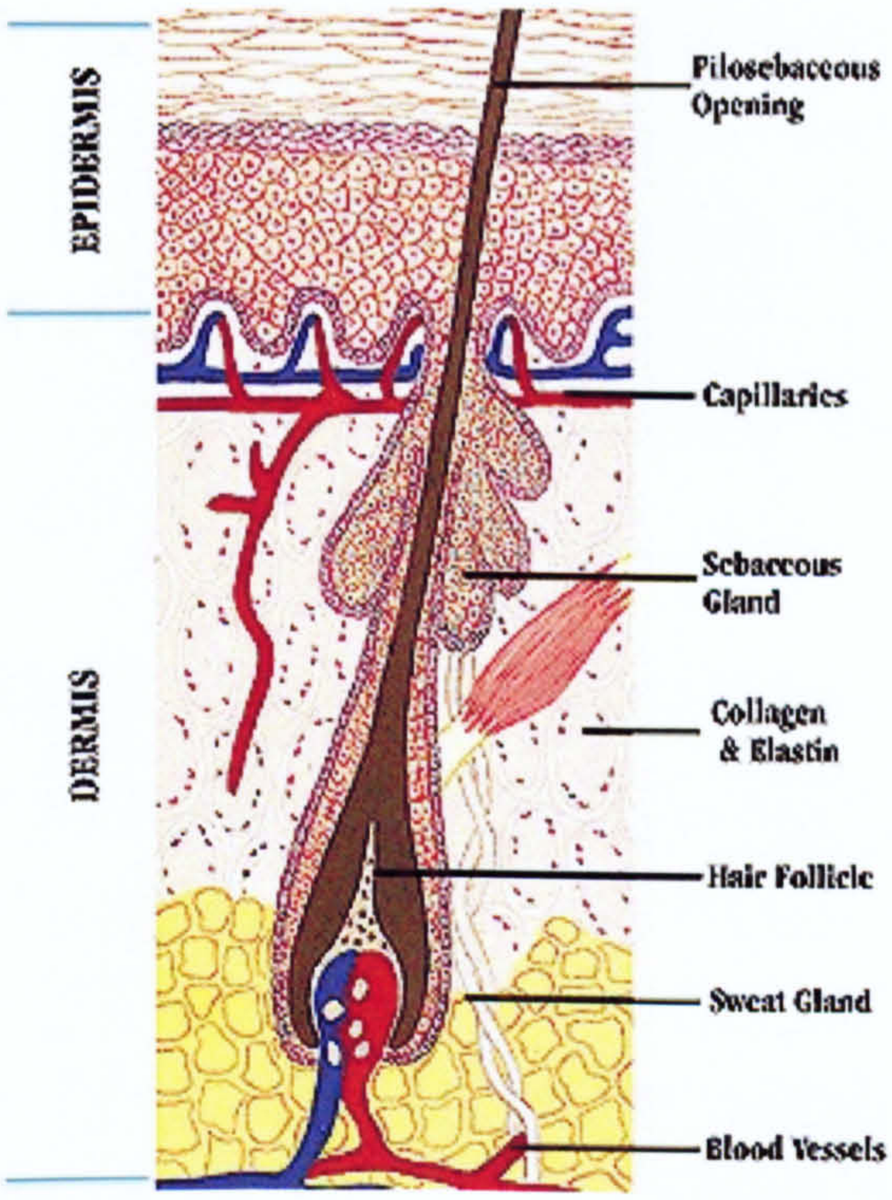

Figure 1.1: The structure of the skin.

Located below the epidermis is the dermis, which is composed of a network of collagen and elastin fibers embedded in a mucopolysaccharide matrix. It contains blood and lymphatic vessels and nerve endings and thereby provides physiological support for the epidermis. This layer is responsible for the maintenance of a supple and healthy skin. However, as the blood vessels approach the interface of the two layers (the epidermis and the dermis) very closely, it is usually not considered as a significant barrier to inward permeation *in vivo*. The epidermis which derives from an active epithelial basal cell population, is approximately 150μm thick. It is the outermost layer of the skin and comprises the viable epidermis (*stratum germinativum, stratum spinosum, stratum granulosum and stratum lucidum*) and the cornified *stratum corneum*.

The viable epidermis comprises a layer of cells that undergoes continuous differentiation. As the cells divide, they move away from the source of nutrient supply and differentiate or undergo a process of keratinisation. The end result of this process is the formation of a thin stratified and extremely resilient dead layer, *the stratum corneum* at the skin surface. This *stratum corneum* is usually regarded as the fundamental barrier to drug permeation. Therefore, the viable epidermis which is often regarded as having the properties of an aqueous gel, does not present a significant barrier to penetration in most circumstances. However, in cases where the *stratum corneum* is damaged, or if extremely lipophilic drugs are being administered, the viable epidermis, can be a rate-limiting factor in percutaneous absorption.

The greatest penetration barrier of the skin is said to reside in the *stratum corneum*. This layer is the least permeable layer of mammalian skin. It is the outermost layer (typically about 10-20μm thick) and offers a formidable barrier to transepidermal water loss and to the percutaneous absorption of most dermally applied drugs (Scheuplein & Blank, 1971, Scheuplein, 1976, Behl *et al.*, 1982, Elias, 1983).

The *stratum corneum* has two major components: the intracellular hydrophilic component, keratin, and the hydrophobic intercellular lipid material. On this basis, Elias (1983) has proposed a two-compartment model of the *stratum corneum* which he describes as a 'brick and mortar' structure (Figure 1.2). In this model, Elias depicts

the keratin-filled corneocytes as the hydrophilic 'brick' and the intercellular hydrophobic lipids as the 'mortar'.

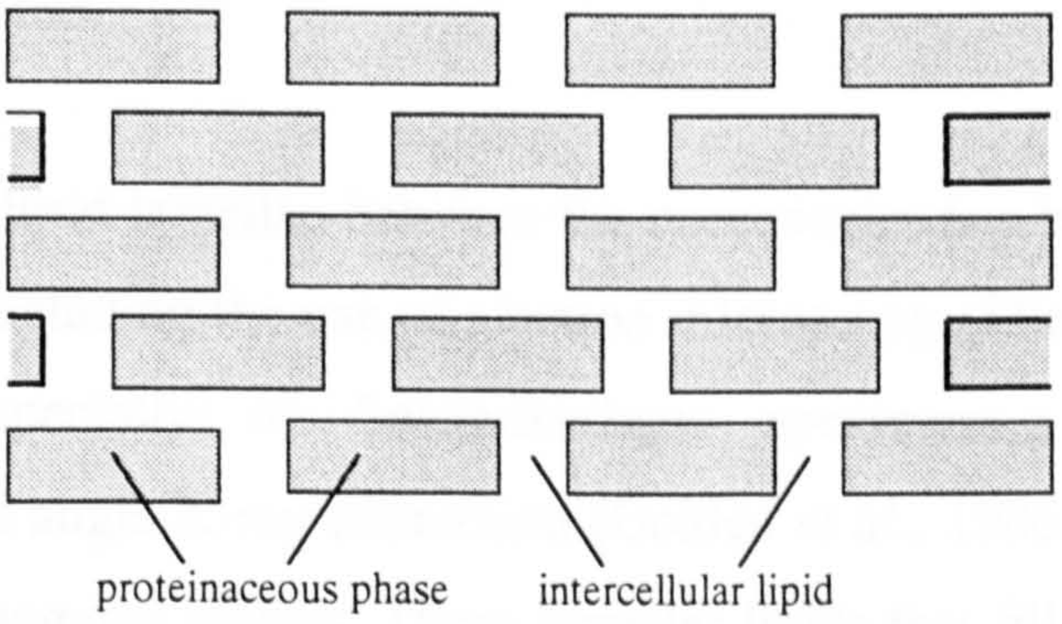

Figure 1.2: Idealised brick and mortar model of the *stratum corneum* adapted from Elias 1983)

The corneocytes contain highly crossed-linked keratins. These keratins are fibrous proteins and under normal circumstances, assume an α-helical conformation which is stabilised by intrachain hydrogen bonding (van Duzee, 1975). The keratin is further stabilised by a large number of disulfide bridges between its cysteine residues. In addition, there are some lipids and carbohydrates in the corneocytes, most of them being present as lipoproteins and glycoproteins respectively (Blank, 1987). These protein components can be subdivided into water soluble and water insoluble (membrane) fractions.

The existence of lipid lamellae between the corneocytes has been demonstrated in a variety of ways including the use of electron microscopy (Elias, 1981, Williams and Elias, 1987) especially of freeze-fractures specimens, differential scanning calorimetry, small angle X-ray diffraction (Golden *et al.*, 1986, Friberg and Osborne, 1985) and histochemical studies. These lamellar lipids that fill the intercellular space are poor in phospholipids and rich in sphingolipids (Bodde *et al.*, 1989), and are said to play a major role in providing the epidermal barrier to percutaneous penetration

Feingold (Feingold, 1991 and the references cited therein) has compiled a large number of observations that strongly suggest the involvement of the lipids in the intercellular domains in maintaining permeability barrier function which include;

i. disturbance in the permeability barrier function was shown by the extraction of *stratum corneum* lipids by topical solvent or detergent treatment. It is also found that the quantity of lipids extracted from the *stratum corneum* correlates directly with the extent or disturbance in barrier function.
ii. the permeability barrier function of essential fatty-acid deficient mice is abnormal and there is a quantitative diminution in intercellular lipids.
iii. in essential fatty acid-deficient animals, or following solvent disruption of the barrier, water soluble substances traverse the intercellular pathways in passing across the *stratum corneum*.
iv. regional variations in the permeability barrier can be linked with quantitative differences in the *stratum corneum* lipid composition: for example the quantity of lipid in the *stratum corneum* of the soles and

palms is small and the barrier is poor, whereas the abdomen has an increased quantity of lipids and provides a better barrier against water movement.

v. there is striking similarity of the lipid compositions of the *stratum corneum* in most terrestrial mammals. However, in non-fur bearing marine mammals, where a strong permeability barrier is not as necessary, the intercellular *stratum corneum* lipid species remain more polar and the fatty acids are of short length and less saturated than terrestrial mammals.

vi. in avians, intercellular lipid deposition in the *stratum corneum* is accelerated when the animals are subjected to water deprivation, and simultaneous with this increase in intercellular lipids there is an improvement in barrier function.

The lipid composition of the *stratum corneum* varies from one part of the body to another, and also according to the degree of keratinocyte differentiation. In general, the *stratum corneum* lipids consists mainly of ceramides (50%), cholesterol (20%), free fatty acids (25%) and very little of phospholipids. The ceramides have been implicated as important in the cohesion/adhesion of the *stratum corneum*, providing links (intercalation) between the *stratum corneum* bilayers (Brain and Walter, (1991)). It has further been shown that the ceramides consist of six chromatographically distinct fractions, varying in polarity according to their content of sphingosine, phytospingosine, and amide-linked fatty or hydroxyacids. The least polar of the ceramides has a most unusual structure in which 30 or 32 carbon ω-hydroxyacids are amide-linked to sphingosine with the ω-hydroxyl groups esterified with a mixture of fatty acids containing a high proportion of linoleic acid (Figure 1.3) (Wertz & Downing, 1989).

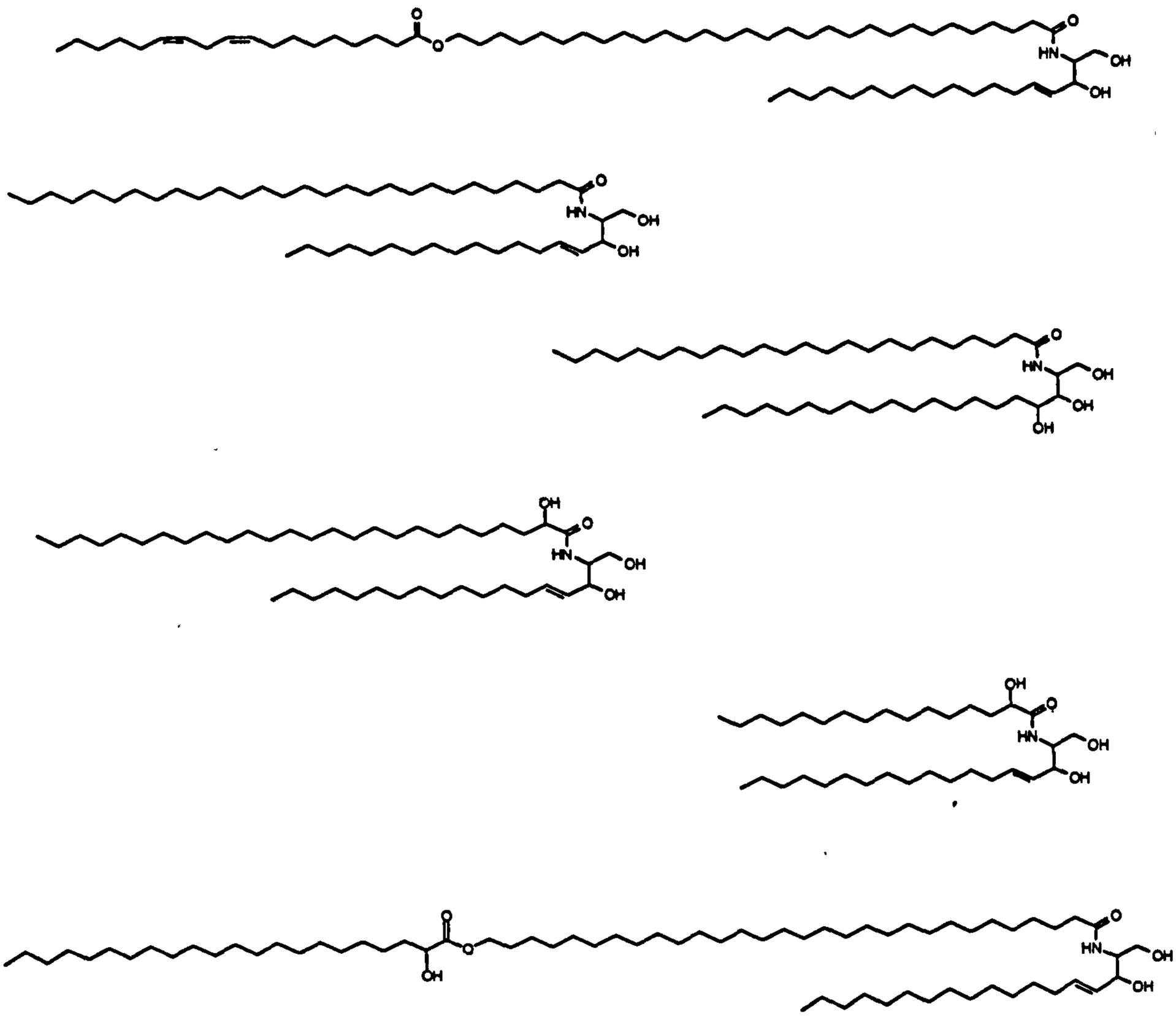

Figure 1.3: Representative structures of the stratum corneum ceramides (Wertz & Downing, 1989)

The bilayer structure of the *stratum corneum* intercellular lipids in itself is insufficient to account for its low water permeability because bilayers consisting of phospholipids offer an insignificant barrier to passage of water (Downing *et al.*, 1986). It has been suggested, therefore, that the resistance of the *stratum corneum* to water permeation requires the hydrocarbon chain regions of its component lipids to be in the crystalline or gel phase. This is normally the case only when the lipids incorporate saturated fatty acids. Thus, the fact that the *stratum corneum* lipids offer a significant barrier to water penetration, is explained on the grounds that the lipids are arranged in a close-packed crystalline manner, with their fatty acid components comprising mostly saturated hydrocarbon chains. This highly ordered rigid structure results in a unique impermeability for many compounds including water (Landmann, 1988).

In the viable epidermis, there are analogues of the *stratum corneum* ceramides that exist in which glucose is attached to the sphingosine, forming a corresponding series of glucosylceramides. These acylglucosylceramides have been proposed to play a role in inducing assembly of lamellar granules (Downing *et al.*, 1983). They may be viewed as stacks of flattened liposomes, that are eventually extruded into the extracellular space (Figure 1.4). Besides glycolipids, the viable epidermis also contains the usual array of phospholipids, but these are degraded when the cells keratinize.

1.2.3 The Routes of Percutaneous Penetration

Identification of the routes of drug penetration through the skin is important in understanding the mode of action of penetration enhancers. There are various potential pathways for permeation through the skin (see Table 1.1). In general, the routes of skin penetration can be subdivided as;

i. the transappendageal routes;
ii. the transepidermal routes.

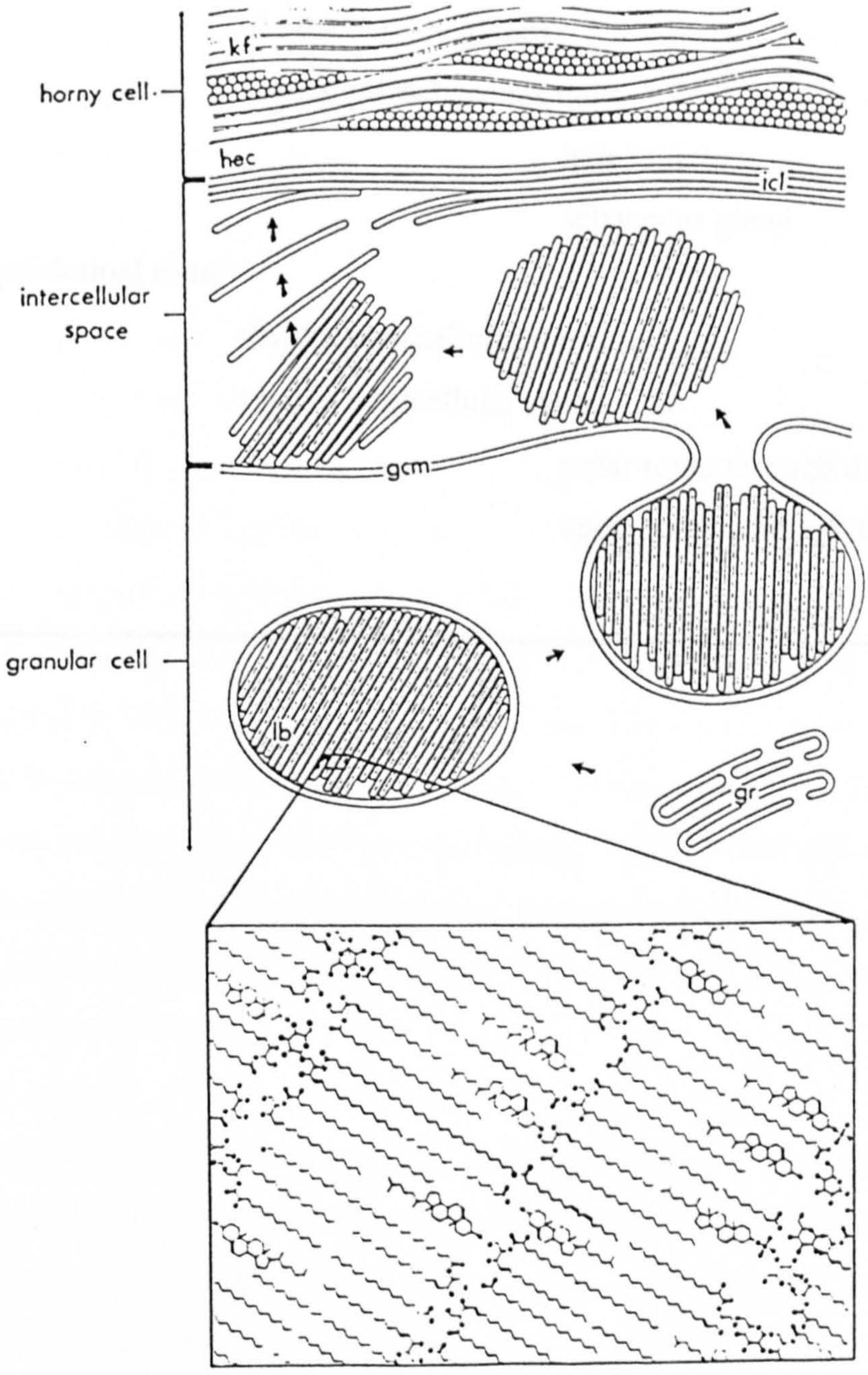

Figure 1.4 Representation of the formation of the *stratum corneum*. The boxed area shows a diagrammatic representation of the role of lipids in the formation of the epidermal lamellar granules. The granules are then extruded into the intercellular space and rearranged into the broad extracellular lipid sheets that constitute the epidermal water barrier (Downing *et al.*, 1986).

Table1.1: Overview of the assumed pathways through the *stratum corneum*

Transappendageal route		
	via the eccrine glands	
	via the pilosebaceous unit:	
		hair follicle
		sebaceous gland
Transepidermal route		
	via the transcellular route	
	via the intercellular route	
		polar route through the bilayer
		apolar route through the bilayer

The transappendegeal routes refer to transport via the sweat glands and along the hair follicles with their associated sebaceous glands (Figure 1.5). These routes circumvent penetration into the *stratum corneum* itself and thus are known as 'shunt routes'. However, because of their relatively small area (less than 0.1% of the total surface area of the skin), these routes are considered to be of minor importance. Nevertheless, these routes may be significant for the penetration of ionic molecules or large polar compounds (Barry, 1987).

The transepidermal routes, on the other hand, due to the large surface area of the epidermis (i.e. about 99% of the total surface area of the skin) are generally considered as the major diffusion pathways for the penetrating molecules. These routes can further be divided into two general pathways; the intercellular pathways and the intracellular pathways. Intracellular pathways provide the diffusion of drug molecules through the cornified proteineous cells. The diffusional resistance is contributed by the whole thickness of the *stratum corneum*. The evidence for this, can be seen by observing the gradual increase in permeability of the *stratum corneum* as layers are removed by adhesive tape stripping (Tregear, 1966) or by the differences in concentration of the drug in the various strippings (Schaeffer et al., 1978). On the other hand, the intercellular pathways offer less diffusional resistance than the intracellular pathways.

It is important to note, however, that most molecules are likely to exploit both the intra- and intercellular routes of passage across the skin (William & Barry, 1992) and that the relative fluxes via the two routes will depend on the molecules' physicochemical characteristics (Scheuplein & Blank, 1971), in particular on their oil-water partition coefficient (Scheuplein, 1973, Flynn *et al.*, 1974, Behl *et al.*, 1982). Hydrophilic (polar) molecules are thought likely to utilise mainly the intracellular pathways and shunt routes when moving across the skin, whilst lipophilic molecules (that is those having logP oct/water typically >2) will traverse the *stratum corneum* mainly via the intercellular route (Williams & Barry, 1992). Another property influencing the route of entry includes the drug's diffusion coefficient which in turn depends on its molecular mass and/or dimensions.

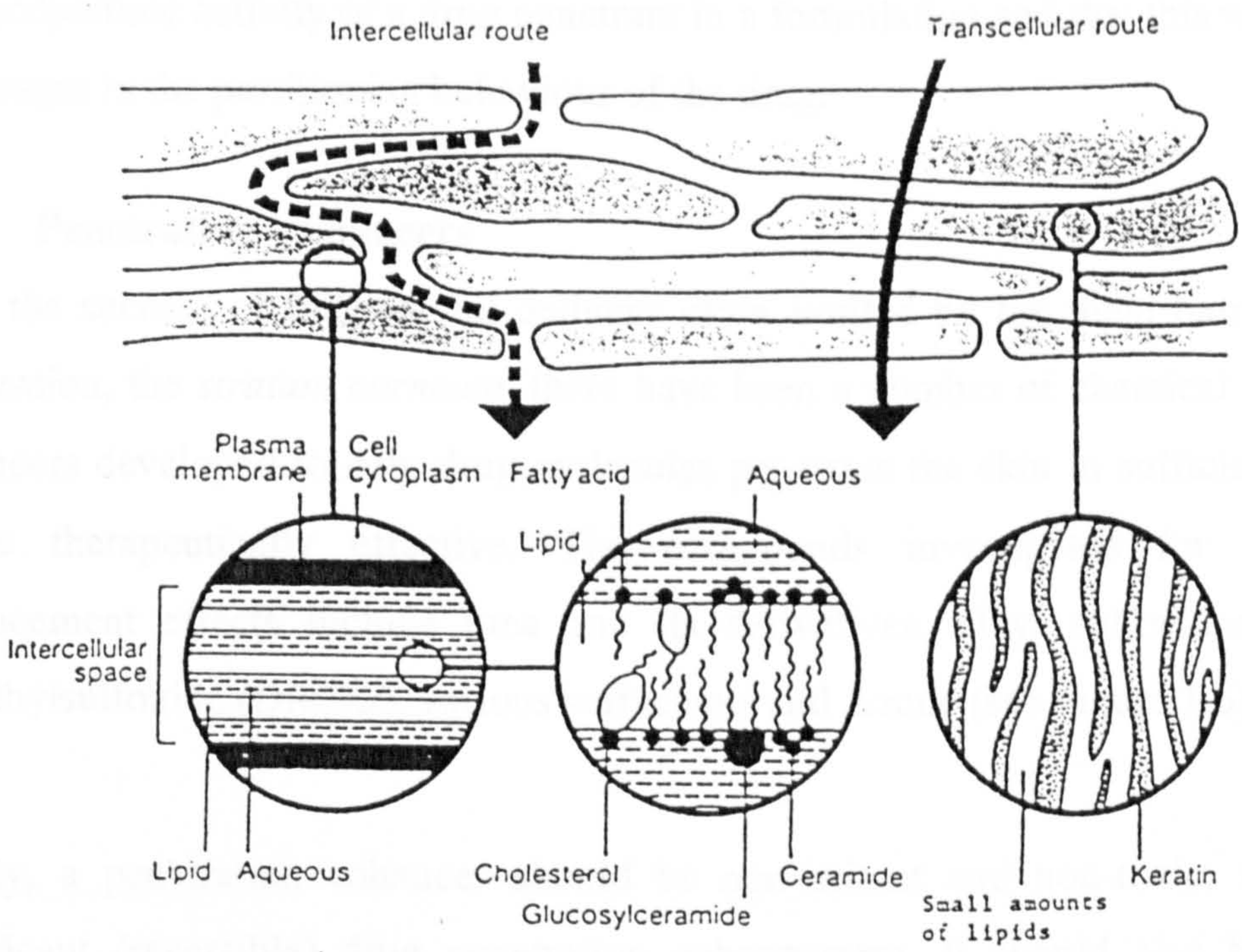

Figure 1.5 The possible diffusional pathways via *stratum corneum*. Two major pathways (trancellular and tortuous intercellular pathways) are illustrated (William & Barry, 1992).

The existence of the inter- and intracellular pathways for permeation across the skin has significant implications in the design, development and use of penetration enhancers. It is unlikely that an enhancer that influences the intercellular pathway, for example, by increasing the fluidity of the extracellular lipid, will have significant effects on the skin permeability of a drug whose primary access route is transcellular. Furthermore, it is entirely feasible that the presence of an enhancer might alter the thermodynamic activity of a drug penetrant in a formulation and that this would result in changes in the partitioning behaviour of the drug.

1.2.4 Penetration Enhancers

With the success of transdermal delivery often limited by the main barrier to drug permeation, the *stratum corneum*, there have been a number of chemical penetration enhancers developed to help drug molecules penetrate the skin in sufficient quantity to be therapeutically effective. The compounds investigated for penetration enhancement effects include urea and its derivatives, alkyl sulfoxides including dimethylsulfoxide (DMSO), various surfactants and Azone (see Figure 1.6).

Ideally, a penetration enhancer should be non-irritant and non-toxic, and give a significant (reversible) drug penetration enhancement. It should also be physico-chemically stable and pharmacologically inert, preferably also odourless, colourless, tasteless and cosmetically acceptable (Barry, 1987).

Unfortunately, however, virtually all of the compounds so far investigated do not meet these ideal criteria. DMSO, for example, only exerts its enhancing activity when used at high concentration (>70%) and at these levels causes significant toxicological problems. Upon topical use, DMSO has been found to produce erythema and wheals, irreversibly damages the skin, and delaminates the *stratum corneum* and denatures its proteins. Moreover, DMSO also produces a bad body odour due to its metabolite dimethylsulfide.

Azone®, on the other hand, is an example of a compound that meets most of the requirements. It was specifically designed as a skin penetration enhancer by Nelson

Research and Development (Hadgraft, 1984). Several studies have shown that it can be used to promote drug penetration in concentrations as low as 1% and is not found to result in any significant irritation to human skin when applied at concentrations of up to 50%. In addition, it has been demonstrated that Azone results in a marked increase in the skin permeation for a variety of drugs including 5-fluorouracil, verapamil and corticosteroids. Synergistic effects of Azone have also been observed when used for the transdermal administration of corticosteroids with propylene glycol.

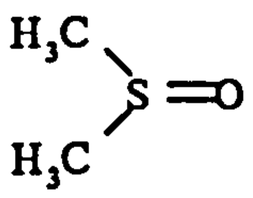

Dimethylsulphoxide
(DMSO)

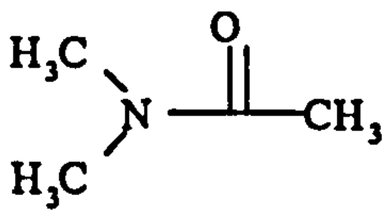

Dimethylacetamide
(DMA)

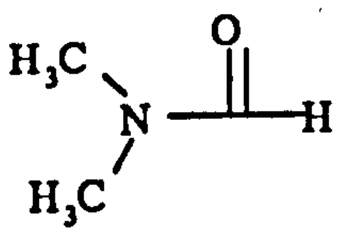

Dimethylformamide
(DMF)

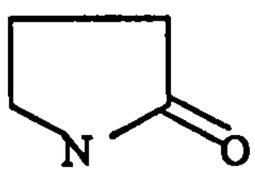

2-Pyrrolidone

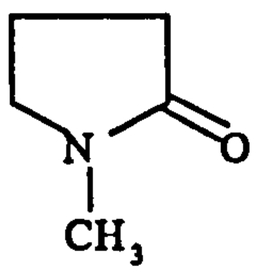

N-Methyl-2-pyrrolidone

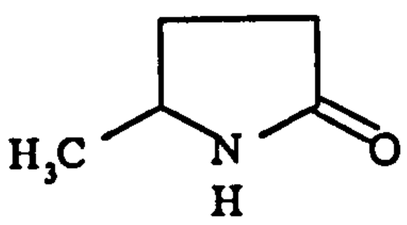

5-Methyl-2-pyrrolidone

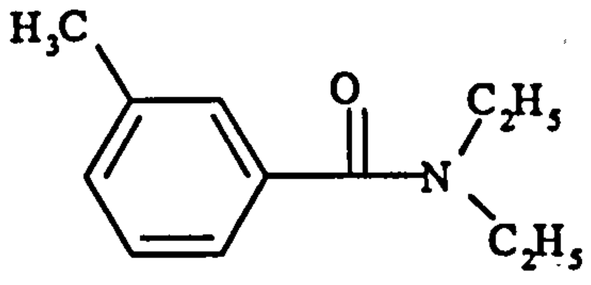

N, *N*-Diethyl- *m*-toluamide

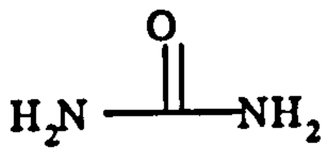

Urea

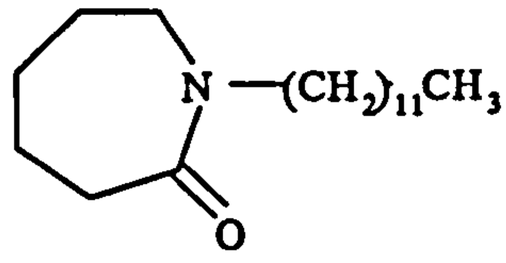

1-Dodecylazacycloheptan-2-one (Azone)

Figure 1.6 : Structures of several reported penetration enhancers

1.2.5 General Description of Azone

Azone (Figure 1.7) at room temperature is a clear, colourless liquid. It has a relative molecular mass of 281.49Da and it has melting and boiling points of -7°C and 160°C respectively at 0.05mmHg. Hadgraft *et al.* (1993) has shown that it has a log P oct/water of 6.21 and that this value is higher than the minimum of ~2 (Barry 1992) required for a molecule to cross the *stratum corneum* via intercellular route.

The solubility of Azone calculated using group increment is 9.06H and is quite close to that of the stratum corneal lipid (9.7–10.0H). Hadgraft *et al.*(1993) postulated that Azone is readily dissolved in the *stratum corneum* but poorly absorbed into the systemic circulation. This is supported by experiments carried out by Weichers and co-workers (1987, 1988) who found that the amount of radiolabelled Azone absorbed through the skin (as assessed by urinary and faeces excretion) was small. Also using a tape-stripping technique, they found that most of the Azone absorbed into the skin resided in the upper layers of the *stratum corneum*.

Azone is compatible with most organic solvents. In the development of topical formulations containing water soluble drugs, it can be incorporated into emulsions, gels and other biphasic systems (Hadgraft *et al.*, 1993).

1.2.6 The Skin Penetration Effect of Azone

Azone has been shown to be an effective enhancer for both hydrophobic and hydrophilic permeants (Weicher & de Zeew, 1993). The hydrophilic molecules in particular benefit from a greater permeation enhancement when incorporated with Azone (Kai *et.al.*, 1993).

Azone is most effective when it is present at a low concentration in a formulation, usually between 1 and 5% (Hadgraft *et al.*, 1993). The concentration of Azone needed to produce optimal penetration however varies from drug to drug (Stoughton & McClure, 1983).

PAGE
NUMBERS
CUT OFF
IN
ORIGINAL

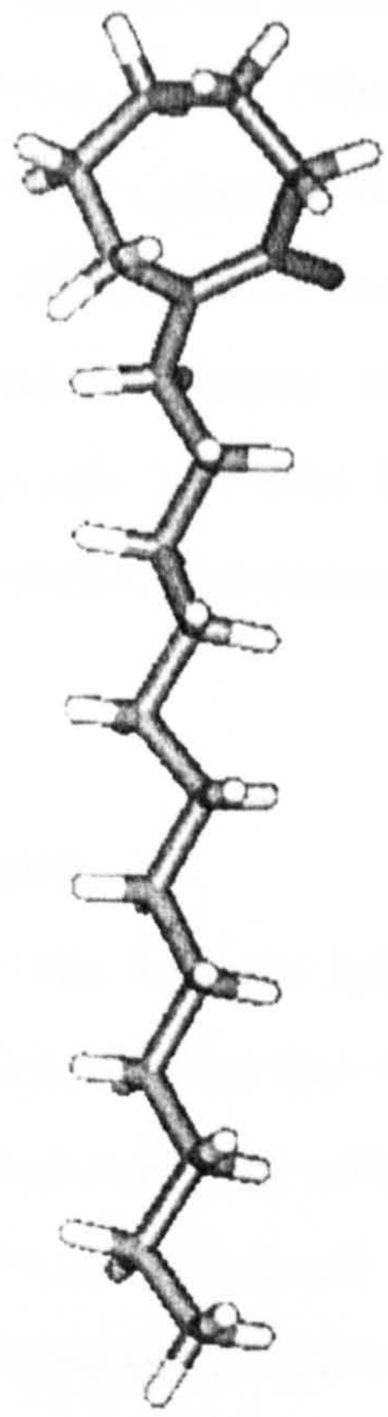

Figure 1.7 The 3D structure of Azone

Azone produces a large penetration enhancement when only a small amount of the active drug is present in the formulation. This can be advantageous when a potentially hazardous or particularly expensive compound is used in conjunction with Azone.

Formulations that may benefit from the use of Azone to enhance drug permeation include those used in the treatment of acne vulgaris, trichomoniasis, amoebiasis, psoriasis, skin inflammation and epithelial neoplasms. In the treatment of acne vulgaris, for example, a maximal penetration enhancement of 0.02% clindamycin formulation was seen with 8% Azone, which had the same activity in inhibiting the growth of *P. Acne* as a vehicle containing 0.1% clindamycin alone, thereby lowering

the amount of the active drug required in the formulation. Azone has also been shown to increase the flux of erythromycin, sodium fusidate and metronidazole.

In addition, Azone can be used to increase the enhancement of *p*-aminobenzoic acid which is an effective topical sunscreen agent. Other drugs that can be enhanced in their skin penetration by Azone include glucocorticosteroids such as triamcinolone which has a high incidence of side effects when used alone. Azone could reduce the amount of this drug needed to produce clinical effects, thereby reducing the side effects. An overview of the compounds that have been investigated in combination with Azone, together with the observed permeation enhancement is given in Table 1.2.

1.2.7 Mechanism of Action of Azone

The mechanism of action of Azone has been the subject of many investigations over the past few years. Several studies have shown that Azone acts by interacting with the intercellular lipids. Using differential scanning calorimetry, it has been shown that Azone fluidises the lipids of the *stratum corneum* (Goodman and Barry, 1985). In another study, using electron spin resonance, Quan and Maibach (1994) found that Azone affects the spin label binding to lipid bilayers and causes an increase in the flexibility and polarity of local bilayers surrounding the spin label. Incorporation of Azone in a skin lipid model has been shown to decrease the gel to liquid crystalline transition temperature sufficiently to induce formation of a liquid phase and increases membrane fluidity below the transition temperature (Beastall *et al.*, 1988). Further work using a fluorescent probe technique has demonstrated that Azone interacts with structured lipids making them more fluid, producing a concomitant reduction in the diffusional resistance experienced by the penetrating species (Beastall *et al.*, 1988).

Table 1.2 Compounds that have been investigated with Azone (Wiechers and de Zeeuw, 1990 and the references cited therein).

Compound	%Azone in formulation	Study type	Skin type	Enhancement factor
Amcinonide	2	*in vivo*	man	>2[a]
Anthracene	3	*in vivo*	hairless mouse	yes[b]
Betamethasone benzoate	2[c]	*in vivo*	man	2.2[a]
	2.5	*in vivo*	man	0.9[a]
8-Bromo cAMP	1	*in vitro*	hairless mouse	12
6-Carboxyfluorescein	3	*in vivo*	rat	2-3
Clindamycin phosphate	8	*ex vivo*	hairless mouse	yes[b]
Desonide	2	*in vivo*	man	>2[a]
Desoximetasone	1	*in vivo*	man	3-4[a]
Dexamethasone				
acetate	5	*in vivo*	rat	yes[b,d]
palmitate	5	*in vivo*	rat	small[b,d]
Difluoromethylornithine	10	*in vitro*	pig	1,3
Erythromycin	5[c]	*in vitro*	hairless mouse	15
	50[c]	*ex vivo*	hairless mouse	yes[b]
Estradiol	2[c]	*in vivo*	man	1.4
	3	*in vitro*	man	1.3
Ethanol	5	*in vitro*	hairless rat	2
Flucinolone acetonide	2	*in vivo*	man	4-5[a]
5-Fluorouracil	1.8	*in vitro*	hairless mouse	>80
	2[c]	*in vitro*	hairless mouse	>130
	2[c]	*in vitro*	man	≈20
	2[c]	*in vitro*	man	100
	3	*in vitro*	hairless rat	yes[b]
	3	*in vitro*	hairless rat	10-100
	3	*in vitro*	hairless rat	≈100
	3	*in vitro*	hairless mouse	>10
	3	*in vitro*	man	8
	3	*in vitro*	man	7
	5	*in vitro*	hairless mouse	50
	10	*in vitro*	hairless rat	≈10
Fusidate sodium	3[c]	*ex vivo*	hairless mouse	2-3
Griseofulvin	3	*in vitro*	man	yes[b]
	5[c]	*in vitro*	hairless mouse	>36
Hematoporphyrin derivative	2	*in vitro*	hairless mouse	8
	10	*in vitro*	man	≈19
Hydrocortisone	5[c]	*in vitro*	hairless mouse	45
	5[c]	*ex vivo*	hairless mouse	≈65
Hydroquinone	0.5	*in vivo*	man	1.2[e]
	2	*in vitro*	hairless mouse	>3
Ibuprofen	5	*in vitro*	hairless rat	3
Idoxuridine	5[c]	*in vitro*	hairless mouse	>3000
Indomethacin	3	*in vitro*	hairless rat	9
	5	*in vitro*	hairless rat	4
	6[c]	*in vitro*	rat	5
	6[c]	*in vivo*	rat	3
	8	*in vitro*	hairless mouse	>7
Indomethacin, Ca	6	*in vitro*	rat	2
	6	*in vitro*	rat	1.3
Insulin	0.1[c]	*in vitro*	rat	7
	0.1[c]	*in vitro*	rat	14

[a]Based on vasoconstriction assay; [b]not quantified or not quantifiable; [c]propylene glycol was co-administrated; [d]based on plasma concentrations; [e]based on amounts retrieved in urine and faeces; [f]spreading due to biphasic pattern in control; [g]pre-treated with 50 mg of Azone for 24 hr.

Compound	%Azone in formulation	Study type	Skin type	Enhancement factor
Isoproterenol	1[c]	*in vitro*	man	8
6-Mercaptopurine	3	*in vitro*	guinea pig	30
Metronidazole	1	*in vitro*	man	25
Mitomycin C	3.3	*in vitro*	rat	yes[b]
	3.3	*in vitro*	rat	60
	3.3	*in vitro*	hairless mouse	40
Nifedipine	5[c]	*in vivo*	rat	8[d]
Popanolol	2	*in vivo*	rabbit	30[d]
	3[c]	*in vivo*	rabbit	1.8[d]
Sulfanilamide	5	*in vitro*	hairless rat	≈70
Thymidine	2	*in vitro*	hairless mouse	>3
	2	*in vivo*	hairless mouse	yes[b]
triamcinolone acetonide	1.6[c]	*in vivo*	man	>3[e]
	1.6[c]	*in vivo*	man	4-9[a]
	2	*in vitro*	hairless mouse	>120
	3	*in vivo*	man	>2[a]
	10	*in vitro*	hairless mouse	>5
Trifluorothymidine	5	*in vitro*	guinea pig	224
	5[c]	*in vitro*	guinea pig	287
	5[c]	*in vivo*	guinea pig	yes[b]
	10[c]	*in vitro*	guinea pig	large[b]
	10[c]	*in vitro*	man	large[b]
Vasopressin	5	*in vitro*	hairless mouse	65
	5	*in vitro*	rat	15
	unknown	*in vivo*	rat	yes[b]
Verapamil, HCL	2[c]	*in vivo*	rat	6[d]
	3	*in vitro*	rat	≈5
	3	*in vitro*	hairless mouse	44-130[f]
	3	*in vitro*	man	3
	12	*in vitro*	rat	>20
Vidarabine (Ara-A) and esters				
Ara-A	3	*in vitro*	hairless mouse	170
	pretr.[g]	*in vitro*	hairless mouse	360
Ara-A-2',3'-di-*O*-acetate	15	*in vitro*	hairless mouse	100-1000
	pretr.[g]	*in vitro*	hairless mouse	100
Ara-A-5'-*O*-valerate	15	*in vitro*	hairless mouse	100-1000

[a]Based on vasoconstriction assay; [b]not quantified or not quantifiable; [c]propylene glycol was co-administrated; [d]based on plasma concentrations; [e]based on amounts retrieved in urine and faeces; [f]spreading due to biphasic pattern in control; [g]pre-treated with 50 mg of Azone for 24 hr.

In another study, Bodde and co-workers (1989) using X-ray diffraction techniques also concluded that Azone intercalated into the lipid bilayer of a *stratum corneum* model, causing a small decrease in the interlamellar spacing as well as inducing lateral swelling. Sugibayashi and co-workers (1992) compared the effects of Azone on the skin components with that of other penetration enhancers, including isopropyl myristate, dodecyl acetamide, dodecyl pyrrolidone, DMSO, methyl pyrrolidone, sodium salicylate, ethanol and urea. They found that incorporation of Azone resulted in a more marked fluidisation of liposomal lipids compared with other enhancers. Also, Azone did not extract the *stratum corneum* lipid and had no direct effect on the keratin of the *stratum corneum.* Furthermore, it was observed that Azone increased the water content in the *stratum corneum*, as measured by the changes in skin conductance.

Azone, which has a polar head group and a long alkyl chain, is thought to incorporate into structured lipids with the ring structure lying in the plane of the polar head groups. This has been suggested from the broadening of the phase transition on addition of Azone to the polar membrane (Beastall *et al.*, 1988). The presence of such a seven membered ring is considered to force the alkyl chains of the skin lipids apart, to give the lipid molecules more free space to move. This induces the disorder of the structured lipid and thus changes the skin permeability (Quan and Maibach, 1994).

1.3. MOLECULAR DYNAMICS SIMULATION OF LIPID MEMBRANE

1.3.1 Overview

The earlier sections have briefly discussed the physical aspects of transdermal drug delivery and the challenges involved, and how chemical enhancers can be used to overcome the barrier to drug permeation. Various experimental techniques that have been used to elucidate the mechanism of penetration enhancement of Azone have been mentioned. Unfortunately, no single experimental technique available to date can give us an accurate description at the *molecular level* of how this compound exerts its penetration enhancement effect. In the work reported here a computer simulation technique, molecular dynamics (MD) is employed in an effort to understand the mechanism of interaction between this molecule with a model lipid bilayer.

1.3.2 Lipid polymorphism

The most important components of biological membranes in general are phospholipids. The belief is that phospholipids form the major framework of membranes (Gennis, 1989). The most common include diacylphosphatidylethanol-amines, phosphatidylcholines (lecithins), phosphatidylserines and sphingomyeline. Table 1.3 shows the composition of phospholipids in various human cell membranes. The lecithins are the major phospholipids present in the mammalian tissues. However, many biological membranes contain mixtures of these different classes and their proportions vary within a particular tissue from one animal to another (van Deenan, 1965, Chapman & Wallach, 1968).

Due to their amphiphatic nature, phospholipids can form a variety of phases (Figure 1.8). The most important and familiar arrangement of phospholipids in biological membranes is the lamellar or bilayer (Epand, 1990). However, under certain conditions, some phospholipids can adopt non-bilayer phases such as micelles or the hexagonal phases. Micelles are formed when a critical concentration of polar lipids is reached in an aqueous medium. Above the critical micelle concentration, other phases such as hexagonal and bilayer can be present.

Table 1.3 Phospholipid Composition of Human Tissues

Tissue	*Phospholipid composition*								
	PC	**CP**	**LPC**	**PE**	**EP**	**PI**	**PS**	**SM**	**DPG**
Brain	33.9	0.1	-	13.2	20.2	2.6	10.5	13.8	1.9
Heart	22.0	16.9	1.7	14.0	11.9	4.3	3.2	5.5	14.5
Lung	41.7	1.1	1.1	9.6	10.5	3.8	7.4	15.0	2.7
Liver	45.2	-	0.7	28.4	1.1	6.5	3.8	6.7	5.5

key: PC - Phosphatidylcholine
LPC -Lysophosphatidylcholine
EP - Ethanolamine Plasmalogen
PS - Phosphatidyl Serine
DPG -Diphosphatidyl glycerols
CP - Cardiolipin
PE - Phosphatidylethanolanmine
PI - Phosphatidylionositol
SM - Sphingomyelin

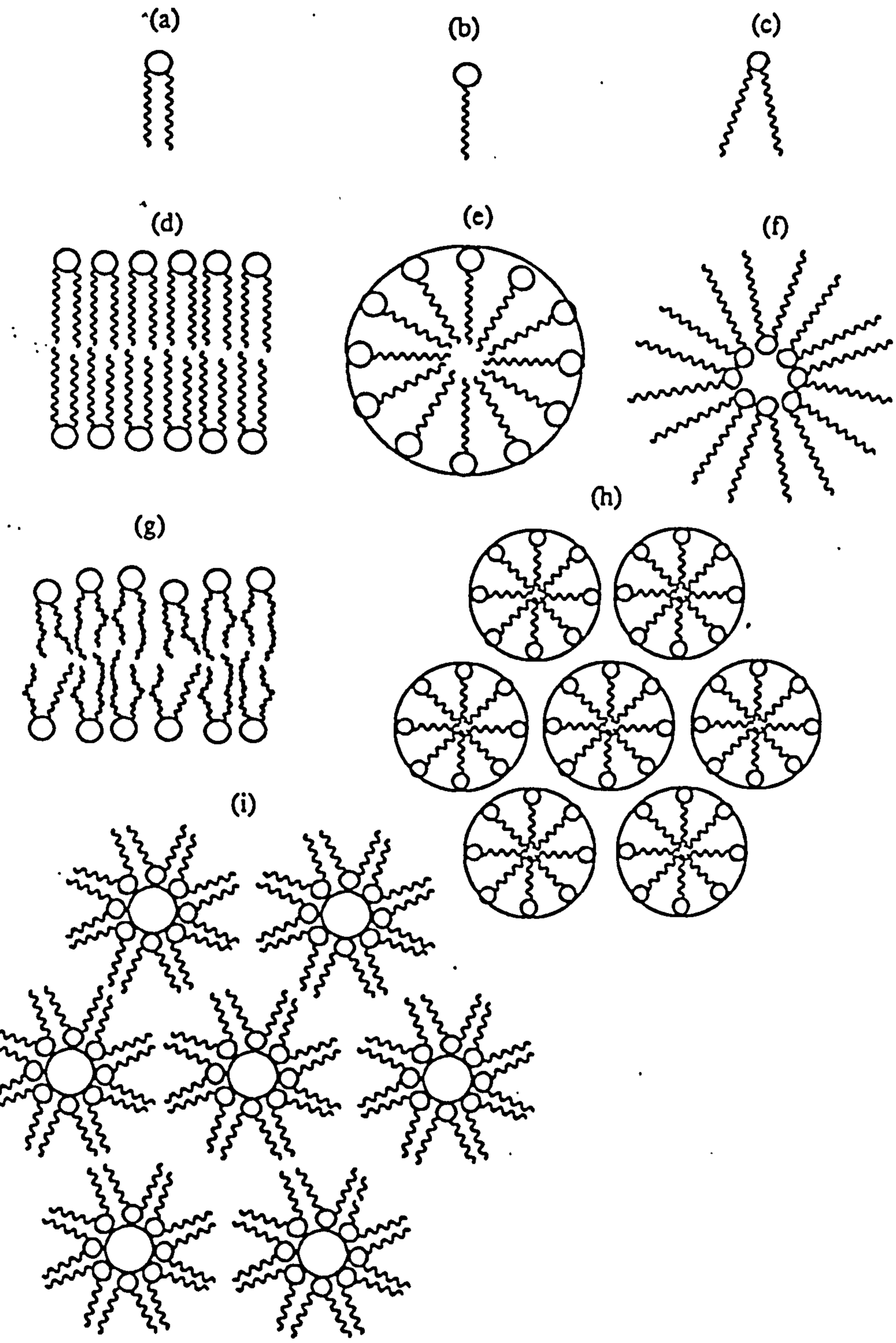

Figure 1.8: Structures of various lipid assemblies: (a)-(c) different type of lipid monomer. (d) highly ordered lamellar structure (LC or Lβ) (e) micelle (f) inverted micelle (g) liquid crystalline (Lα lamellar (h) hexagonal, H_I (i) inverted hexagonal, H_{II}.

In the hexagonal phases, (hexagonal H_I and H_{II}), the phospholipids are arranged as hollow cylinders filled with solvent. As the name implies, each cylinder is surrounded by six other cylinders. The H_I structure has the headgroup located at the outer circumference of the cylinder; in contrast, the H_{II} arrangement has its headgroup facing the inner core. In general, the formation of these phases in biological systems is not common. This is due to the fact that these structures represent a gross rearrangement of the lipid morphology that could result in a breakdown of the permeability barrier. However, in the pure form, in aqueous suspensions, certain lipid components of biological membranes can form the hexagonal phases, H_I spontaneously. One such example is ethanolamine plasmalogen (Epand, 1990).

The lamellar or bilayer arrangements are usually regarded as basic structures in biological membranes. These arrangements are important as they allow the headgroups to protect the hydrocarbon portions of the membrane from the aqueous environment. Luzzatti (1968) has reviewed the different types of lamellar phases extensively. The phases include liquid crytalline (Lα), gel phases (Lβ, Lβ'), lamellar rippled (Pβ and Pβ') and crystalline phase, C. These types of lamellar structures differ from one another as a result of thermotropic and lyotropic polymorphism as well as other variable external influences.

In thermotropic mesomorphisms, phospholipids do not pass directly from the crystalline phase to an isotropic liquid, but form a liquid crystalline state at intermediate temperatures. In the crystalline state, the hydrocarbon chains of the phospholipids adapt a fully extended, *trans* configuration. At the first transition (transformation to the liquid-crystalline state) the hydrocarbon chains melt. Furthermore, their mobility increases and they lose their fully extended all *trans* state; the number of *gauche* conformations increases and their chains display 'kinks' (Chapman, 1983).

At low temperature, in excess water, the bilayer remains in the gel phase (Lβ'), which like the crystalline state, is characterised by an ordered hydrocarbon chain structure, low interfacial surface area and low lipid mobility. At a characteristic transition temperature, this phase transforms into the liquid crystalline phase (Lα). Above this temperature, the mobility of the hydrocarbon chains of the lipid increases, the bilayer becomes thinner and the area per lipid molecule increases. A typical phase diagram of a phospholipid is represented in Figure 1.9.

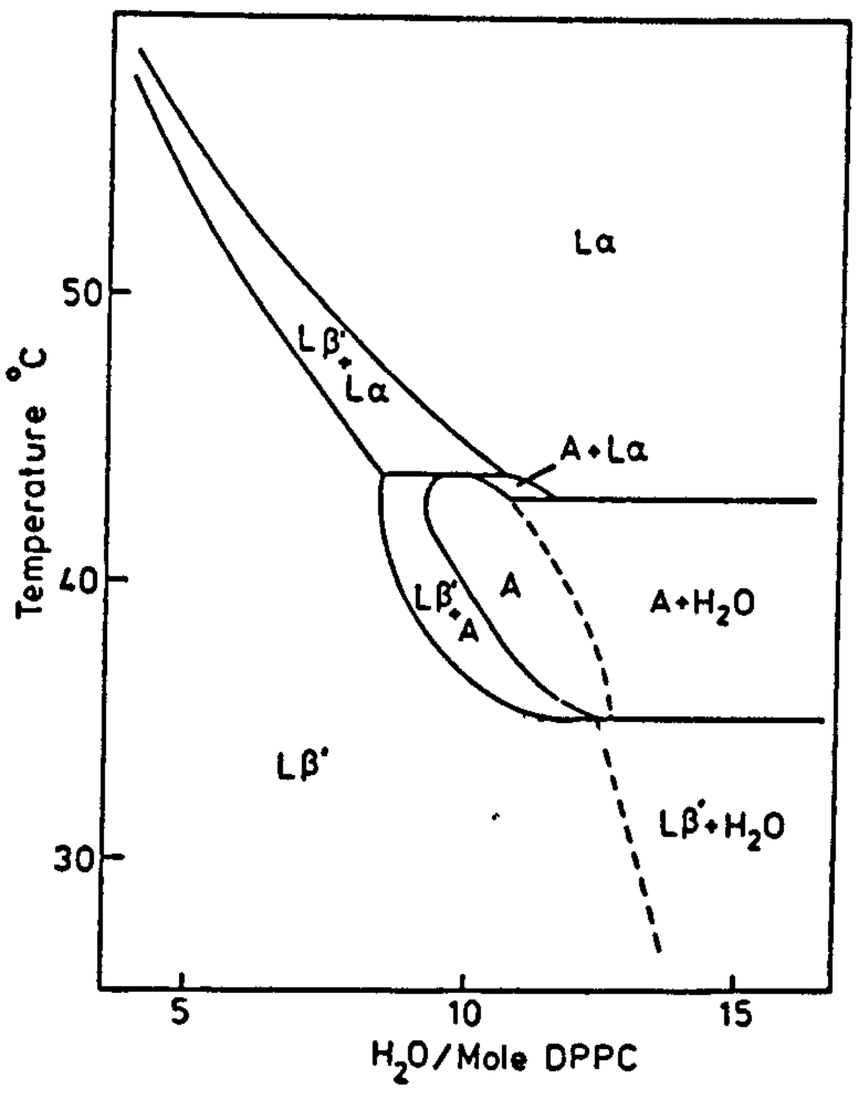

Figure 1.9. A typical phase diagram of dipalmitoyl phosphatidylcholine. Tm is the transition temperature. A is either Pβ' or Lβ'. L denotes a one-dimensional lamellar lattice, P a two-dimensional monoclinic lattice. In the α and β phases the hydrocarbon chains are liquid-like and solid-like respectively. The prime on β indicates that the chains are tilted with respect to the bilayer plane. Broken lines denote an uncertain phase boundary. Taken from Egbert, (1988).

1.3.3 Fundamentals of Molecular Dynamics

Karplus and Petsko (1990) refer to MD as the science of simulating the motions of a system of particles. Other workers, Allen and Tildesley (1987) define it in a slightly different manner; MD is the term used to describe the solution of the classical equations of motion (Newton's equations) for a set of molecules. The key word addressed by these workers nevertheless is the same, that is *motion*—which describes how positions, velocities and orientations change with time.

In MD the motions of atoms are simulated as a function of time, usually in terms of calculations based on Newton's Laws of motion. The time-dependent behaviour of a system consisting of N atoms, with masses m_ι is described by Newton's equation of motion:

$$F_\iota = m_\iota a_\iota \quad \text{.....1.1}$$

where $\iota=1,...N$ and a_ι and F are respectively, the accelerations and forces exerted on the atoms. In order to solve this equation it is necessary to evaluate the forces acting on the atoms in the system, and these can be obtained by taking the derivatives of the potential energy function, U, with respect to the atom positions r (i.e. with respect to their Cartesian co-ordinates, x_ι, y_ι and z_ι).

$$dU/dr_\iota = F_\iota \quad \text{.....1.2}$$

The acceleration, a_ι, of each particle can then be determined as:

$$a_\iota = F_\iota/m_\iota \quad \text{.....1.3}$$

With knowledge of the accelerations of all atoms, it is then possible to calculate the changes in the atom velocities and positions. Thus one obtains a trajectory of the atoms followed as a function of time.

The calculation of the atomic trajectories (eqn. 1.1-1.3) can be solved numerically using various algorithms such as the Verlet algorithm (Verlet, 1967), the Gear Predictor (Gear, 1971) and the Beeman Predictor (Beeman, 1976), for evaluating the forces and accelerations iteratively over small time steps, Δt. The most widely used algorithm in MD simulation is the Verlet algorithm (Haile, 1997). Given the positions and velocities of all atoms at time t, the forces exerted on each atom by the remaining atoms are calculated. Then, assuming that the forces do not change appreciably in the small time interval Δt, the positions, r_i and velocities, v_i of the atoms at time $(t + \Delta t)$ in response to these forces, at time t, can be determined using the Verlet algorithm:

$$r_i(t + \Delta t) = 2r_i(t) - r_i(t-\Delta t) + \Delta t^2 F_i(t)/2m_i \quad \text{.....1.4}$$

$$v_i(t) = \frac{(r_i(t+ \Delta t) - r_i(t- \Delta t)}{2\ \Delta t} \quad \text{.....1.5}$$

The new co-ordinates are then used to calculate the new set of forces acting on the atoms at time $(t + \Delta t)$. When this procedure is applied repeatedly, a description of the system as a function of time can be obtained.

As an alternative to the Verlet algorithm, the velocities and positions of the atoms can be obtained as:

$$v_i(t + \tfrac{1}{2}\Delta t) = v_i(t - \tfrac{1}{2}\Delta t) + F_i(t)/m_i\ \Delta t \quad \text{.....1.6}$$

$$r_i(t + \Delta t) = r_i(t) + r_i\ (t + \tfrac{1}{2}\Delta t)\ \Delta t \quad \text{.....1.7}$$

using the co-ordinates of the atoms at intervals of Δt and their times $\frac{1}{2}\Delta t$. This algorithm is also referred to as the half-step 'leap-frog' scheme (Allen & Tildesley, 1987) and is very efficient from computational point of view, as it is simple and requires less CPU time and memory. The magnitude of the time step used in these calculations is critical, and must be sufficiently small to allow the simulation of the bond vibrations which occur on a time scale of femtoseconds (fs). The time step used is usually is in the range of 0.5 to 2.0 fs. Clearly, for most chemical and physical processes such as diffusion, which occur on nanoseconds and/or larger time scales, the computation involved will be very long.

Another essential element in an MD study is the choice of an appropriate potential energy function. In principle, the potential energy of a system can be obtained using *ab initio* quantum mechanics calculations (using programs such as Gaussian 90 (Frisch et al., 1990)) but such calculations are computationally prohibitive for systems involving more than 50 atoms. As an alternative, semi-empirical potential energy calculations are more common. These calculations are based on classical mechanical principles and allow a good approximation of the potential energy. The energy function which is employed is also called the force field. A force field has three components:

i. A set of equations defining how the potential energy of a molecule varies as a function of its constituent atoms' positions.
ii. A series of atom types, defining the characteristics of the elements within specific chemical contexts. The atom type depends on hybridisation, charge and the nature of the other atoms to which it is bonded.
iii. One or more parameter sets that fit the equations and atom types to experimental data. Parameter sets define constants, used in the equations to relate atomic characteristics to energy components and structural data such as bond lengths and bond angles.

Molecular mechanics calculations do not explicitly treat the electrons in a molecular system. Instead, the computations are based upon the interactions between the atomic nuclei. Electronic effects are implicitly included in the force field calculations through the force field parameters. This approximation makes molecular mechanics computations relatively inexpensive, and allows them to be used for very large systems containing many thousands of atoms. However, certain points must be borne in mind when using molecular mechanics among the most important of which are that:

i. Each force field achieves good results only for a limited class of molecules, related to those for which it was parameterised and no force field can be generally used for all molecular systems of interest.

ii. Processes such as that involving bond formation and bond breaking cannot be simulated by molecular mechanics as the electronic effects are neglected.

The potential function derived from molecular mechanics usually has two main contributions; bonded and non-bonded terms. The most common form of a potential energy functions is :

$$U = \Sigma E_{bond} + \Sigma E_{angle} + \Sigma E_{torsion} + \Sigma E_{improper} + \Sigma E_{eel} + \Sigma E_{vdw} \quad ....1.8$$

where $E_{bond} + E_{angle} + E_{dihedral}$ are the energy contributions due to bond stretching, and angle bending and dihedral torsions in the system. Bond energy is usually described by a harmonic function;

$$E_{bond} = \tfrac{1}{2}K_b (b - b_o)^2 \quad .....1.9$$

where b is the observed bond length, b_o is the equilibrium bond length and K_b is the force constant. Similarly, the angle energy can also be described by a harmonic function:

$$E_{angle} = \tfrac{1}{2}K_a(a - a_o)^2 \quad .....1.10$$

where a is the observed angle, a_o is the equilibrium angle and K_a is the force constant.

The dihedral angle energy term in the equation is usually described by a cosine function:

$$E_{torsion} = \tfrac{1}{2}K_d[1+\cos(n\delta - \lambda)] \quad .....1.11$$

where δ is the observed dihedral angle, n is the multiplicity, λ is the phase and K_d is the force constant. Improper dihedral angle strain is usually described as:

$$E_{improper} = \tfrac{1}{2}K_i[1-\cos 2\delta] \quad .....1.12$$

where K_i is the force constant and δ is the improper dihedral angle.

As the name implies, the non-bonded energy terms describe the atomic interactions not associated with covalent bonds. The electrostatic energy (for atoms *i and j*) is usually defined by Coulomb interactions:

$$E_{eel} = q_i q_j / 4\pi\varepsilon_o \varepsilon r \quad \text{.....1.13}$$

where, q_i, q_j, are the atomic partial charges, r is the non-bonded distance, ε_o is the permittivity in vacuum and ε is the dielectric parameter. Finally, the last term that describes the nonbonded interaction (for atoms *i and j*) is the van der Waal energy which is usually represented by a Lennard-Jones potential (a 6-12 potential)

$$E_{vdw} = 4\varepsilon_{ij} [(\sigma_{ij}/r)^{12} - (\sigma_{ij}/r)^{6}] \quad \text{.....1.14}$$

where, σ_{ij} is the Lennard-Jones distance, ε_{ij} is the dispersion well depth and r is the non-bonded distance (Figure 1.10).

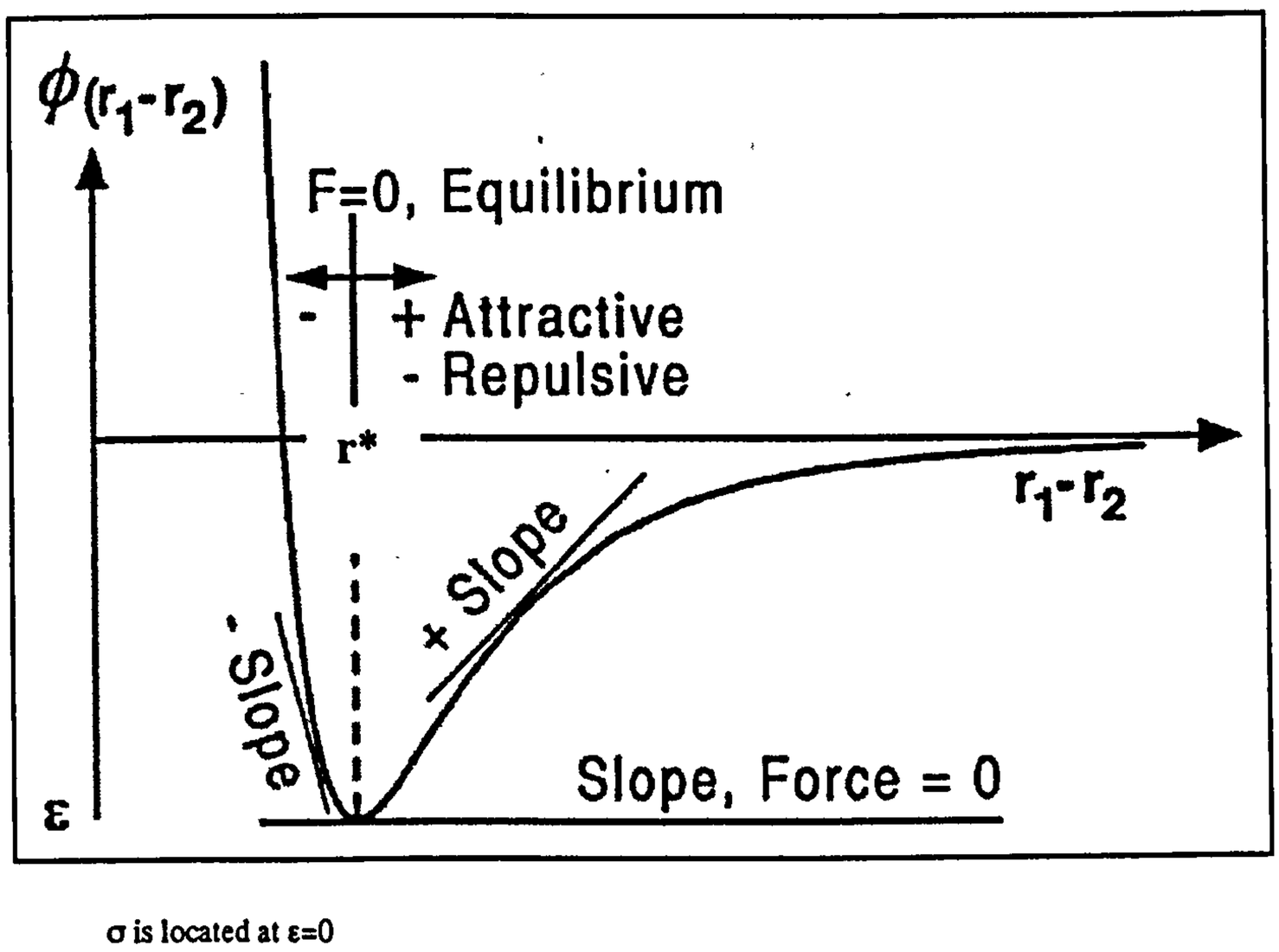

σ is located at ε=0

Figure 1.10. Lennard-Jones Potential

An MD simulation is initiated by defining the number of particles (N), assigning the atomic positions and velocities of the particles at time t=0. Initial positions $r_i(0)$, can be assigned according to some lattice structure or taken from a previous simulation. The initial velocities $v_i(0)$ are usually assigned randomly. Lack of available storage on the host computer as well as the speed of execution limit simulation sizes to systems involving a small number of molecules (Allen & Tildesley, 1987). The size of system simulated is typically in the range of a few hundred to several thousand molecules, which is very small compared to a real microscopic system. Small systems are dominated by surface effects which usually are not of interest. These effects can be eliminated by employing periodic boundary conditions (pbc).

In simulations employing pbc, the positions (co-ordinates of the particles) are assigned in a cell called the simulation or primary cell. The primary cell is surrounded by exact replicas of itself, representative of the bulk material. Periodic boundary conditions in two dimensions are shown in Figure 1.11. The co-ordinates of the particles in the image boxes can be computed simply by adding or subtracting integral multiples of the box sides. Should a particle leave the box during the simulation then it is replaced by a corresponding image entering from the appropriate adjacent cell. The number of particles within the central box thus remain constant.

In MD simulations, the calculation of non-bonded interactions between all pairs of atoms is too expensive as the increase in computing time is of the order of N^2. One way to deal with this problem is by applying a *non-bonded cut-off* and *minimum image convention* (Figure 1.12). The minimum image convention states that each atom 'sees' at most just one image of every other atom in the system (which is repeated infinitely via pbc). A cut-off (R_{cut}) is a distance outside of which interactions are considered to be negligible and therefore ignored. In general, the cut-off should not exceed half of the smallest dimension of the primary cell in order to prevent a particle from interacting with its own image or indeed the same particle twice.

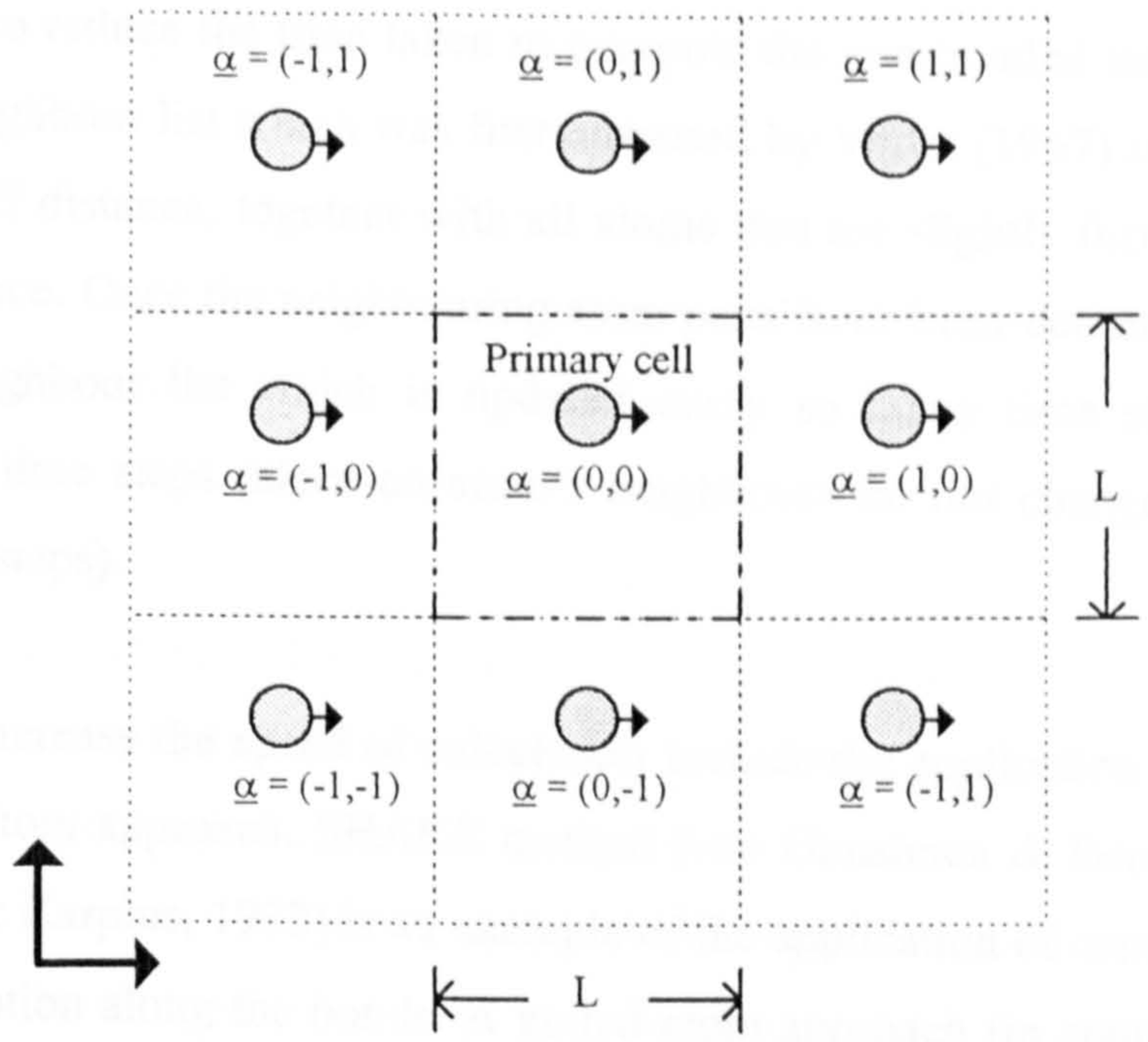

Figure 1.11. Periodic boundary conditions in two dimensions. The primary cell surrounded by eight image cells and each cell is identified by a cell translation vector $\underline{\alpha}$. Each cell has a reference frame whose origin is the lower left corner of the cell. Since the events in the primary cell are duplicated in each image cell, there is conservation of mass in each cell. As atom *i* leaves the primary cell, an image of *i* enters the primary cell from an adjacent cell.

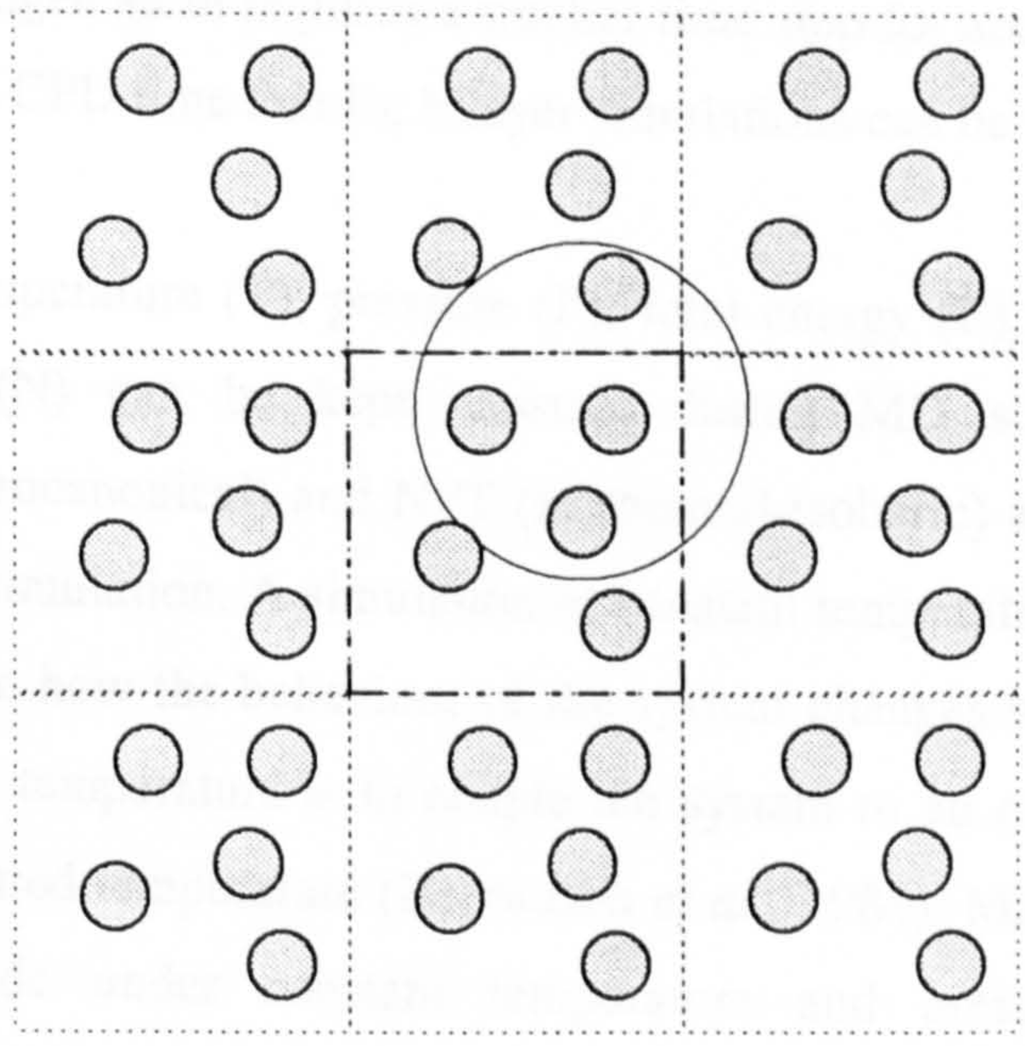

Figure1.12 : The spherical cut-off and minimum image convention The circle represents the spherical cut-off.

The use of a non-bonded neighbour list in conjunction with the use of a non-bonded cutoff could also reduce the time taken to compute the non-bonded interactions. The non-bonded neighbour list which was first proposed by Verlet (1967) stores all atoms within the cutoff distance, together with all atoms that are slightly further away than the cutoff distance. Once the neighbouring atom pairs have been determined, they are stored in a neighbour list which is updated every so many time steps, typically between 10-20 time steps (since an atom's neighbours do not change significantly over these time steps).

Other ways to increase the speed of calculation include the application of constraints and the united atom approach. SHAKE method (van Gunsteren & Berendsen, 1977; van Gunsteren & Karplus, 1982) is an example of the application of constraints which constrain the motion along the bonds. A united-atom approach (in contrast to an all-atom approach where all atoms in the system are included explicitly in the calculation) involves hydrogen atoms being subsumed into the atoms to which they are bonded. This reduces the size of the system studies, which results in fewer nonbonded interactions and internal degrees of freedom. One advantage of this, is that it is feasible to use a larger dynamic integration time step in MD simulations since the small mass of the hydrogen atom requires a smaller time step for accurate integration. This allows a saving in CPU time that for bilayer simulations can be very costly.

Parameters such as temperature (T), pressure (P), total energy (E), volume (V) and number of particles (N) can be kept constant during MD simulations. NVT (canonical), NVE (microcanonical) and NPT (isothermal-isobaric) are three types of ensemble used in MD simulation. A simulation at constant temperature is desirable if one wishes to determine how the behaviour of the system changes with temperature. One way to control the temperature is to couple the system to an external heat bath that is fixed at the required temperature (Berendsen *et al.*, 1984). Many experimental measurements are made under constant temperature and pressure, thus NPT simulations are most directly relevant to experimental data. In this type of ensemble, the system maintains its pressure at constant value by changing the volume of the simulation cell.

1.3.4 Application of MD to the Simulations of Lipid Bilayer

The application of MD to a condensed phase system was first devised by Alder and Wainwright (1957), using a hard-sphere model. However, it is not until 1982, that MD was first applied in the modelling of lipid bilayers by van der Ploeg and Berendsen (1982, 1983). Their model consisted of a single bilayer which was made up of two opposing monolayers. Each monolayer contained 16 decane molecules arranged in a square and constrained to be periodic in two dimensions. The headgroups of the decane molecules were treated as 'united atoms' and restrained by means of a harmonic force. This system was further improved by Egbert and co-workers (Berendsen & Egbert, 1986, Egbert, 1988) where the headgroups of the molecules were treated in full atomic detail. In this system, they included the atomic partial charges and sodium ions that constituted the counterions for decanoate ions. In both simulations, the structures were analysed by calculating bond order parameters, density profiles, pair distribution functions and other dynamics properties of the lipid bilayer. The earlier simulations performed by van der Ploeg and Berendsen (1982) were found to be more successful in the prediction of static properties of the model membrane. The bond order parameters obtained by averaging over the time-dependent orientations of the chain segments, for example, were in excellent agreement with those measured experimentally. However, the simulation by Egbert (1988) demonstrated a more successful prediction of the dynamic properties of the lipid membrane.

With increased computer power, Egbert and co-workers (1994) further improved their molecular dynamics simulations by employing a more realistic model of a lipid membrane which consisted of 64 molecules of dipalmitoyl phosphatidylcholine (using a united atom model) arranged in a bilayer. The computational cell also included 736 water molecules, giving a total number of atoms of 5408. It is interesting to note that, in using their original force field, the model membrane showed gel-like characteristics and that with a slight modification of the force field, the system was found to behave as a liquid crystalline phase. The results obtained, including the bilayer repeat distance, surface area per lipid, bond order parameters and atomic distributions were again in close agreement with the available experimental results, and showed that the MD simulations could provide realistic models of phospholipid membranes (Egbert, 1988, Egbert *et al.*, 1994).

Since these simulations by Egbert and co-workers, numerous other workers have carried out MD simulations of the liquid phase systems and the research in this area has been reviewed by Pastor (1994), Merz and Roux (1996) and Merz (1997). It is necessary therefore to set this work in context by reviewing the important aspects of the methodology and significant results from MD simulations of lipid bilayer models.

One of the most important aspects of MD simulations of lipid bilayers is the development of a potential function and associated parameters suitable for lipid membrane models. Several potential energy functions and parameters have been used successfully in the simulations of lipid bilayers. These include the use of the AMBER force fields (Weiner *et al.*, 1984) for bonds, angles and torsions with the combination of OPLS parameters (Jorgensen & Triado-Rives, 1988) for non-bonded interactions in the simulation of dilauryl phosphatidyl ethanolamine (DLPE) (Damodaran *et al.*,1992), DLPE, DOPC and DOPE (Huang *et al.*, 1994) and DMPC (Robinson *et al.*, 1993). The use of AMBER force field parameters along with Discover parameters (Hagler *et al.*, 1979(a) 1979(b)) for the Lennard-Jones 6-12 potential parameters have been found to be satisfactory in the force field development for crystalline lipid systems (Stouch *et al.*, 1991). Although the force field parameters were successfully refined for modelling DMPC lipid bilayers (Stouch, 1993, Stouch *et al.*, 1994) there has been a lot of effort expended recently to develop a better force field for the simulation of lipid membranes. This task has been undertaken by Schlenkrich and co-workers (1996) who derived an all-atom potential energy function for phospholipids. The parameters were derived to be consistent with the all-atom CHARMM 22 potential for peptides, proteins and nucleic acids. With the availability of such a force field, it is possible to simulate complex membrane systems that contain peptides and proteins as well as lipids. These potential parameters have been successfully used to study DPPC bilayer models (Feller *et al.*, 1997, Tu *et al.*, 1996).

The use of 'united atom' versus 'all atom' models in (lipid) MD simulations has long been a subject of debate. Usually, with united atom models, hydrogen atoms are subsumed into the atoms to which they are bonded. This reduces the size of the system studied, which results in fewer nonbonded interactions and internal degrees of freedom. One advantage of this, is that it is feasible to use a larger integration time

step in MD simulations since the small mass of the hydrogen atom requires a smaller time step for accurate integration. This allows a saving in CPU time which in some cases in bilayer simulations can be costly. Earlier MD simulations of liquid crystalline systems (Egbert, 1988, Egbert *et al.*, 1994), Damodaran *et al.* (1992), Huang *et al.*, (1994), Robinson *et al.* (1994) and Zhou & Schulten (1995) all employed united-atom models where the methylene and methyl groups were treated as united-atoms. The use of united-atom models has been shown to produce artificially high diffusion rates, which therefore preclude their use for studying diffusion in the biomembrane. Moreover, other studies on n-alkanes strongly suggest that all hydrogen atoms must be included to reproduce experimental data (Bassolino-Klimas *et al.*, 1993 and the references therein). As a consequence of these deficiencies all of the most recent MD simulations of membrane systems, (Stouch, 1991; Damodaran & Merz, 1995; Tu *et al.*, 1995, 1996; Feller *et al.*, 1996; Feller & Pastor 1995; Feller *et al.*, 1997) have moved towards employing the all atom approach to give a better representation of experimental data.

Another important issue in the MD studies of lipid bilayers is the type of ensemble employed in the simulation. Earlier bilayer simulations used constant volume and temperature (NVT or canonical) ensembles (Alper *et al.*, 1993; Venable *et al.*, 1993; Damodaran & Merz, 1992, 1994; Robinson *et al.*, 1994). Such ensembles are better than constant volume-constant energy (NVE) ensembles since they provide constant temperature (which mimics experimental conditions). They also have a clear advantage over constant pressure-constant temperature (NPT) ensembles, because of the time saved in not scaling the periodic box dimensions. This time can be particularly significant when the system to be simulated is large and the available computing resources are limited. However, this type of ensemble does have limitations. The problem with the NVT ensemble is that the starting configuration must be based on a good estimate of the dimensions and density to reproduce the experimentally observed features of the lipid membrane. If the estimate is bad, the results obtained do not reproduce the experimentally observed characteristics of the bilayer. For example, if the density is too low in a fluid phase membrane, a gap can develop between the monolayers or the two monolayers may bend because of their inherent curvature. Another concern that arises from the use of this ensemble is that if the density is adjusted to the appropriate value, the simulation might produce a good

might produce a good result even if the force fields are not right, because the constraints of the constant volume would prevent the system from evolving to an incorrect density (Jakobsson *et al.*, 1996). Clearly, the best solution is to employ constant NPT ensembles.

In NPT simulations, the dimensions of the cell of the system are allowed to change in response to the change in pressure within the box (Merz, 1997). The use of this type of ensemble has been reported by Huang *et al.*, (1994), Egberts, (1988) and Egberts *et al.* (1994). The simulations carried out by Egbert and co-workers (1994) for example, demonstrated a defect in the NPT scheme used as shown by the model produced at the end of the simulation. This model exhibited characteristics of the gel phase whereas it was expected to behave as a liquid crystalline phase. By arbitrarily reducing the partial charges of the lipid molecules by a factor of two, the system was shown to transform from its gel state to the liquid crystalline phase. Recently, Parinello-Rahman NPT simulations with a Nosé thermostat have been carried out by Tu *et al.* (1995) and Shinoda *et al.* (1995) and this type of ensemble is claimed to be the correct one to use in bilayer simulations. This claim has been counter-argued by Chiu *et al.*, (1995) and Feller & Pastor (1996) who suggested that the correct way of simulating the biomembranes is by employing a constant surface tension-constant temperature (NPγT) ensemble since fully hydrated bilayers have an inherent surface tension. Objections to this were raised by Jahnig (1996), who pointed out that the surface tension of unstressed bilayers is zero. This is further supported by the work of Tielman and Berendsen (1996) who demonstrated that there is little practical difference in the simulations between the use of either constant pressure ensembles (Merz, 1997, Jakobsson *et al.*, 1996).

Most bilayer simulations have one common goal, that is to produce a bilayer model which gives an accurate picture of lipid bilayer structure and dynamics. With this model, further simulations could be carried out to study the effects of biomolecules such as cholesterol or proteins bound in the membrane and the study of pharmaceutically important processes such as diffusion and transport of small molecules.

Edholm & Nyberg (1992), Robinson *et al.*, (1995) and Gabdoline *et al.*, (1996) have all attempted to study the interaction of cholesterol in model membranes. Edholm & Nyberg (1992) studied the perturbing effect of cholesterol in a DPPC bilayer. In the fluid phase of the bilayer, at 13% (w/w) concentration of cholesterol they found that a local ordering of the hydrocarbon chains is induced. At low concentration, there was a slight increase in the thickness of the membrane close to cholesterol but no increase observed in bond order parameters or trans-rotamer content of the lipid alkyl chains was observed. In another study, Robinson *et al.* (1995) successfully reproduced the main physical effects of cholesterol on lipid membranes. Using DMPC as a model membrane, they found that the number of trans-rotamer conformations increased in lipid molecules adjacent to the cholesterol, suggesting that these lipids are more ordered. In addition, they were able to observe that cholesterol is hydrogen bonded to the phosphate oxygen atoms of the lipid headgroups, and to ester groups as well as water molecules. Another interesting finding was that the cholesterol molecules were only slightly tilted with respect to the bilayer normal. All of these observations were in agreement with the observed experimental results (Gennis, 1989).

Vanderkooi (1994), performed an energy minimisation on DMPC-cholesterol bilayers at 1:1 ratio and found that the structures correspond to the available experimental data as judged from the molecular areas and bilayer thickness. This work was extended in a molecular dynamics study, using NPT simulations (Gabdouline *et al.*, 1996). The system studied consisted of 16 DMPC and 16 cholesterol molecules. Even though they observed an increase in area per lipid and area per cholesterol, the observed experimental area per lipid is never reached for the liquid crystalline phase. As pointed out by Merz (1997) this is probably due either to the deficiencies in the potential function used or to the use of an inappropriately short the time scale for the simulation (100-300ps). Nevertheless, as with the work by Robinson et al (1995), they also observed an increase in trans conformation (30%) as compared with the neat DMPC bilayer.

Other MD simulations of lipid bilayers have been concerned with the interaction and diffusion of drugs in the bilayer. Huang and co-workers (1995) investigated the interaction of trichloroethylene (an inhaled general anaesthetic) on the structure of a

DOPC lipid bilayer. By comparing with the pure bilayer, they observed three major effects caused by the drug -

i) an increase in the ratio of the effective hydrocarbon tails to the headgroup per lipid, suggesting a tendency for the lipids near the anaesthetic's site of action to form a hexagonal (H_{II}) phase;
ii) a slight increase in *gauche* rotamer conformations in the DOPC hydrocarbon chains
iii) a significant increase in the lateral mean-square displacement of lipid molecules, indicating an increase in lipid lateral diffusion and membrane fluidity.

The same authors also studied the effect of pressure on the behaviour of the anaesthetic. Here they found that at 200atm the perturbing effect of the anaesthetic was partially inhibited and virtually eliminated at 400atm. These results correlate well with experimental observations, where the effect of anaesthesia is reduced with an increase in pressure.

An investigation of solute diffusion in a lipid bilayer has been carried out in Stouch's laboratory (Bassolino-Klimas *et al.*, 1993; Alper & Stouch, 1995; Bassolino-Klimas *et al.*, 1995; Bassolino *et al.*, 1996) looking at the effect of size on the mechanism of membrane diffusion of small molecules including methane, benzene, a nifedipine analogue and adamantane. From their various MD simulations these authors concluded that molecules of a size on the order of that benzene or smaller diffuse faster in the bilayer centre than elsewhere in the bilayer. The increased rate appears tied to the ability of the small solutes to make rapid, large motions, jumps, between and within the plentiful voids that exist in the bilayer centre. This enhanced diffusion is unavailable for molecules such as adamantane and nifedipine whose volumes are two and three times larger than benzene respectively. Voids seldom appear that can accommodate the larger molecules. It seems likely that this increased rate of diffusion is at least partly responsible for the faster-than-expected permeation of small molecules (Stouch & Bassolino, 1996).

Other notable MD studies of liquid bilayer systems include those concerned with bilayer /peptide and bilayer/protein interactions carried out by Shen *et al.*, (1997), Woolf & Roux (1994, 1996), Damodaran & Merz (1995), and Kothekar (1996).

1.4 Content of the thesis

This chapter has reviewed the various aspects of transdermal drug delivery and MD simulations of lipid bilayers. The experimental observations of the effect of Azone on the *stratum corneum* or *stratum corneum* models and the application of MD in lipid bilayer modelling has also been discussed.

In Chapter 2, the methodology involved in carrying out the experiments is described. Basically, the work is divided into three studies; MD simulations of Azone in various environments where the conformations of Azone in these systems are investigated; three different forms of MD simulations of a pure DPPC bilayer carried out to determine the appropriate model to use in studying the incorporation of Azone in the system; and MD simulations of DPPC bilayers containing Azone, where the effects of Azone on the membrane are measured.

In Chapter 3, the results of all of the simulations are presented. Chapter 4 discusses and compares the results with the available experimental data and Chapter 5 gives general conclusions drawn from the three studies.

2. METHODOLOGY

2.1 Overview

The molecular dynamics (MD) simulations reported here are divided as three separate but related studies. In the first, the simulations were performed for liquid Azone, and Azone in water, in the presence and absence of dipalmitoyl phosphatidylcholine (DPPC). The trajectories of these simulations were analysed in terms of the conformations adapted by Azone. In the second study, the MD simulations were performed for solvated bilayer of DPPC. These simulations were carried out under varying conditions, exploring the use of both the AMBER4.1 and CHARMm22 force fields; the aim of the studies being to determine the most appropriate methodology to use in simulating the effects of Azone on the DPPC bilayer. The final study involved MD simulations of solvated DPPC bilayers incorporating, in the one case, Azone localised in just one monolayer of the bilayer, and in the second case, with Azone present in both monolayers. These studies were conducted to determine the disordering effects of Azone on the lipid bilayer.

2.2 Force Field and Model Parameters

All of the simulations were performed using the SANDER program from AMBER version 4.1 (Pearlman *et al.*, 1995) and with the exception the one simulation performed for an Lα-DPPC bilayer (2.4.4) involved the used of the AMBER force field potentials. In the case of the Lα-DPPC bilayer studies, one simulation was carried out using the CHARMm22 force field (Schlenkrich *et al.*, 1996) with the exception of improper torsion parameters which are taken from the AMBER force fields. Since these parameters are not included in AMBER package, tests were carried out to ensure that the energies obtained using the CHARMm22 lipid potentials

calculated using CHARMm22 molecular modelling implementations were essentially the same as those obtained using the SANDER module of AMBER. For this purpose, we used hexane as our test model since the molecule does not have an improper torsion. The first-step energies calculated during minimisation were compared from the same configuration, and the results obtained showed that CHARMM22 and AMBER4.1 values were essentially the same, see Appendix 1.

The atomic partial charges for DPPC and Azone which were used in the Azone/water, Azone/DPPC/water and liquid Azone simulations were calculated using Gaussian94 (at the 6-31G* level, see Table 2.1). The DPPC charges used in the Lβ'-DPPC bilayer simulation were calculated using the turbomole program (at 3-21G level). In the CHARMm modelling of the La-DPPC bilayer, the DPPC charges were taken directly from the literature (Schlenkrich *et al,* 1996).

A TIP3P water model (Jorgensen *et al.*, 1983) was used in all simulations involving water. In this model each water molecule has its oxygen atom bearing a charge of -0.8340, balanced by charges of +0.4170 carried on each of the two hydrogen atoms.

Table 2.1 6-31G* charges for DPPC * (in the all-atom models)

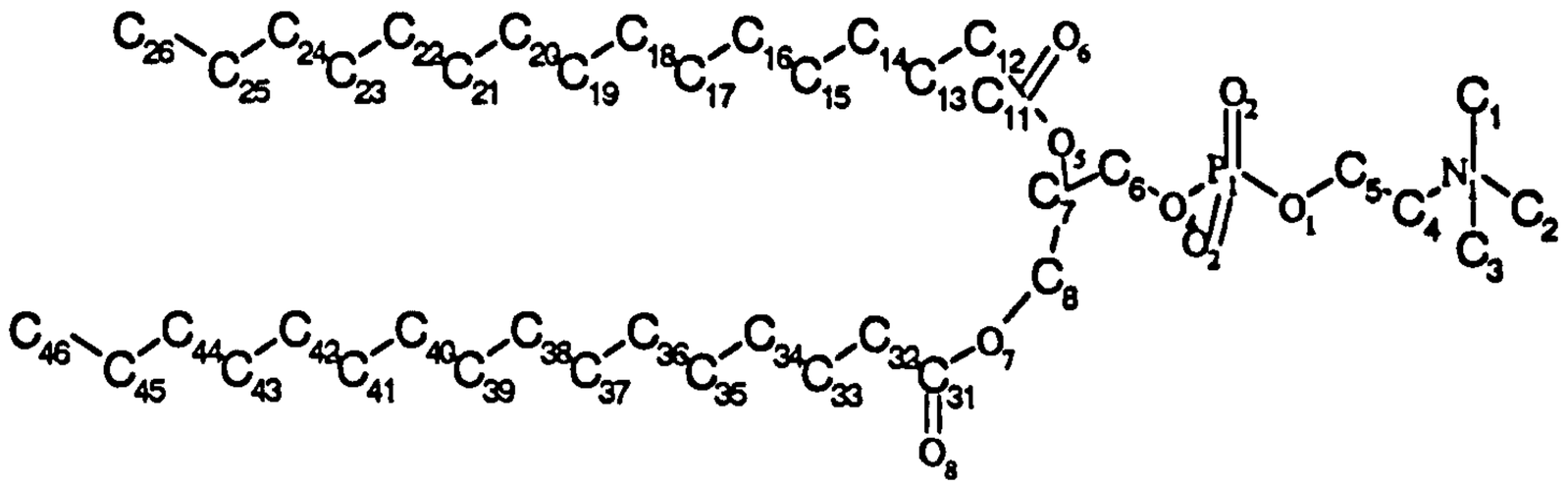

Atom	Charge	Atom	Charge	Atom	Charge
N1	0.3988	H24	0.0884	C33	-0.0304
C1	-0.5033	C16	0.2597	H52	0.0464
H1	0.2097	H25	-0.0096	H53	0.0464
H2	0.2097	H26	-0.0096	C34	0.1711
H3	0.2097	C17	-0.3781	H54	0.0072
C2	-0.5033	H27	0.0934	H55	0.0072
H4	0.2097	H28	0.0934	C35	-0.4656
H5	0.2097	C18	0.1492	H56	0.1054
H6	0.2097	H29	-0.0037	H57	0.1054
C3	-0.5033	H30	-0.0037	C36	0.2773
H7	0.2097	C19	-0.2374	H58	-0.0288
H8	0.2097	H31	0.0644	H59	-0.0288
H9	0.2097	H32	0.0644	C37	-0.2627
C4	-0.3314	C20	0.1155	H60	0.0669
H10	0.1588	H33	0.0063	H61	0.0669
H11	0.1588	H34	0.0063	C38	0.0661
C5	0.3243	C21	-0.3825	H62	0.0090
H12	-0.0042	H35	0.0929	H63	0.0090
H13	-0.0042	H36	0.0929	C39	-0.2484
O1	-0.5262	C22	0.3439	H64	0.0692
P1	1.2443	H37	-0.0286	H65	0.0692
O2	-0.7135	H38	-0.0286	C40	0.1897
O3	-0.7135	C23	-0.4993	H66	-0.0036
O4	-0.5262	H39	0.1071	H67	-0.0036
C6	0.2075	H40	0.1071	C41	-0.4895
H14	0.007	C24	0.1237	H68	0.1142
H15	0.007	H41	0.0037	H69	0.1142
C7	0.0482	H42	0.0037	C42	0.3174
H16	0.0975	C25	0.0947	H70	-0.0170
O5	-0.4744	H43	-0.0011	H71	-0.0170
C11	0.9538	H44	-0.0011	C43	-0.3337
O6	-0.6504	C26	-0.3154	H72	0.0715
C12	-0.3909	H45	0.0669	H73	0.0715
H17	0.1086	H46	0.0669	C44	0.0317
H18	0.1086	H47	0.0669	H74	0.0112
C13	-0.0817	C8	0.1013	H75	0.0112
H19	0.0488	H48	0.0973	C45	0.1485
H20	0.0488	H49	0.0973	H76	-0.0111
C14	0.1844	O7	-0.4763	H77	-0.0111
H21	0.0076	C31	0.8222	C46	-0.3324
H22	0.0076	O8	-0.5663	H78	0.0731
C15	-0.4000	C32	-0.3876	H79	0.0731
H23	0.0884	H50	0.0952	H80	0.0731
		H51	0.0952		

* note that the hydrogen atoms were omitted from the structure of DPPC for clarity. The hydrogen atoms listed in the table are arranged below their respective methyl or metylene carbons.

Table 2.2 6-31G* charges for Azone**

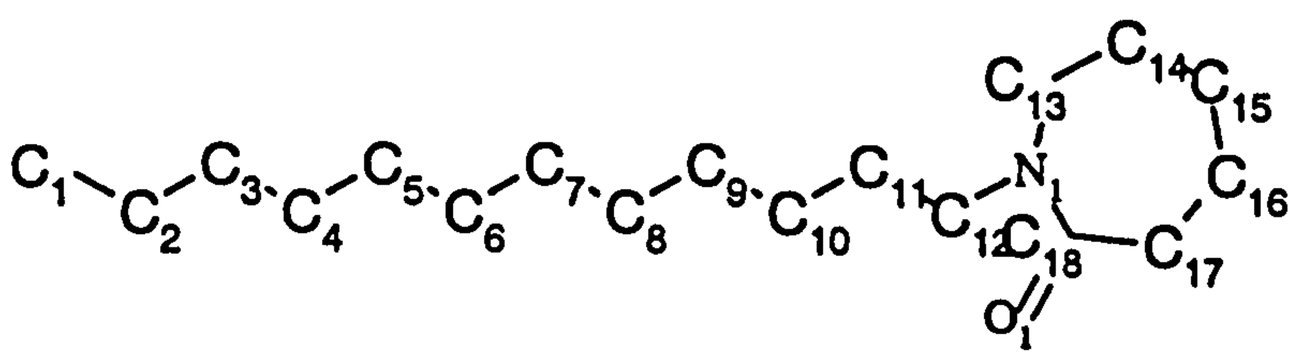

Atom	Charge	Atom	Charge
C1	-0.310	H19	-0.009
H1	0.066	C10	0.038
H2	0.066	H20	-0.015
H3	0.066	H21	-0.015
C2	0.198	C11	-0.048
H4	-0.032	H22	0.022
H5	-0.032	H23	0.022
C3	0.014	C12	0.093
H6	-0.001	H24	0.054
H7	-0.001	H25	0.054
C4	-0.104	N1	-0.405
H8	0.012	C13	-0.269
H9	0.012	H26	0.126
C5	0.109	H27	0.126
H10	-0.025	C14	0.152
H11	-0.025	H28	-0.007
C6	0.014	H29	-0.007
H12	-0.007	C15	-0.116
H13	-0.007	H30	0.031
C7	-0.018	H31	0.031
H14	-0.003	C16	0.140
H15	-0.003	H32	0.001
C8	0.030	H33	0.001
H16	-0.010	C17	-0.347
H17	-0.010	H34	0.105
C9	0.030	H35	0.105
H18	-0.009	C18	0.714
		O1	-0.596

** note that the hydrogen atoms were omitted from the structure of Azone for clarity. The hydrogen atoms listed in the table are arranged below their respective methyl or metylene carbons.

2.3 MD simulations of Azone in various environments

2.3.1 Liquid Azone

This system comprised 36 molecules of Azone, initially arranged in two monolayers. The atomic coordinates for the Azone molecules were generated using Hyperchem® molecular modelling package (Hypercube, 1996) and the resulting structure was then geometry-optimised using the same program. Since the initial arrangement of the Azone molecules in the system bore little resemblance to the arrangement expected in the liquid state, the simulation was initiated under full isotropic NPT conditions in order to allow the system to adjust its density continuously and naturally.

All the bond lengths in the system were constrained using the SHAKE method. The integration time step used was 1.5 femtosecond and was first minimised at 0K, using the NVT periodic boundary conditions. Once minimised, the system was then equilibrated at 298K and 1 atm. using NPT periodic boundary conditions. A residue-based non-bonded pairlist (updated every 20 timesteps) was used, along with a cutoff distance of 12Å. Temperature and pressure relaxation time-constants of 0.2ps were applied. The establishment of equilibrium was monitored by following the fluctuations in energy, temperature, pressure and density of the system. Unfortunately at the end of the equilibration run, i.e. after 600ps, the system failed to achieve the known density of liquid Azone (0.92g/cm^3). Thus, a new system was constructed with the positions of the molecules were scaled so as to give the desired density values (Figure 2.1). This system was re-minimised and then re-equilibrated at 298K under NVT conditions (with the density of the system kept constant throughout the simulation). This simulation was run for a total time of 1 nanosecond and the trajectory was collected and analysed for the last 500ps of the simulation.

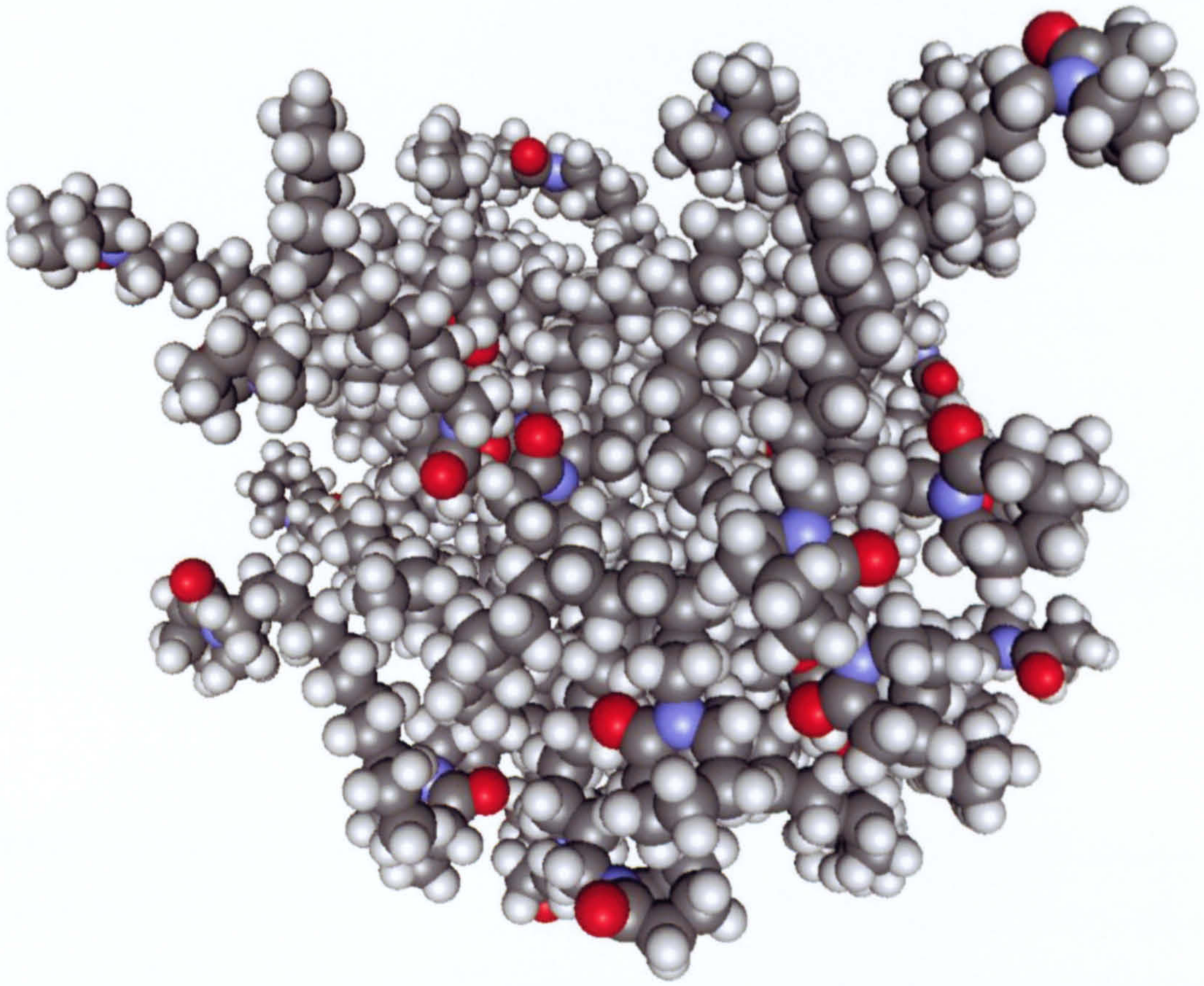

Figure 2.1 The starting model used in the simulation of liquid Azone. The density of the system was fixed at 0.92g/cm^3.

2.3.2 Azone in Water

A single Azone molecule (chosen at random from the well-equilibrated liquid Azone system) was used here as a starting structure and solvated in a total of 898 water molecules using the EDIT module in. All bond lengths in the system were constrained using the SHAKE method. The integration time step used was 1.5 fs and the system were first minimised at 0K, using the NVT ensemble. After minimisation, the system was then equilibrated at 323K and 1 atm. using the NPT ensemble. A residue-based non-bonded pairlist (updated every 20 timesteps) was used, along with a cutoff distance of 12Å. Temperature and pressure relaxation time-constants were both 0.2ps. Equilibration was monitored by the fluctuations in energy, temperature, pressure and density of the system. The simulation was run for a total time of 1 nanosecond and the trajectory was collected and analysed for the last 500ps of the simulation.

2.3.3 Single Azone and single DPPC molecules in water (1Azone-1DPPC/water)

The starting structure for this system involved an Azone molecule chosen at random from the liquid Azone run and a DPPC molecule taken from the all atom simulation of the liquid crystalline DPPC bilayer (2.4.3). The two molecules were initially arranged side by side. The molecules were then solvated with 898 water molecules using the EDIT module in AMBER. All bond lengths in the system were constrained using the SHAKE method. The integration time step used was 1.5 fs. The system was first minimised at 0K, in the NVT ensemble. After minimisation, the system were then equilibrated using NPT periodic boundary conditions, the pressure was kept constant at 1 atm with a pressure relaxation time constant of 0.2ps. A residue-based non-bonded pairlist (updated every 20 timesteps) was used, along with a cutoff distance of 12Å. The temperature of the system was also kept constant at 323K using a temperature relaxation constant of 0.2ps. The equilibration was monitored by the fluctuations in energy, temperature, pressure and density of the system. Following the equilibration the system was further run for the period of 1nanosecond and the trajectory was collected and analysed for the last 500ps of the simulation.

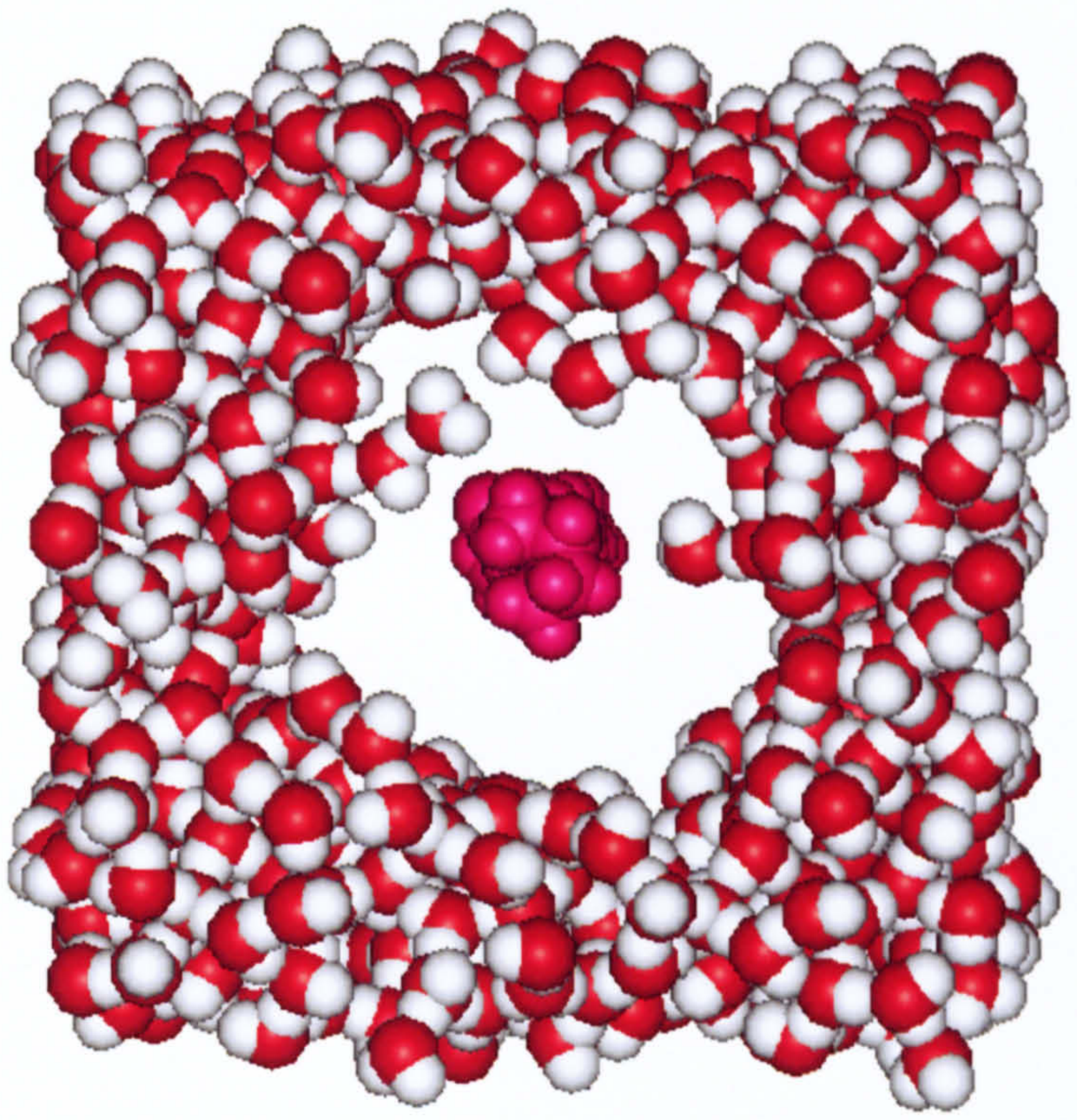

Figure 2.2 The starting structure for the simulation of Azone in water, with the Azone molecule (shown in red) revealed by the removal of obscuring solvent.

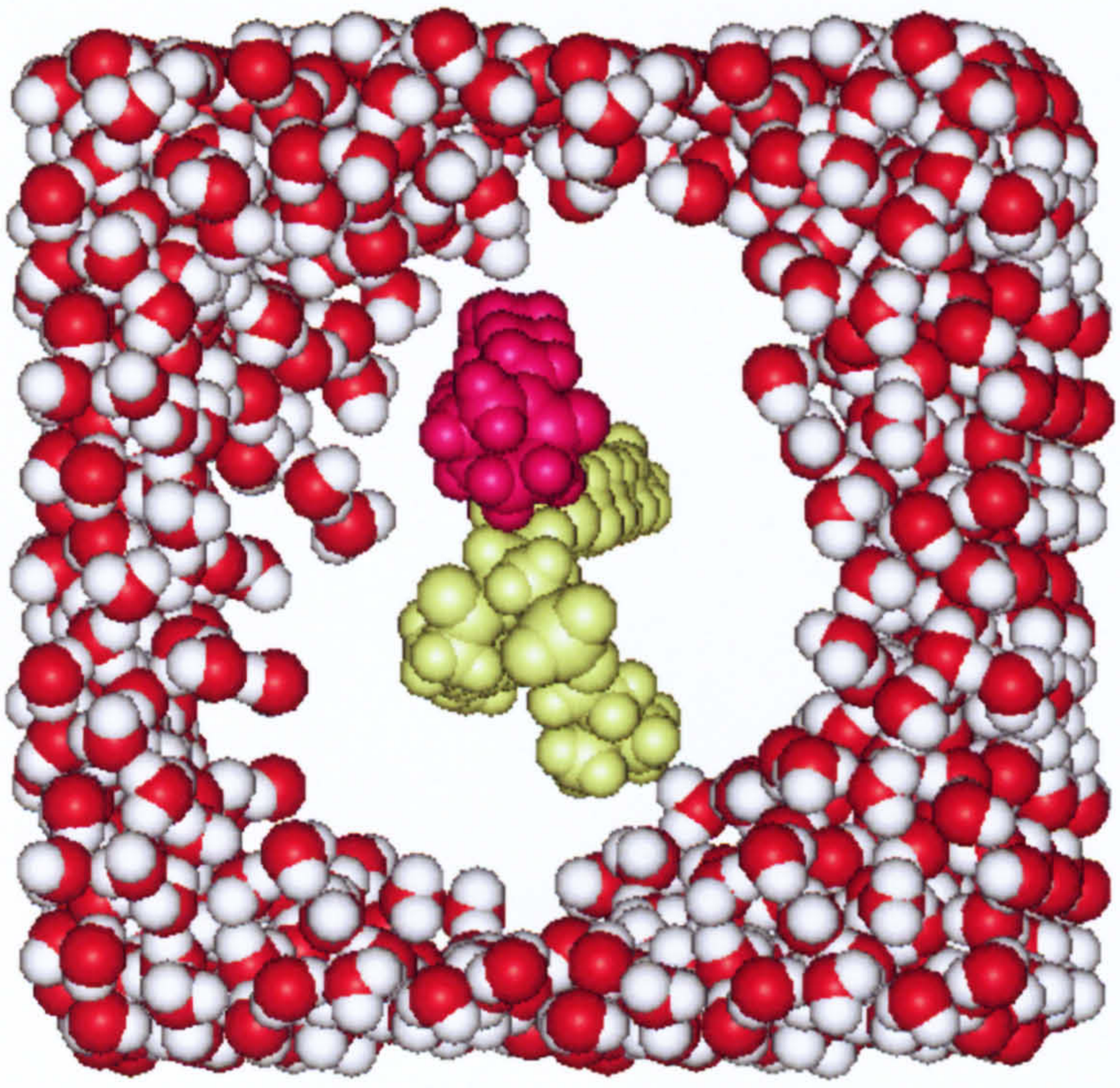

Figure 2.3 The starting structure for the simulation of Azone and DPPC in water with the Azone and DPPC molecules (shown in red and green, respectively) revealed by the removal of the obscuring solvent.

2.4 MD simulation of pure lipid bilayer

2.4.1 Choice of lipid

As the first task in carrying out the MD simulations of lipid bilayers, it was necessary to decide on the appropriate system for modelling the lipid lamellae in the *stratum corneum* (SC). The SC lipids consist of many different species of lipids, in general mainly ceramides (50%), steroids (20%) and free fatty acids with small amounts of phospholipids (Yardley & Summerly, 1981).

Ideally, therefore, it would have been most appropriate to use ceramides for the simulation studies, but because there are little or no experimental data available on these systems, it was elected instead to use a simple phospholipid model, specifically, a bilayer of dipalmitoylphosphatidyl choline (DPPC). Although ceramides and phospholipids have rather different head groups, both types of lipid have hydrophobes involving two saturated hydrocarbon chains, and experimental studies carried out using extracted skin ceramides have produces results that are qualitatively similar to those obtained with phospholipids (Brain & Walters, 1991). More importantly, DPPC is well characterised and experimental data on this lipid are readily available. Moreover, there have been a number of other MD studies of phospholipid systems, and these would provide useful data to compare with the proposed simulations (Egbert, 1988, Egbert *et al.*, 1994, Marrink *et al.*, 19943, Edholm & Nyberg, 1992). The structures of DPPC and a ceramide are compared in Figure 2.4

The atomic co-ordinates for DPPC were obtained using the known X-ray crystal structure of dilauroylphosphatidyl ethanolamnine DLPE (Elder *et al.*, 1977). The necessary modifications were made using the Hyperchem® modelling package (Hypercube, 1996) and the DPPC structure is geometry-optimised using the same program.

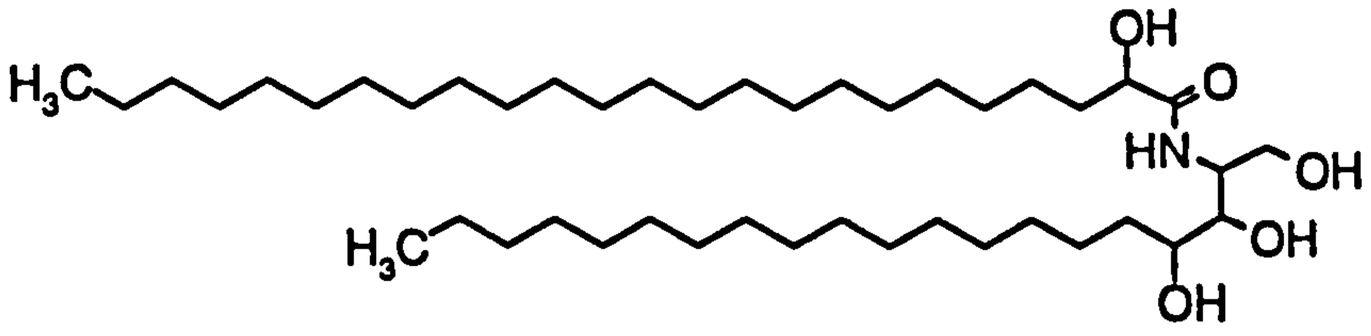

Ceramide 6

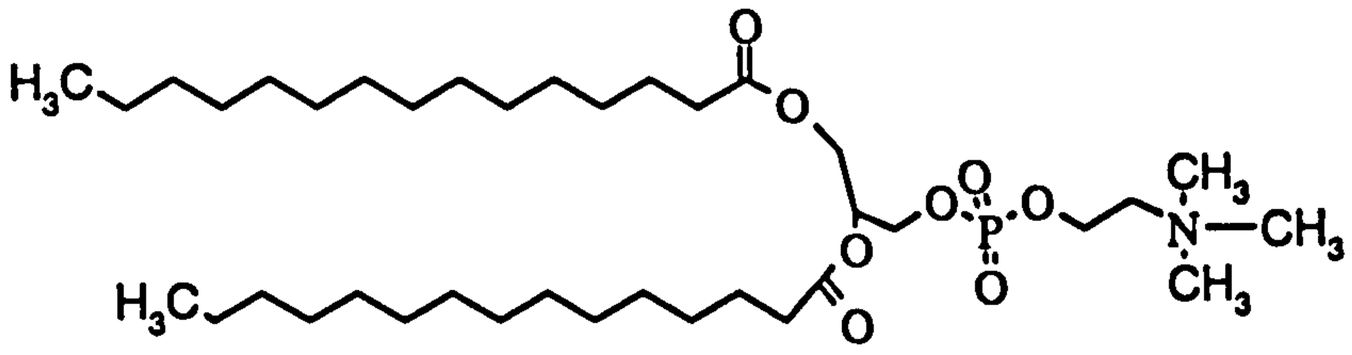

DPPC

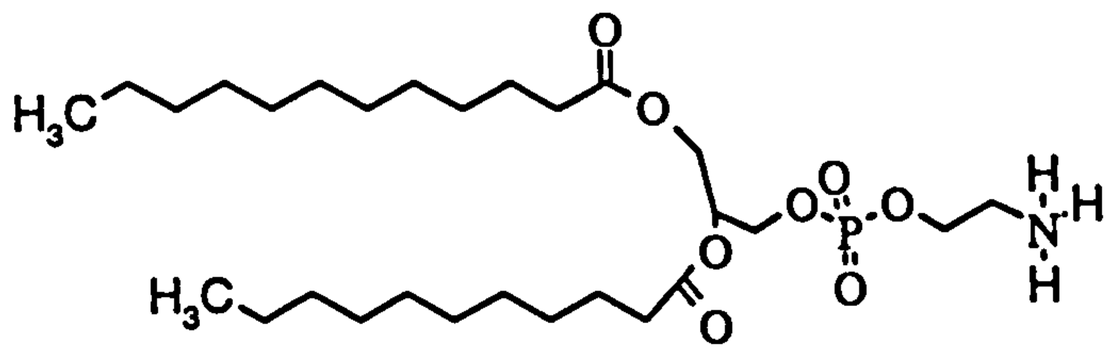

DLPE

Figure 2.4 : The structures of DPPC, DLPE and ceramide 6.

2.4.2 Lβ' DPPC bilayer

The simulation of the Lβ' DPPC bilayer was performed using a united-atom approximation for the methylene and methyl groups, but with polar hydrogen atom treated explicitly. The initial bilayer was generated with 48 molecules of DPPC arranged in two monolayers. The bilayer was then solvated with 552 molecules of water (which corresponds to 11.5 water molecules per lipid or 22% water by weight) using the EDIT program of AMBER4.1. The resulting model occupied a periodic box of dimensions 75.5Å x 35.4Å x 31.0Å. These dimensions provided an interfacial area per lipid of 46 $Å^2$, which is close to the experimental value of 47.5 $Å^2$ (Tardieu *et al.*, 1973). The system was subjected to energy minimisation at 0K in the NVT ensemble. This was followed by an equilibration of the system in various stages.

In the first stage, the minimised structure (Figure 2.5) was subjected to a 'belly' simulation of water molecules. Here only water molecules were allowed to relax. The temperature of the system was raised slowly using a temperature coupling of 0.5ps. The temperature was raised to 100K in the first 9ps, to 200K over the next 9ps, and then to 292K over a further 9ps. After this, a simulation was carried out in which only the water and the headgroup atoms of the lipid molecules were allowed to move, and then a further simulation in which all atoms of the system were allowed to move (in both cases using the same heating scheme as used during the water run). In all these simulations, NVT ensembles were employed, with a residue-based non-bonded pairlist updated every 20 timesteps and a cutoff distance of 9Å. (The use of an NVT, rather than NPT ensemble in these 'belly' runs was essential to prevent the atoms that were allowed to move from approaching too closely to the 'stationary' atoms).

The next stage of the simulation was to get the desired bilayer repeat distance and bilayer thickness. The simulation was carried out in such a way that the X-dimension of the periodic box (which represented the normal to the bilayer) was allowed to vary under a constant pressure of 1 atm., whilst the dimensions in the other two directions were held constant. Once the bilayer repeat distance had equilibrated, a full isotropic NPT simulation was carried out until equilibration was reached. Following the

equilibration phase, the atomic coordinates and velocities of the system were collected every 50 time steps (that is every 0.075ps) using a NVT ensemble.

2.4.3 Lα-DPPC bilayer (AMBER simulation)

An MD simulation of the Lα-DPPC bilayer structure was first performed using the AMBER force field. In this simulation all DPPC atoms were treated explicitly. The starting bilayer model was constructed by arranging 32 molecules of DPPC in two opposing monolayers, each involving 16 DPPC molecules. The lipid-lipid spacing was arranged so as to give an initial surface area per molecule of 64Å. (Using the same NPT scheme the structure did equilibrate to give the surface area per molecule of ~62 Å which is the value determined experimentally by Nagle, (1993)-refer Appendix 4).

The resultant bilayer was subsequently placed in a periodic box and a total of 898 water molecules using the EDIT module of AMBER4.1. This corresponds to ~28 water molecules per lipid or 40% water by weight, which, from the phase diagram, given a temperature of 323K, was correct for liquid crystalline (Lα phase) DPPC bilayer.

The minimisation, equilibration (refer Appendix 6) and trajectory collection procedures were carried out in the same way for the Lβ' bilayer simulation (2.4.2) except that the temperature of the system was kept constant at 323K and the non-bonded cut-off used was 12 Å. The neighbour pairlist was updated every 20 time-steps. The system were equilibrated for 180ps and the total run for this simulation is 600ps.

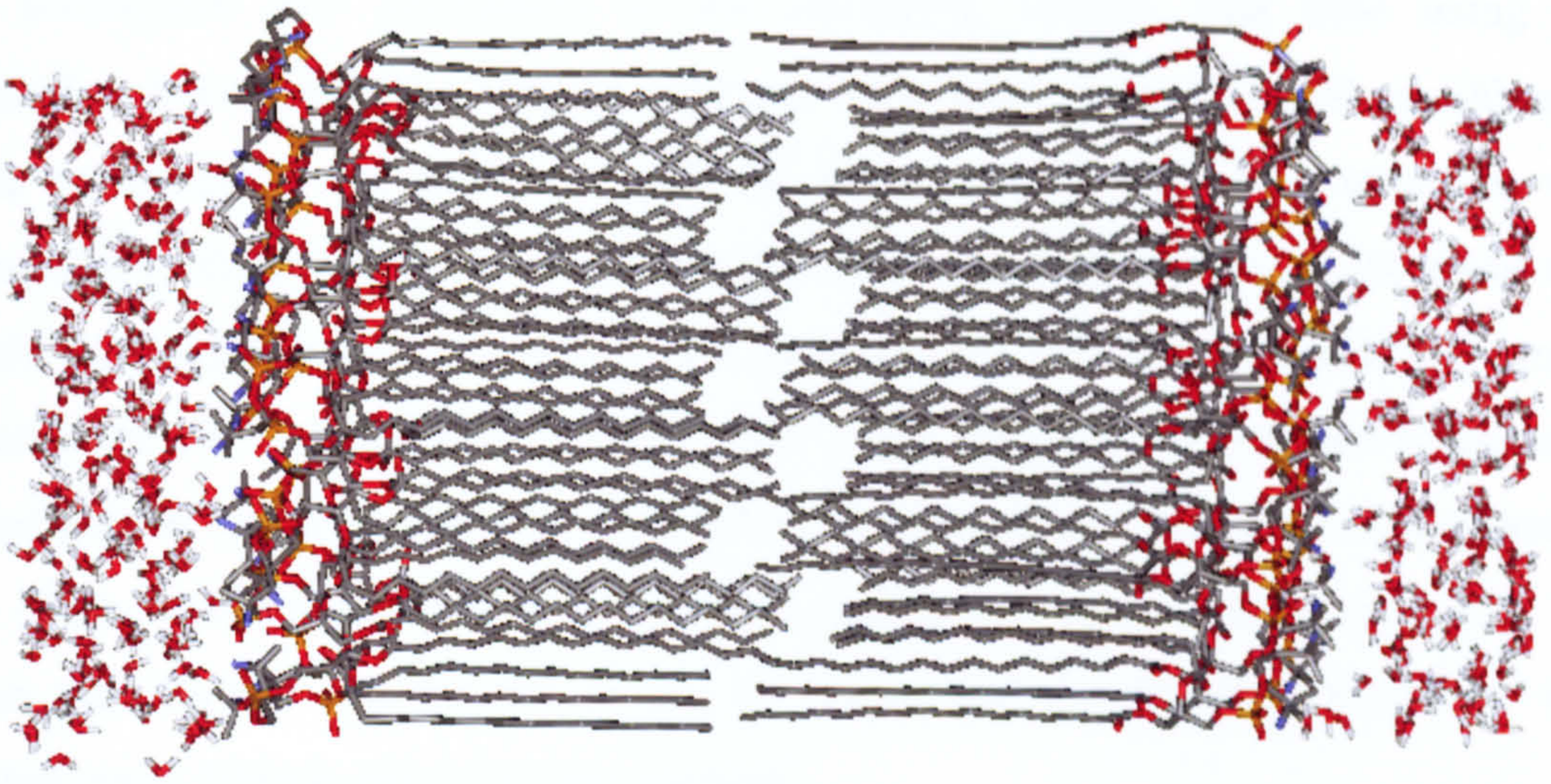

Figure 2.5 The minimised structure of the Lβ' DPPC bilayer

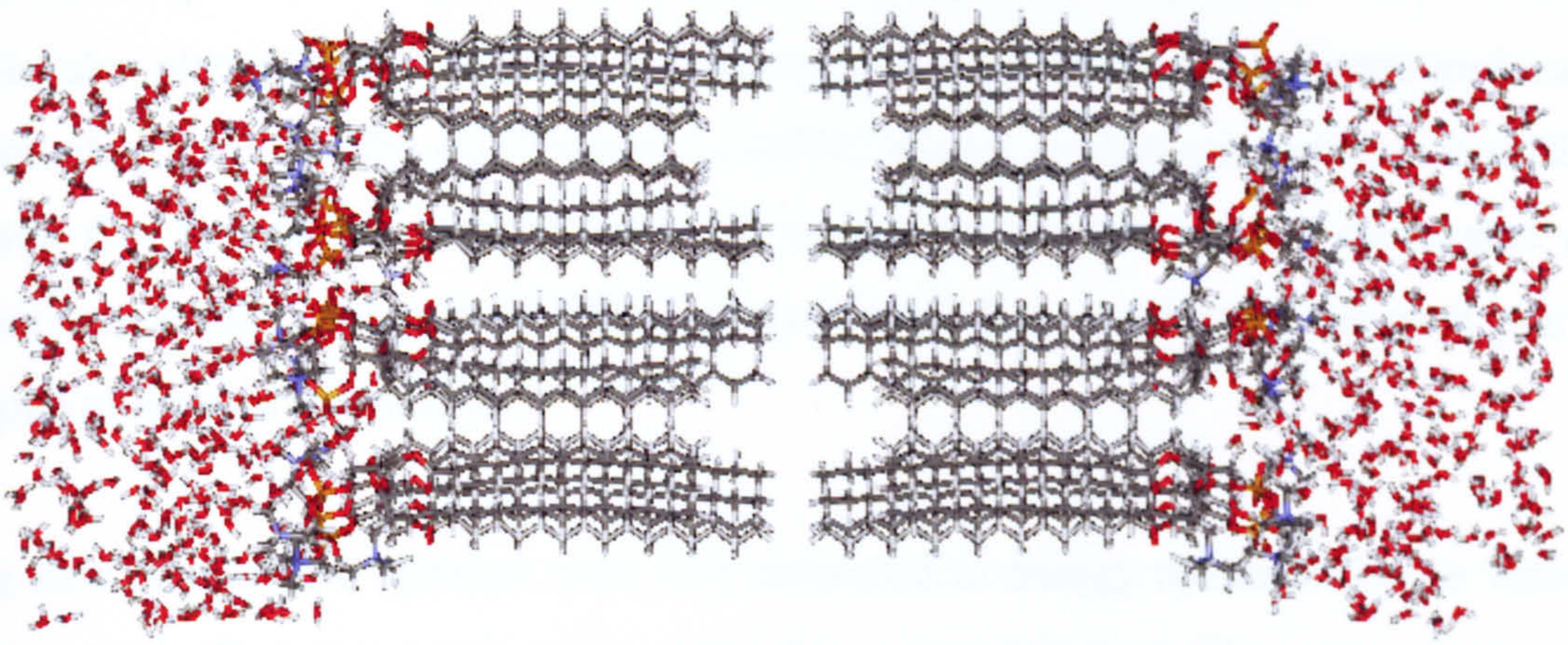

Figure 2.6 The minimised structure of Lα DPPC bilayer (modelled using the AMBER parameters).

2.4.4 Lα DPPC bilayer (CHARMm simulation)

In a subsequent MD simulation of the Lα-DPPC bilayer, this time using the CHARMm force field, the starting structure was taken from the well equilibrated model generated in the previous AMBER simulation (2.3.3). This structure was subsequently minimised at 0K employing the NVT ensemble. Since this structure was already well equilibrated, the system was subsequently allowed to equilibrate under full-isotropic NPT conditions at 323K and 1atm. pressure. A residue-based non-bonded pairlist (updated every 20 timesteps) was used, along with a cutoff distance of 12Å. Once equilibrium had been achieved (using the same criteria as 2.4.3), the system was further run for the period of 600ps and the dynamic trajectory was sampled every 50time-steps for data analysis.

2.5 Studies of the perturbation effect of Azone on the lipid model

Two separate studies were carried out to investigate the perturbing effects of Azone on the Lα-DPPC bilayer. In the first study, there were 2 Azone molecules localised in one monolayer of the lipid bilayer, and in the second study there were 2 Azone molecules placed in each of the 2 monolayers. For both systems, the Azone molecules were introduced into the equilibrated La-DPPC bilayer models generated as described above (2.4.3) and the amount of water in the system kept at 28 molecules per lipid/Azone. One molecule of DPPC was removed from the bilayer for each pair of Azone molecules introduced.*

The new Azone/lipid systems were first subjected to energy minimisation in various stages. In the first stage, only water molecules were minimised. Then water molecules were held fixed in their minimised positions while the Azone and DPPC molecules were minimised, and then in the final stage all atoms of the system were minimised.

---

* see appendix 9.

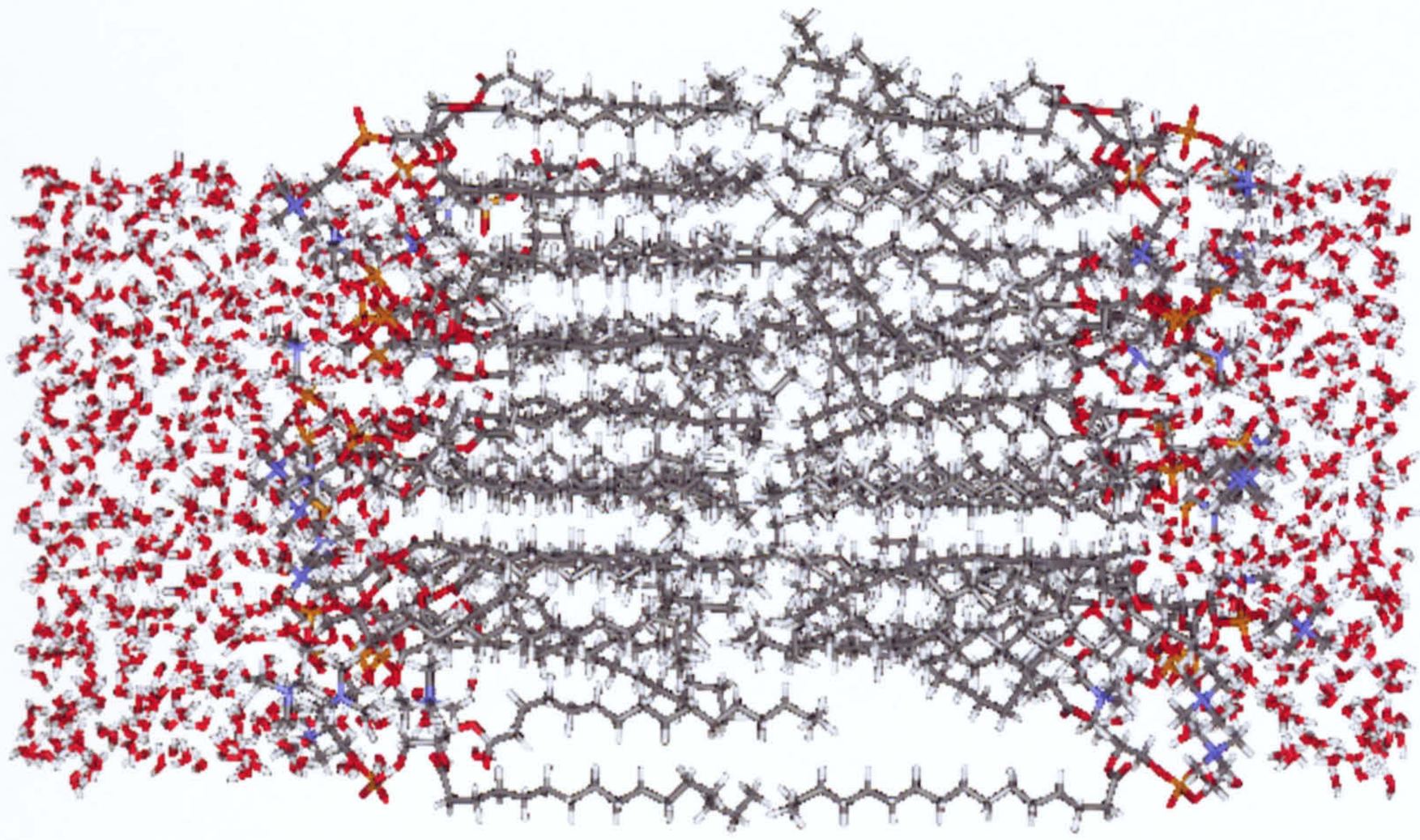

Figure 2.7 The minimised structure of Lα DPPC bilayer (modelled using the CHARMm force field parameters).

The equilibration of the Azone/lipid/water systems was then carried out following the same stepwise approach. During these equilibration runs, the temperature of the systems was kept fixed at 325K. The NVT ensemble was applied during these equilibration stages followed by the MD of all atoms in the system under the same NVT conditions. After this, the systems were simulated using NPT ensemble, with the pressure and temperature fixed at 1 atm. and 325K, respectively, until all thermodynamic properties and box dimensions of the systems were equilibrated. Following this equilibration phase, the atomic coordinates and velocities of the systems were sampled for data analysis every 50 time-steps. The systems were allowed to equilibrate for 500ps (Appendix 4 shows the equilibration of the bilayer repeat distance) and the systems were further subjected to 500ps giving the total run of 1ns.

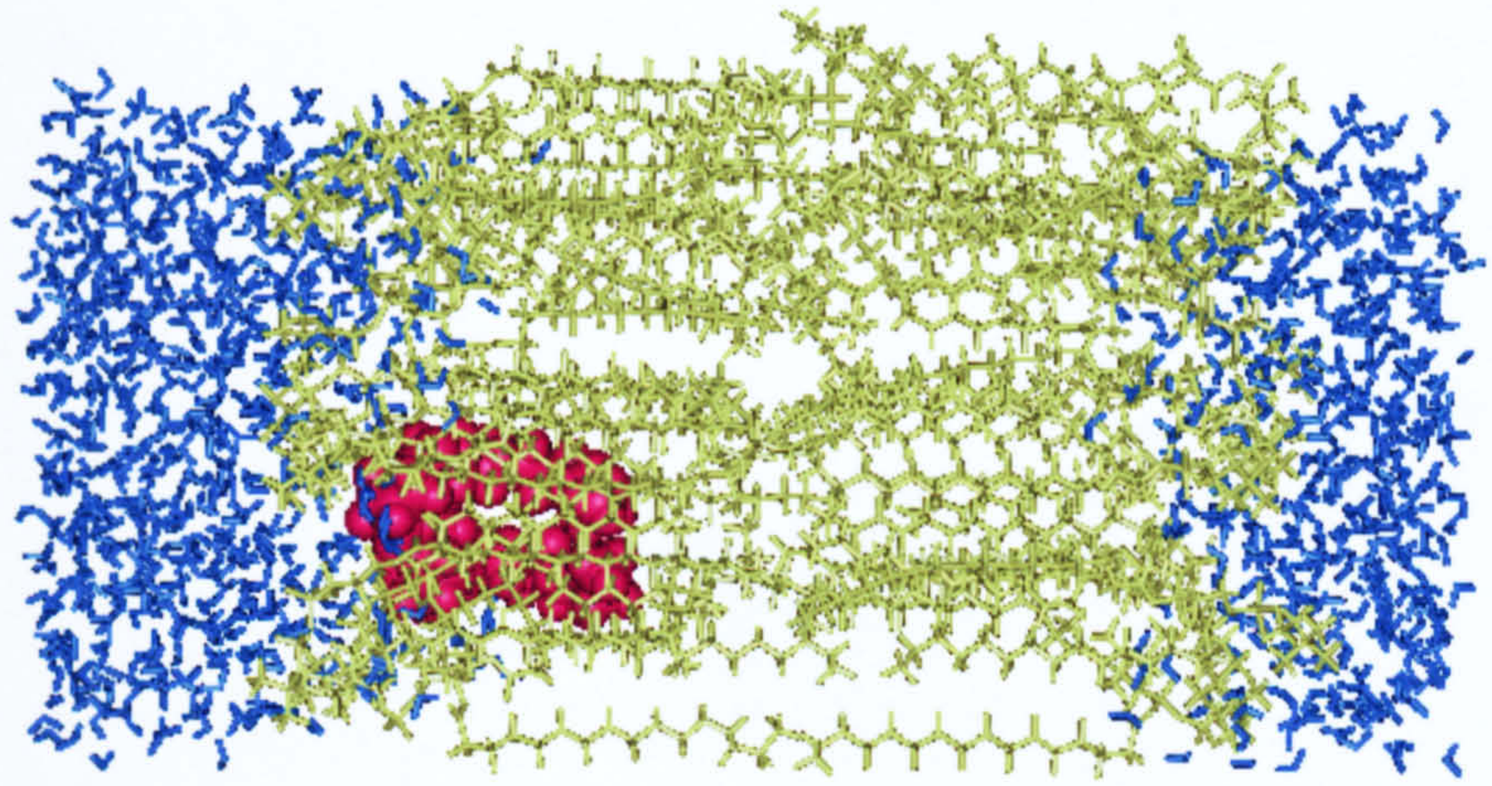

Figure 2.8 The minimised structure of the 2Azone-DPPC bilayer. Colour coding: red, Azone; green, DPPC; blue, water

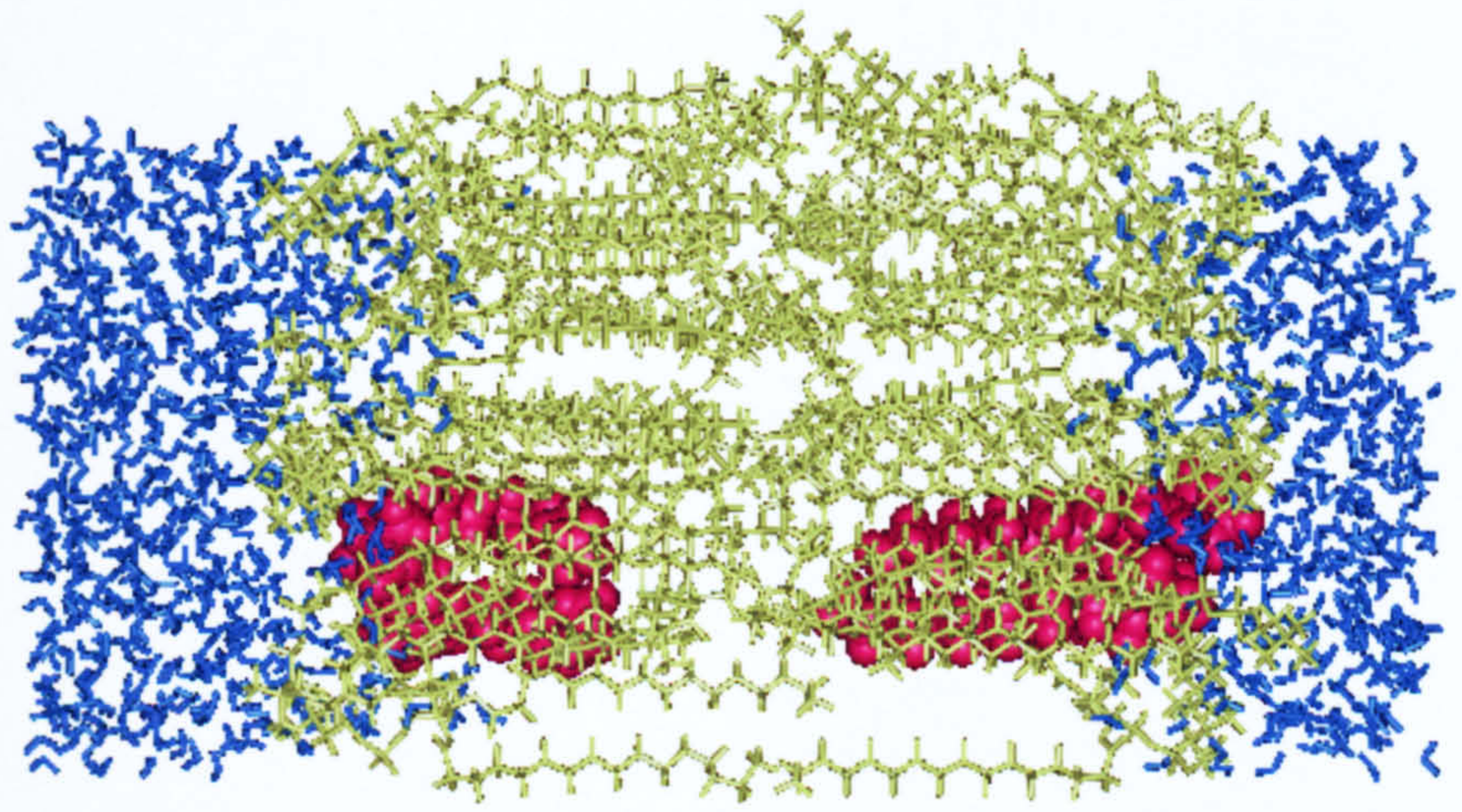

Figure 2.9 The minimised structure of the 4Azone-DPPC bilayer. Colour coding: red, Azone; green, DPPC; blue, water

3.RESULTS

3.1 MD of Azone in Various Environments

The results of the trajectory analyses for the three simulations involving Azone in different environments (Azone in water, Azone with DPPC in water, liquid Azone) are presented in this section. The analyses carried out here are mainly focused on the conformations adopted by the Azone molecule and to a lesser extent on the interactions of Azone and DPPC molecules with water.

3.1.1 Conformation of Azone

The conformations of a molecule are traditionally defined as those arrangements of its atoms in space that can be inter-converted purely by rotation about single bonds. This definition is usually relaxed in recognition of the fact that small distortions in bond angles and bond lengths often accompany conformational changes, and that rotation can occur about bonds in conjugated systems that have an order between one and two (Leach, 1996).

In this study, the conformations of Azone adopted during the MD simulations were investigated using cluster analysis to identify families of conformers, and calculating the distributions of the dihedral angles and the methyl carbon to headgroup nitrogen separations. Cluster analysis of Azone conformers was carried out according to the methods described by Perkins and Barlow (1990).

Figures 3.1.2-3.1.4 show the various major (representatives) conformations formed for all the three systems (i.e. Azone in water, Azone with DPPC in water and Liquid Azone) derived from the cluster analysis. It is noted that in most cases the Azone molecule adopts

a structure in which the headgroup is oriented parallel with the principle axis of the alkyl chain.

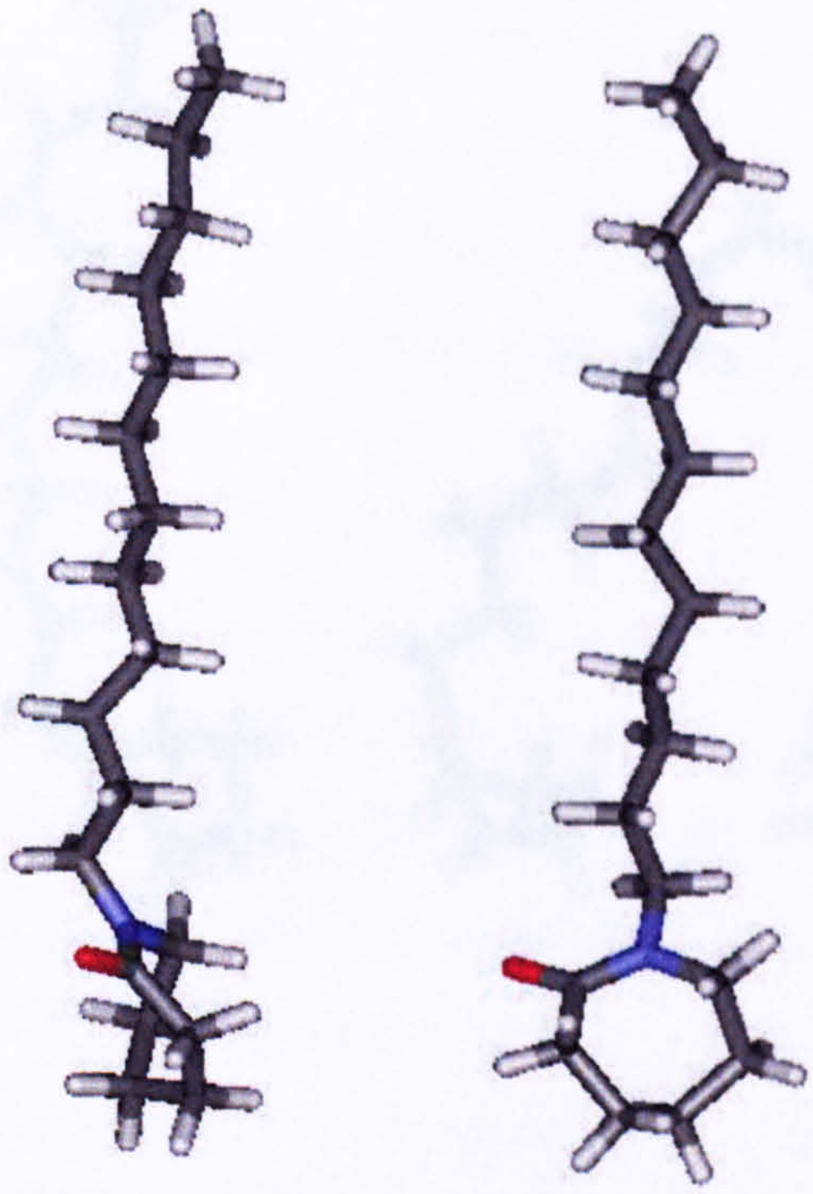

(a) (b)

Figure 3.1.1 : The global minimum energy conformation of Azone. (a) side-projection, (b) front-projection.

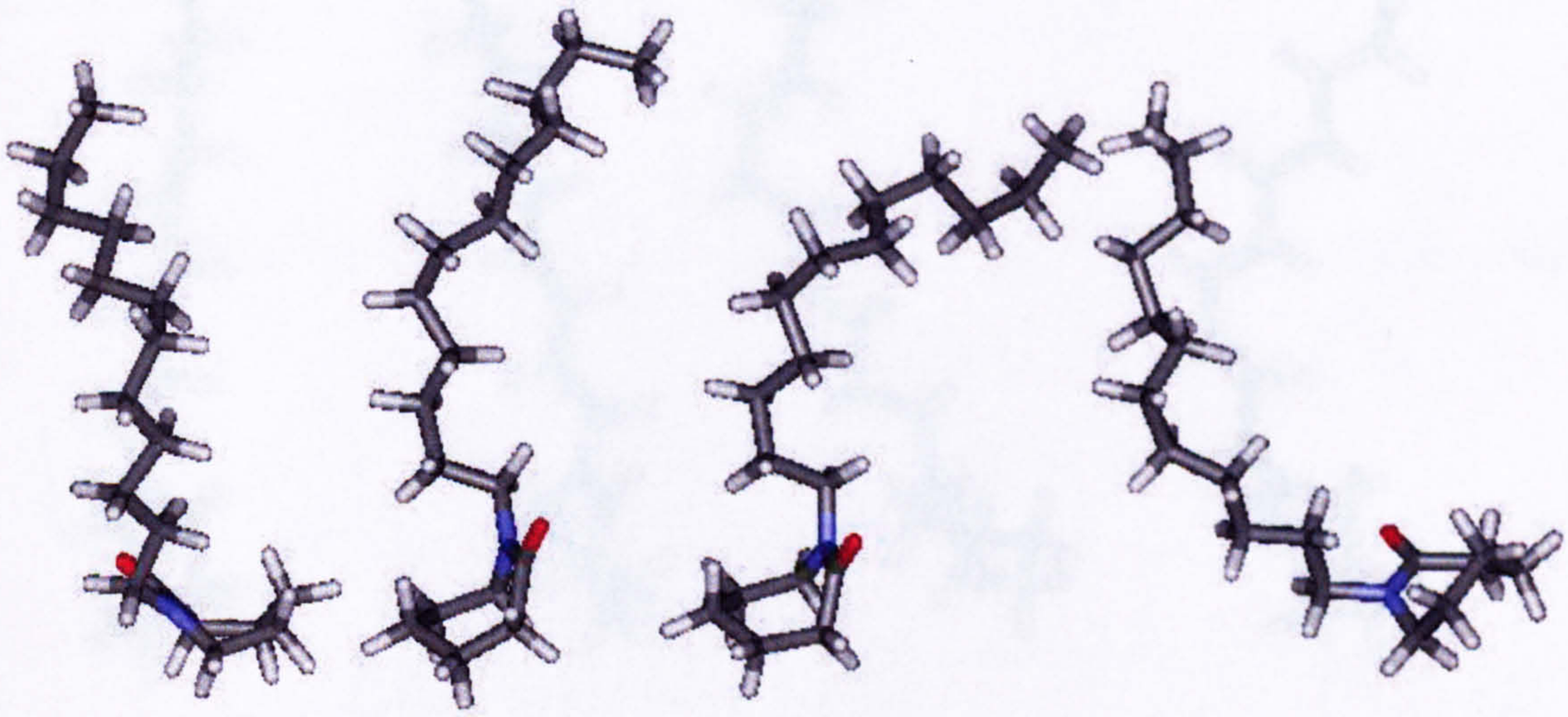

Figure 3.1.2: Representative Azone conformers found for Azone in water.

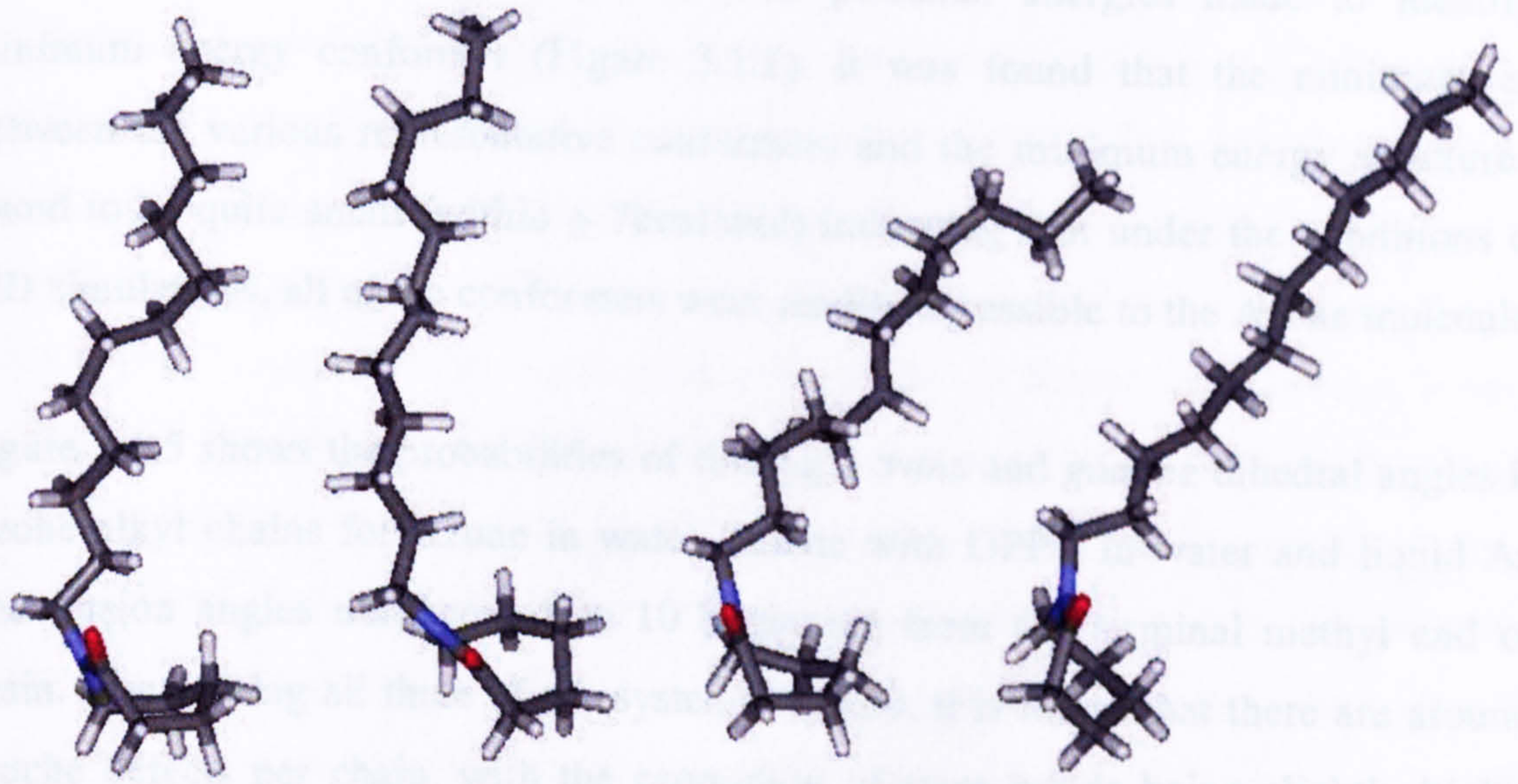

Figure 3.1.3 Representative Azone conformers found for Azone with DPPC in water.

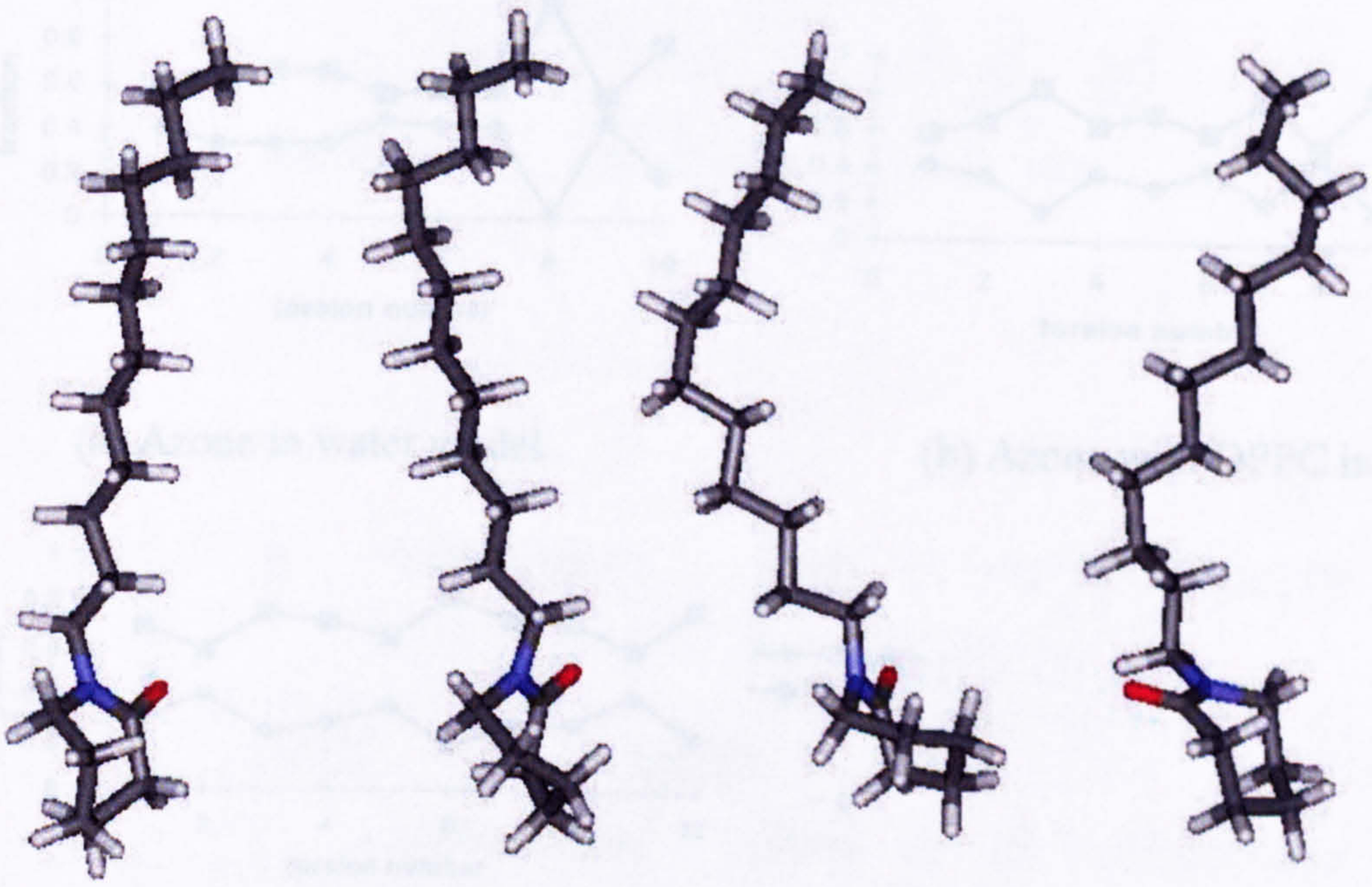

Figure 3.1.4 Representative Azone conformers found for liquid Azone.

In separate studies, in vacuo energy minimisations of these representative conformers were performed and comparisons of their potential energies made to identify the minimum energy conformer (Figure 3.1.1). It was found that the minimum energy between the various representative conformers and the minimum energy structure were found to be quite small (within ± 7kcal/mol) indicating that under the conditions of the MD simulations, all of the conformers were readily accessible to the Azone molecule.

Figure 3.1.5 shows the probabilities of finding a *trans* and *gauche* dihedral angles in the Azone alkyl chains for Azone in water, Azone with DPPC in water and liquid Azone. The torsion angles numbered 1 to 10 beginning from the terminal methyl end of the chain. Considering all three of the systems studied, it is found that there are around 2-4 gauche defects per chain, with the proportion of trans bonds being slightly higher for liquid Azone compared with Azone in water (with or without DPPC). It is interesting also to note that for Azone in water, torsion 8 appears only to adopt a trans configuration, but why this should be so is not clear.

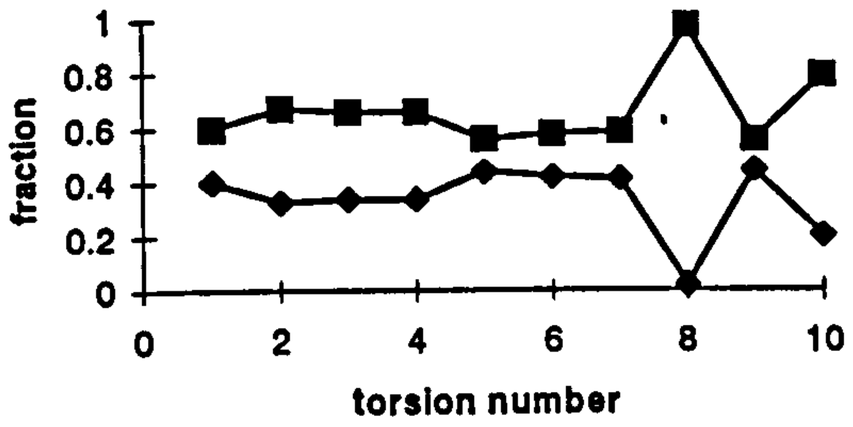

(a) Azone in water model

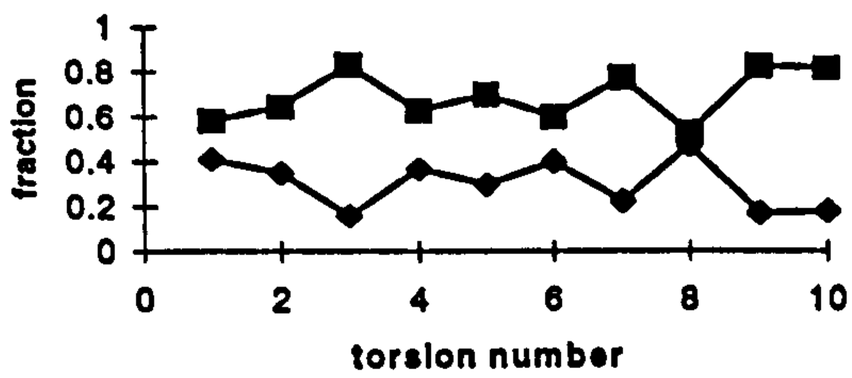

(b) Azone with DPPC in water

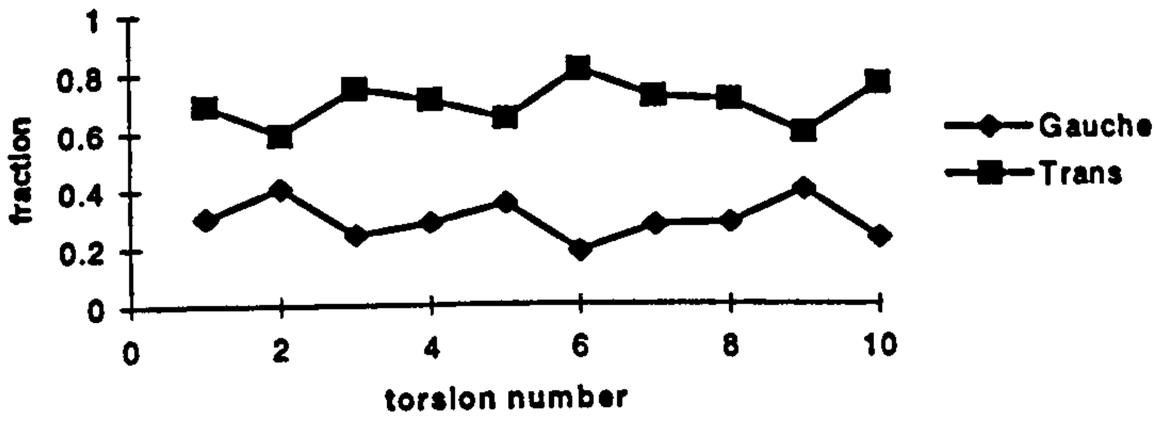

(c) liquid Azone

Figure 3.1.5. Fractions of *trans* and *gauche* dihedral angle vs. torsion number.

The variation of the individual dihedral angles were also monitored as a function of time for the Azone in water and Azone with DPPC in water systems (Figures 3.1.6 & 3.1.7). Comparisons made between these two sets of data reveal that Azone alkyl chain exhibit significantly difference behaviour in the presence of DPPC. For example, the transition between *trans* and *gauche* rotamers in Torsion 1 is much more rapid for Azone alone in water than for Azone with DPPC in water. The same is also true for torsion 5 and to a lesser extent Torsion 4. The most striking difference in behaviour, however, is seen for Torsion 8. In the presence of DPPC Torsion 8 undergoes several *trans-gauche* transitions, but for the Azone molecule alone in water this torsion exists almost entirely in the *trans* state. The two systems do show same features in common, however, in particular that the mid-section of the Azone alkyl chain undergoes more frequent *trans-gauche* transitions than either of the two chain ends, and also that the chain nearest the headgroup tends to exist for most of the time in an extended state.

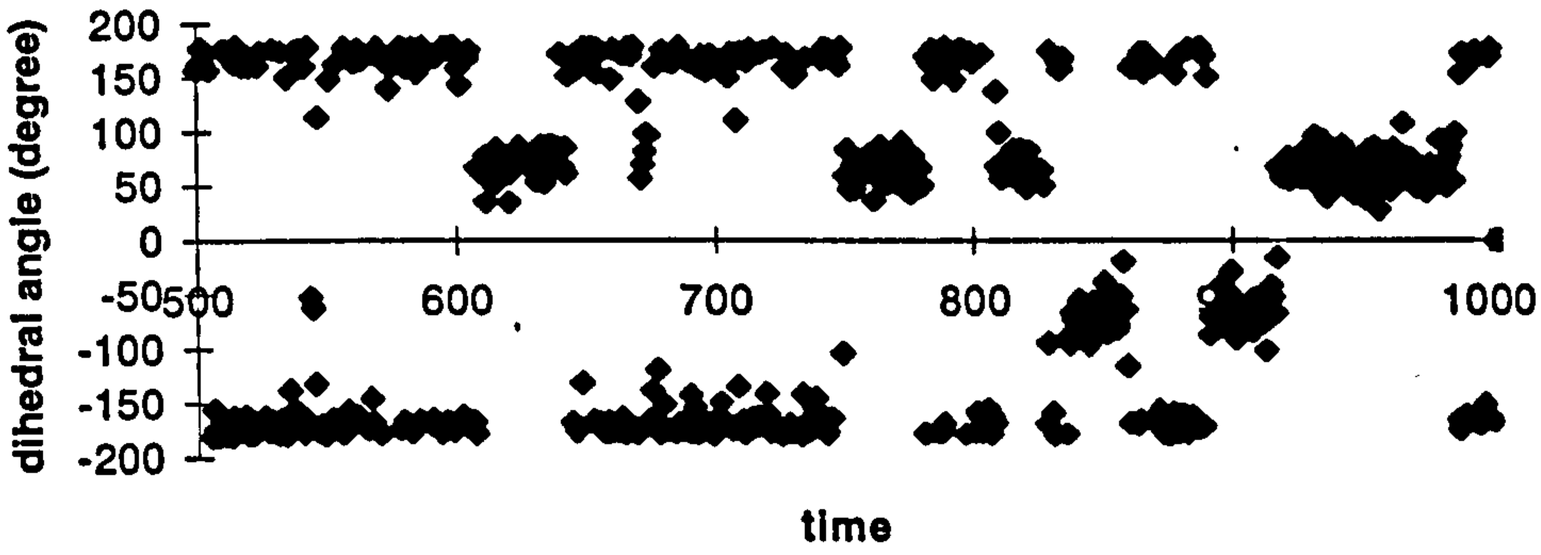

(a) Torsion 1

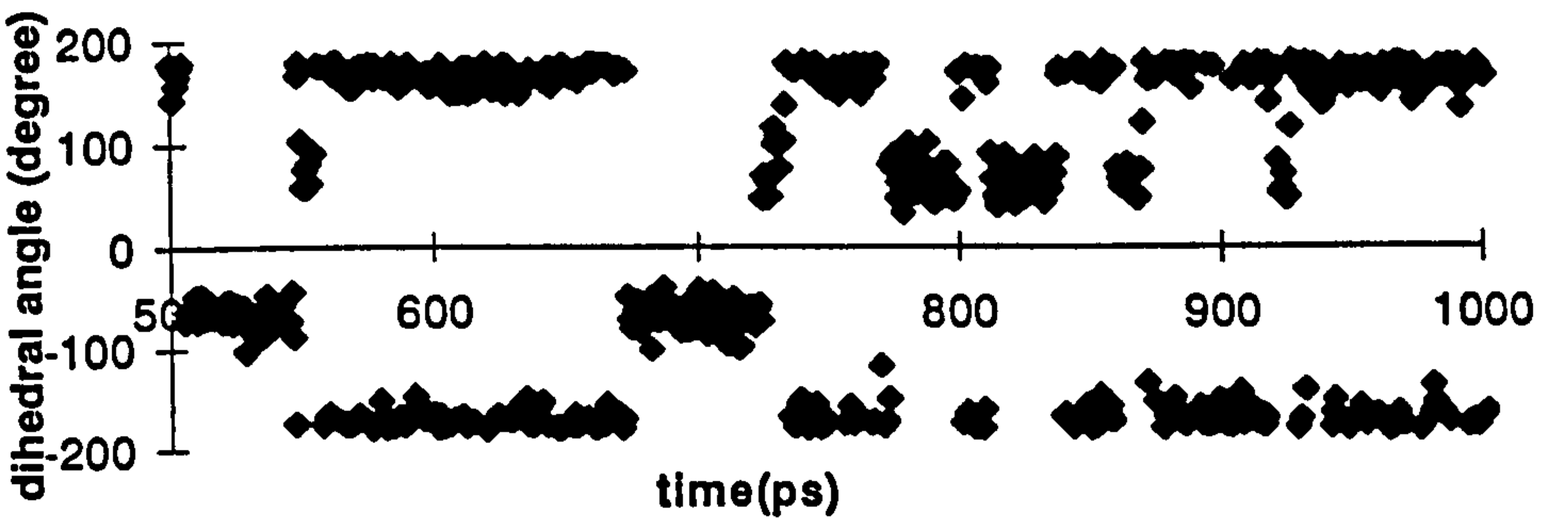

(b) Torsion 2

Figure 3.1.6: The changes in dihedral angle vs. time for Azone in water.

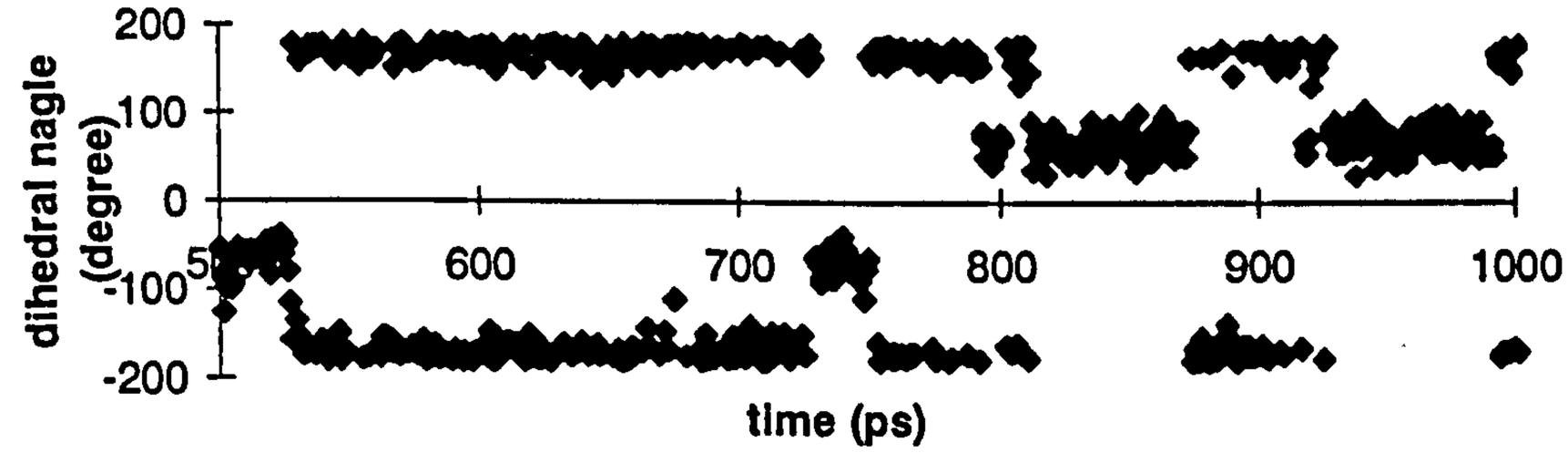

(c) Torsion 3

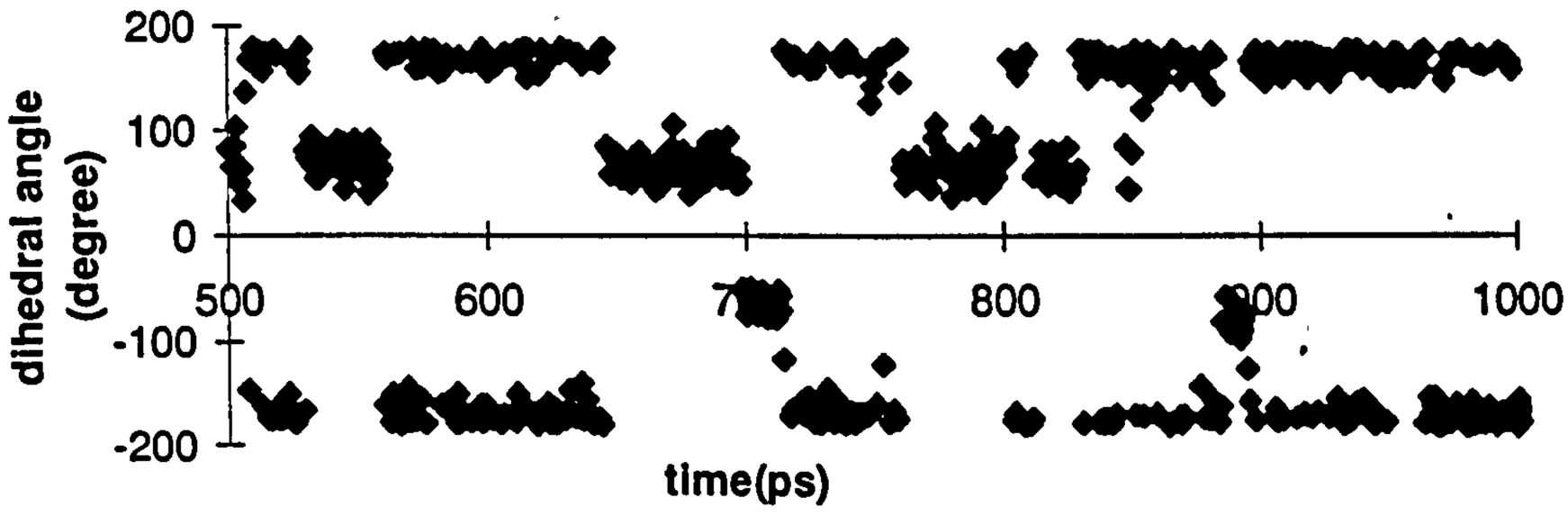

(d) Torsion 4

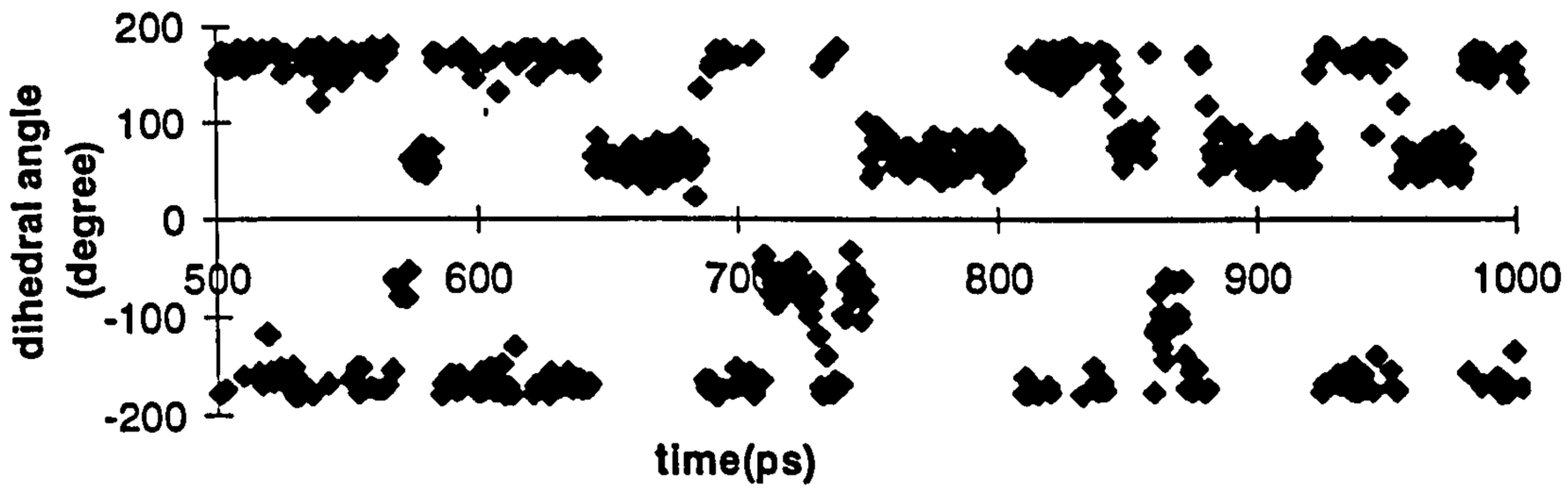

(e) Torsion 5

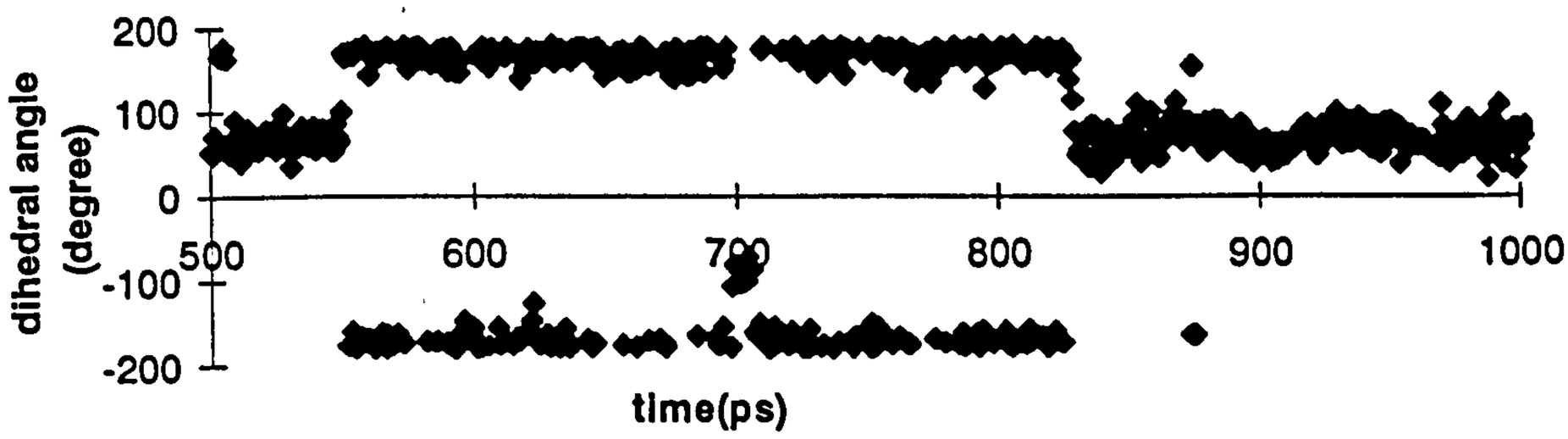

(f) Torsion 6

Figure 3.1.6: (ctd.) The changes in dihedral angle vs. time for Azone in water.

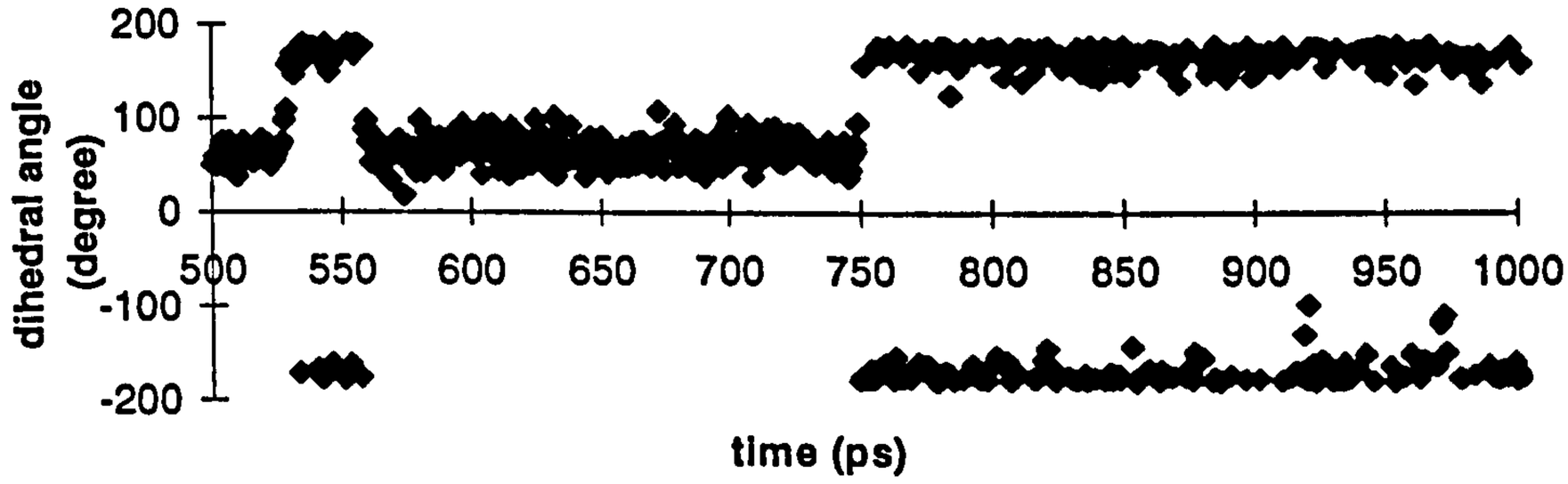

(g) Torsion 7

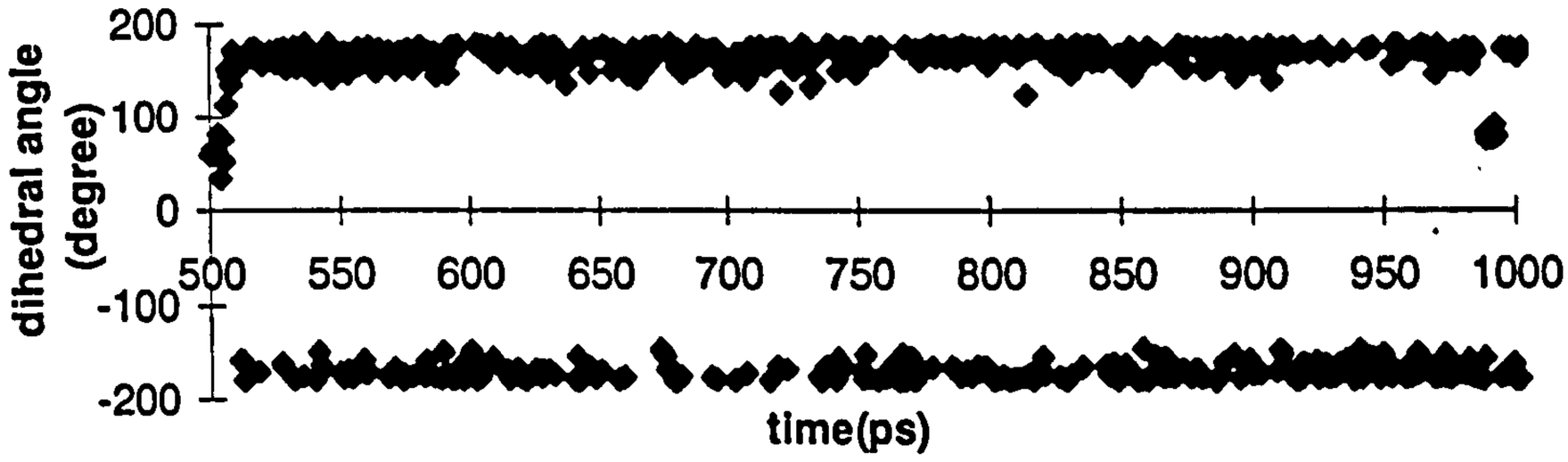

(h) Torsion 8

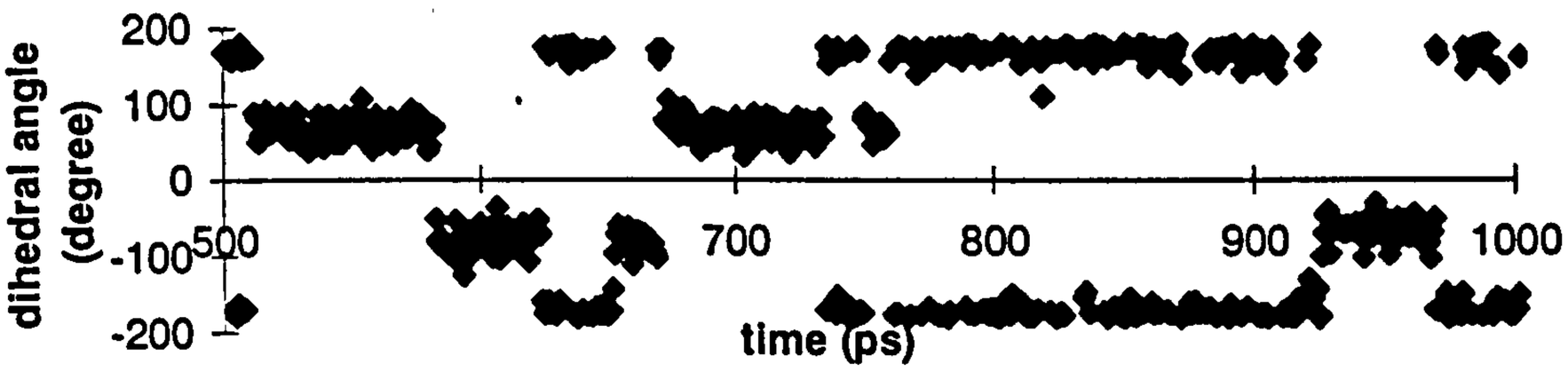

(i) Torsion 9

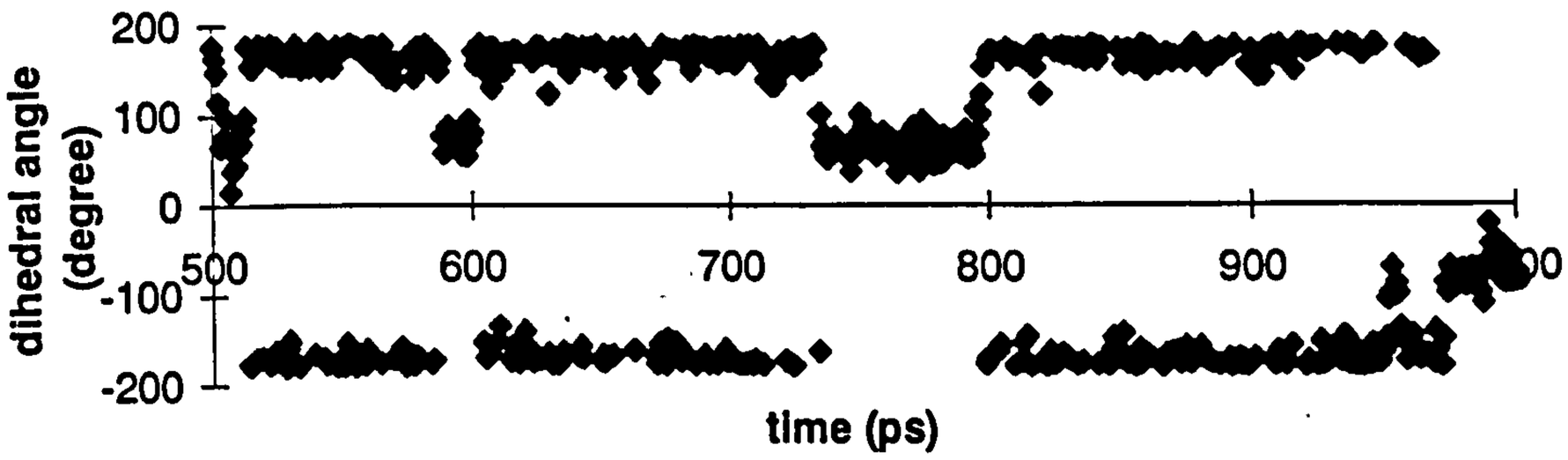

(j) Torsion 10

Figure 3.1.6 (ctd.): The changes in dihedral angle vs. time for Azone in water.

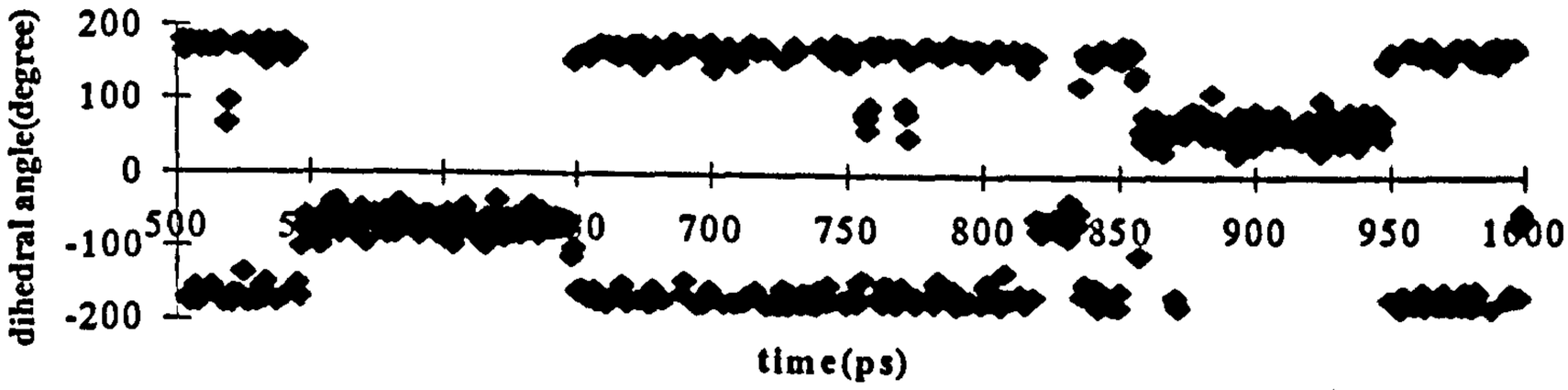

(a) Torsion 1

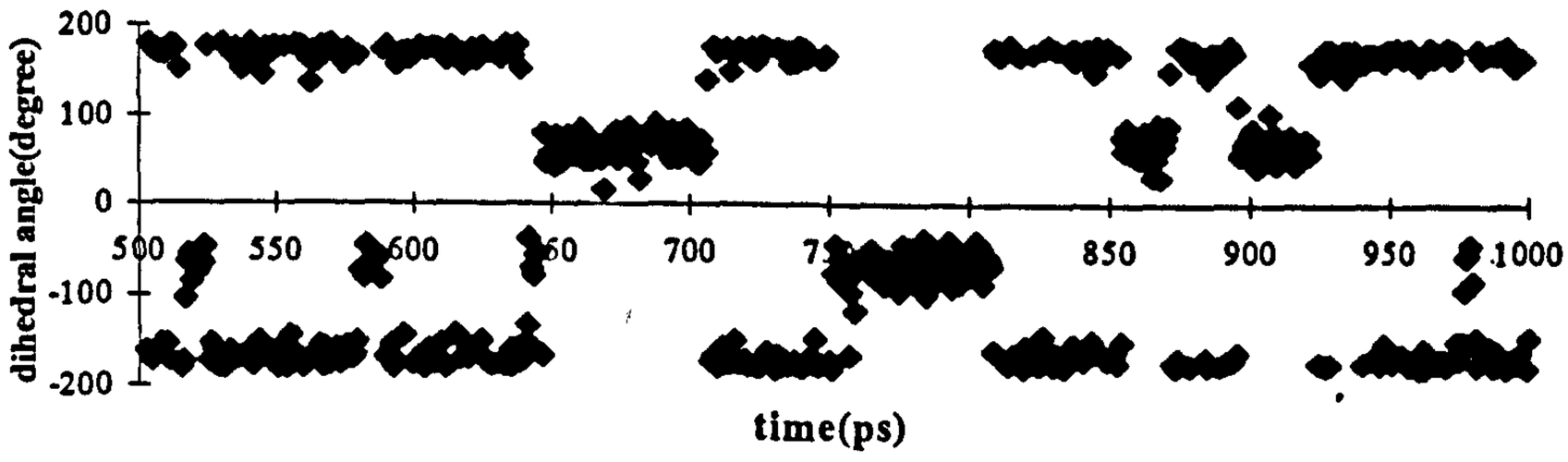

(b) Torsion 2

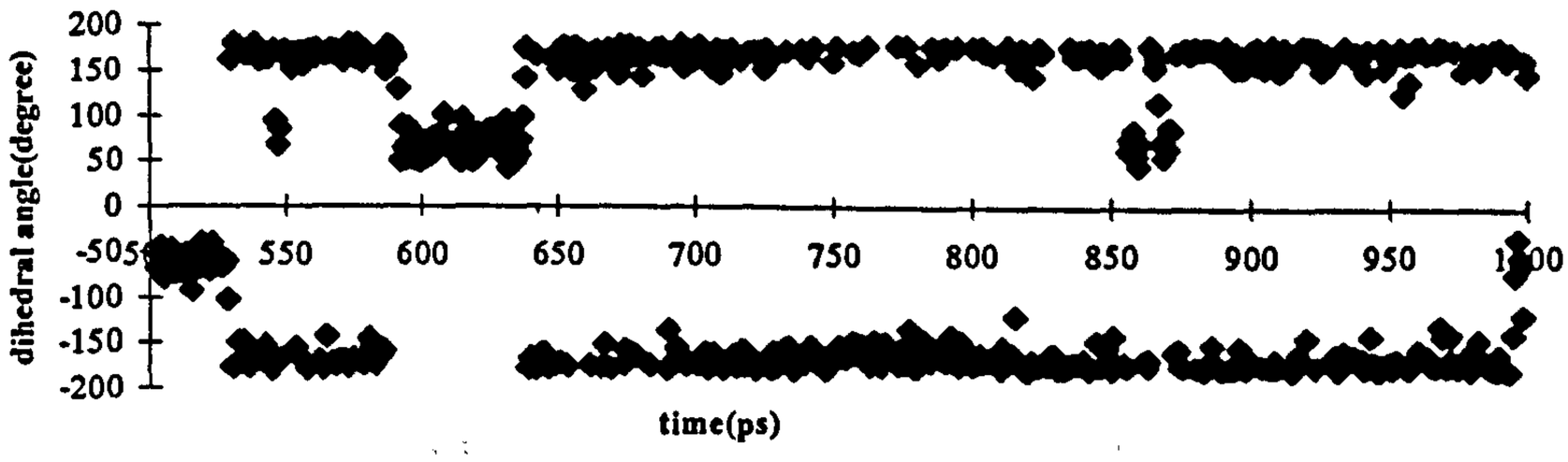

(c) Torsion 3

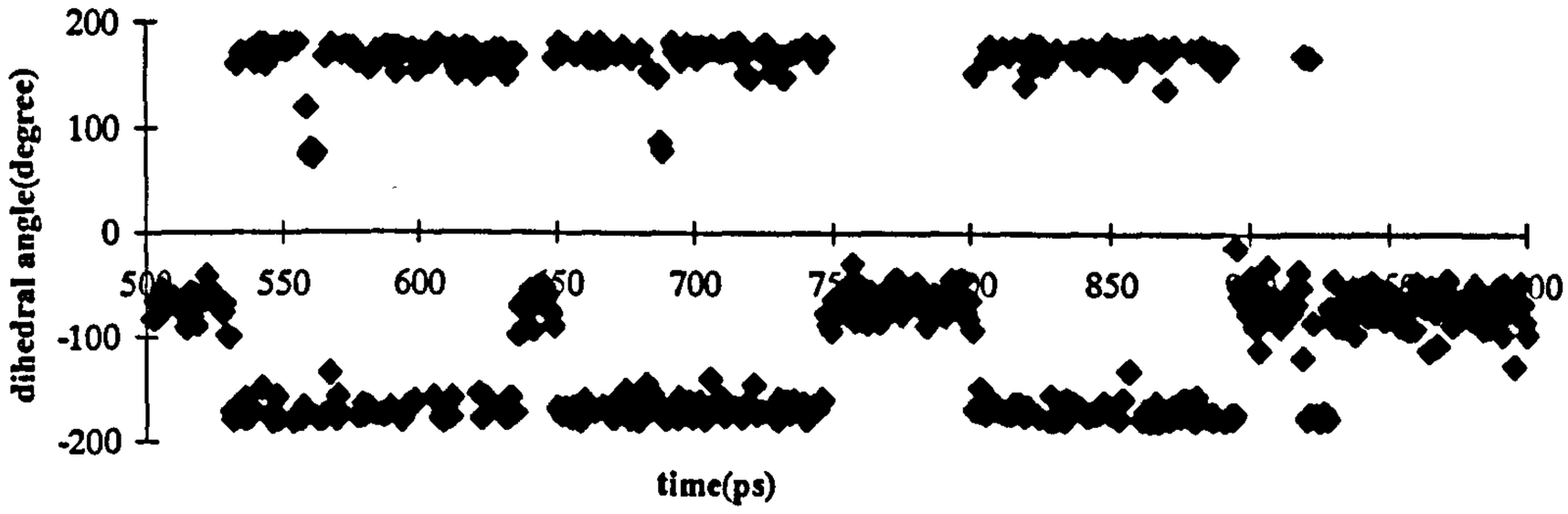

(d) Torsion 4

Figure 3.1.7: The changes in dihedral angle vs. time for Azone with DPPC in water.

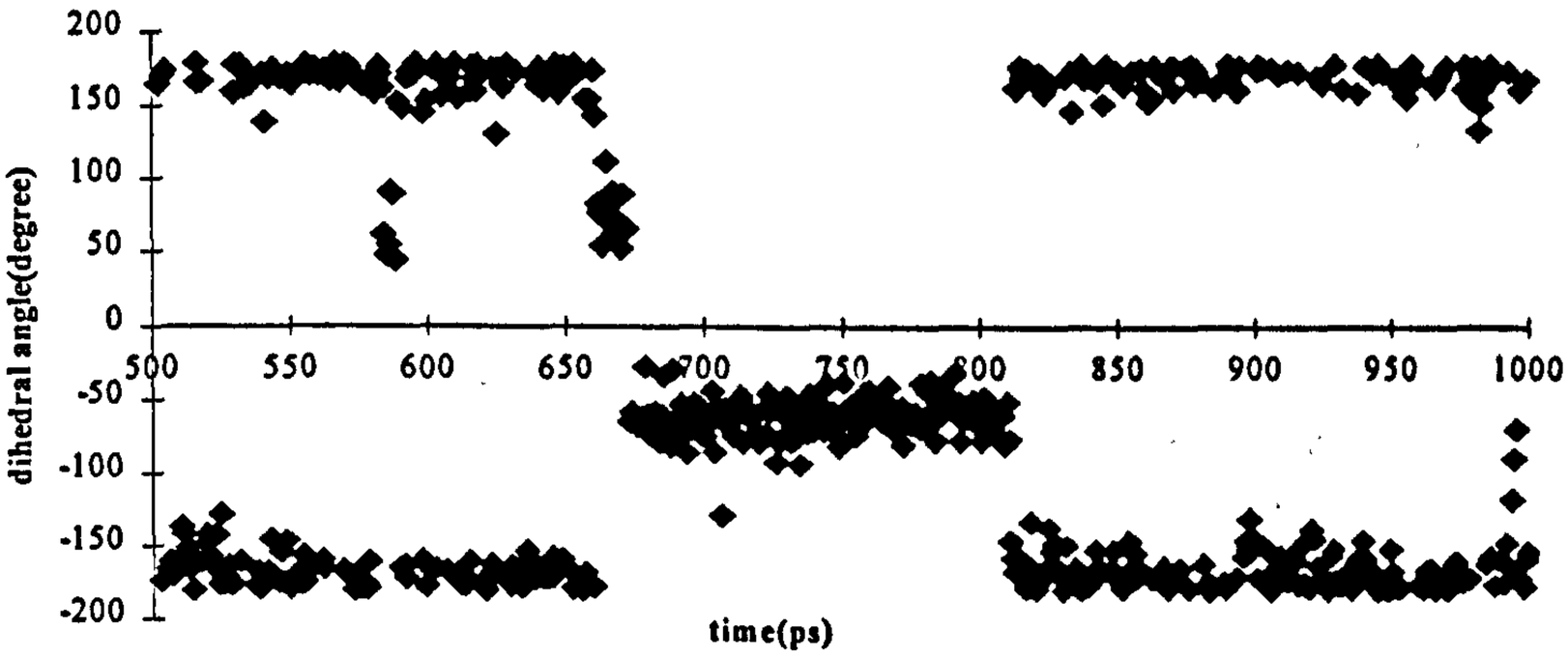

(e) Torsion 5

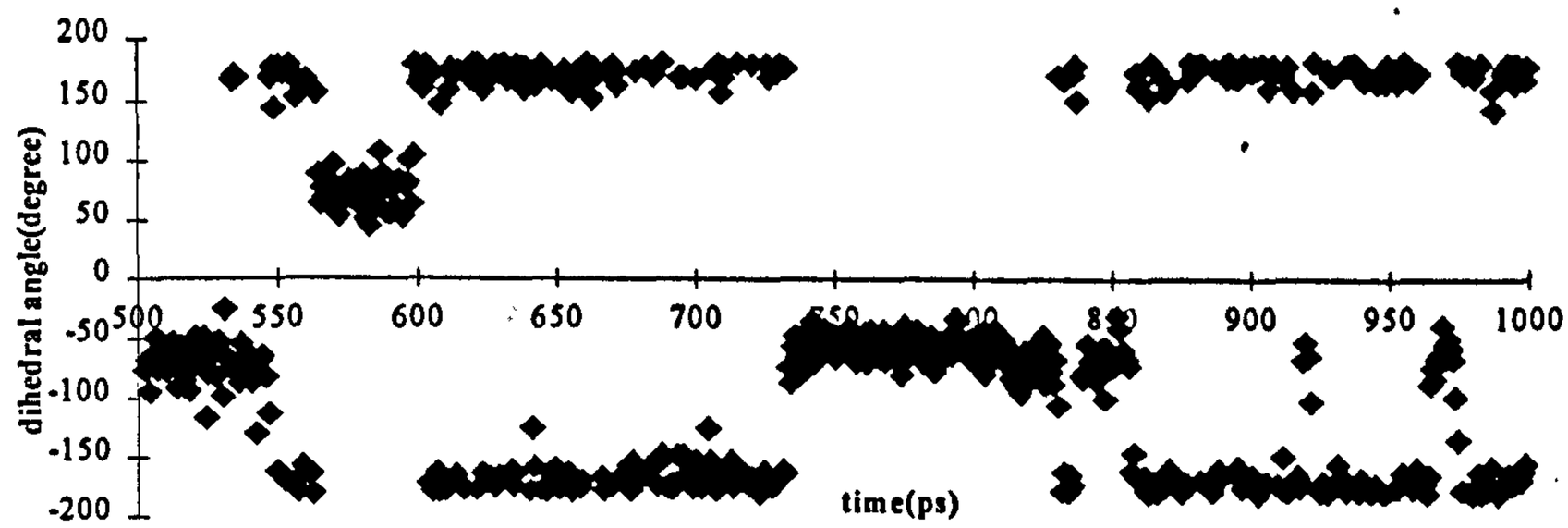

(f) Torsion 6

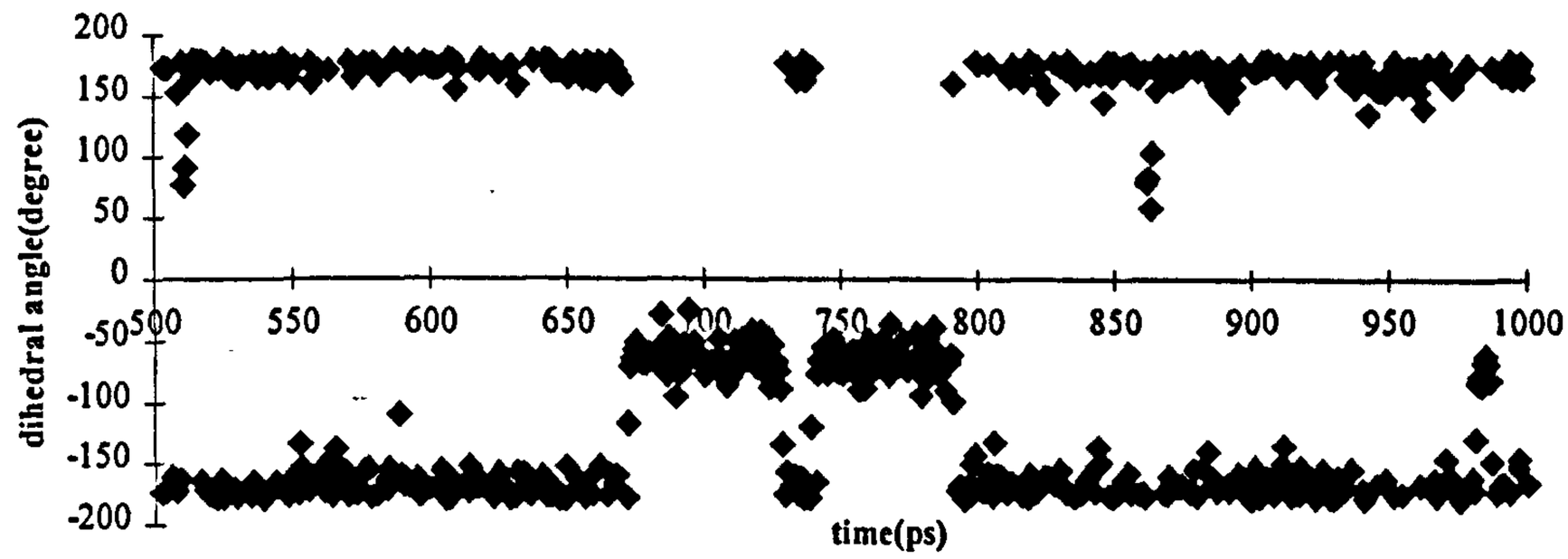

(g) Torsion 7

Figure 3.1.7 (ctd.): The changes in dihedral angle vs. time for Azone with DPPC in water.

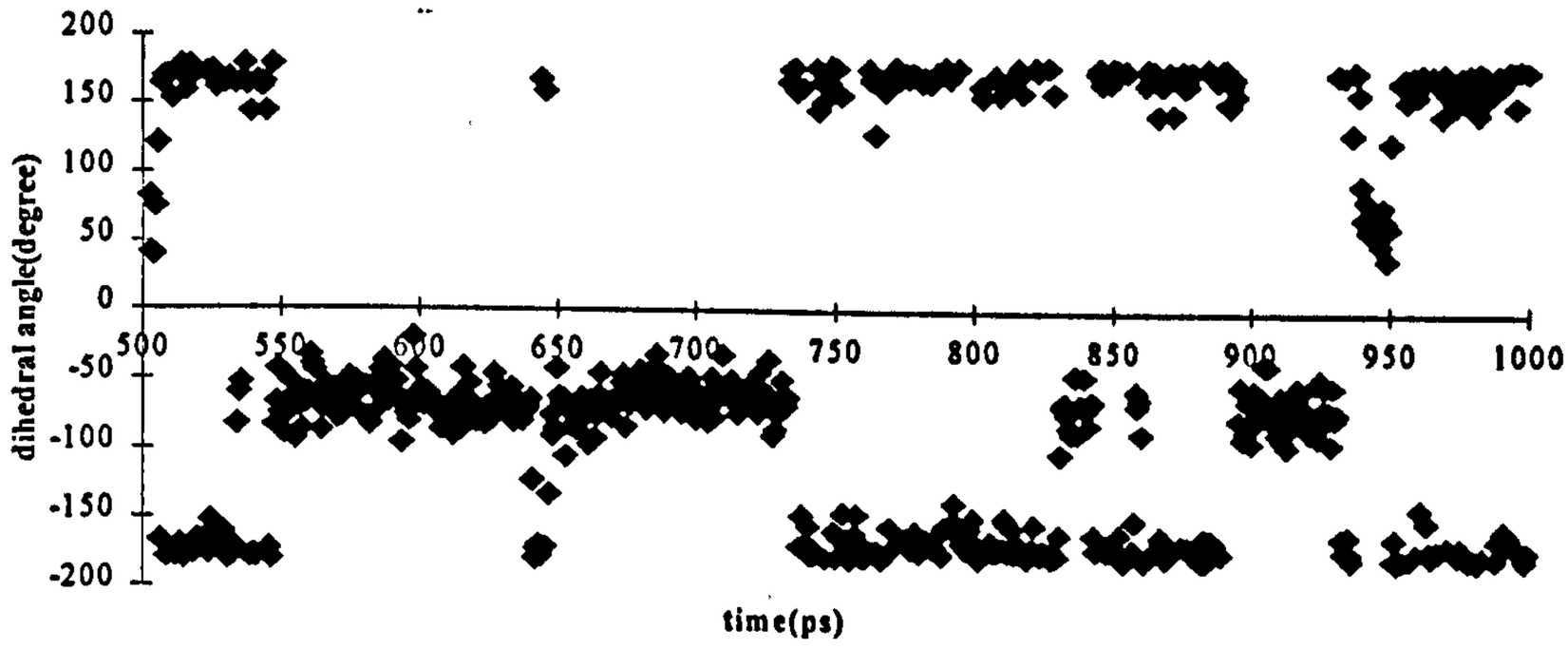

(h) Torsion 8

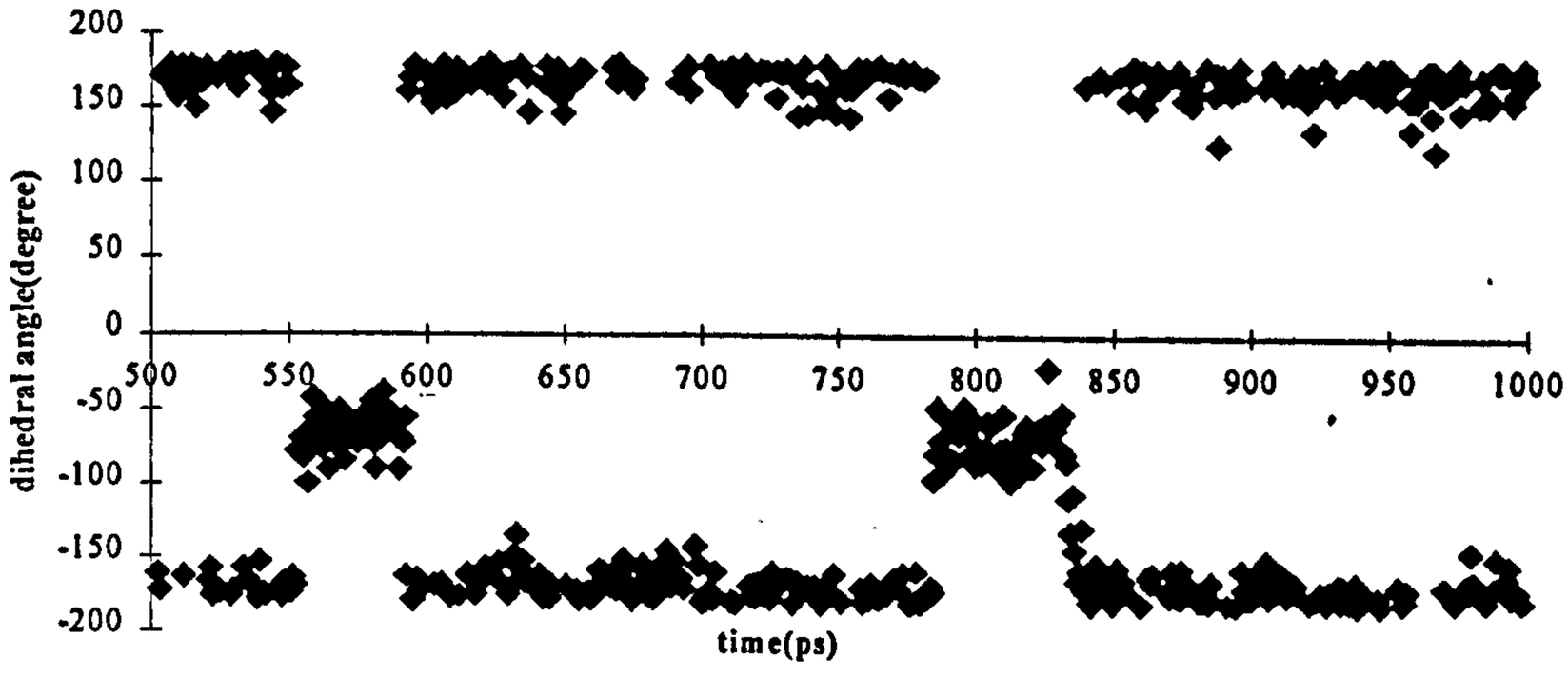

(i) Torsion 9

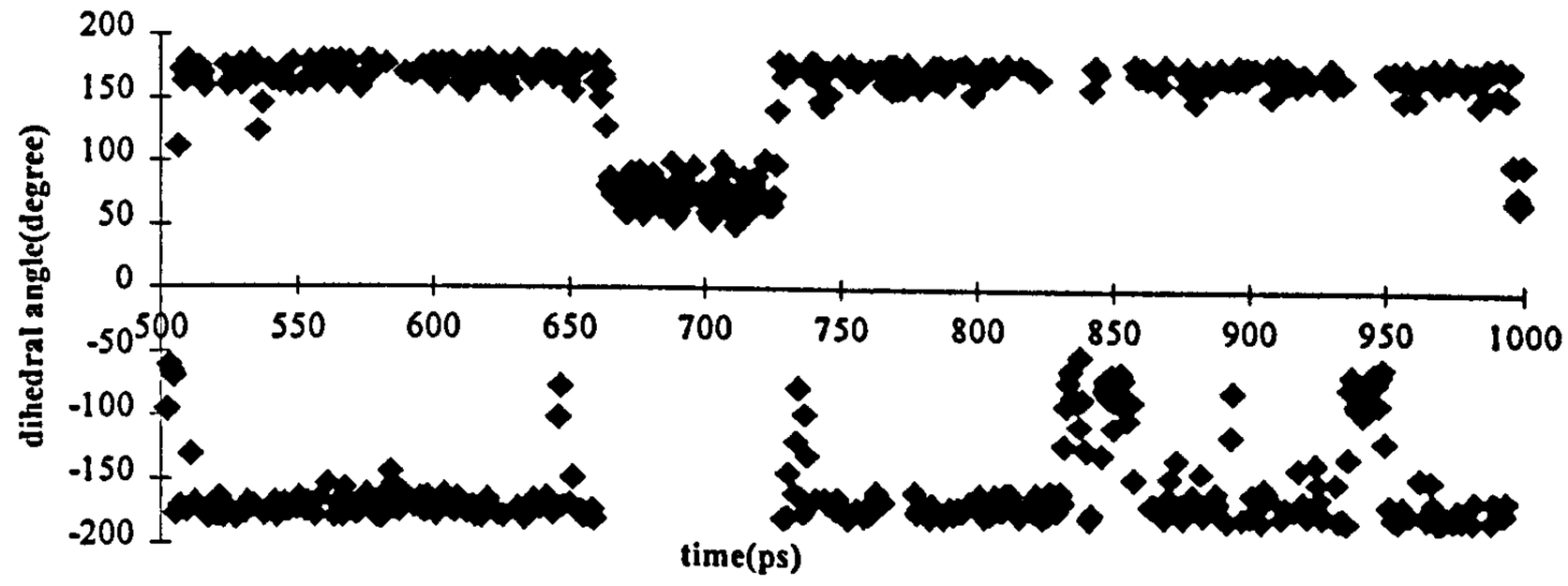

(j) Torsion 10

Figure 3.1.7 (ctd.): The changes in dihedral angle vs. time for Azone with DPPC in water.

Besides cluster analysis and dihedral angle analysis, another simple way to investigate the conformation of Azone is by measuring the average distance between the terminal methyl carbon and the nitrogen on the headgroup. This gives us some idea as to the overall shape of the molecule. Figure 3.1.8 illustrates various conformations of Azone showing how the shape of the molecule changes as the distance between these two atoms varies. The distance is obviously greatest (14.8Å) when the alkyl chain is fully extended. The average separations of these two atoms calculated over the whole of each trajectory were found to be 11.3Å, 12.5Å and 12.2Å for the Azone in water, Azone with DPPC in water and liquid Azone, respectively. It is interesting to note that the value calculated for the liquid Azone model lies between the values calculates for the two other systems, but this is probably due only to the fact that the value for liquid Azone was calculated by averaging over 36 molecules. The slightly shorter mean end-to-end distance calculated for Azone in water compared with Azone with DPPC in water is simply a reflection of the fact that there are more *gauche* defects present in the alkyl chain in the former system (as shown in the previous dihedral angle analysis).

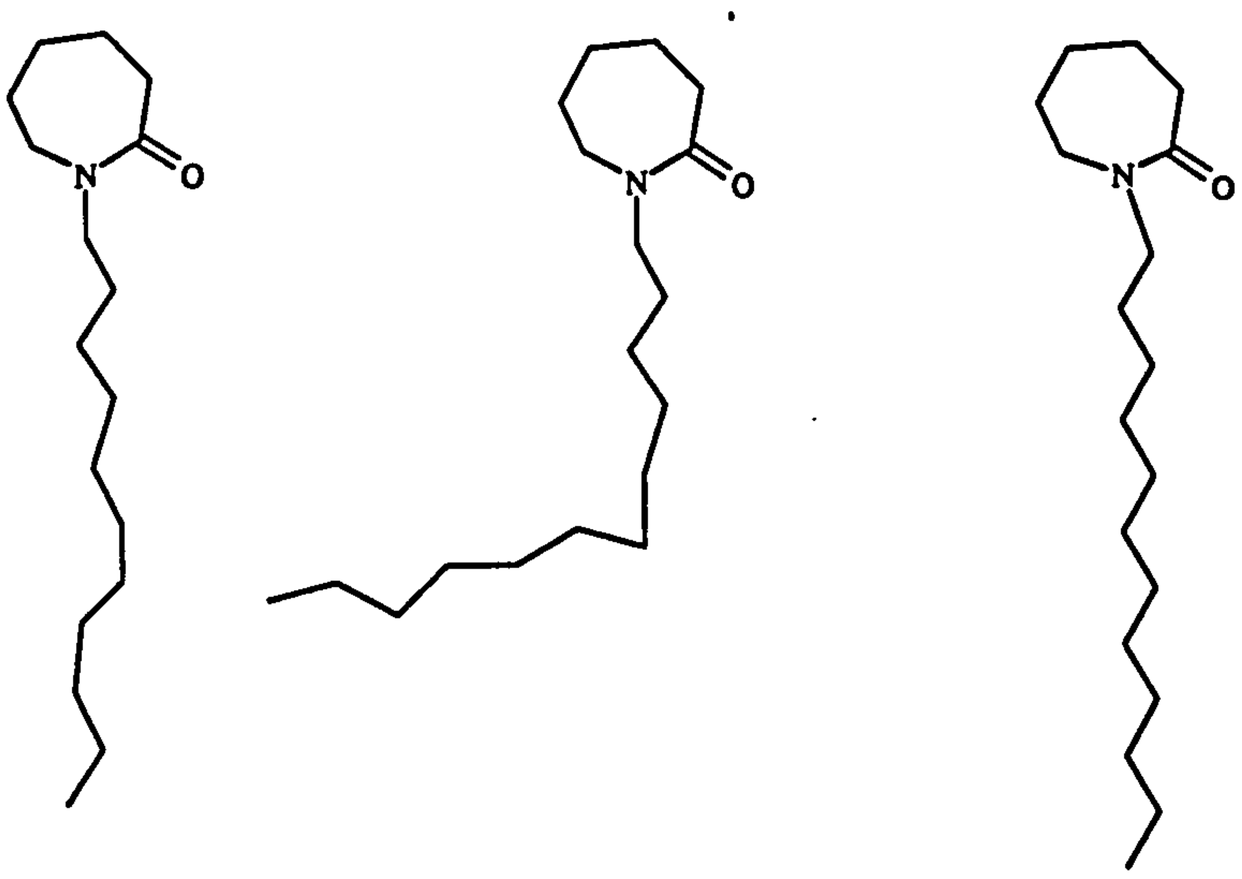

Figure 3.1.8 Structures of Azone reflected exhibiting different end-to-end chain length.

3.1.2 Hydration of Azone

The interactions of Azone molecule with water were investigated by calculating the pair distribution functions of the Azone nitrogen and oxygen atoms with respect to the water oxygen and hydrogen atoms. Figure 3.1.10 shows the pair distribution functions for the Azone nitrogen with respect to the water oxygen and hydrogen atoms. The absence of any first neighbour peak in the plot for the Azone nitrogen atom indicates that this atom has no specific hydration. Figures 3.1.11 (a) & (b) however, show that there are strong first neighbour peaks for the Azone oxygen (at a distance ~1.95Å). It is evident, therefore, that there is strong water hydrogen bonding to the amide oxygen, and the co-ordination number calculated as 1.

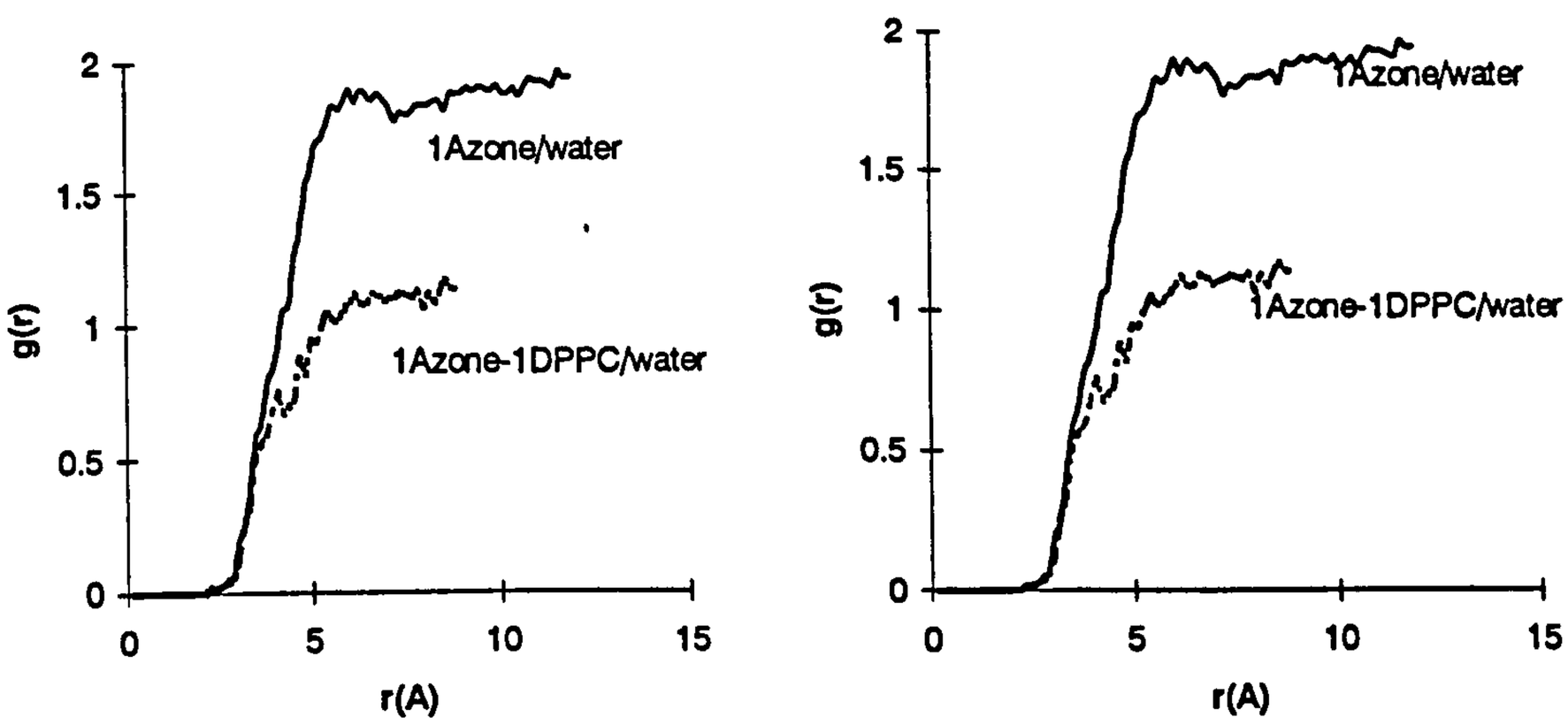

Figure 3.1.10 Pair distribution function of Azone's nitrogen with (a) respect to water's oxygen and (b) respect to water's hydrogen.

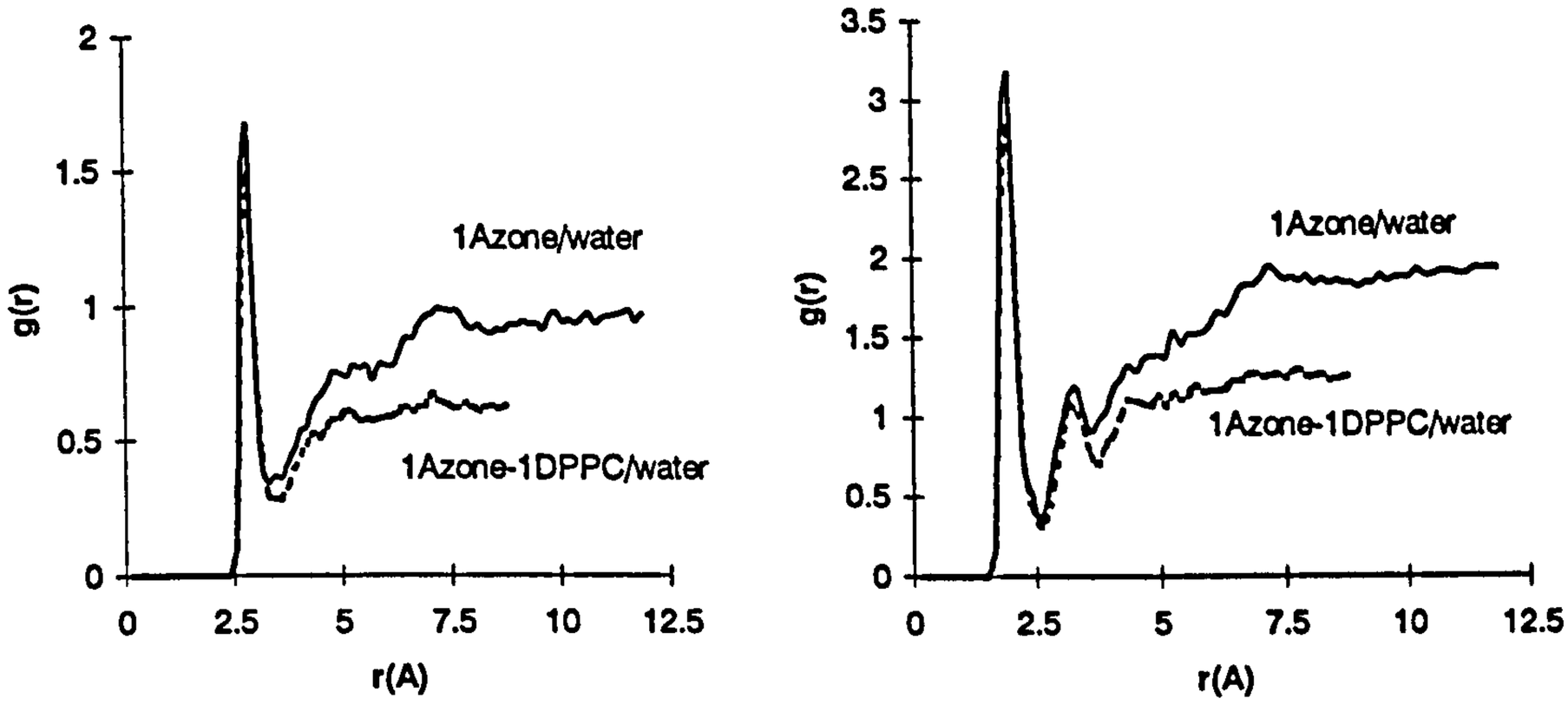

(a) (b)

Figure 3.1.11 Pair distribution functions for the Azone oxygen (a) with respect to the water oxygen and (b) with respect to the water hydrogen

3.2 MD OF PURE DPPC/WATER BILAYER SYSTEM

3.2.1 Electron density profile

The structural properties of a lipid bilayer such as bilayer thickness can be derived from an electron density profile which can be determined experimentally by X-ray diffraction. In a typical electron density profile for DPPC (Figure 3.2.1), the regions of high electron density can be clearly distinguished from those of low electron density. The electron dense region is interpreted as being due to the choline and phosphate moieties in the lecithin head group. The low density region (the central trough) is attributed to the methyl terminus of the hydrocarbon region. The region between the peaks and trough is attributed to the methylene groups and the narrow regions at the outer edges of the profile are attributed to the water layers sandwiched between adjacent bilayers (Lesslauer *et al.*, 1972; Zacchai *et al.*, 1975).

In this MD study, the electron density was calculated as the total number of electrons associated with the atoms within a slice, divided by the volume of the slice, and this is averaged over the simulation time. From Figure 3.2.2 we can see that in the profiles calculated for the various MD models of the DPPC bilayers closely resemble the experimental electron density profile. Comparing the three profiles, we can see that the width of the low density region due to terminal methyl groups is greatest in the Lα-DPPC CHARMm model followed by the Lα-DPPC AMBER system and then the Lβ' system. This implies that the Lα-DPPC bilayer is more disordered in the CHARMm model than in the AMBER model. The profile of the gel system shows a sharp trough in the low-density region which is consistent with a higher order of chain packing in the system.

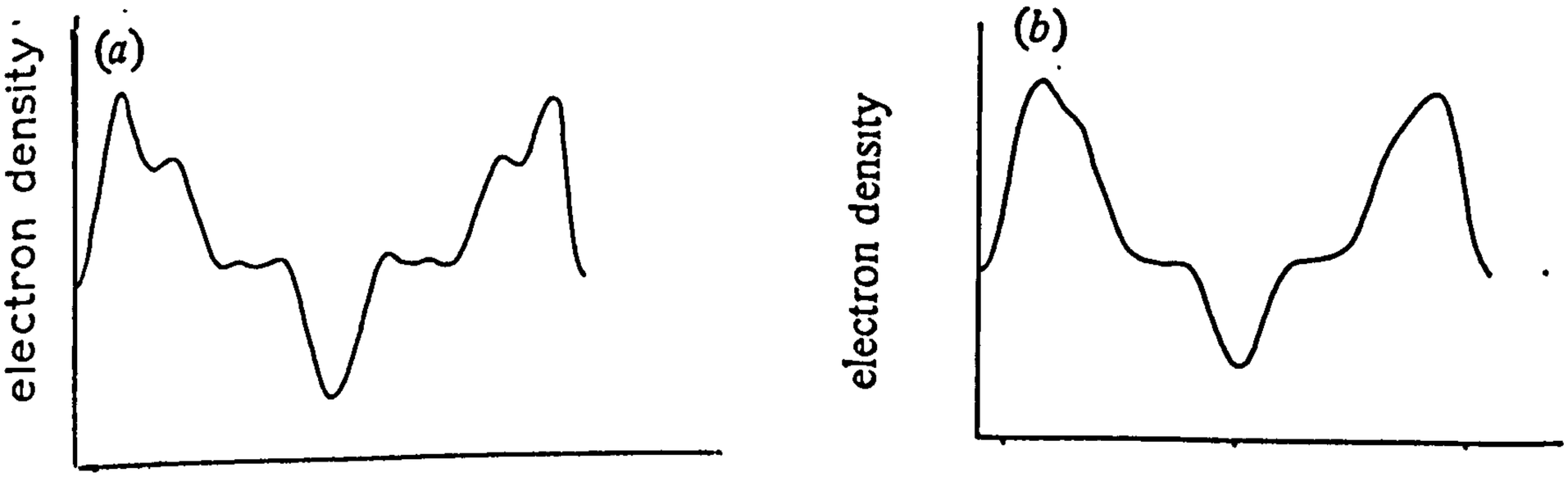

Figure 3.2.1 : Typical experimental electron density profiles of a lecithin bilayer in the (a) gel phase and (b) liquid crystalline phase(McKintosh, 1980)

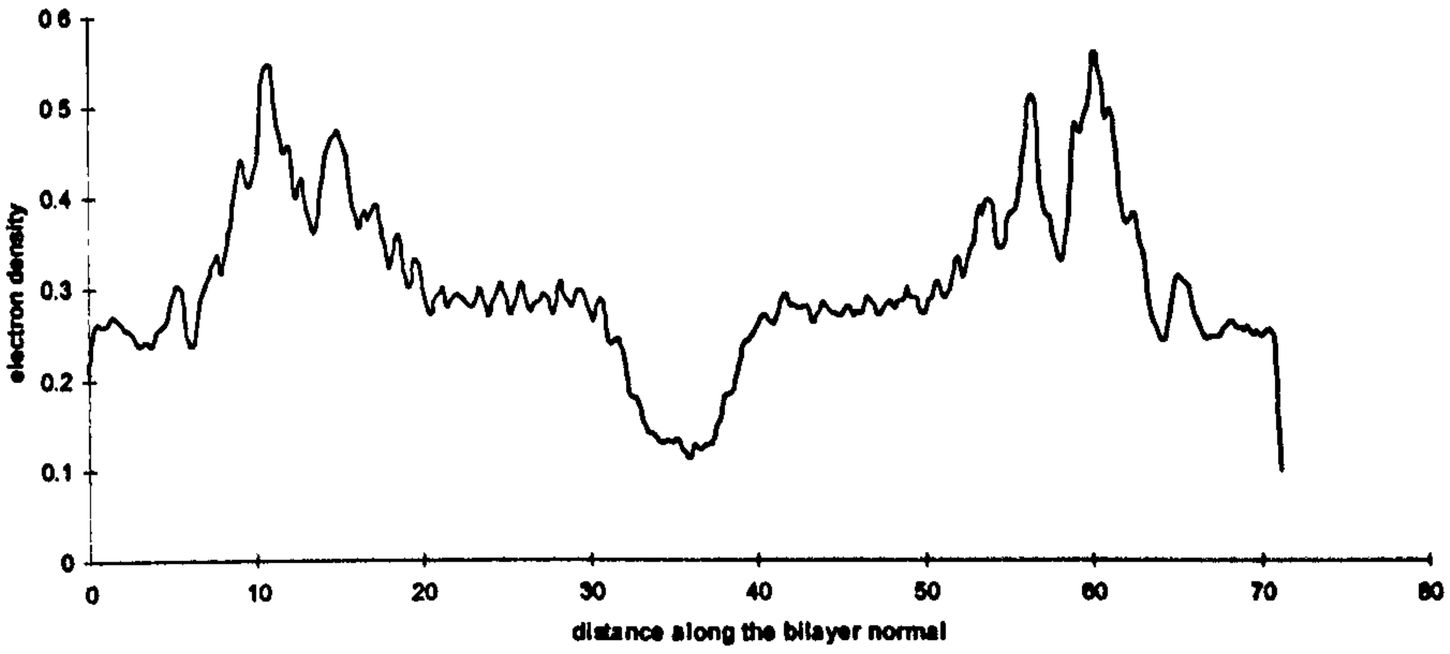

a) Lβ' DPPC model

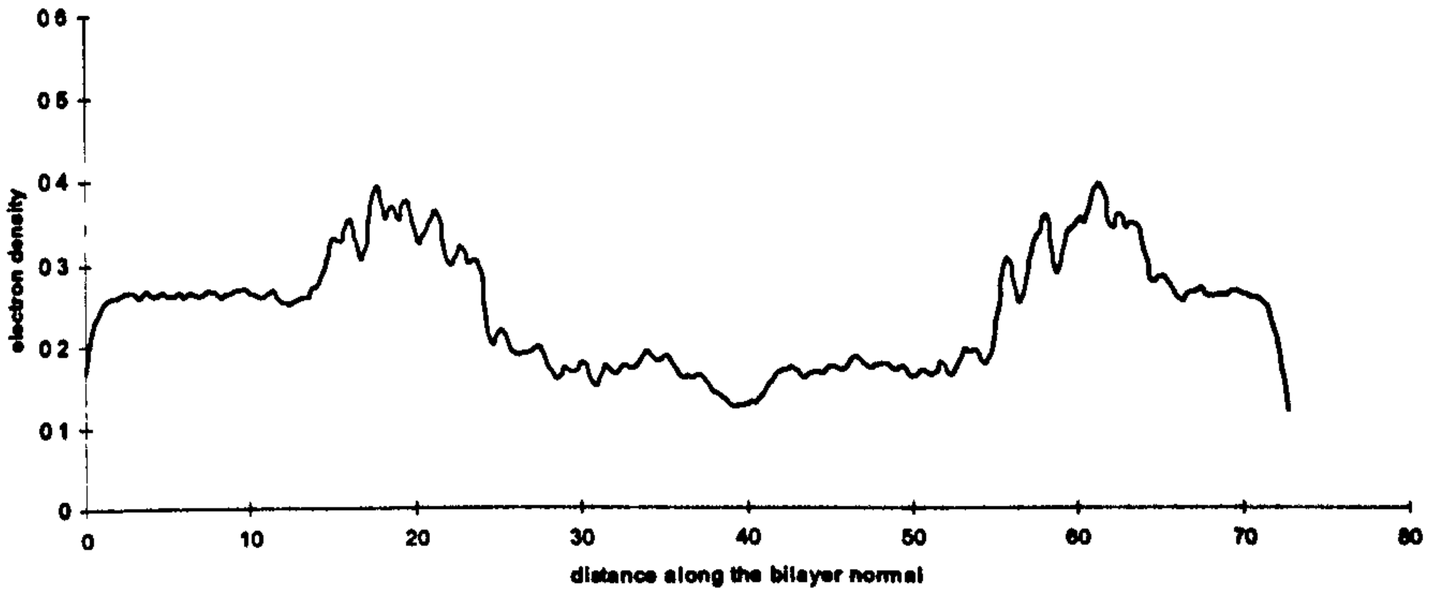

b) Lα-DPPC AMBER model

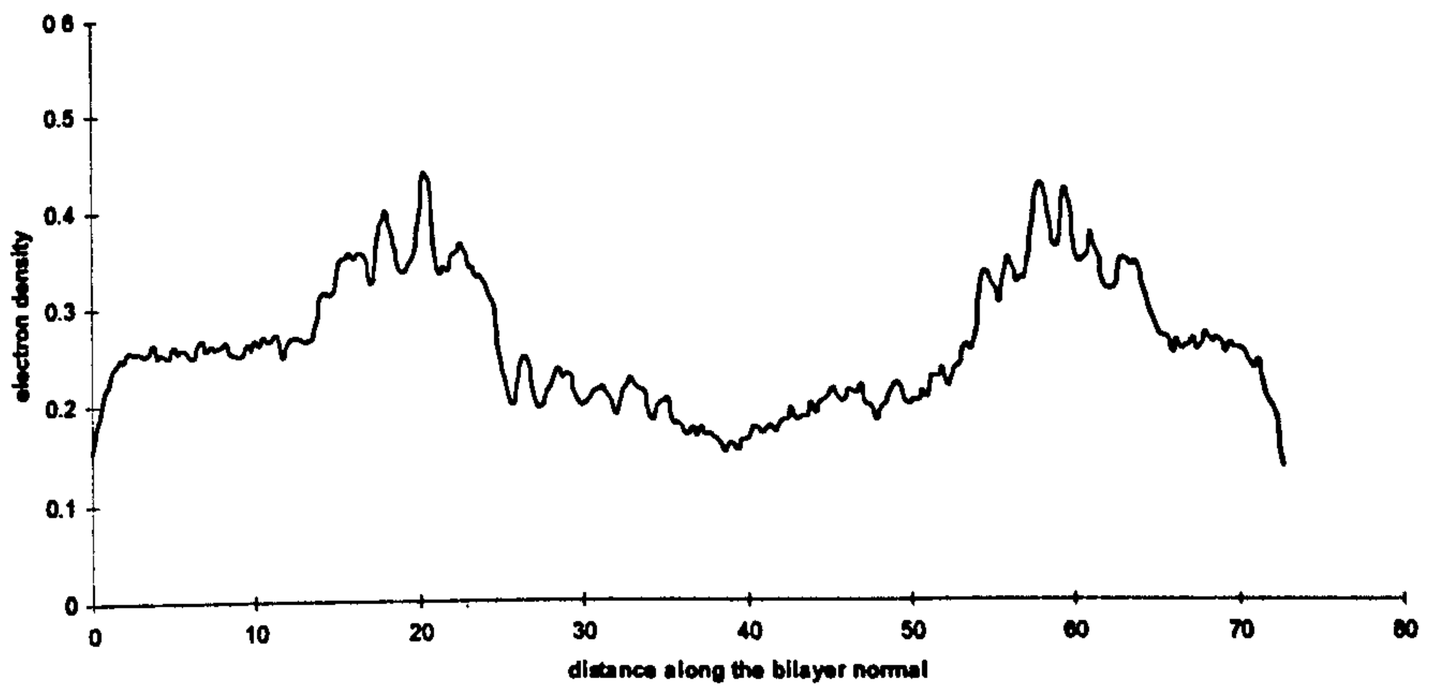

c) Lα-DPPC CHARMM model

Figure 3.2.2 Total electron density profiles of calculated for the various MD models of DPPC bilayers.

In Figure 3.2.3, the electron density profiles for the various DPPC bilayer models are deconvulated to show the individual contributions made by the phospholipids' phosphate, choline and the alkyl chain methyl group. The results confirm the experimental findings, in that the electron rich and the electron poor regions are found to be due to the headgroup phosphate and choline groups and the methyl terminus groups, respectively.

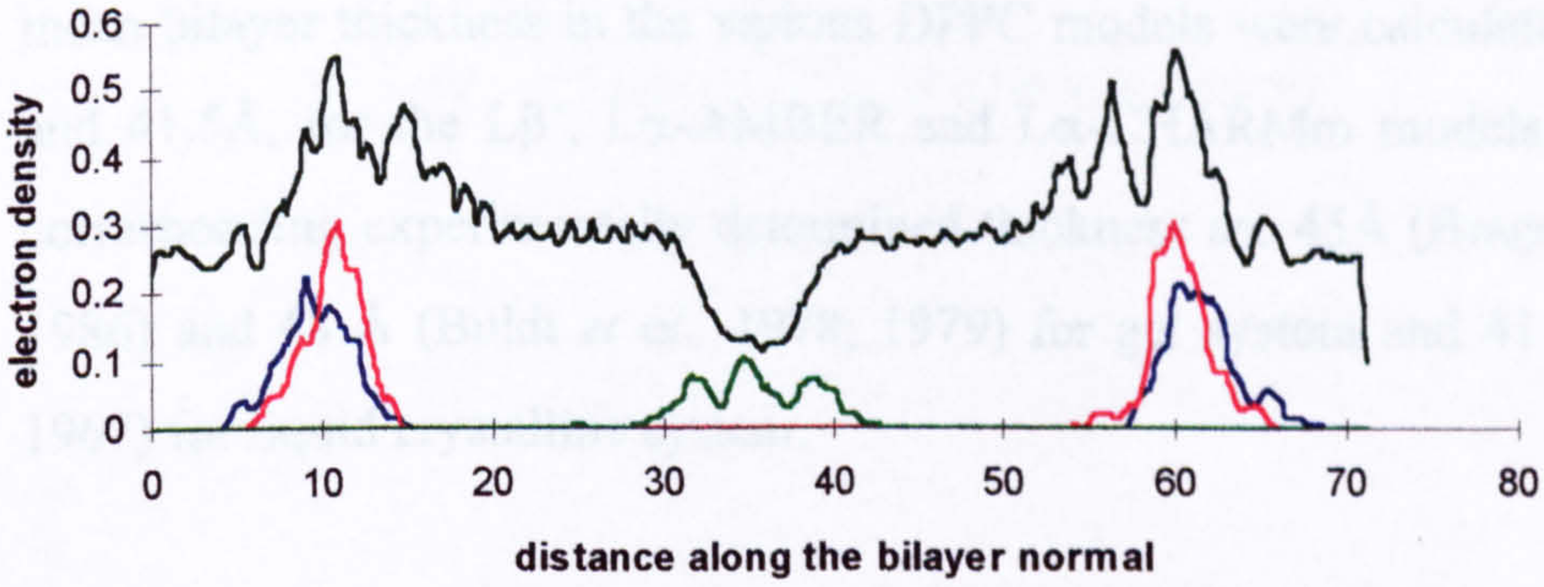

(a) Lβ' DPPC model

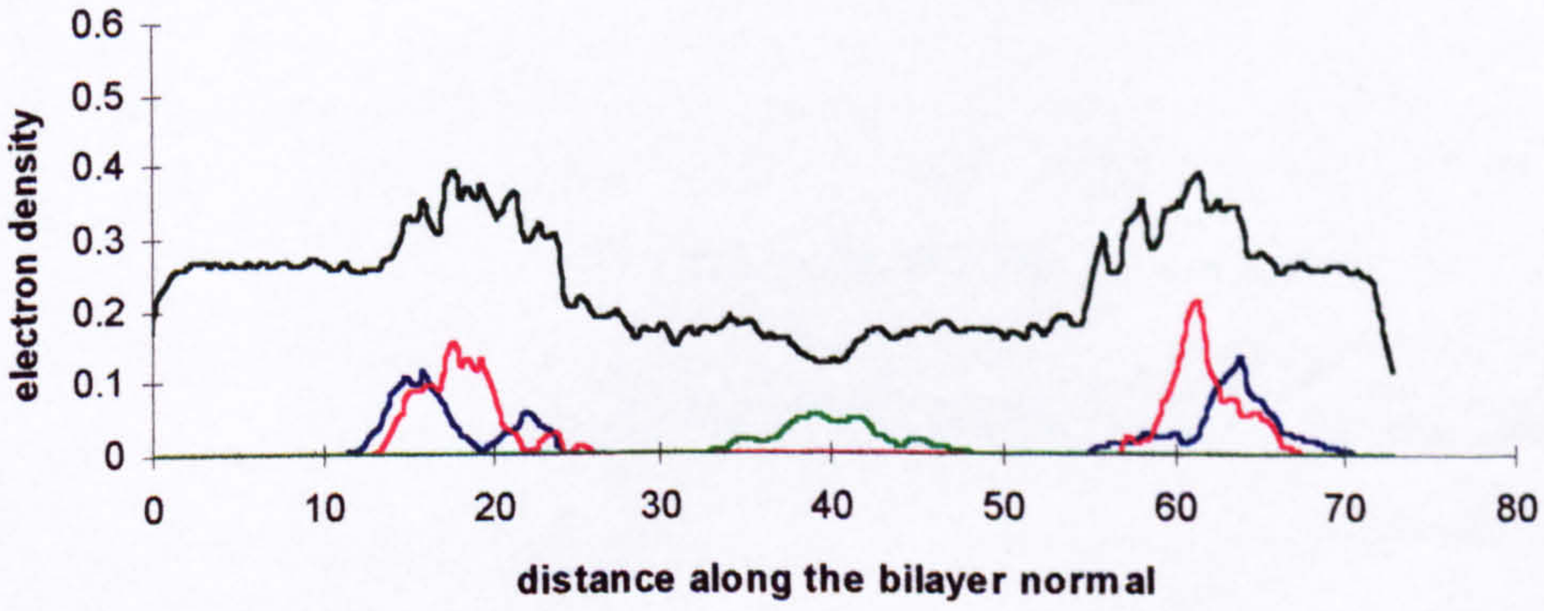

(b) Lα-DPPC AMBER

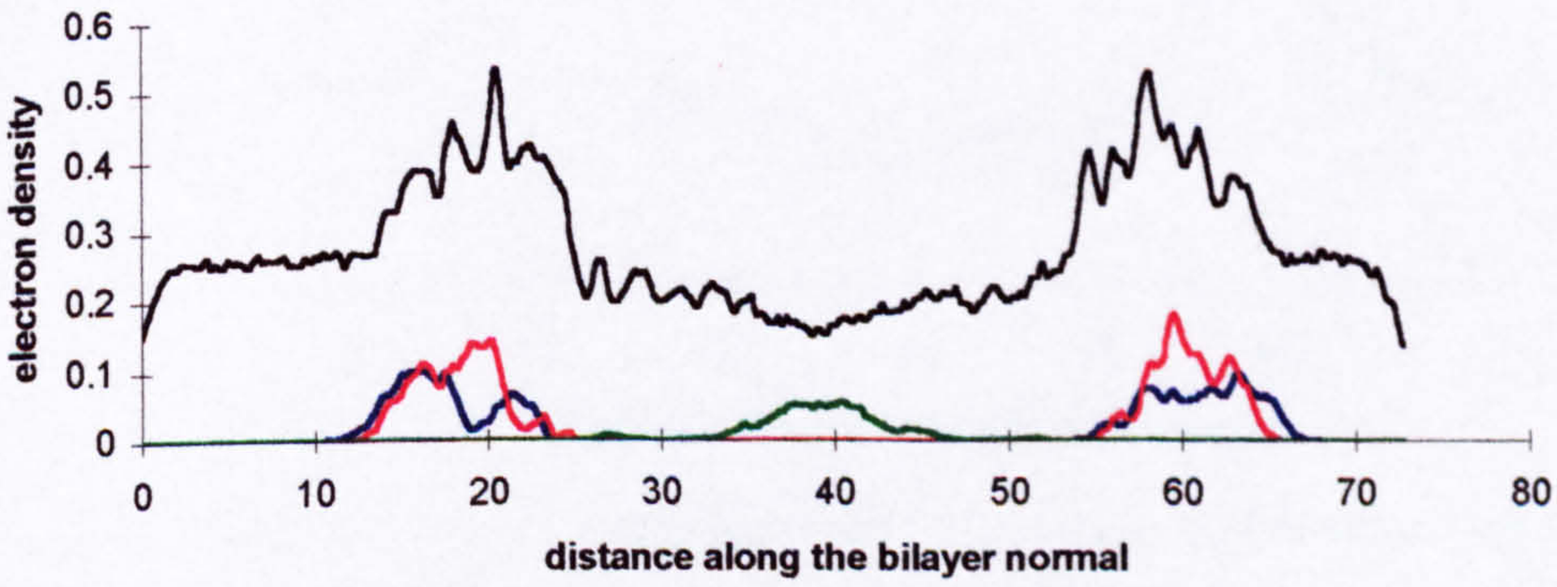

(c) Lα-CHARMm

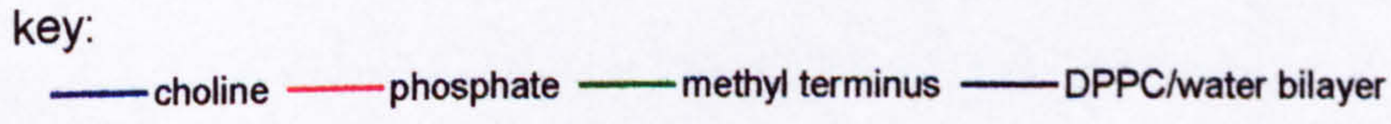

Figure 3.2.3 Group contributions to the electron density profiles for the DPPC bilayer models.

Besides giving an indication of the degree of disorder of the system, the electron density profiles can also be used to determine the bilayer thickness, conventionally measured simply on the mean intermonolayer phosphorus-phosphorus or nitrogen-nitrogen separation distance. By dissecting the electron density profiles further to show the density contributed by the phosphorus and nitrogen atom (Figure 3.2.4) the mean bilayer thickness in the various DPPC models were calculated as 47.5Å, 44 Å and 41.5Å, for the Lβ', Lα-AMBER and Lα-CHARMm models respectively. The corresponding experimentally determined thickness are 45Å (Braganza & Worcester, 1986) and 48 Å (Buldt *et al.*, 1978; 1979) for gel system and 41 Å (Reiss-Husson, 1967) for liquid crystalline system.

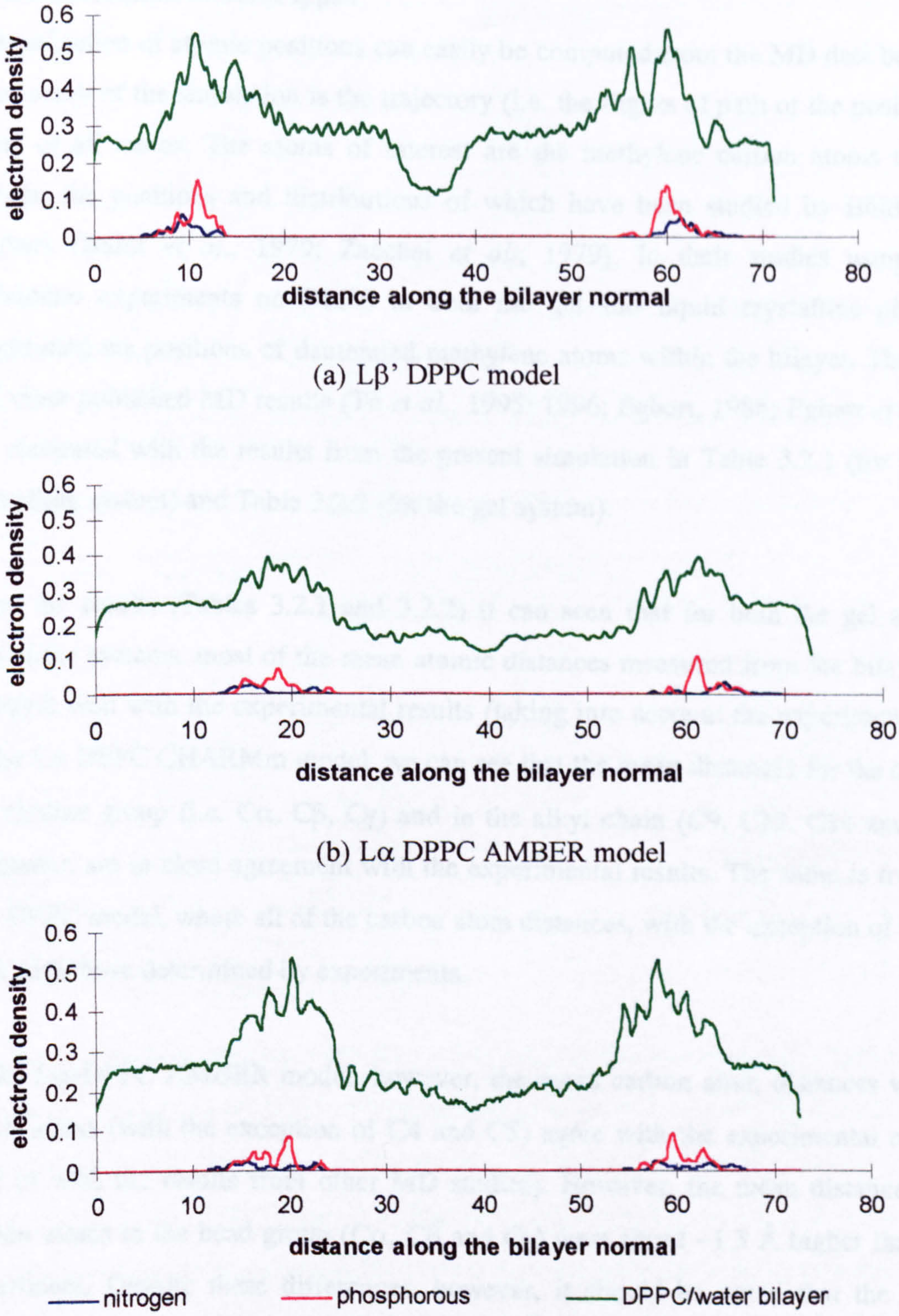

Figure 3.2.4 The contributions to the DPPC bilayer electron density by the headgroup phosphorus and nitrogen atoms. Note that the peak in the phosphorus distribution corresponds to the peak in the total electron density profile.

3.2.2 Distribution of atom types

Determination of atomic positions can easily be computed from the MD data because the main result of the simulation is the trajectory (i.e. the flights of path or the positions with time) of all atoms. The atoms of interest are the methylene carbon atoms within the bilayer, the positions and distributions of which have been studied by Büldt and co-workers (Büldt *et al.*, 1979; Zacchai *et al.*, 1979). In their studies using neutron diffraction experiments on DPPC in both the gel and liquid crystalline phase, they determined the positions of deuterated methylene atoms within the bilayer. Their results and other published MD results (Tu *et al.*, 1995; 1996; Egbert, 1988; Egbert *et al.*, 1994) are compared with the results from the present simulation in Table 3.2.1 (for the liquid crystalline system) and Table 3.2.2 (for the gel system).

From the results (Tables 3.2.1 and 3.2.2) it can seen that for both the gel and liquid crystalline systems, most of the mean atomic distances measured from the bilayer centre compare well with the experimental results (taking into account the experimental error). In the Lα DPPC CHARMm model, we can see that the mean distances for the carbons in the choline group (i.e. Cα, Cβ, Cγ) and in the alkyl chain (C9, C12, C14 and C15) in particular, are in close agreement with the experimental results. The same is true for the Lβ' DPPC model, where all of the carbon atom distances, with the exception of C5, agree well with those determined by experiments.

In the Lα-DPPC AMBER model, however, the mean carbon atom distances within the alkyl chains (with the exception of C4 and C5) agree with the experimental results (as well as with the results from other MD studies). However, the mean distances for the carbon atoms in the head group (Cα, Cβ and Cγ) were about ~1.5 Å higher than that of experiment. Despite these differences, however, it should be noted that the distances calculated for Cα, Cβ and Cγ atoms are almost the same, indicating that the headgroups are aligned approximately parallel to the bilayer plane - a result which is consistent with the observations recorded in the neutron diffraction experiments (Büldt *et al.*, 1979) and in other MD studies (Tu *et al.*, 1996).

Table 3.2.1: Mean distances of various DPPC atoms from the bilayer centre (Lα phase)

carbon atom	exp. (Å)*	MD SIMULATIONS			
		Egbert et al.(1994) (Å)	*Tu et al., (1995)* (Å)	*Lα- AMBER* (Å)	*Lα- CHARMm* (Å)
Cα	21.0 + 1.0	na	20.2 + 2.4	22.53 + 2.9	21.4 + 2.75
Cβ	21.2 + 1.0	na	20.3 + 2.6	22.79 + 2.11	21.7 + 1.13
Cγ	21.8 + 0.6	na	21.1 + 3.0	23.27 + 1.73	21.8 + 1.43
C	17.4 + 1.5	na	17.4 + 2.1	20.93 + 2.1	19.7 + 1.9
C4	12.2 + 1.5	13.3 + 3.9	11.7 + 1.7	14.59 + 2.35	13.4 + 2.11
C5	10.5 + 1.5	12.4 + 3.5	10.7 + 1.8	13.63 + 2.2	12.2 + 2.42
C9	8.1 + 1.0	8.4 + 4.0	6.9 + 2.0	8.81 + 1.98	8.05 + 2.18
C12	5.7 + 3.4	5.6 + 4.1	na	5.5 + 2.1	5.2 + 1.92
C14	3.6 + 1.0	4.1 + 4.4	2.6 + 2.0	3.34 + 2.15	3.1 + 2.11
C15	1.9 + 1.0	3.1 + 6.0	1.9 + 2.1	2.83 + 2.4	2.2 + 2.23

* Büldt *et al.*, (1979) and Zacchai *et al.* (1979)

Table 3.2.2 *:* Mean distances of various DPPC atoms from the bilayer centre (Lβ' phase)

carbon atom	exp.(Å)*	MD SIMULATIONS		
		Egbert et al. (1994) (Å)	*Tu et al., (1995)* (Å)	*Lβ'*(Å)'
Cα	24.4 + 0.6	na	24.5	25 + 2.05
Cβ	24.1 + 1.0	na	23.7	24.98 + 4.9
Cγ	23.6 + 1.0	na	23.4	26.15 + 4.38
C	21.6 + 1.5	na	20.7	21.6 + 2.2
C4	15.4 + 1.5	15.9 + 6.6	14.3	15.53 + 2.5
C5	13.7 + 1.5	14.7 + 6.5	13.3	14.39 + 3.43
C9	9.8 + 1.0	10.0 + 5.8	9.1	9.565 + 3.5
C12	na	6.9 + 5.6	na	5.997 + 3.37
C14	4.1 + 1.0	4.7 + 5.6	3.8	3.76 + 3.1
C15	2.5 + 1.0	4.7 + 5.6	12.8	2.87 + 3.05

* Büldt *et al.*, (1979) and Zacchai *et al.* (1979)

Number density profiles were also calculated for the various DPPC bilayer models, firstly considering all DPPC atoms and water (Figure 3.2.5) and then considering the separate contributions from different parts of the DPPC molecule (dissected as shown in Figure 3.2.6; profiles shown in Figure 3.2.7). From Figure 3.2.5, it is seen that the central hydrocarbon region of the bilayer is always devoid of water and that there is a diffuse interface with water penetrating into the bilayer to a depth of 13.5Å in the Lβ' system, and to depths of 11.25Å and 9Å in the Lα-AMBER and Lα-CHARMm systems (with the depths measured relatives to the bilayer centre). The results from neutron diffraction experiments on DPPC/water multilayers in the gel phase at low water content, and in the liquid crystalline phase at 25% hydration show that water penetrates up to 15Å from the middle of the bilayer, - penetrating, therefore down to

the DPPC acyl ester group (Büldt *et al.*, 1979, Zacchai *et al.*, 1980). The fact that in the Lα DPPC systems, water penetrates more deeply into the bilayer than is seen by experiment is explained by the fact that the liquid crystalline MD models are more hydrated (i.e. 33%) than bilayers studied by experiment.

The details of the internal structure of the lipid bilayer (for all three models) can clearly be seen in Figure 3.2.7. Interestingly, all three models have similar features; For examples, the position of the trough in the centre of the alkyl chain methylene (CH_2) distribution corresponds to the maximum in the alkyl chain methyl distribution (CH_3), at the centre of the bilayer. It is also seen that the mean positions of the ester carbonyl groups lie at the boundary of the hydrocarbon region, with the polar headgroups distributed about 20Å, 15 Å and 12Å away from the bilayer centre in the Lβ', Lα-AMBER and Lα-CHARMm models, respectively. These data thus indicate the length of the lipid is shortest in the Lα-CHARMm model followed by Lα-AMBER model and then the Lβ' model. This shortening of the lipid length can be attributed to a higher incidence of *gauche* defects in the liquid crystalline modelled DPPC alkyl chain. In addition, it is noted that the distributions of the various DPPC fragments are broadest in the Lα-CHARMm model followed by Lα-AMBER model and the Lβ' model, suggesting that the mobility of the fragments follows the rank ordering Lα-CHARMm > Lα-AMBER > Lβ'.

The extent of water penetration in the DPPC bilayers was also investigated in relation to the location of the various DPPC fragments. As it can be seen from Figure 3.2.7, for all three systems, the water penetrates to the boundary of the hydrocarbon region, where the ester carbonyl groups are located. The phospholipid headgroups are almost fully immersed in water. Thus, despite the fact that water penetrates to a greater absolute depth in the Lα DPPC bilayers compared with the Lβ' DPPC bilayers, the relative extent of water penetration remains the same, that is, to the limit of the phospholipid ester moieties.

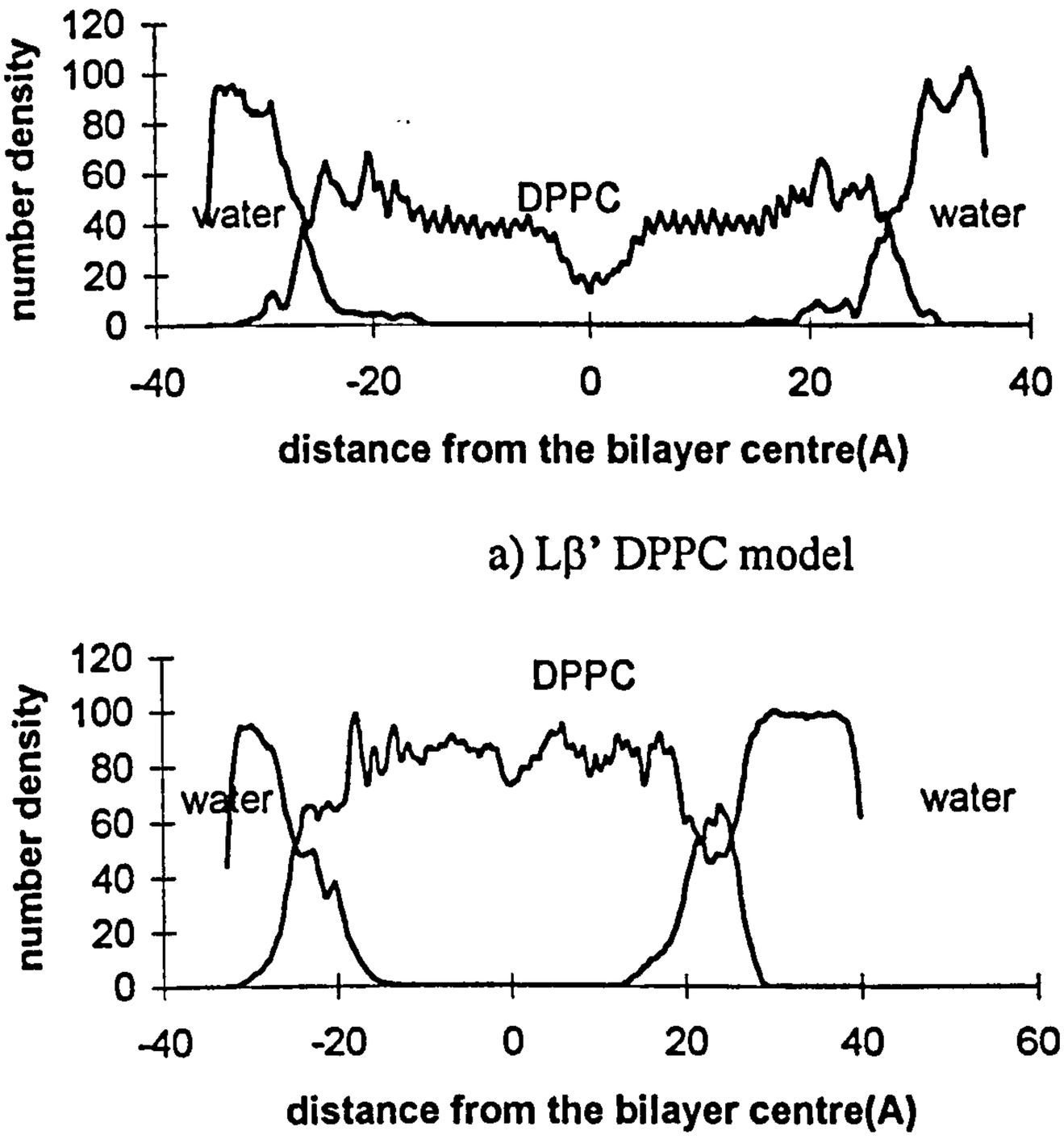

a) Lβ' DPPC model

(b) Lα DPPC AMBER model

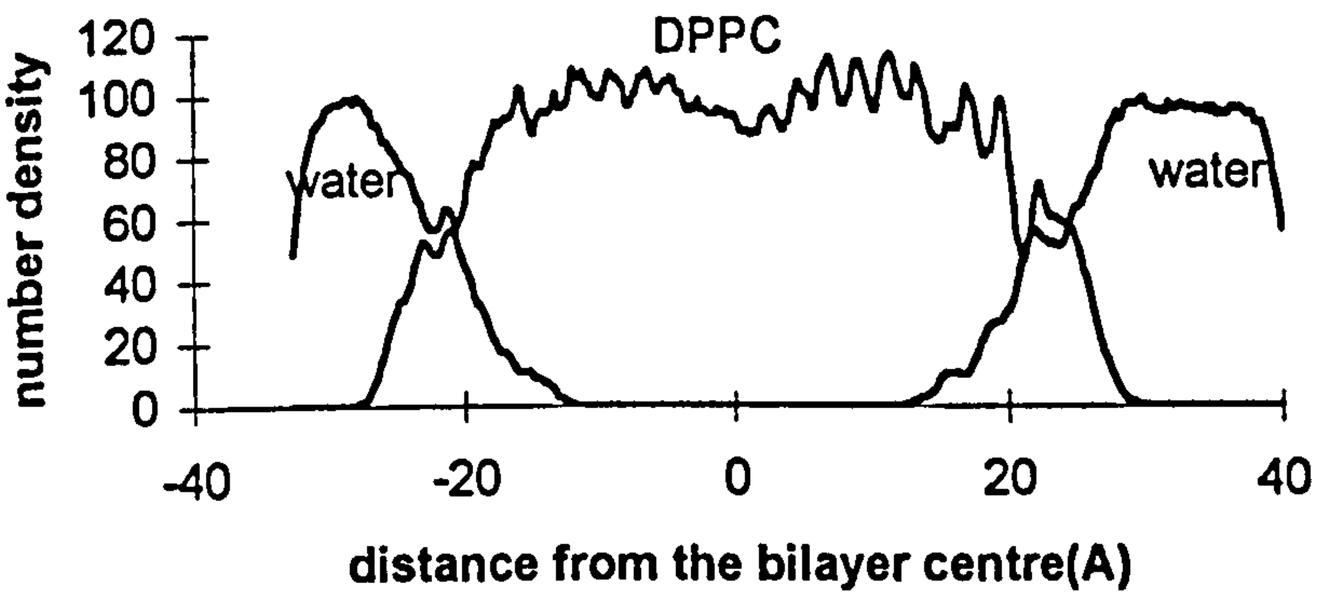

(c) Lα DPPC CHARMm model

Figure 3.2.5: DPPC and water number density profiles for the various DPPC bilayer models.

Figure 3.2.6: The parsing of DPPC into the quasimolecular parts used in the calculation of the number density profiles.

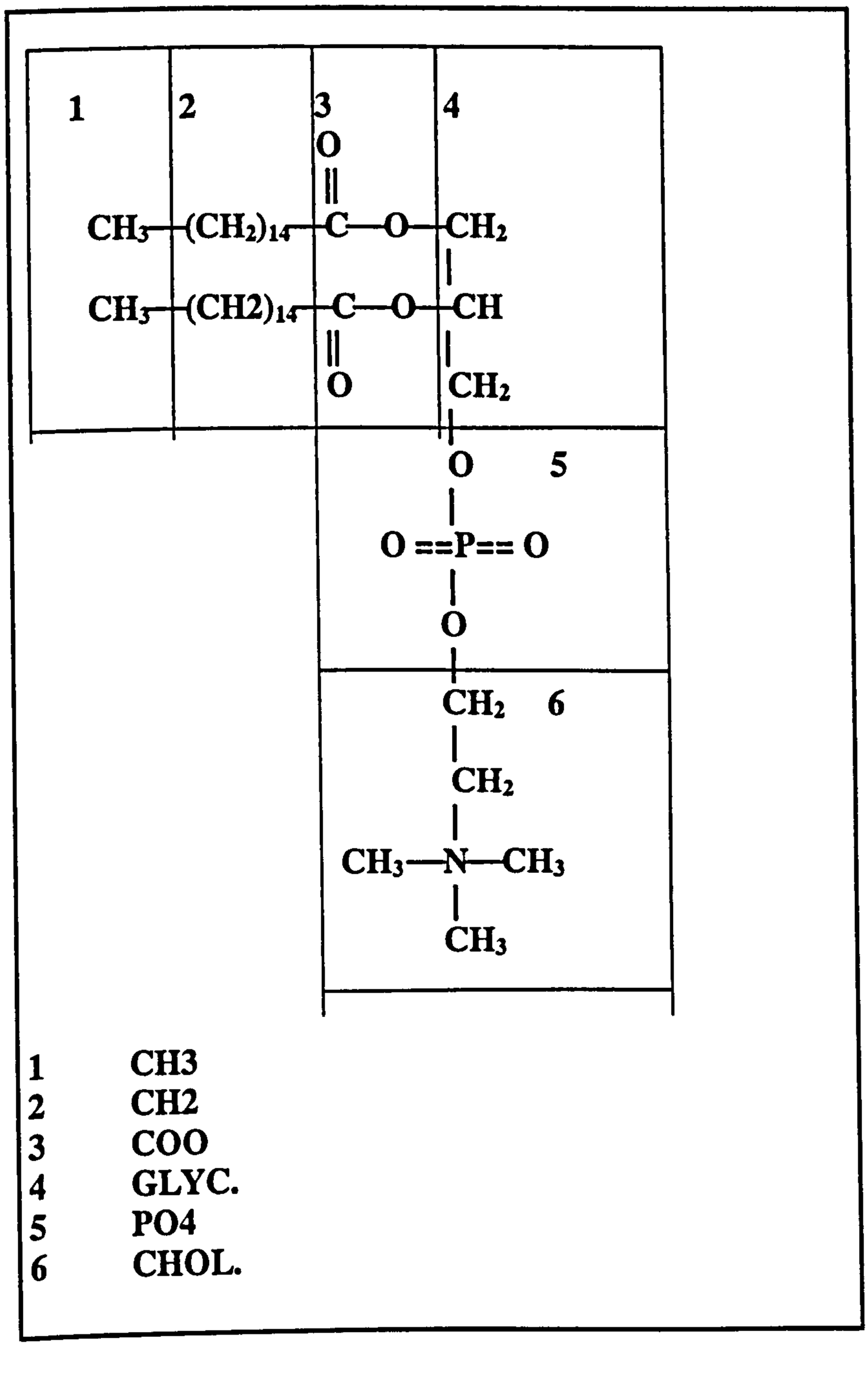

1 CH3
2 CH2
3 COO
4 GLYC.
5 PO4
6 CHOL.

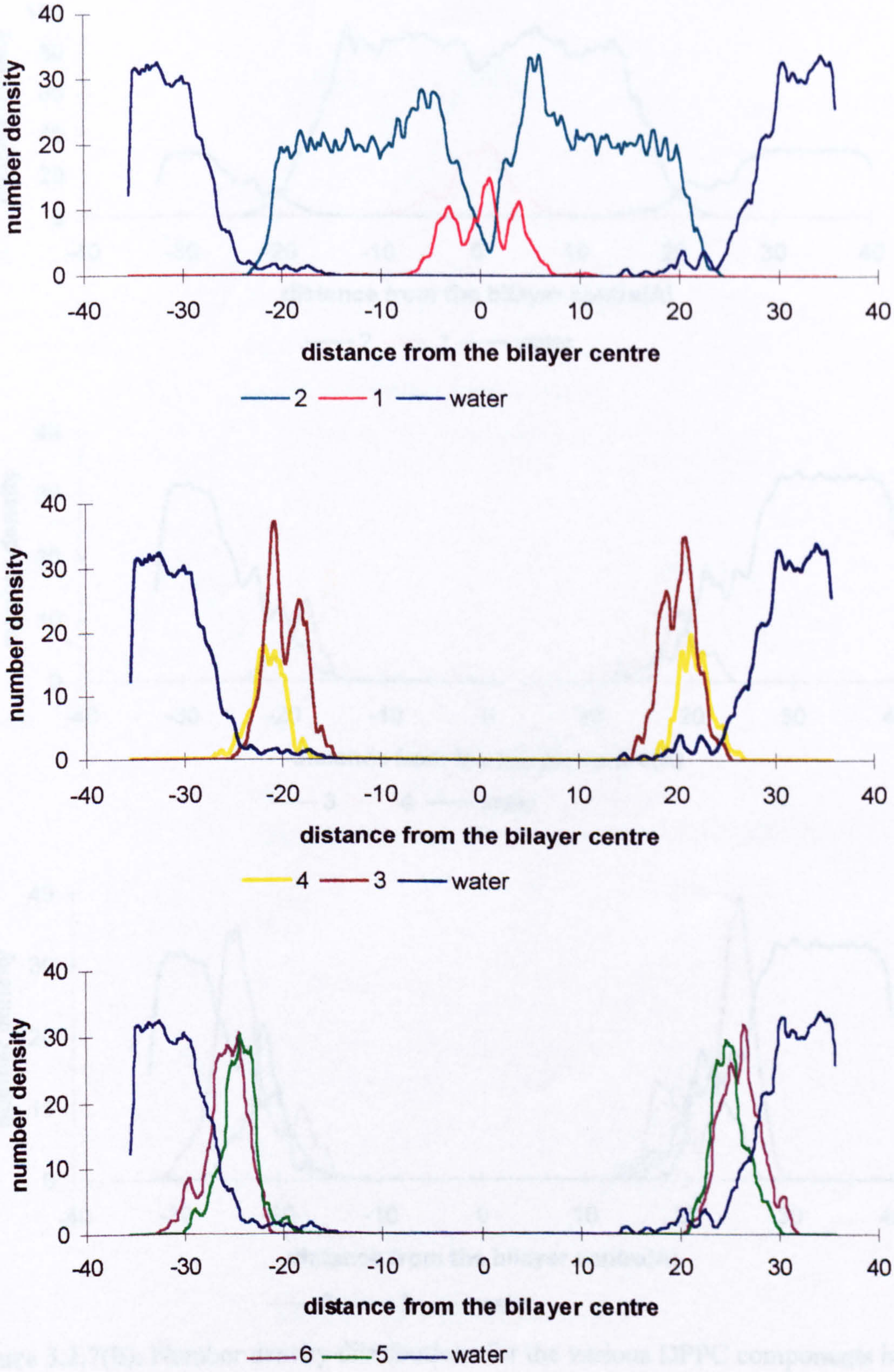

Figure3.2.7(a): Number density distributions for the various DPPC components in the Lβ' bilayer system (DPPC components numbered as shown in Figure 3.2.6).

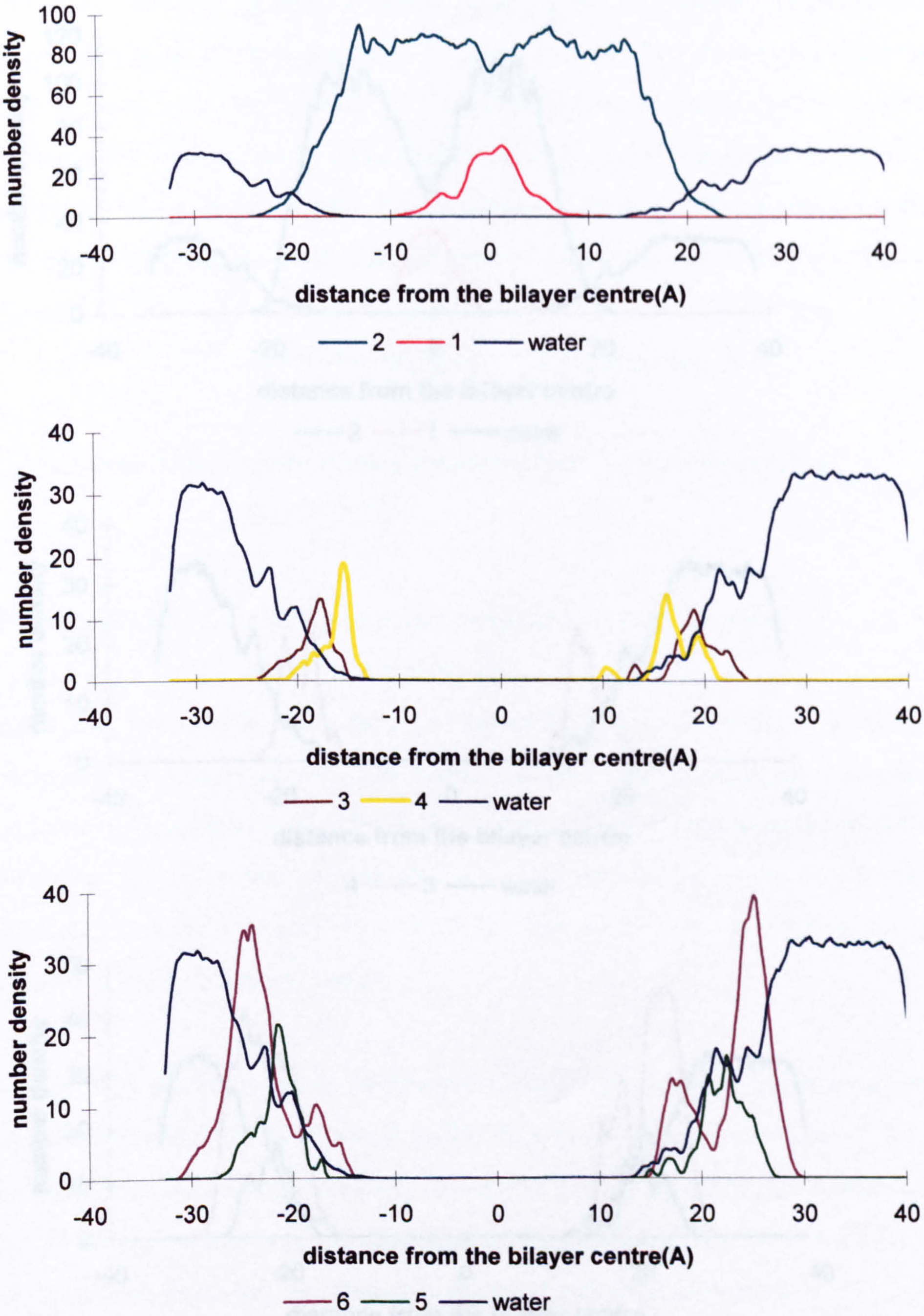

Figure 3.2.7(b): Number density distributions for the various DPPC components in the Lα DPPC AMBER bilayer system (DPPC components numbered as shown in Figure 3.2.6).

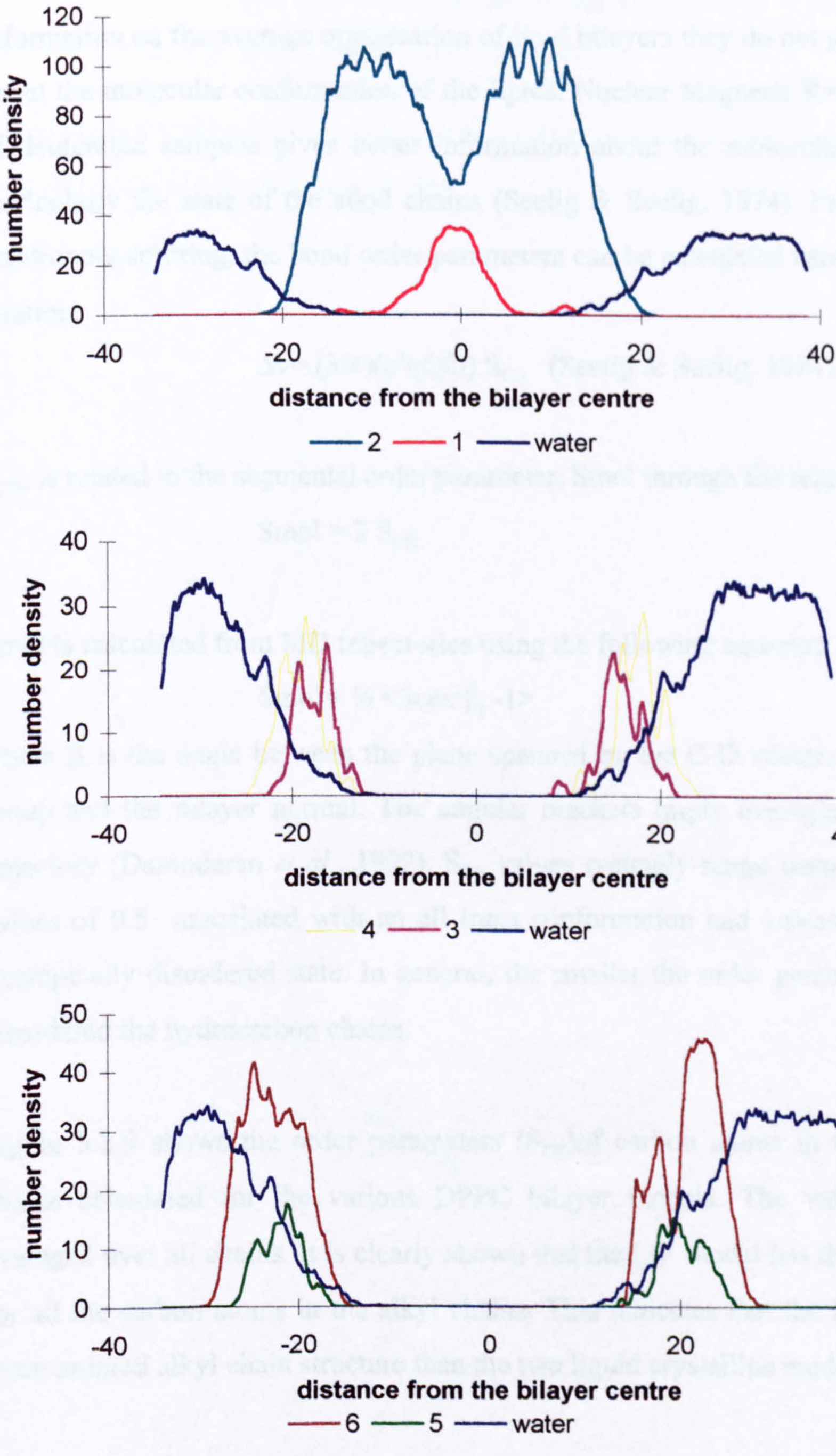

Figure3.2.7(c): Number density distributions for the various DPPC components in the Lα DPPC CHARMm bilayer system (DPPC components numbered as shown in Figure 3.2.6).

3.2.3 Order Parameter

While the electron density obtained from X-ray diffraction studies provides information on the average organisation of lipid bilayers they do not give information about the molecular conformation of the lipids. Nuclear Magnetic Resonance (NMR) of deuterated samples gives better information about the molecular conformation, particularly the state of the alkyl chains (Seelig & Seelig, 1974). From the residual quadrupole splitting, the bond order parameters can be calculated using the following relation:

$$\Delta\nu = (3/4)(e^2qQ/h)\, S_{CD} \quad \text{(Seelig \& Seelig, 1974)}$$

S_{CD}, is related to the segmental order parameter, Smol through the relation;

$$Smol = 2\, S_{CD}$$

Smol is calculated from MD trajectories using the following equation;

$$Smol = \tfrac{1}{2} \langle 3\cos^2\beta_j - 1 \rangle$$

where β_j is the angle between the plane spanned by the C-D vectors of a methylene group and the bilayer normal. The angular brackets imply averaging over the MD trajectory (Damodaran *et al.*, 1992). S_{CD} values typically range from 0.0 to 0.5 with values of 0.5 associated with an all trans conformation and values of 0.0 with an isotropically disordered state. In general, the smaller the order parameters, the more disordered the hydrocarbon chains.

Figure 3.2.9 shows the order parameters (S_{CD})of carbon atoms in the hydrocarbon chains calculated for the various DPPC bilayer models. The values of S_{CD} are averaged over all chains. It is clearly shown that the Lβ' model has the highest values for all the carbon atoms in the alkyl chains. This indicates that the Lβ' model has a more ordered alkyl chain structure than the two liquid crystalline models.

For most of the carbon atoms in the alkyl chains, the Lα-CHARMm model gives lower S_{CD} values compared with the Lα-AMBER model. However, the Lα-AMBER model has lower S_{CD} values for C2 and C15, suggesting that the Lα-AMBER model is more

disordered in the first and the end segments of the alkyl chains while in general Lα-CHARMm is more disordered in the middle segment.

First and the last segments of the alkyl chains while, in general, the Lα-CHARMm model is more disordered in the middle segment.

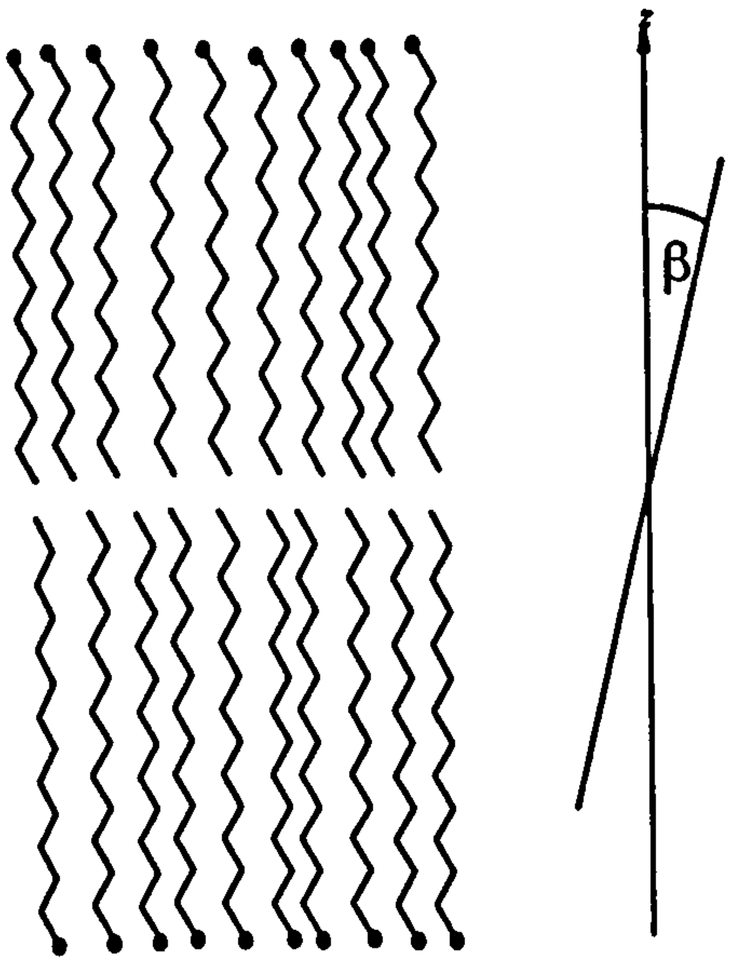

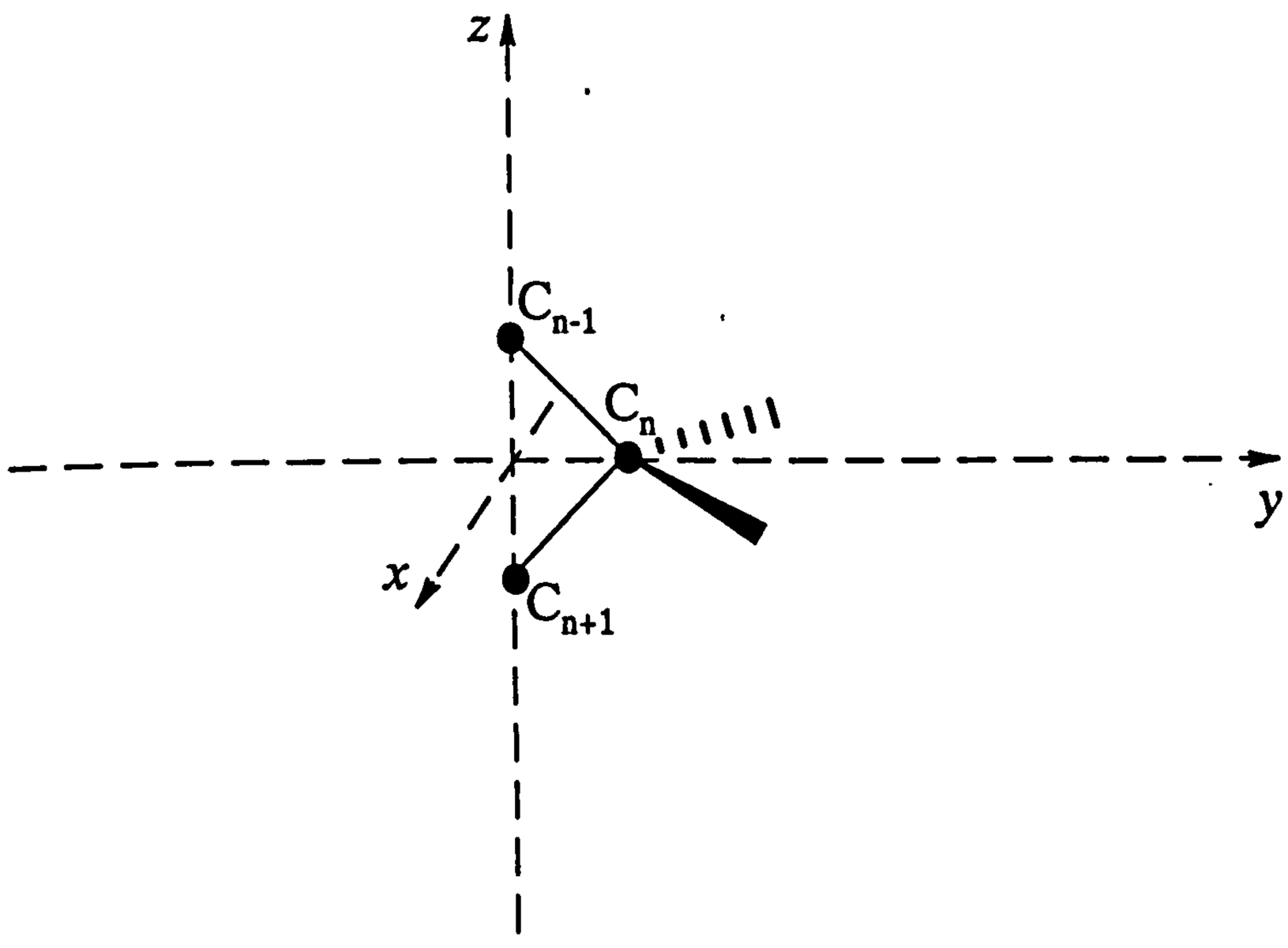

Figure 3.2.8 : Definition of order parameter. β is the angle between the bilayer normal and the vector joining C_{n-1} to C_{n+1} (C-D vector).

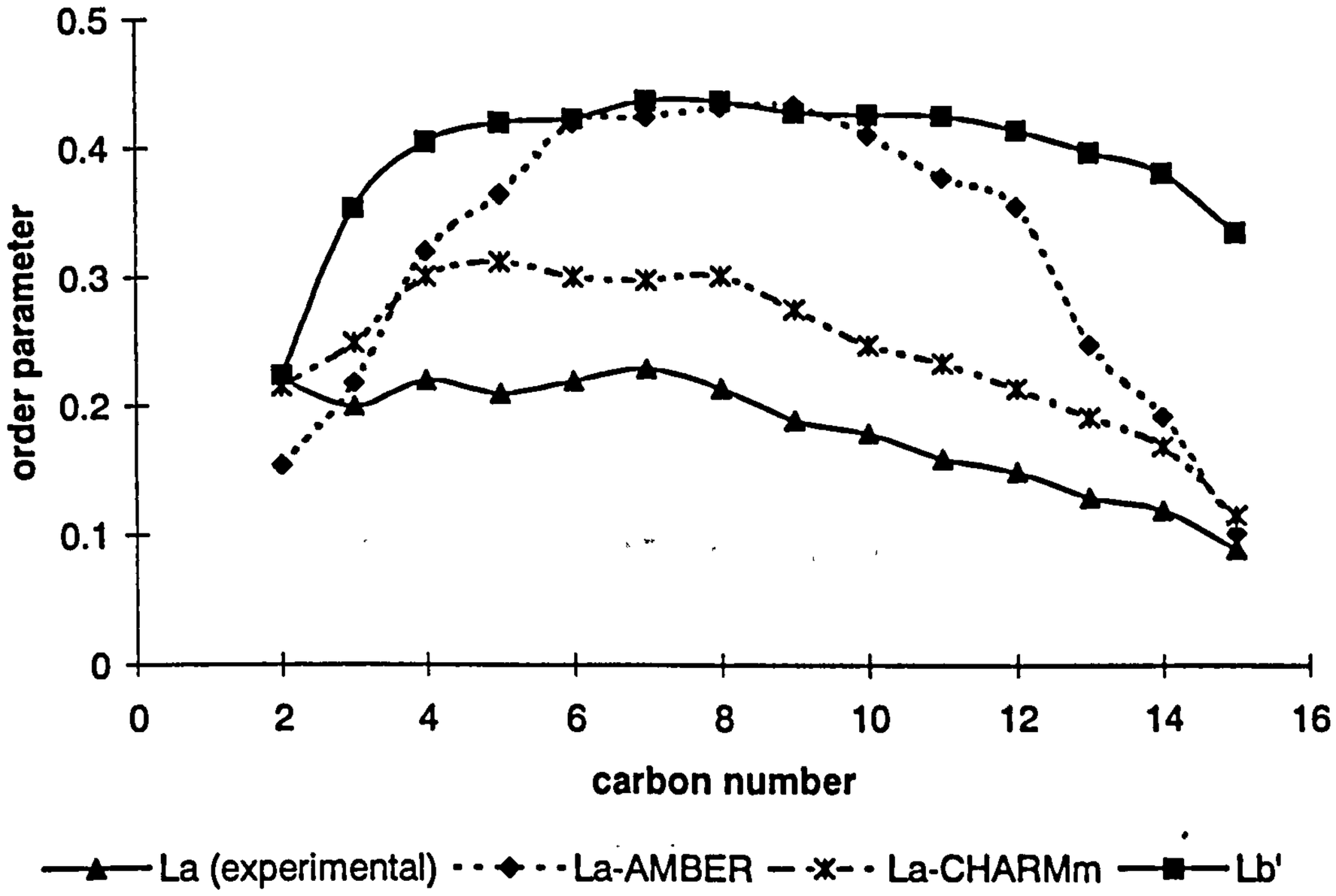

Figure 3.2.9: Order parameter profiles for the DPPC alkyl chains in DPPC bilayers (averaged over both chains).

Both liquid crystalline models show S_{CD} profiles similar to those determined by experiment with the Lα-CHARMm model matching more closely than the Lα-AMBER model.

With the order parameters calculated separately for the DPPC S_{N1} and S_{N2} hydrocarbon chains (Figure 3.2.10). It is found that the S_{N2} chain has lower S_{CD} values than the S_{N1} chain indicating that the S_{N2} chain is just slightly more disordered.

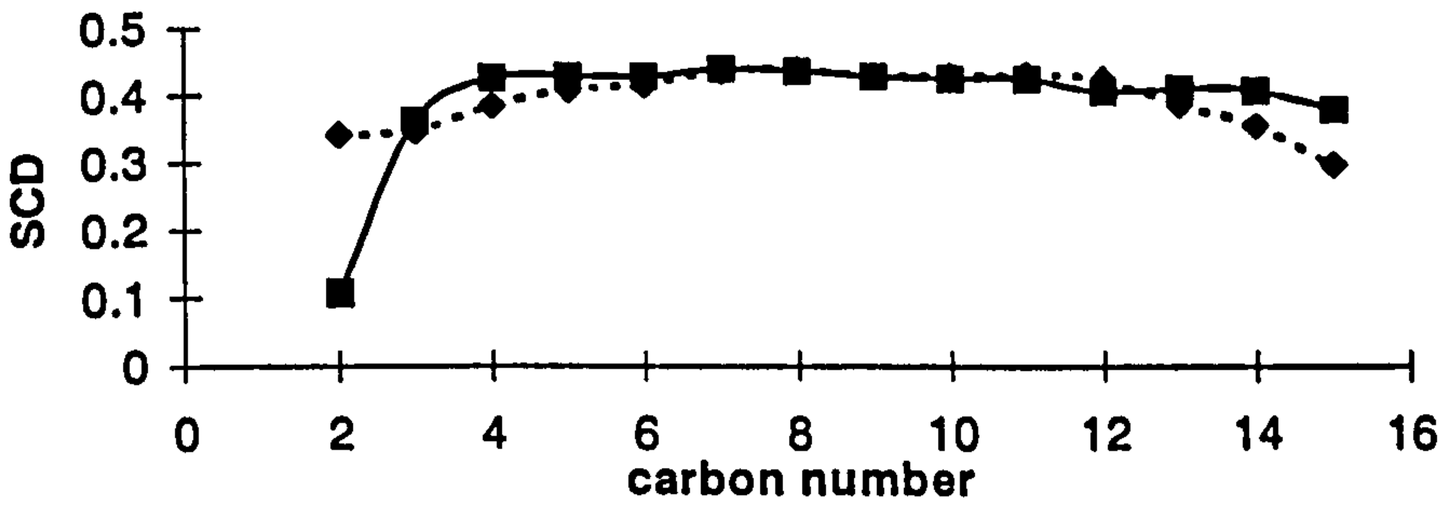

(a) Lβ' model

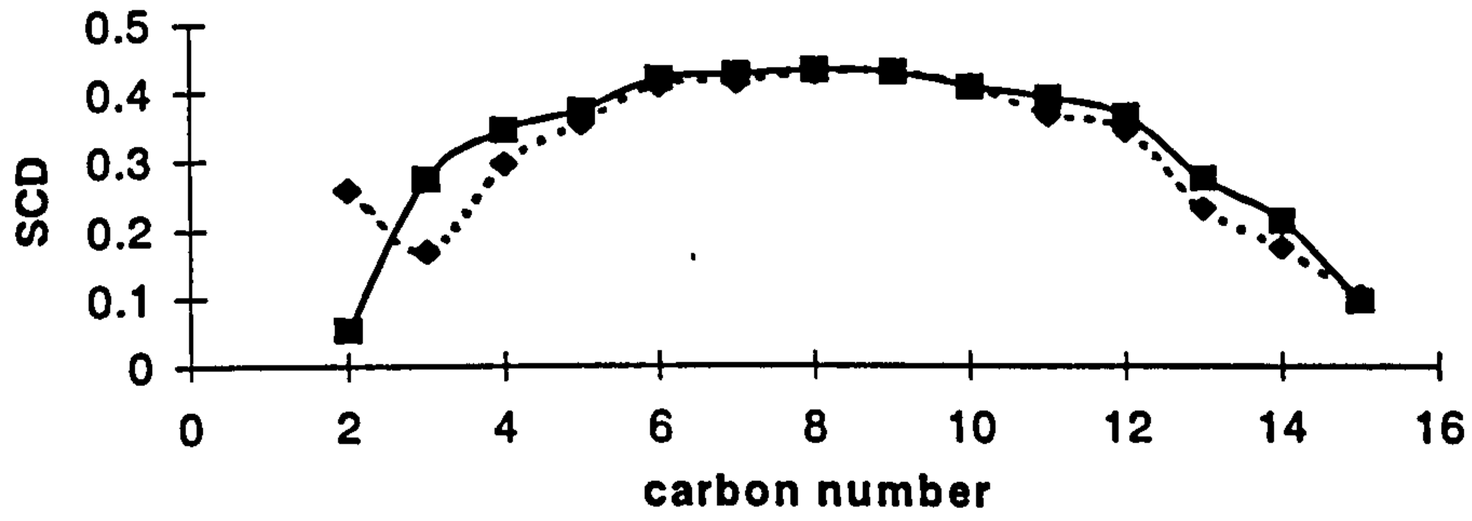

(b) Lα DPPC AMBER model

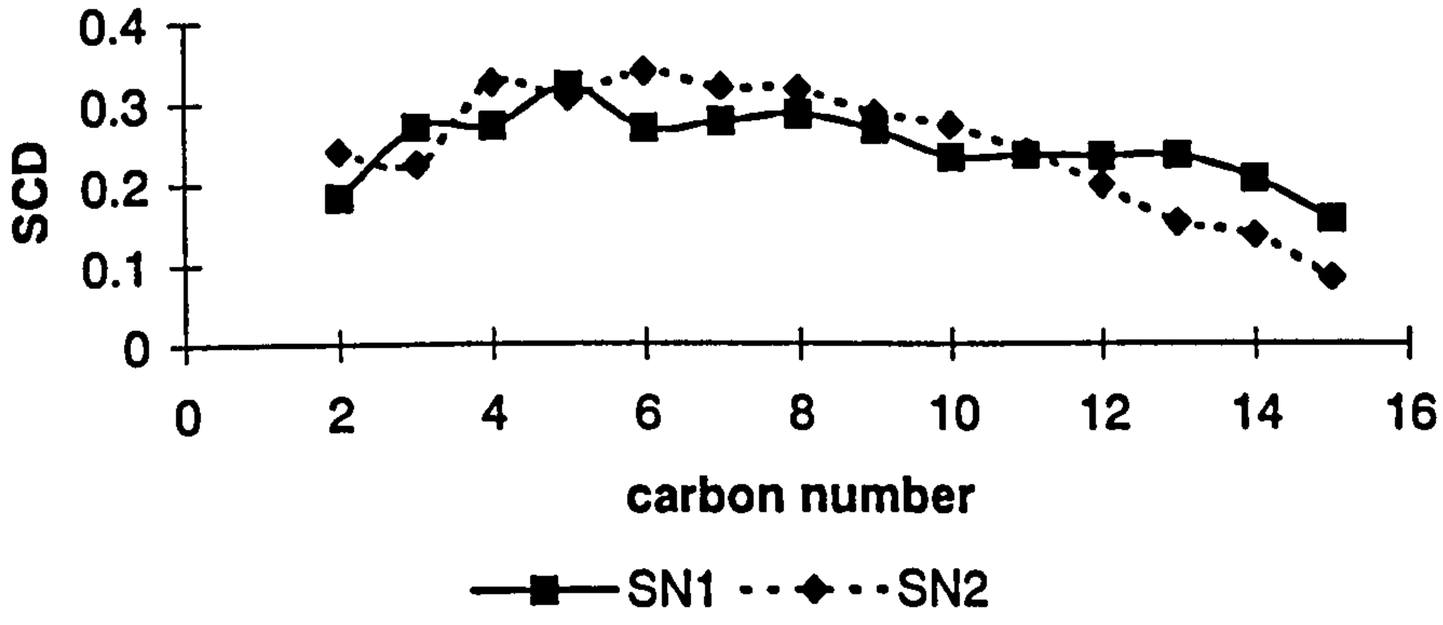

(c) Lα DPPC CHARMm model

Figure 3.2.10 : Order parameter profiles for the DPPC S_{N1} and S_{N2} alkyl chains in various pure DPPC bilayer models.

3.2.4 Hydration of the phosphatidylcholine and acyl ester groups

The extent of hydration of the lipid atoms was investigated by calculating the radial distribution functions [g(r)] which were obtained as:

$$g(r) = N(r)/(4\pi r^2 \delta r \rho_o)$$

where N(r) is the number of water molecules between r and r + δr Å from the reference atom. ρ_o is the water number density taken as 1g/cm^3. The g(r) for the choline nitrogen and carbonyl carbon atoms, phosphate phosphorous and oxygen atoms with respect to the water oxygen (OW) were calculated. Figure 3.2.11 shows the g(r) plots for the choline nitrogen and phosphate phosphorous atoms with respect to the water oxygen.

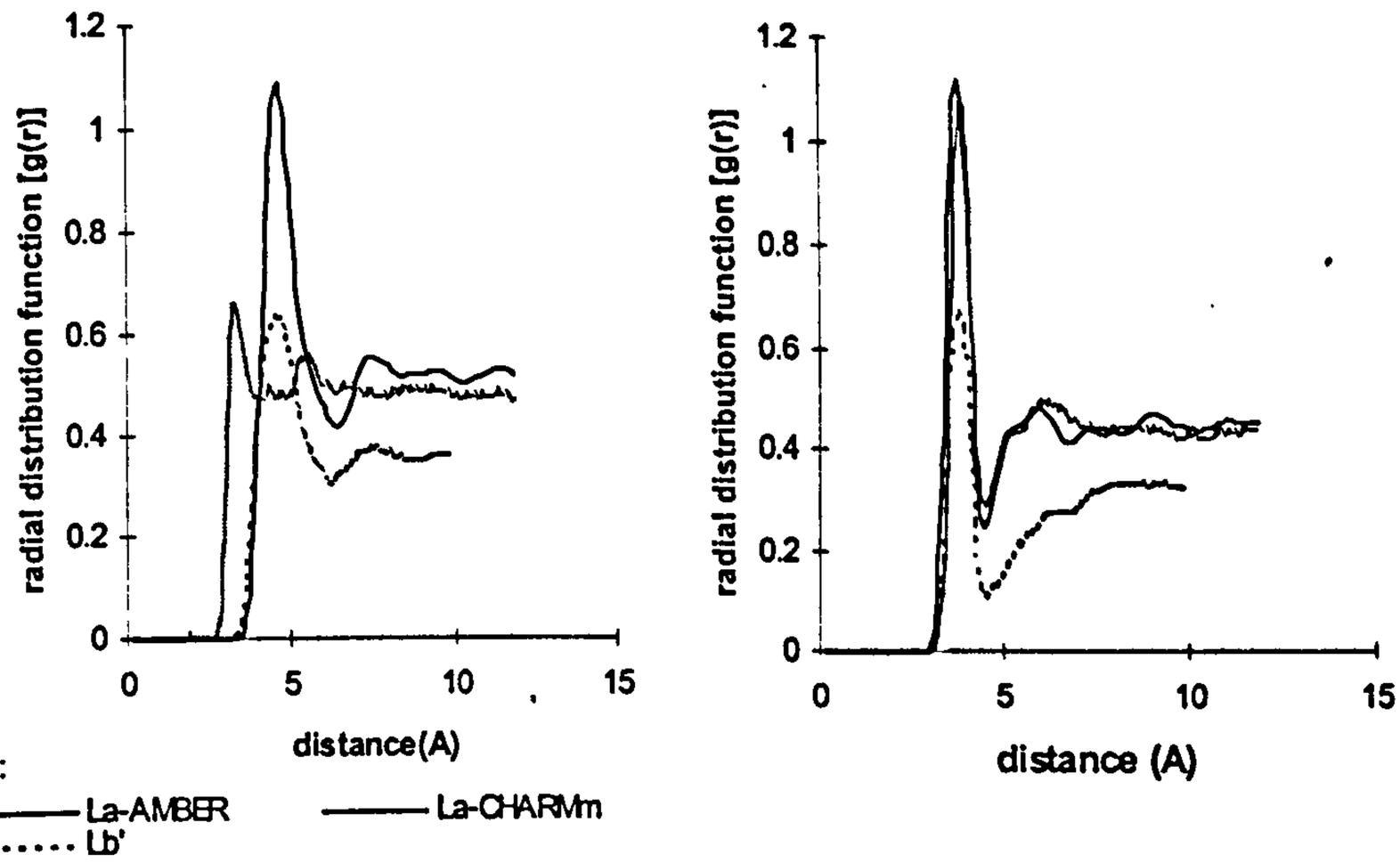

(a) (b)

Figure 3.2.11 : Radial distribution functions for the DPPC (a) choline-nitrogen, and (b) phosphate-phosphorus calculated with respect to the water oxygen.

An atom is considered 'hydrated' if a well-defined first neighbour peak is present in the g(r) for the atom when calculated with respect to OW (Egbert, 1988). Except for the carbonyl oxygen on the SN1 chain (O7), the rest of the atoms studied appear to be hydrated. The extent of hydration of the DPPC molecule (calculated as the coordination number of OW) is evident from Table 3.2.3, where it is seen that water penetrates as far as the lipid carbonyl groups in all three models, a result which agrees with the observation made in consideration of the number density profiles.

Table 3.2.3: Hydration of the phosphatidylcholine head groups and the acyl ester groups

radial distribution function	*Hydration Level(*coordination number)*		
	AMBER	CHARMm	GEL
C1-OW	4.426(4.35)	4.774(4.35)	4.406(4.65)
C2-OW	5.840(4.65)	6.427(4.8)	3.740(4.5)
C3-OW	5.070(4.5)	4.881(4.5)	4.811(4.5)
N-OW	19.17(6.45)	18.06(6.45)*	11.90(6.15)
O1-OW	10.74(5.55)	10.40(5.55)	5.072(5.4)
O2-OW	2.642(3.45)	2.033(3.3)	1.612(3.15)
O3-OW	2.216(3.3)	1.766(3.3)	1.552(3.15)
O4-OW	0.797(3.45)	0.889(3.45)	0.368(3.6)
P-OW	5.636(4.5)	5.132(4.5)	3.236(4.5)
C11-OW	2.620(4.35)	2.206(4.35)	0.512(4.5)
C31-OW	1.392(4.35)	1.026(4.2)	0.258(4.35)
O5-OW	0.636(3.6)	0.601(3.6)	0.140(3.45)
O6-OW	0.161(3.35)	1.106(3.45)	0.183(3.3)
O7-OW	0.366(3.3)	No clear minimum	No clear minimum
O8-OW	0.746(3.45)	0.818(3.6)	0.1983

Note

The numbers in parenthesis give the locations (in Å) of the first minimum in the radial distribution function. In most cases there is a clear first minimum.

- The coordination number was calculated as the average number of water oxygen atoms whose distance lies in the interval of (r, r+δr) from a given lipid atom and this is given by the following formula:
    - $N(r) = nrdo / (nlip*nsdrf)$ where

N(r) is the coordination number of the water oxygen atoms, nrdo is number of water oxygen - lipid atom pairs, nlip is the number of lipid molecules and nsrdf is the number of frames in the simulation runs where rdf are accumulated. From this, g(r) can be calculated using the equation :

$$g(r) = N(r) /(4\pi r^2 \delta r \rho_o)$$

- the program for this calculation is described in Appendix 7. g(r) and N(r) are the direct outputs of the program.

plots for the same atom sometimes vary from one model to another (see Table 3.2.3 and Figure 3.2.11). In general, however, it is clear that the Lβ' model appears to be less hydrated than the Lα-models. The results also show that atoms nearest to the alkyl chain appear to be less hydrated than the ones near the headgroup/water interface. Another way to measure the extent of hydration is by calculating the amount of bound water in the system. It was found that approximately 196, 336 and 368 water molecules bind to the DPPC headgroups in the Lβ', Lα-AMBER and Lα-CHARMm models, respectively. These represent about 35.5%, 37.75% and 40% of the water present in the Lβ', Lα-AMBER and Lα-CHARMm models, respectively. There are therefore, more bound water molecules in the Lα-CHARMm model compared with the Lα-AMBER model, and both of the liquid crystalline models are more hydrated than the Lβ'.

3.2.5 Diffusion constants of DPPC and water molecules

Another aspect of the dynamics of the DPPC bilayer system which has been investigated was , the diffusion of water and DPPC molecules in the systems. The diffusion of the molecules was calculated as the mean squared displacement (MSD) of the centres of mass of the molecules using the formula:

$$MSD(t) = \langle |r(t) - r(0)|^2 \rangle$$

where r( ) represent the coordinates referred to the centre of mass of the molecule of interest, with the angular brackets indicating an averaging over the entire MD trajectory. The diffusion constants were obtained from the slopes at the long time region of the MSD vs. t plot (as examplified by Figure 3.2.12):

$$D = 1/6(\Delta MSD/\Delta t) \qquad \text{(Allen \& Tildesley, 1987)}$$

Our results for the water diffusion constants in the three systems are almost the same, (Table 3.1.13). The values are higher than those determined by experiment (2.5×10^{-5} cm²/s) and the simulated TIP3P water (3.98×10^{-5}cm²/s) (van der Spoel et al., 1998 and the refernces therein).

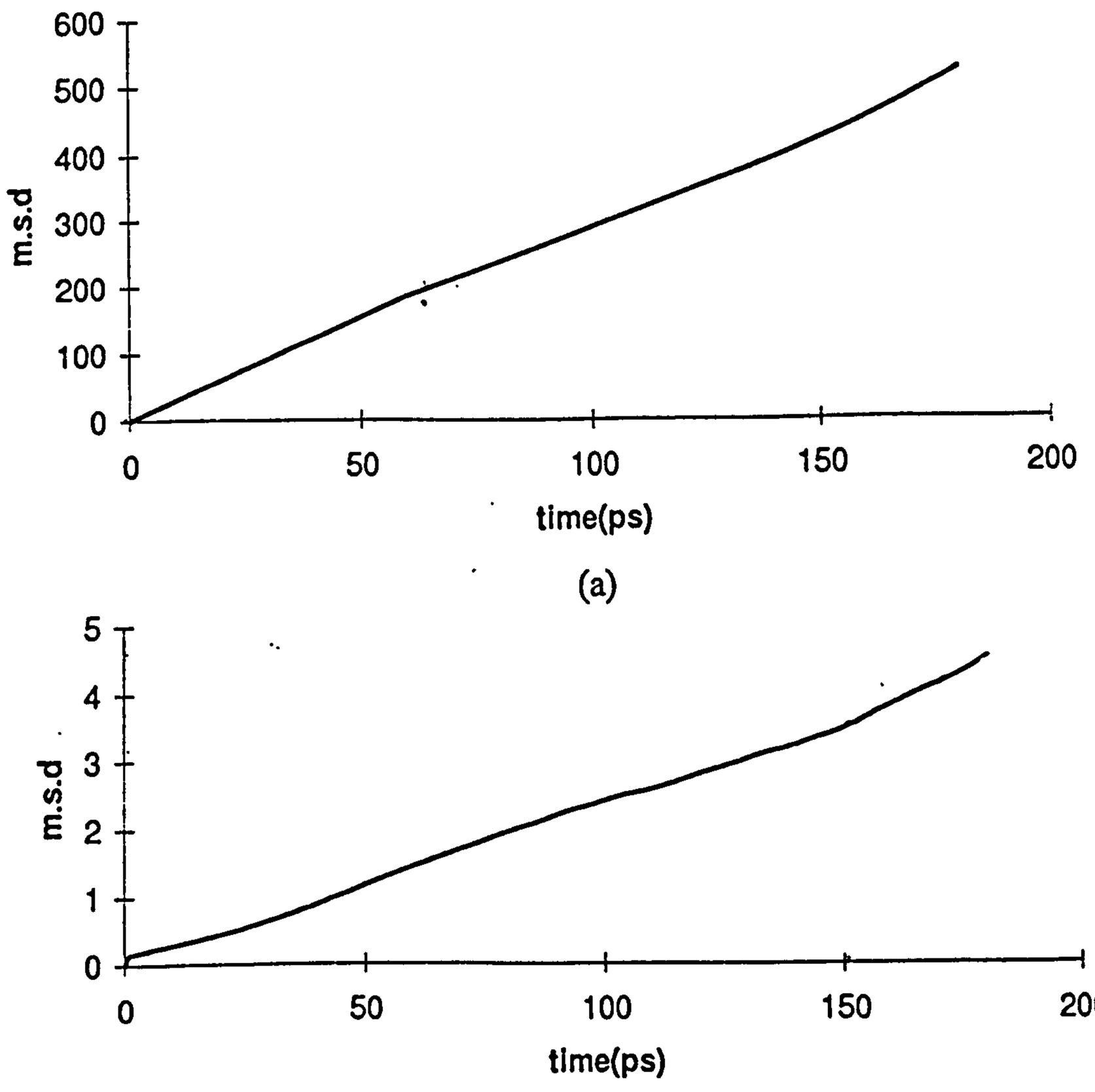

Figure 3.2.12 MSD plot vs time for the (a) water and (b) lipid molecules in the La-DPPC AMBER model. Time t=0, refers to the time after equilibrium is achieved (equilibrium was monitored as in Appendix 6).

These calculated values do not distinguish between bulk and bound water. If one assumes that there is a considerably large amount of bound water in the system, then it would be expected that the values should be lower than those calculated for pure water. The fact that our diffusion constants are higher than the values calculated for the pure water, is probably due to the higher simulation temperature (50°C for Lα and 25°C for Lβ vs. 25°C for TIP3P water).

Table 3.2.4 : Calculated diffusion constants for water and DPPC molecules in the simulated models

Bilayer Model	Diffusion constant	
	Waters ($x\ 10^{-5}cm^2/s$)	DPPC ($x10^{-7}cm^2/s$)
Lβ'	4.27	3.55
Lα-AMBER	5	4.79
Lα-CHARMm	4.83	9.03

The calculated diffusion constants for the lipid are $3.55x10^{-7}cm^2/s$, $4.79x10^{-7}cm^2/s$, and $9.03\ x10^{-7}cm^2/s$ for Lβ', Lα-AMBER and Lα–CHARMm models, respectively. In general, there is no significant difference in the lateral diffusion of phospholipids with different polar headgroups. The experimental values for the lipid diffusion constants are about $10^{-8}\ cm^2/s$ for the Lα phase and $10^{-10}cm^2/s$ for the Lβ phase in pure phospholipid multilayers or large unilamellar vesicles (Gennis, 1989). The calculated values in the simulations are thus much larger than the cited experimental values but, are consistent with the values calculated in other MD results (Egbert, *et al.*, 1994, Essex *et al.*, 1994).

Experimental observations show that the rate of lipid lateral diffusion reduces by more than two orders of magnitude in the transition from an Lα to a gel phases (Gennis, 1989). Even though this scale of reduction was not observed in our MD simulations, it was found that the lipid diffusion constant was lower for Lβ' model compared with the two crystalline models (about 25 times lower in the case of the Lα–CHARMm model and just slightly lower in the case of Lα-AMBER). It is interesting to note here

thus much larger than the cited experimental values but, are consistent with the values calculated in other MD results (Egbert, *et al.*, 1994, Robinson *et al.*, 1994).

Experimental observations show that the rate of lipid lateral diffusion reduces by more than two orders of magnitude in the transition from an Lα to a gel phases (Gennis, 1989). Even though this scale of reduction was not observed in our MD simulations, it was found that the lipid diffusion constant was lower for Lβ' model compared with the two crystalline models (about 25 times lower in the case of the Lα–CHARMm model and just slightly lower in the case of Lα-AMBER). It is interesting to note here lipid diffusion constant calculated for the Lα–CHARMm model is about twice that calculated for the Lα-AMBER model indicating that the former system is much more fluid.

3.3 MD OF DPPC/WATER BILAYER CONTAINING AZONE

In this section, the results of the two MD simulations for DPPC bilayers containing Azone are presented, and comparisons made with the results obtained for the Lα-AMBER model.

For convinience, the MD model of the DPPC bilayer incorporating two Azone molecules in one monolayer of the bilayer is referred to as the 2Azone-DPPC model, and the same system incorporating two Azone molecules in each of the DPPC monolayers is referred to as the 4Azone-DPPC model.

3.3.1 Electron Density Profile

Figure 3.3.1 shows the electron density profiles calculated for the Lα-AMBER, 2Azone- and 4Azone-DPPC bilayer systems. In general there is not much difference in the profiles among the three systems. The peak-to-peak distances in the profiles are about 43Å and 42Å for the 2Azone- and the 4Azone-DPPC bilayer models respectively. The corresponding distance in the Lα-AMBER model is ~44Å, and it appears, therefore, that there is a slight decrease in the bilayer thickness in the systems containing Azone.

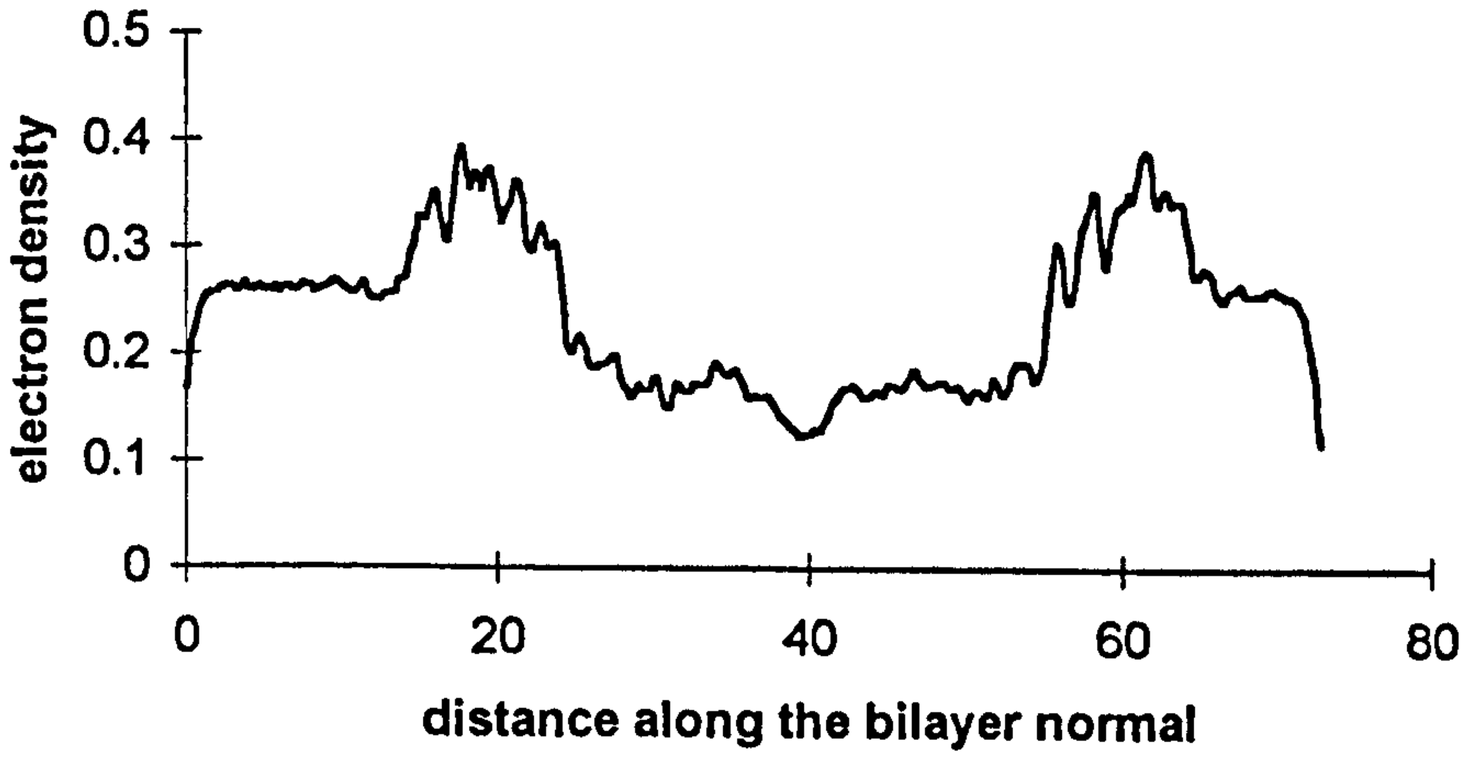

a) Lα-AMBER bilayer

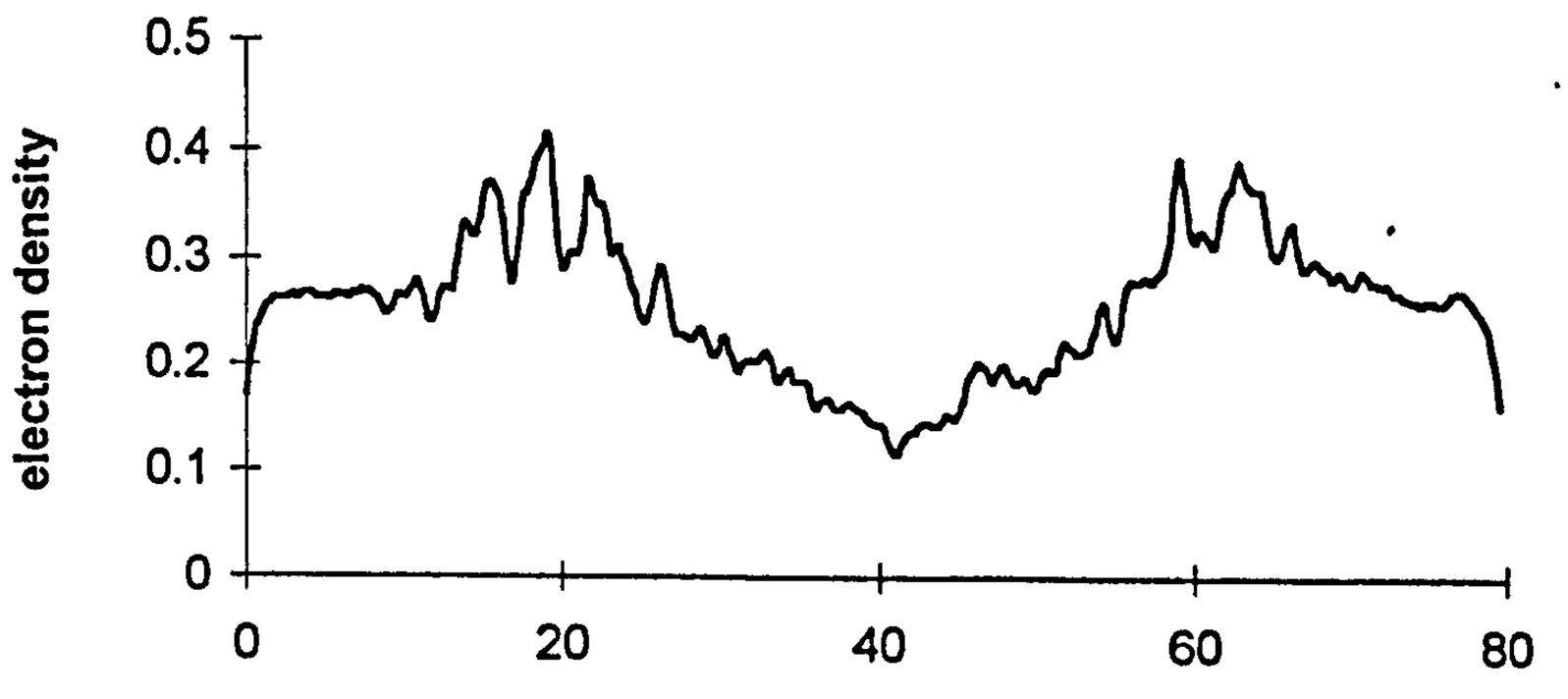

b) 2Azone-DPPC bilayer

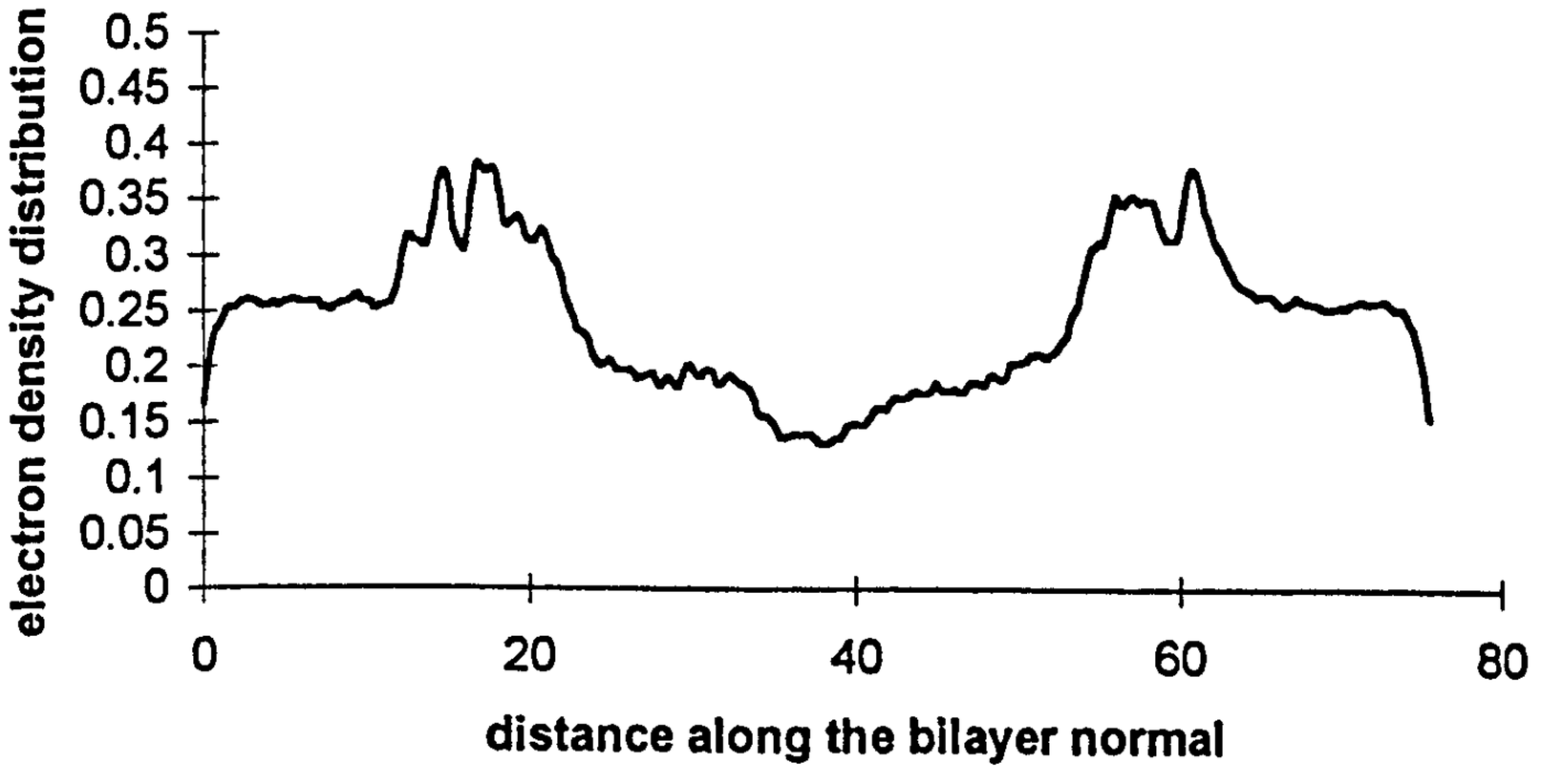

b) 4Azone-DPPC bilayer

Figure 3.3.1: The total electron density profiles for the Lα-AMBER, 2Azone-DPPC and 4Azone-DPPC models.

3.3.2 Number Density Distribution

Figures 3.3.2 and 3.3.3 show the time-averaged number density distributions calculated for the different DPPC structural fragments along the bilayer normal (X-axes). Those shown in Figure 3.3.2(a) and 3.3.3(a), are the profiles of DPPC, Azone and water molecules distributions. These data show that the Azone molecules are confined within the lipid bilayer, spanning a region of ~20 Å thick, lying mostly in one of the DPPC monolayers but with some parts of the molecule penetrating into the adjacent monolayer.

With the distribution profile for the Azone molecules deconvulated to show the separate contributions from their chains and headgroups, the locations of these groups were determined in relation to the various DPPC fragments defined in Figure 3.2.9 (see Figures 3.3.2 (c)-(f)). It was found that the hydrocarbon chains of the Azone molecules cover a region ~18Å thick in the 2Azone-DPPC model and a region ~38Å thick in the 4Azone-DPPC model. It was also observed that there was a bimodal distribution for the Azone headgroups in the 2Azone-DPPC and a unimodal distribution for these groups in the 4Azones-DPPC bilayer. In both cases the peak(s) in the headgroup distribution(s) lie essentially about 10-20 Å from the bilayer centre, with the Azone's headgroups located slightly more deeply in the bilayer than the DPPC headgroups.

These density profiles were also used to determine the influence of the Azone molecules on the distributions of the lipid segments. The Azone molecules effectively increase the widths of the distributions of the methyl, methylene, glycerol, ester, choline and phosphate groups of the lipid, resulting in a more disordered bilayer structure.

The number density profiles were also examined critically to study the effect of Azone on the penetration of water into the bilayer. It is interesting to note that the presence of the Azone molecule caused the water to penetrate deeper into the

bilayer than was seen in the pure DPPC bilayer, penetrating to depths of about 10Å and 12Å from the bilayer centre in the 2-Azone-DPPC bilayer and 4Azones-DPPC bilayer, respectively. It was also observed that the water distribution peaks at a location corresponding to the position of the choline and phosphate groups in the bilayer, and further investigation revealed that in the 2Azone-DPPC model there are also peaks in the water density profile in the locations corresponding to the mid-points of the distributions for the nitrogen and oxygen atoms of the Azone headgroups. This behaviour, however, is not apparent in the 4Azone-DPPC bilayer model.

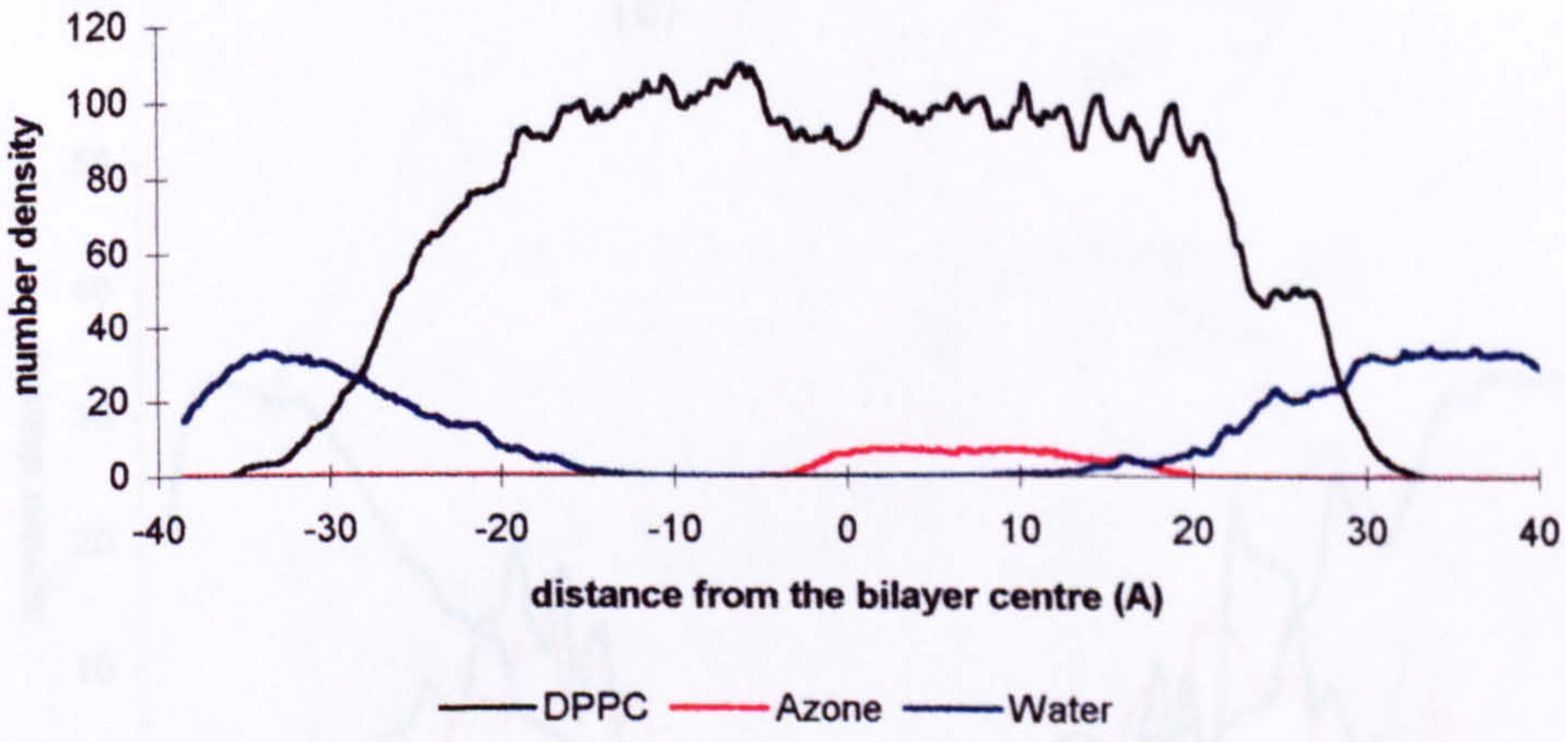

(a)

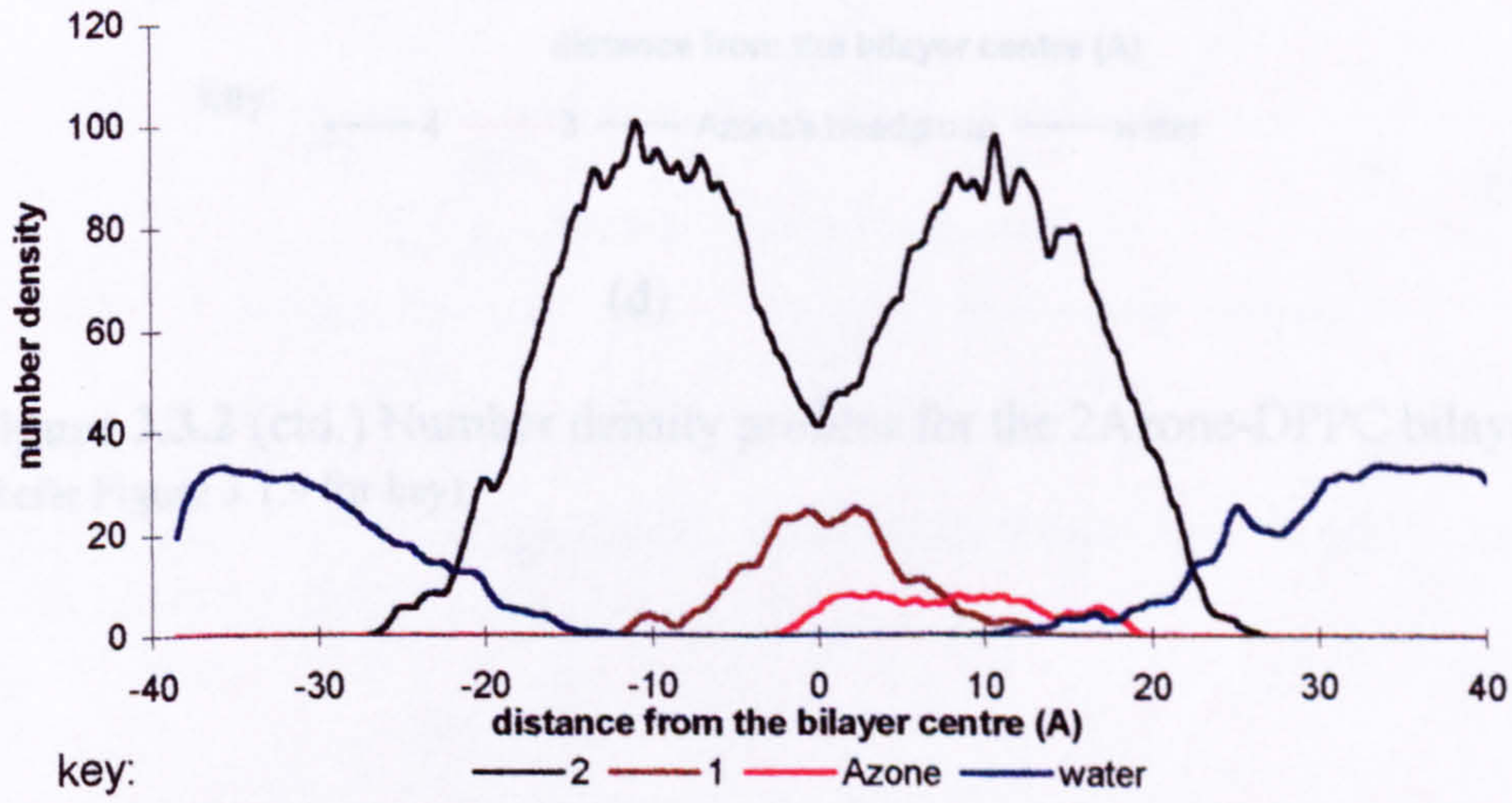

(b)

Figure 3.3.2 Number density profiles for the 2Azone-DPPC bilayer model (Refer Figure 3.1.9 for key).

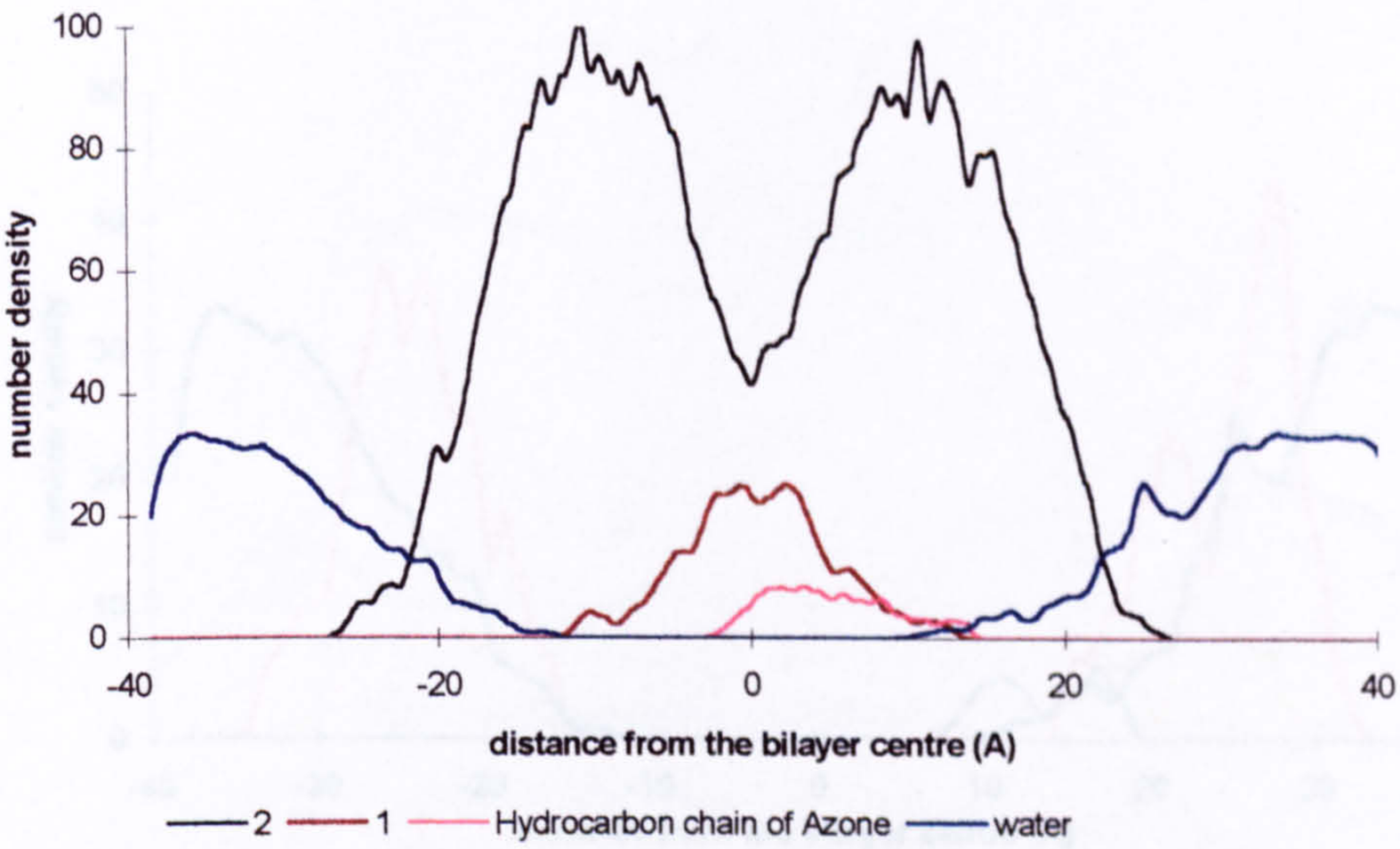

(c)

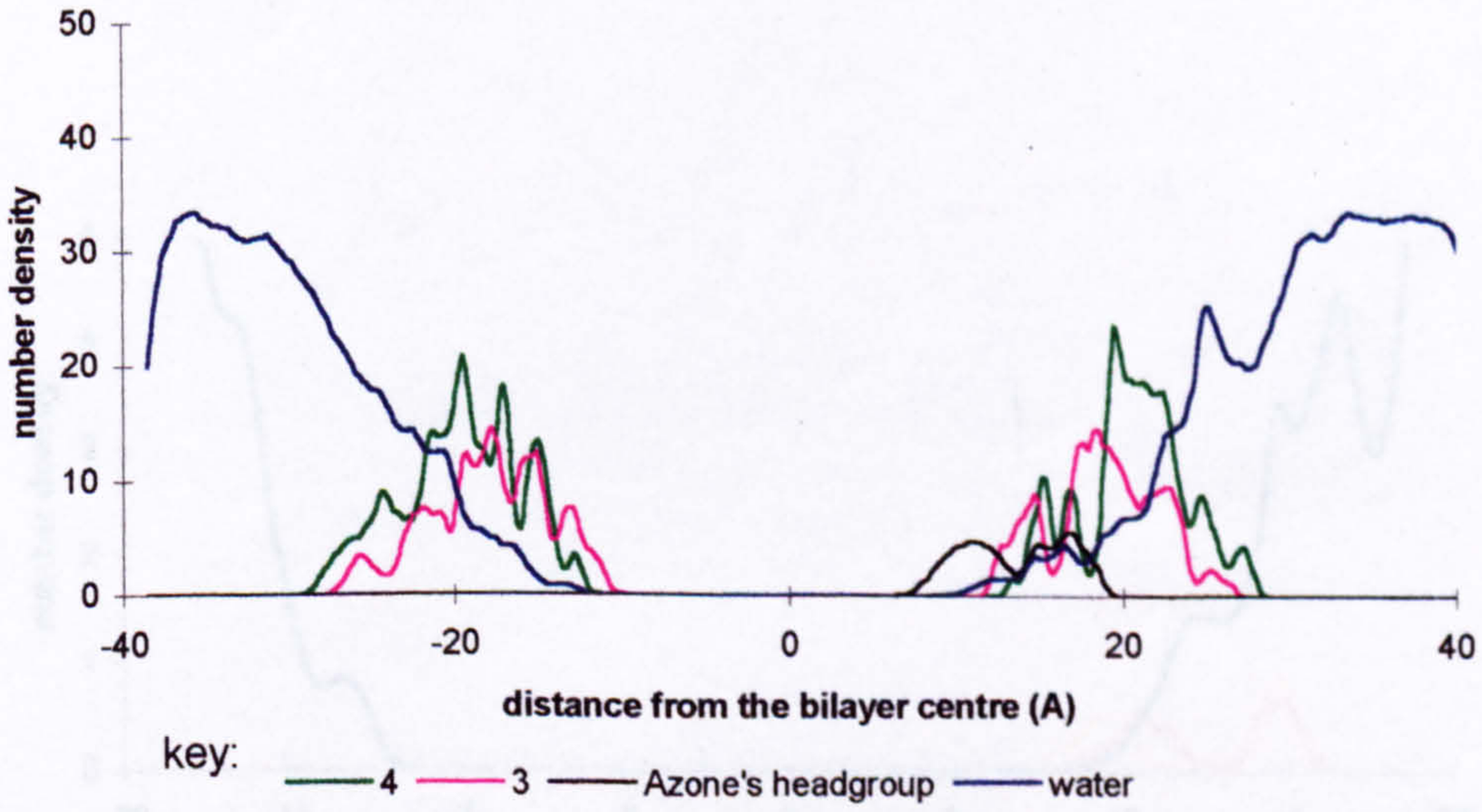

(d)

Figure 3.3.2 (ctd.) Number density profiles for the 2Azone-DPPC bilayer model (Refer Figure 3.1.9 for key).

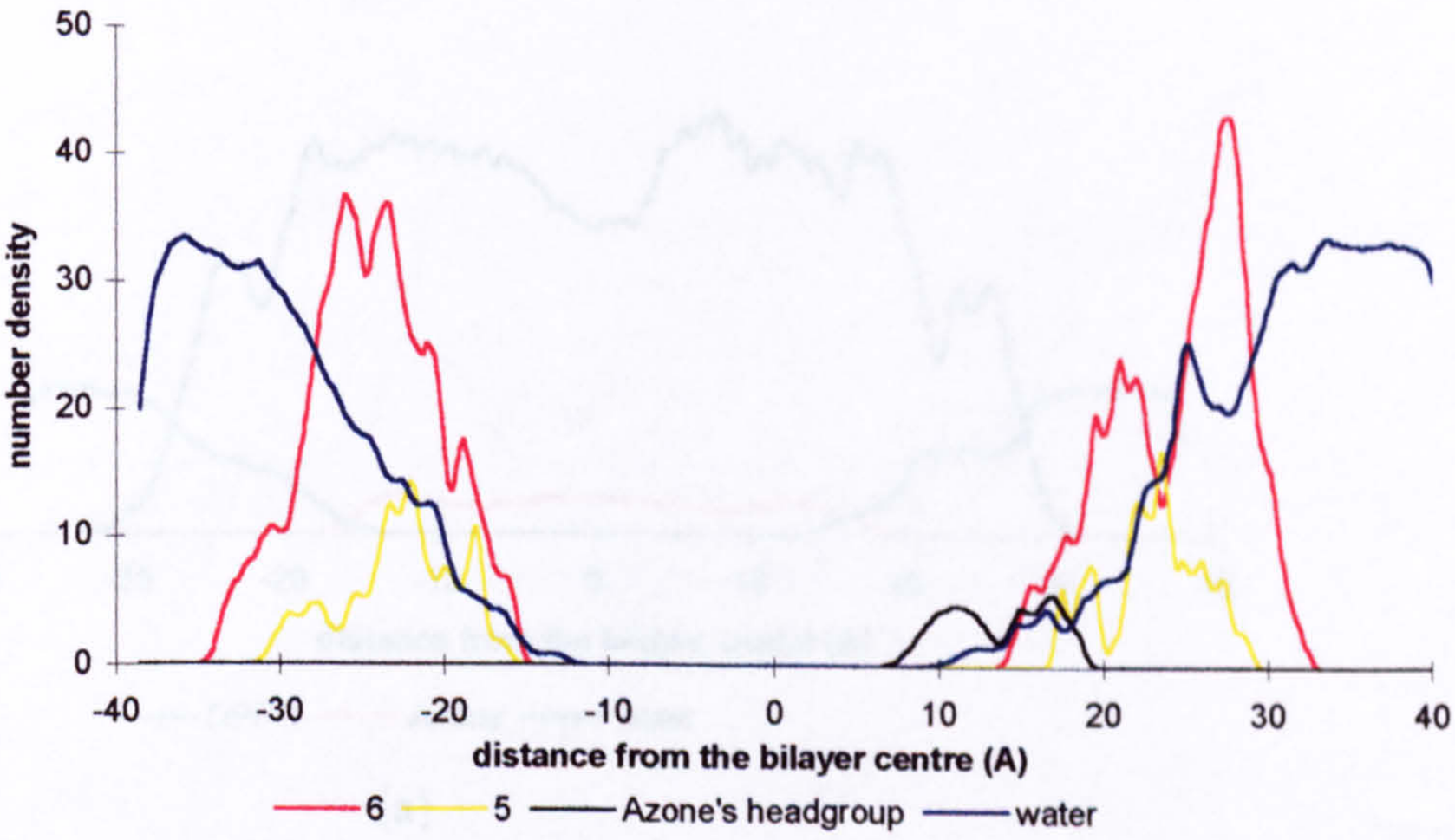

(e)

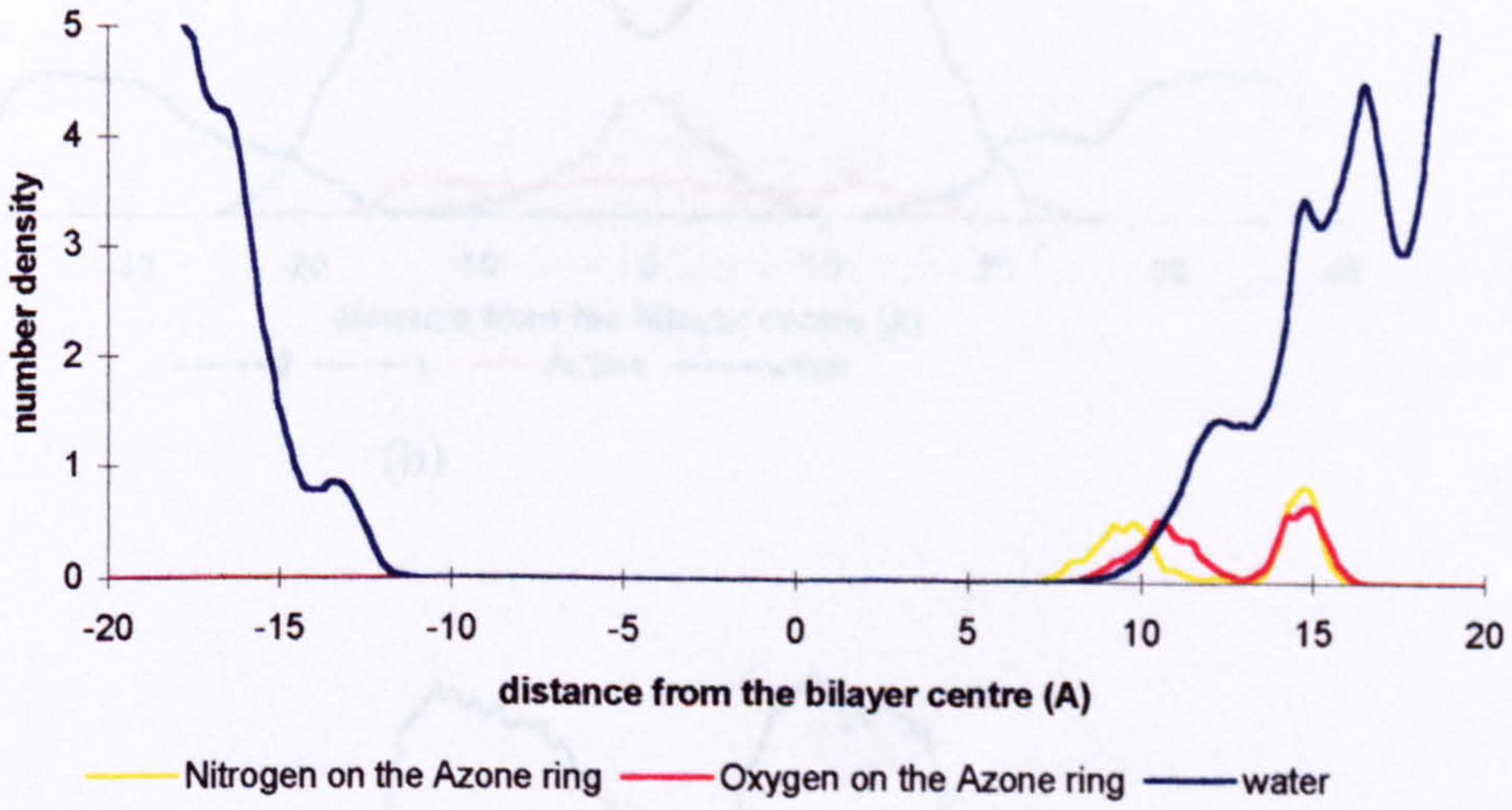

(f)

Figure 3.3.2 (ctd.) Number density profiles for the 2Azone-DPPC bilayer model (Refer Figure 3.1.9 for key).

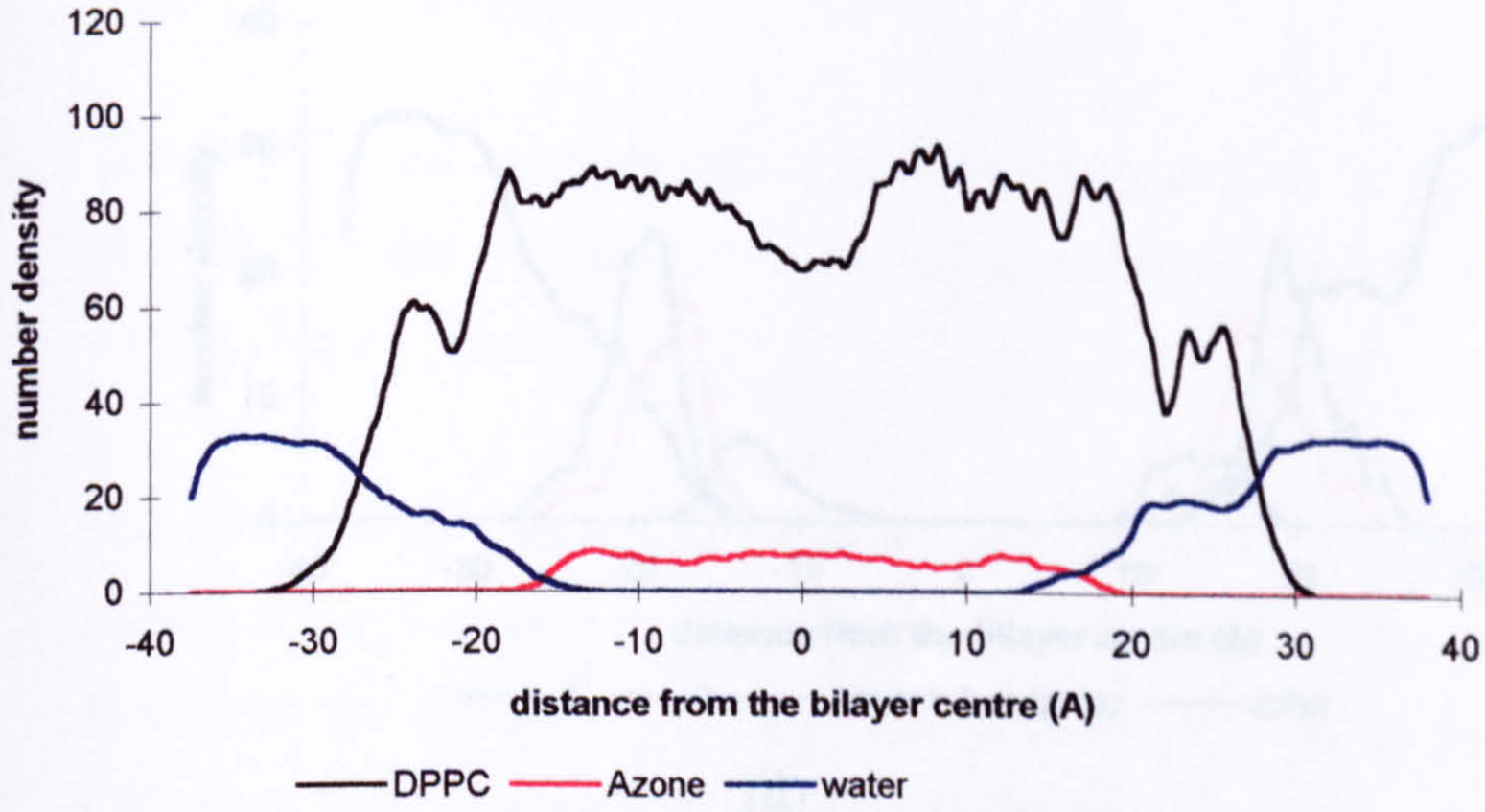

(a)

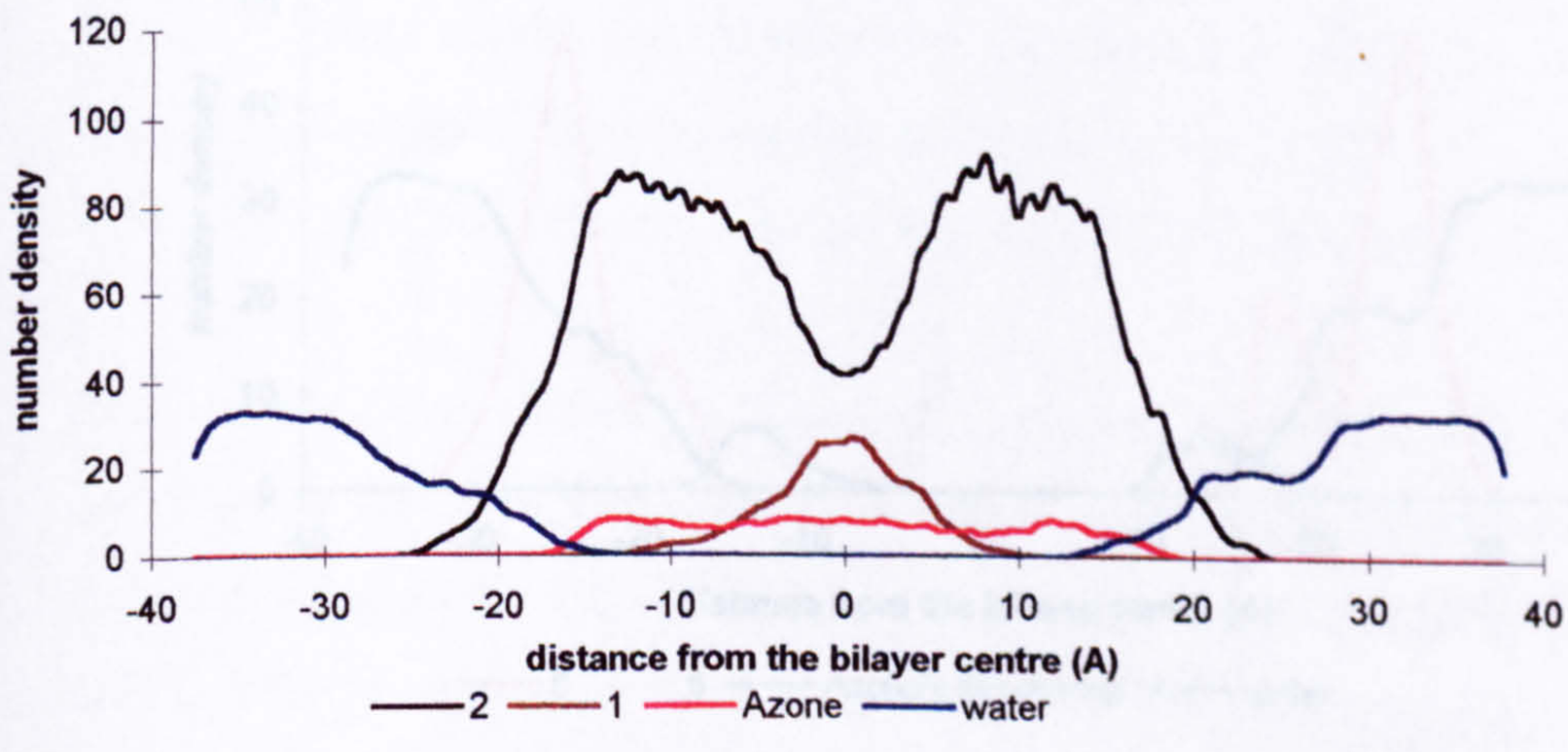

(b)

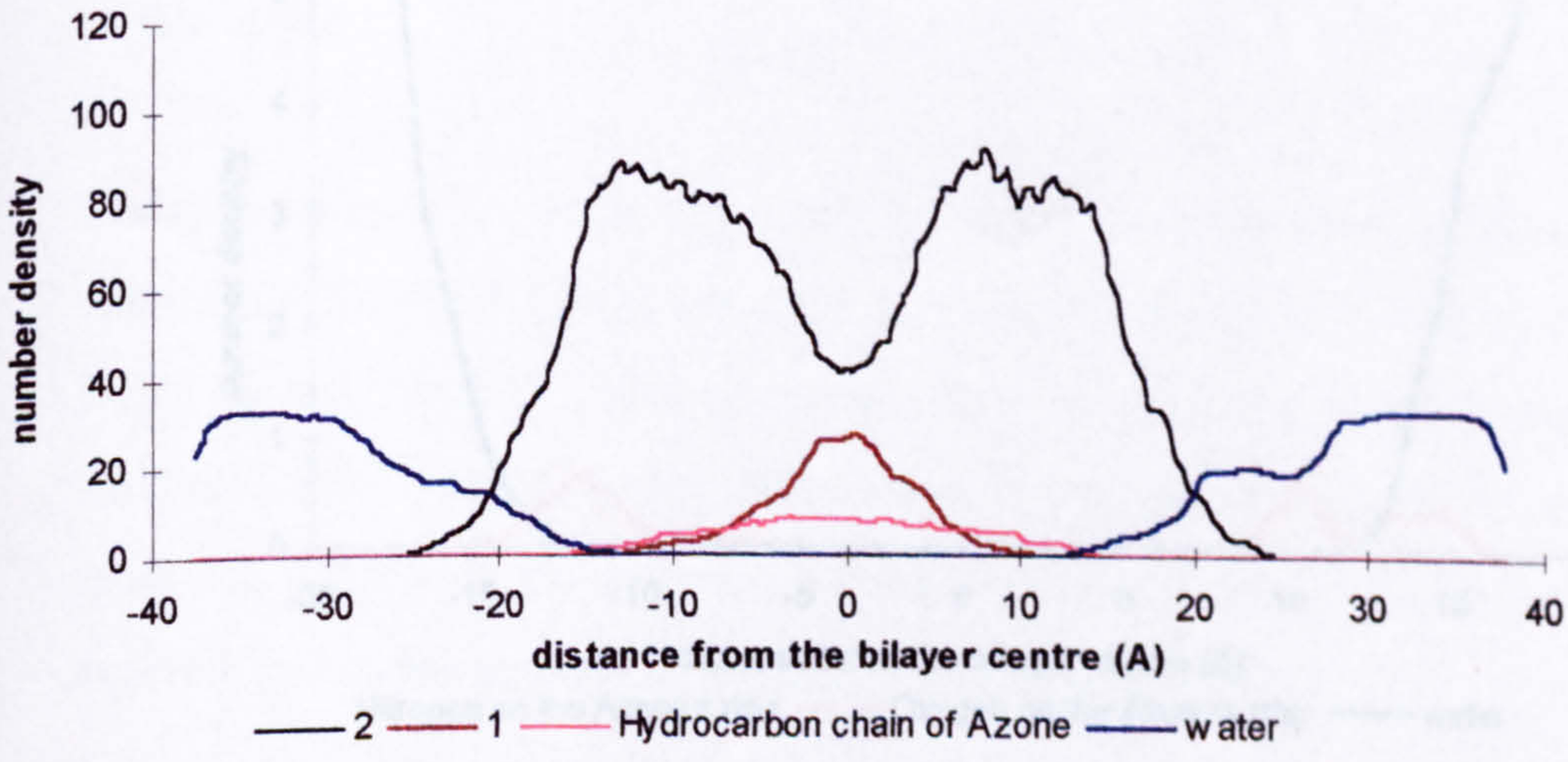

(c)

Figure 3.3.3 Number density profiles for the 4Azone-DPPC bilayer model (Refer Figure 3.1.9 for key).

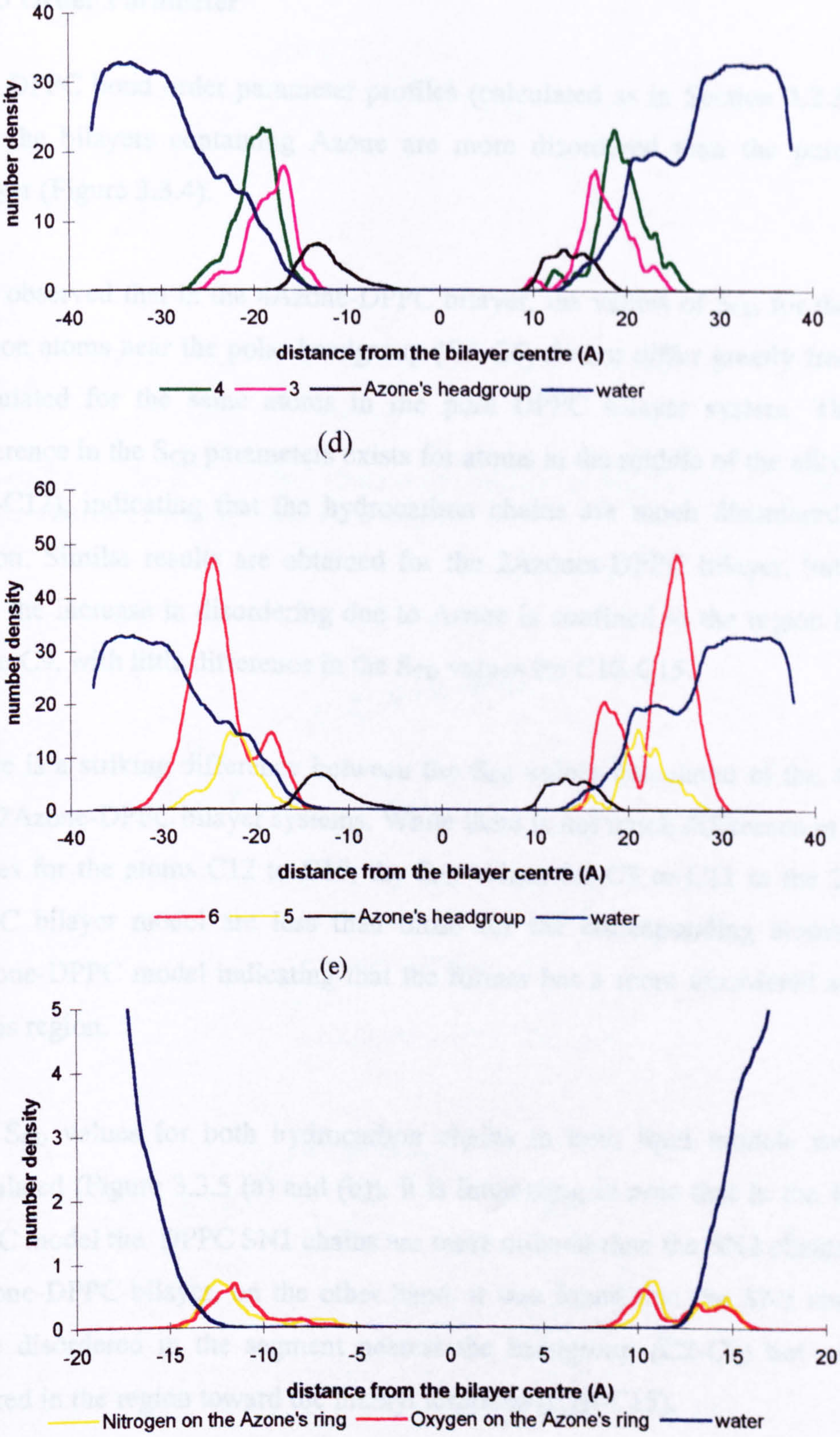

Figure 3.3.3 (ctd.) Number density profiles for the 4Azone-DPPC bilayer model (Refer Figure 3.1.9 for key).

3.3.3 Order Parameter

The DPPC bond order parameter profiles (calculated as in Section 3.2.3), show that the bilayers containing Azone are more disordered than the pure DPPC bilayer (Figure 3.3.4).

It is observed that in the 4Azone-DPPC bilayer, the values of S_{CD} for the DPPC carbon atoms near the polar headgroup (C3-C6) do not differ greatly from those calculated for the same atoms in the pure DPPC bilayer system. The main difference in the S_{CD} parameters exists for atoms in the middle of the alkyl chains (C7-C12), indicating that the hydrocarbon chains are much disordered in this region. Similar results are obtained for the 2Azones-DPPC bilayer, but in this case the increase in disordering due to Azone is confined to the region between C3 to C9, with little difference in the S_{CD} values for C10-C15.

There is a striking difference between the S_{CD} values calculated of the 4Azone-DPPC bilayer and 2Azone-DPPC bilayer systems. While there is not much difference in the S_{CD} values for the atoms C12 to C15, the S_{CD} values for C3 to C11 in the 2Azone-DPPC bilayer model are less than those for the corresponding atoms in the 4Azone-DPPC model indicating that the former has a more disordered structure in this region.

The S_{CD} values for both hydrocarbon chains in both lipid models were also calculated (Figure 3.3.5 (a) and (b)). It is interesting to note that in the 4Azone-DPPC model the DPPC SN1 chains are more ordered than the SN2 chains. In the 2Azone-DPPC bilayer, on the other hand, it was found that the SN1 chains are more disordered in the segment nearest the headgroup (C2-C9) but are more ordered in the region toward the methyl terminus (C10-C15).

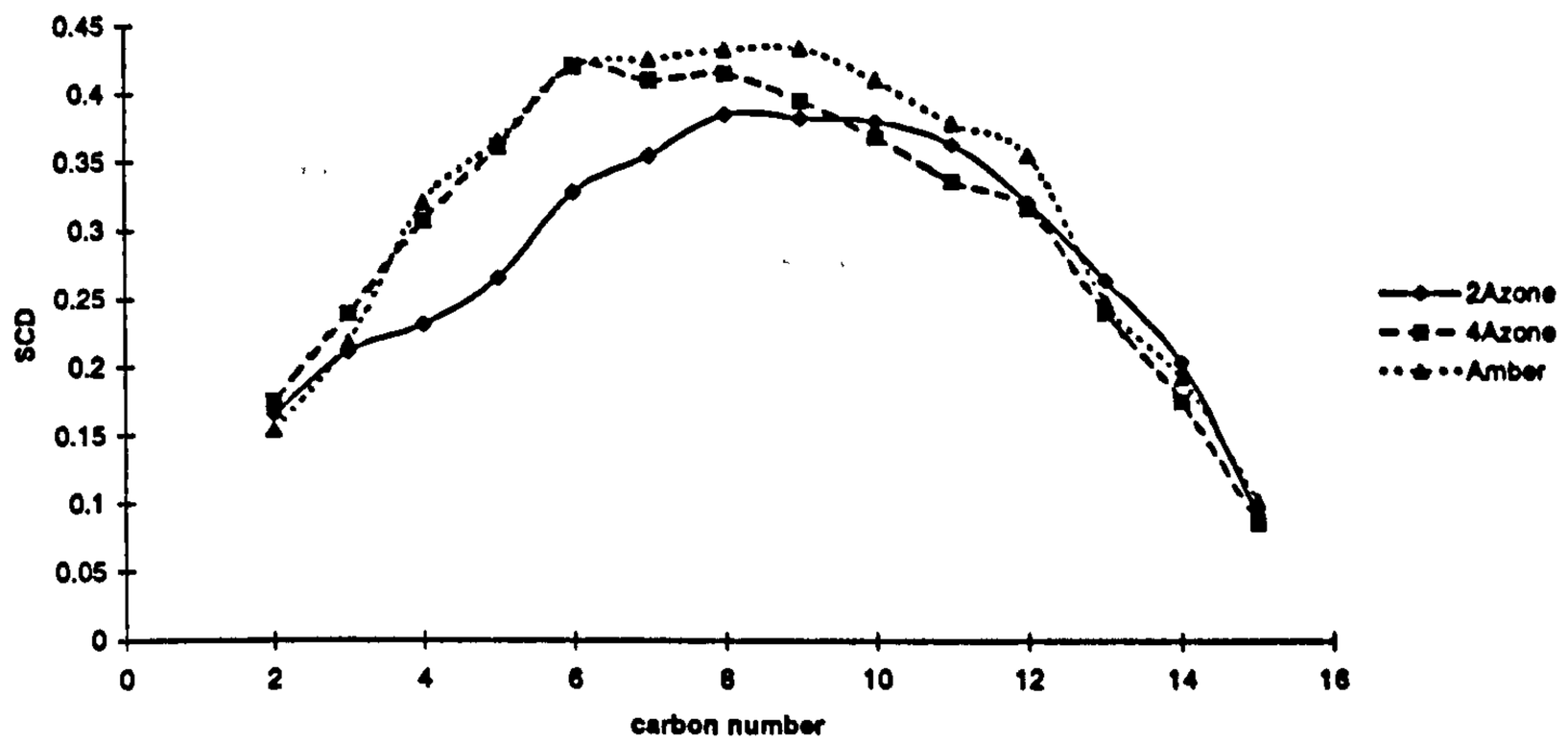

Figure 3.3.4: The DPPC alkyl chain order parameter profiles for the lipid bilayer models (averaged over both hydrocarbon chains).

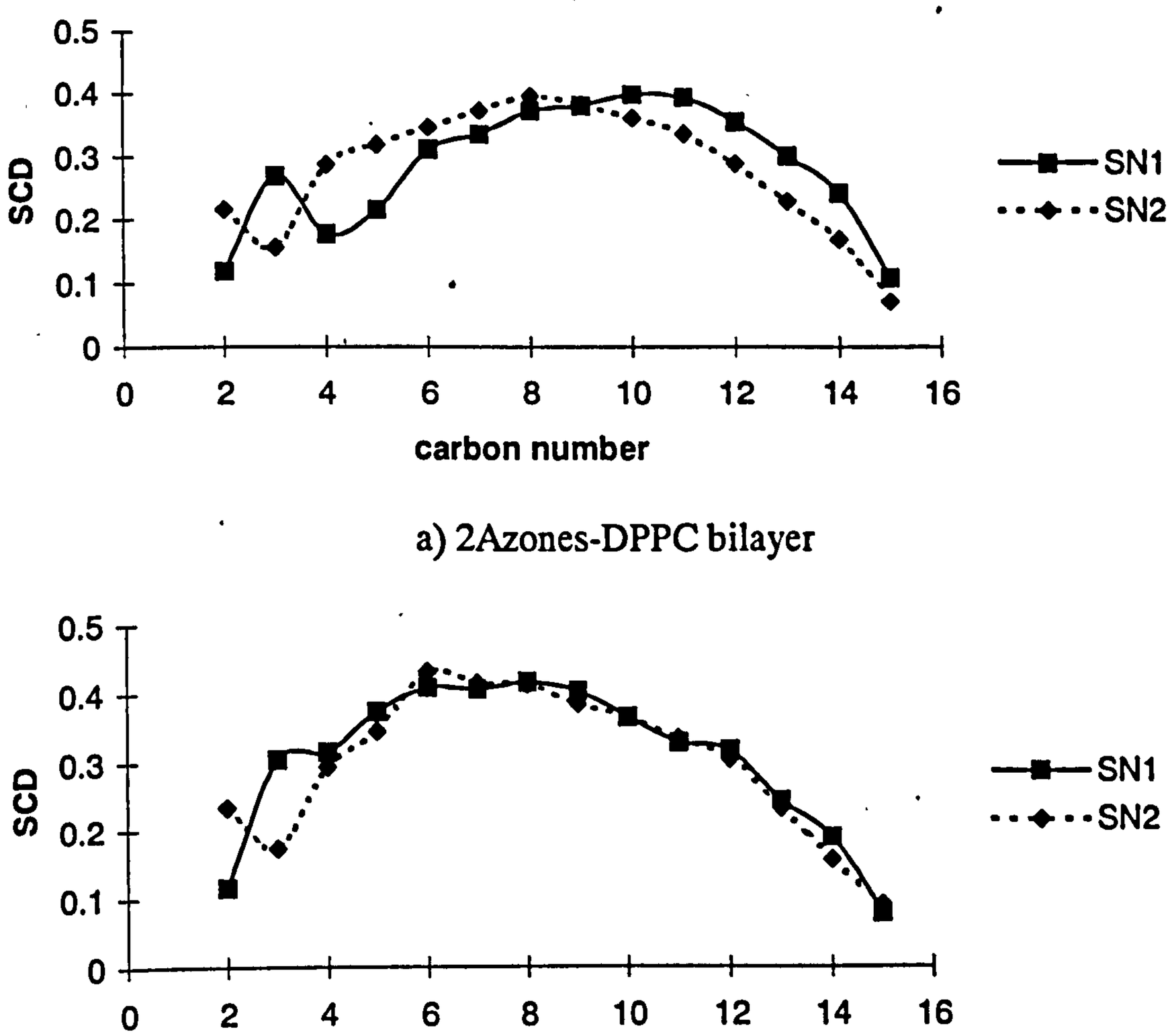

a) 2Azones-DPPC bilayer

b) 4Azone-DPPC bilayer

Figure 3.3.5: Order parameter profiles for the DPPC SN1 and SN2 alkyl chains in the Azone-containing bilayer.

Figure 3.3.6 shows the order parameter profiles calculated separately for the two DPPC monolayers in the 2Azone-DPPC model. The profiles show that there is no significant difference between the monolayer with Azone and the one without. The results also show that the carbons 5-13 are only slightly disordered in the presence of Azone.

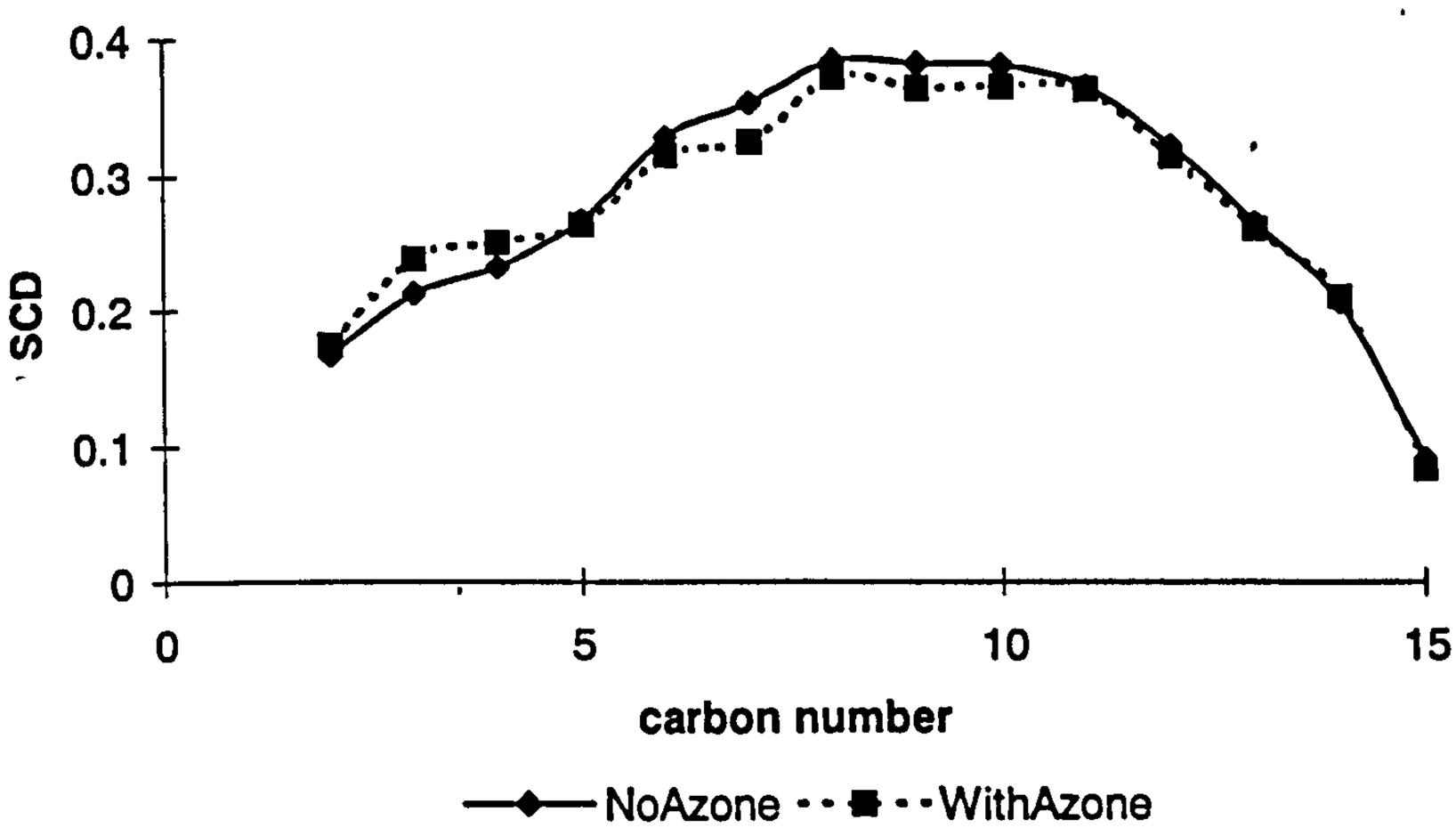

Figure 3.3.6 Order parameter profiles for the monolayers with and without Azone molecules in the 2Azone-DPPC model.

The degree of disordering of the DPPC alkyl chains is also measured by calculating the fractions of *gauche* bonds in the chains (Figure 3.3.7). The results obtained show that, in general, there is a greater disorder (that is, a larger fraction *gauche* bonds) for the DPPC chains in the presence of Azone. (Figure 3.3.7). In addition it is seen that the fraction of *gauche* bonds is higher in the 4Azone-DPPC bilayer than the 2Azone-DPPC bilayer. As found from the calculations of S_{CD}, the DPPC SN1 chain in the 2Azone-DPPC bilayer has a higher fraction of *gauche* bonds than the DPPC SN2 chain (Figure 3.37 (a)&(b)). It is also observed that there is a marked increase in the *gauche* fraction in Torsions 2-6 in the SN1 chain of the bilayer containing Azone molecules compared to that in the pure DPPC bilayer, with the increase more pronounced for the 2Azone-DPPC bilayer than the 4Azone-DPPC bilayer.

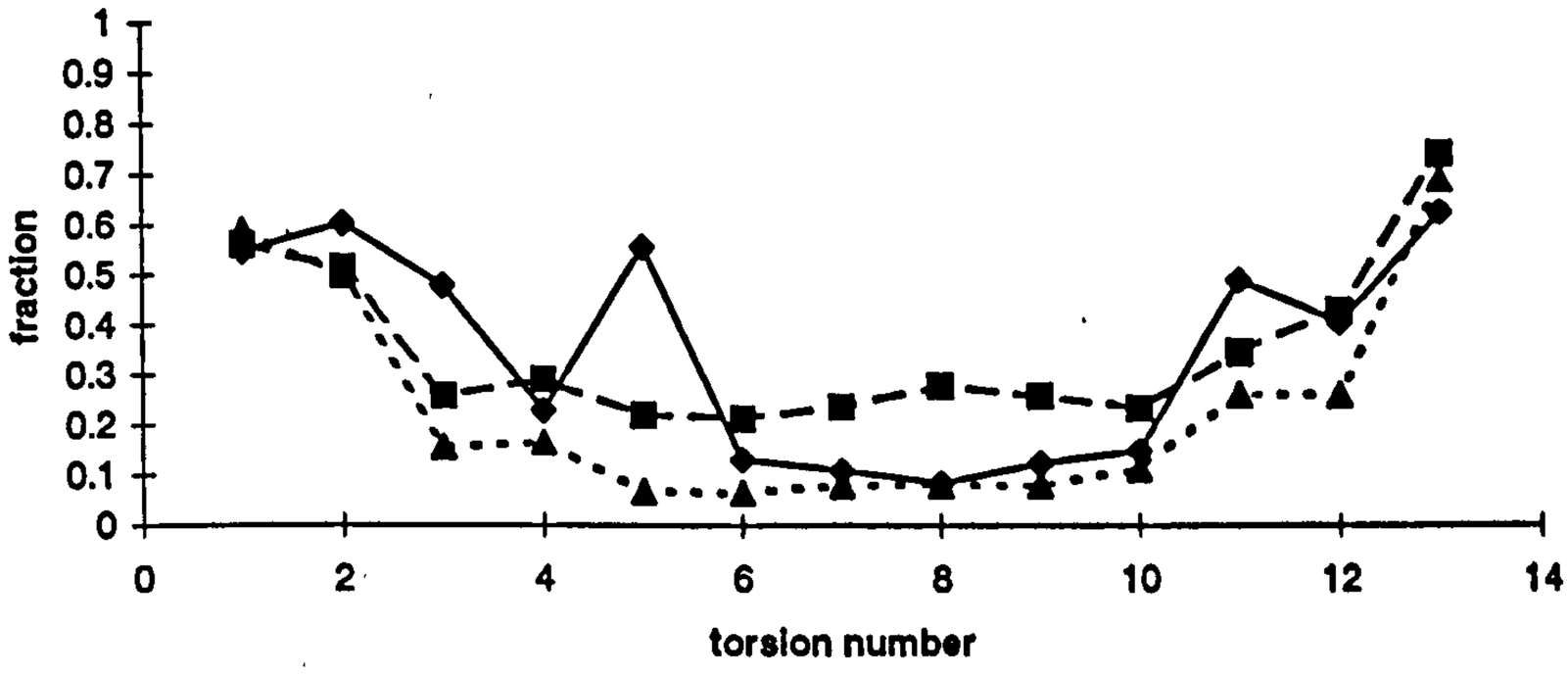

(a) average of both SN1 and SN2 chains

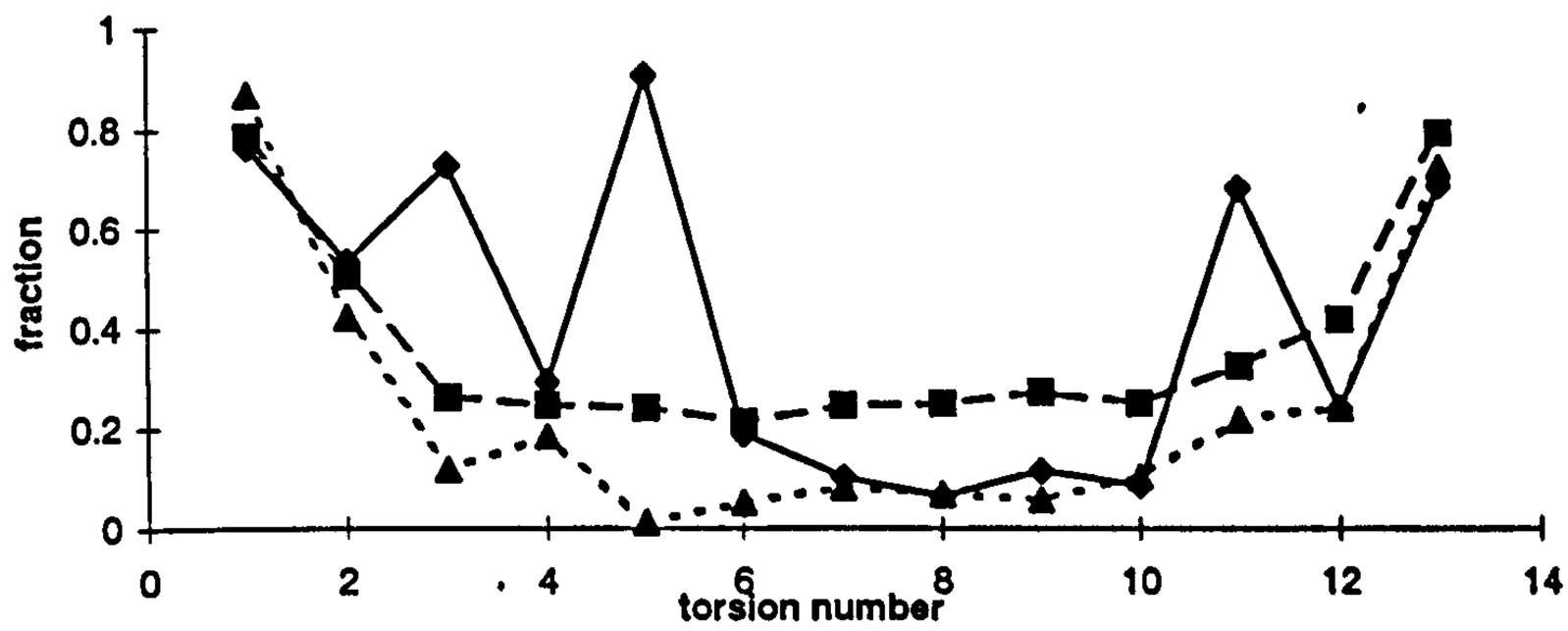

(b) SN1 chain

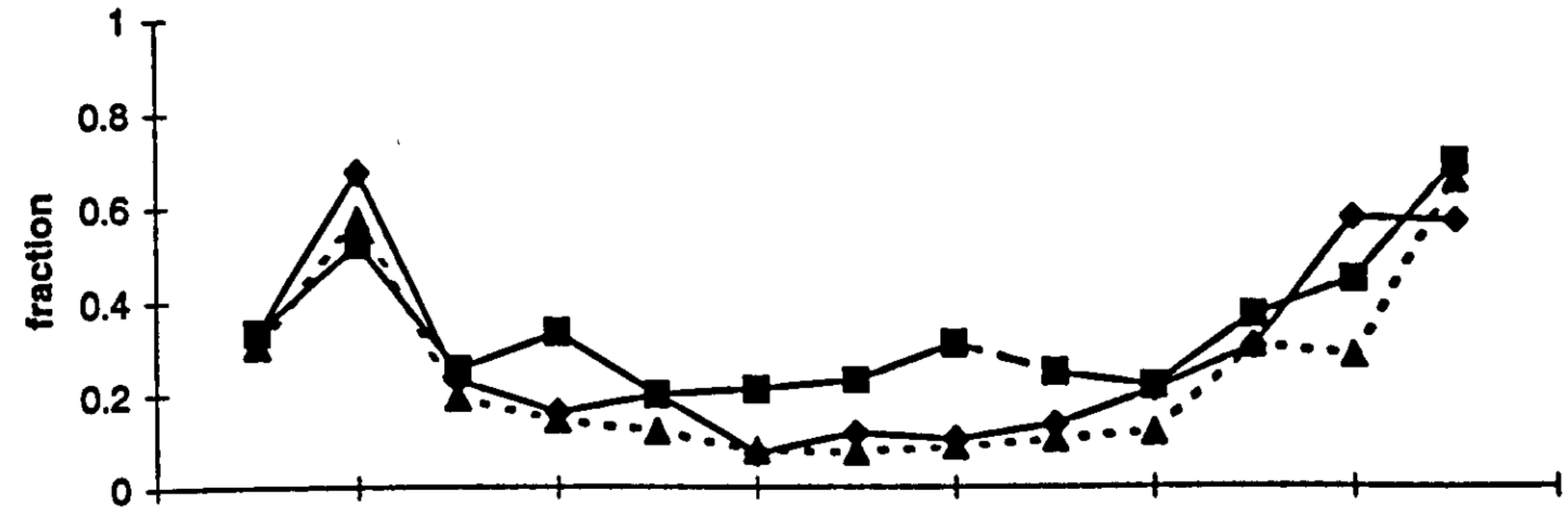

(c) SN2 chain

Figure 3.3.7 Fraction of *gauche* bonds in the alkyl chains of DPPC. The bond torsion angles are numbered 1-13 starting at the methyl ends of the chains.

3.3.4 Hydration Level

In the previous section, it was shown how the density profiles for the DPPC bilayers gave evidence for a greater water penetration into the headgroup region in the bilayers containing Azone. To investigate this issue further, the pair correlation functions, g(r) (see section 3.3.3) for the DPPC headgroup phosphorus and nitrogen atoms were calculated with respect to the water oxygen atoms. The results obtained (Figure 3.3.8) show pronounced peaks at ~ 3.8Å and 4.8Å for the g(r) of phosphorous and nitrogen atoms, respectively. The co-ordination numbers calculated for the two atoms are roughly the same in all three models, indicating about 20 and 6 waters hydrating the nitrogen and phosphorus atoms, respectively.

In order to further study the extent of the DPPC headgroup solvation, the g(r) for various other atoms in the headgroups were calculated. The results obtained (Table 3.3.1) show that in all three models the water penetration into the headgroup region decreases markedly as one travels into the bilayer beyond the carbonyl ester oxygen atom. However, it was observed that in the case of the bilayer containing Azone, there is an approximately 10 fold increase in the co-ordination number for the acyl ester oxygen in the SN1 chain compared to that seen for the pure DPPC bilayer model. Comparisons between the two bilayers containing Azone shows no significant difference in the extent of the hydration of the DPPC headgroups.

For the 2Azone-DPPC model the number density profiles indicated that there was a significant difference in the structure of the monolayer leaflet containing Azone compared to those without. Figure 3.3.9 shows the water g(r) for the DPPC nitrogen and phosphorus atoms for these two monolayers containing Azones calculated separately. It is interesting to note here that although there is little difference in the N-water g(r), there is a pronounced increase in the peak intensity for the P-water g(r) in the monolayer containing Azone. However, since the first

minimum of these functions in the monolayer with Azone is lower than that for the one without, the calculated co-ordination numbers are more or less the same.

Table 3.3.1: Hydration of the DPPC head groups and acyl ester groups for the pure DPPC and Azone-DPPC bilayers (results averaged over both monolayers)

radial distribution function	**Hydration Level(Co-ordination number)**		
	Lα–AMBER	2AZONE	4AZONE
N-OW	19.17(6.45)	19.54(6.45)	20.11(6.45)
C1-OW	4.426(4.35)	6.00(4.65)	4.682(4.35)
C2-OW	5.840(4.65)	5.07(4.5)	5.41(4.5)
C3-OW	5.070(4.5)	6.32(4.8)	5.25(4.5)
O1-OW	10.74(5.55)	10.54(5.55)	10.85(5.55)
P-OW	5.636(4.5)	6.41(4.65)	5.89(4.5)
O2-OW	2.642(3.45)	2.75(3.45)	2.54(3.3)
O3-OW	2.216(3.3)	2.61(3.45)	1.61(3.15)
O4-OW	0.797(3.45)	1.035(3.45)	0.80(3.3)
O5-OW	0.636(3.6)	0.62(3.45)	0.72(3.6)
C11-OW	2.620(4.35)	2.36(4.35)	2.97(4.35)
O6-OW	0.161(3.35)	1.36(3.6)	1.51(3.3)
O7-OW	0.366(3.3)	0.32(3.3)	0.31(3.15)
C31-OW	1.392(4.35)	2.47(5.1)	1.64(4.35)
O8-OW	0.746(3.45)	1.05(3.6)	0.85(3.3)

Note
The numbers in parentheses are the locations (Å) of the first minimum in the radial distribution function. In most cases there is a clear first minimum.

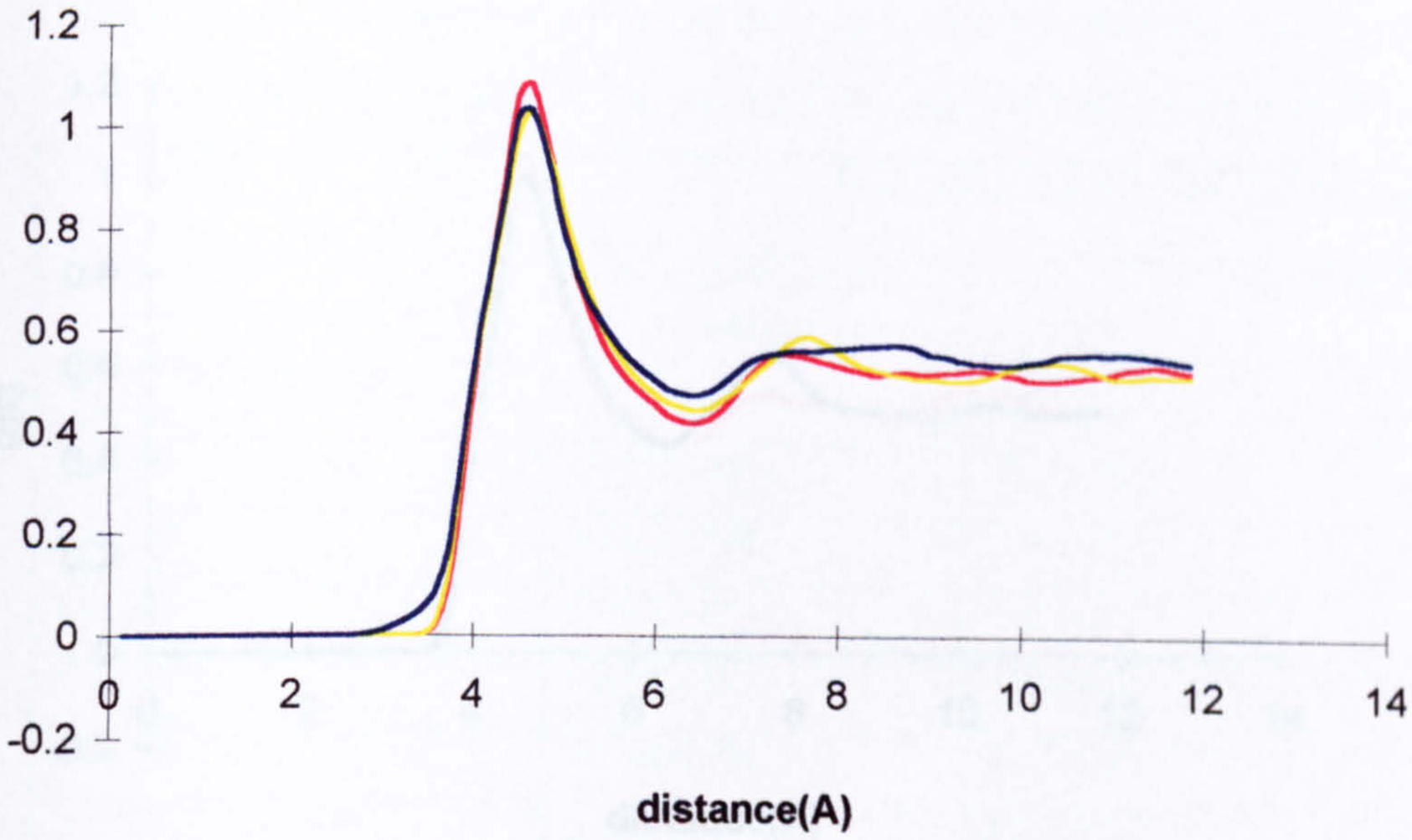

a) with respect of nitrogen

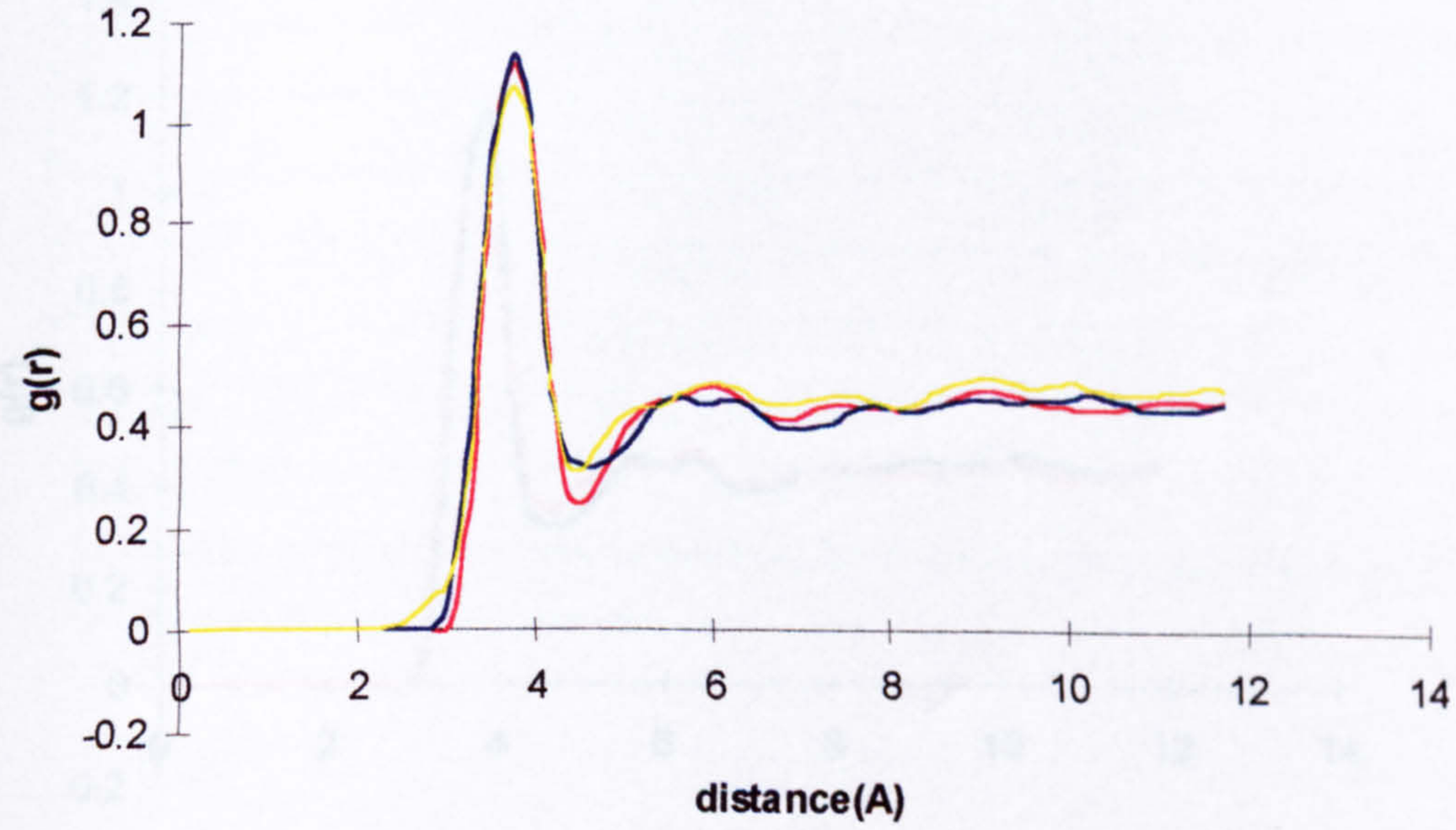

b) with respect to phosphorus

key:
AMBER
2AZONE
4AZONE

Figure 3.3.8: Pair distribution functions for the DPPC choline nitrogen and phosphate phosphorus atoms calculated with respects to the water oxygen (averaged over both monolayers).

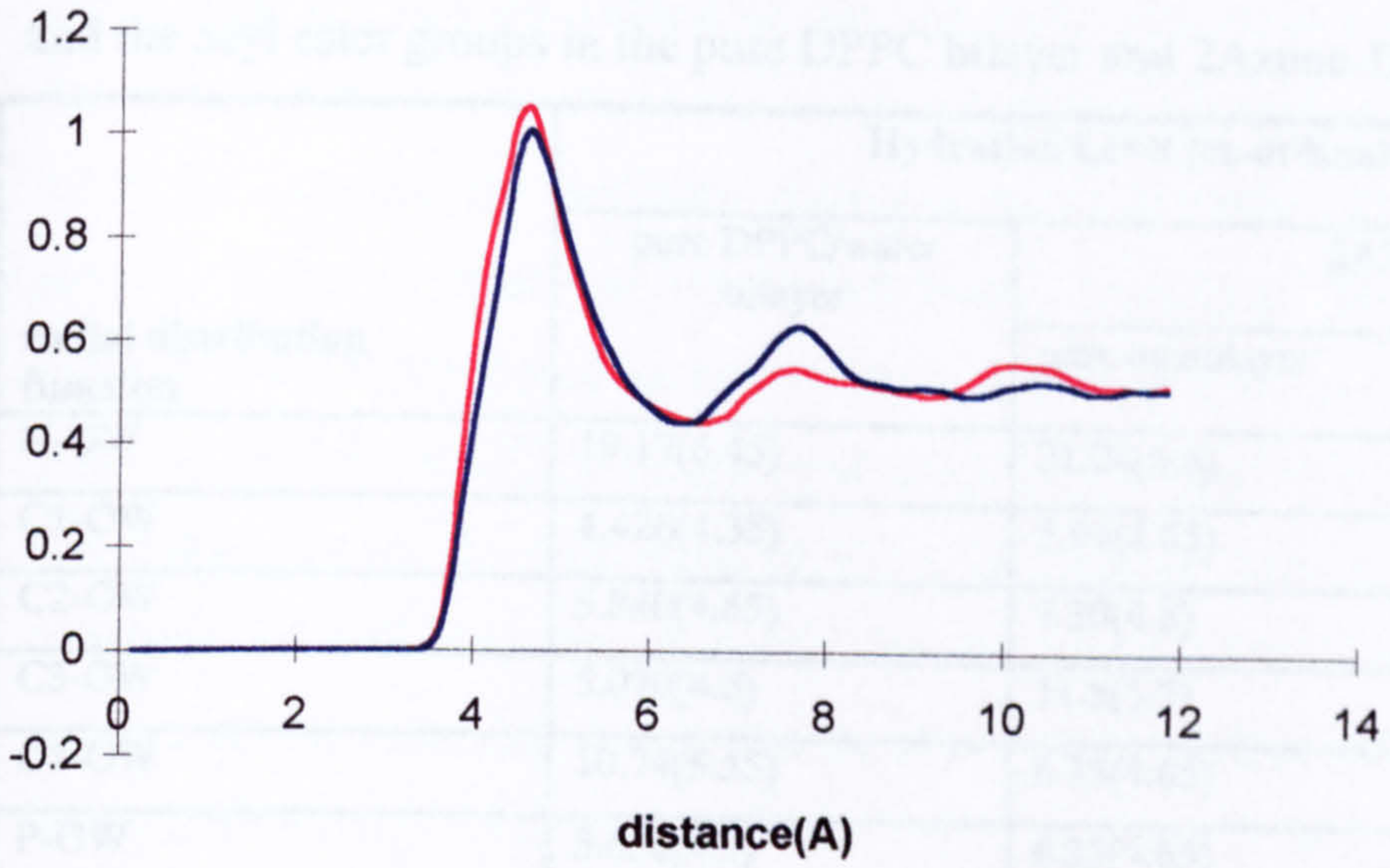

a) nitrogen

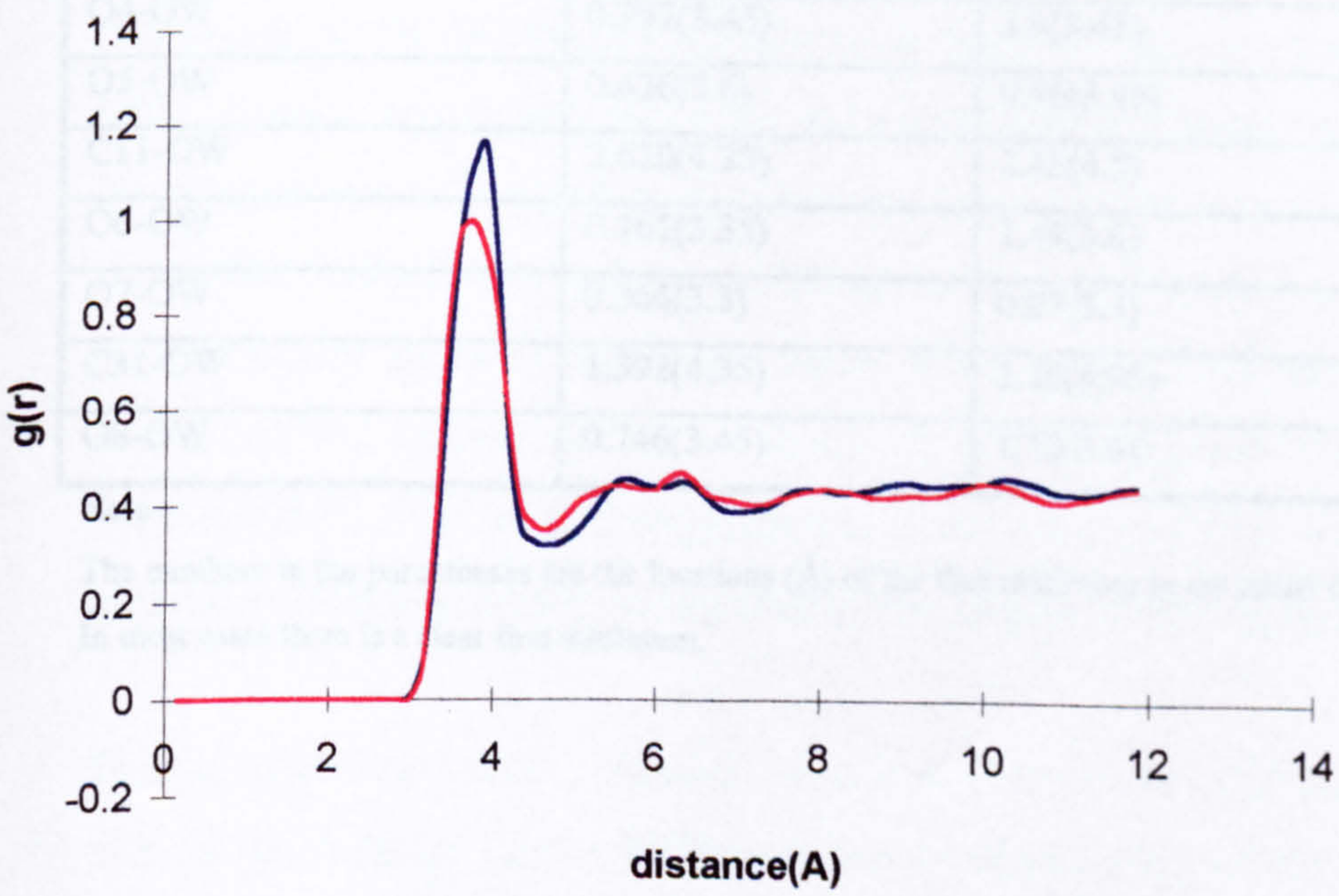

b) phosphorus

key:
monolayer without Azones
monolayer with Azone

Figure 3.3.9 Pair distribution functions for the DPPC choline nitrogen and phosphate phosphorus atoms calculated with respects to the water oxygen in the 2Azone-DPPC model (results shown separately for the two monolayers)

Table 3.3.2: Comparison of the hydration of the phosphatidylcholine head groups and the acyl ester groups in the pure DPPC bilayer and 2Azone-DPPC bilayer.

	Hydration Level (co-ordination number)		
	pure DPPC/water bilayer	2AZONE-DPPC	
radial distribution function		pure monolayer	monolayer with Azones
N-OW	19.17(6.45)	21.04(6.6)	19.26(6.45)
C1-OW	4.426(4.35)	5.94(4.65)	6.06(4.65)
C2-OW	5.840(4.65)	7.30(4.8)	6.34(4.8)
C3-OW	5.070(4.5)	11.5(5.7)	10.41(5.55)
O1-OW	10.74(5.55)	6.35(4.65)	6.48(4.65)
P-OW	5.636(4.5)	6.35(4.65)	6.48(4.65)
O2-OW	2.642(3.45)	2.96(3.45)	2.54(3.45)
O3-OW	2.216(3.3)	2.39(3.45)	3.13(3.6)
O4-OW	0.797(3.45)	1.0(3.45)	1.07(3.45)
O5-OW	0.636(3.6)	0.46(3.45)	0.66(3.3)
C11-OW	2.620(4.35)	2.46(4.5)	2.5(4.35)
O6-OW	0.161(3.35)	1.49(3.6)	1.24(3.6)
O7-OW	0.366(3.3)	0.27(3.3)	0.29(3.15)
C31-OW	1.392(4.35)	2.16(4.95)	2.20(4.8)
O8-OW	0.746(3.45)	1.12(3.6)	0.97(3.6)

Note

The numbers in the parentheses are the locations (Å) of the first minimum in the radial distribution function.

In most cases there is a clear first minimum.

3.3.5 Diffusion Constants

The diffusion constants calculated for the bulk and bound water molecules, Azone and DPPC molecules in the Azone-containing bilayers are shown in Table 3.3.3. As expected the diffusion constants for bulk water (for all the bilayer models) is higher than that for bound water, indicating that the bulk water diffuses much faster than does bound water. The calculated values for the bound water in the 2Azone-DPPC bilayer system (1.52×10^{-5} cm^2/s) is about ~2.8 times lower than that for the bulk water (4.303×10^{-5} cm^2/s). The calculated diffusion constants for bulk and bound waters for the 4Azone-DPPC bilayer are more similar, but the values still imply that the bound water diffuse slightly slower than do the bulk water.

It was found that the diffusion constants for bound water in the bilayers containing Azone molecules are higher than those for the bound water in the pure DPPC bilayer, suggesting that water molecules traverse faster in the presence of Azone molecules. Comparison between the 2Azone- and 4Azone-DPPC bilayers shows that while there is not much difference in the diffusion constant values for bulk waters in the two systems, the value of this constant for bound water in the 4Azone-DPPC bilayer system is about ~2.75 times greater than that for the 2Azone-DPPC bilayer. This suggests that in the 4Azone-DPPC bilayer, the water molecules diffuse relatively faster than in the 2Azone-DPPC bilayer.

The calculated diffusion constants for Azone demonstrate that Azone molecules diffuse much faster (about 3 times faster) in the 4Azone-DPPC bilayer than in 2Azone-DPPC bilayer. The same is true for the diffusion of DPPC, where it is found that the DPPC molecules diffuse ~3x faster in the 2Azone-DPPC bilayer, and about 24 times faster than that in 4Azone-DPPC/water bilayer. These results are significant in which it showed that there is a co-operative effect of Azones when present in large number.

Table 3.3.3 : Diffusion constants for DPPC, Azone and water molecules in various DPPC bilayers.

Bilayer Model	Diffusion Constants			
	Bulk water ($x\ 10^{-5}cm^2/s$)	Bound water ($x\ 10^{-5}cm^2/s$)	Azone ($x10^{-6}cm^2/s$)	DPPC ($x10^{-7}cm^2/s$)
Pure DPPC/water	6.23	0.93	-	4.0
2Azone-DPPC	4.30	1.52	1.03	11.11
4Azone-DPPC	4.23	4.19	3.92	97

Conformation of Azone

The conformations of Azone molecules in the Azone-DPPC bilayers were probed using cluster analysis (as detailed in section 3.1.1). Throughout the 500ps production phase, there are about three hundred clusters formed for Azone configurations in both the two bilayer models indicating that the conformations that Azone molecules adopted during the simulations are random and not specific. Figure 3.3.10 shows the representatives conformers for the 4 major clusters found in the simulations of the bilayers containing Azone molecules.

Figure 3.3.10: Representative structures showing the 4 main conformations adopted by Azone molecules in the Azone-DPPC bilayer simulations.

4. DISCUSSION

4.1 Choice Of Lipid Bilayer Model

In simulating a lipid bilayer, it is important that the model chosen accurately reproduces the structure and properties for the lipid phase of interest, namely in this case, the *stratum corneum* lipid. As mentioned previously, *stratum corneum* lipids comprise a high concentrations of ceramides and cholesterols. These two lipid components are important in providing a highly ordered structure for the intercellular domain; cholesterol (at the right concentration) by reducing the mobility of the lipid atoms lying next to it, and ceramide by providing a more condensed environment in the *stratum corneum* owing to its high transition temperature (~70°C) (Brain and Walters, 1991).

Having considered the organisation and structure of lipids in the intercellular domains, the studies reported here were initiated by simulating a DPPC bilayer in the gel state, using a united atom approach as described in section 2.4.2, with the intention of studying the effect of Azone within the equilibrated structure. It was apparent from this study, however, that the time required for these simulations would be prohibitive and that it might not have been possible to model the systems adequately within the time frame of the simulation unless the bilayer was simulated in the liquid crystalline (Lα) phase (Merz and Damodaran, 1997). There were also issues about the use of the united atom approximation and the choice of force field used in the simulation of the lipid bilayer (Merz, 1997) with most simulations in recent years are performed using an all-atom approach (see section 1.3.1). Thus an all-atom MD simulation of a DPPC bilayer in the Lα-phase was carried out utilising the AMBER all-atom force field. The development of the CHARMm22 force field for lipids also prompted us to consider the use of this force field in our simulations. In using the CHARMm22 force field, however, initially proved very difficult to equilibrate the

DPPC bilayer (the structure of this unsuccessful simulation is presented in Appendix 5). Since this force field is also very specific for biological molecules (i.e. for lipid, protein and nucleic acid) and its suitability for modelling Azone was uncertain, it was elected to use the AMBER force field which, although specially developed for protein and nucleic acid, nevertheless has been used successfully for other small molecules in this laboratory (Hadgigeorgio, 1997, Devani, 1998).

The choice of the AMBER force field was further justified by the results obtained in using this in the MD simulations of the DPPC bilayer. Even though the Lα-CHARMm model has been shown to be superior to the Lα-AMBER model in some aspects of the results when compared with those obtained by experiment, the Lα-AMBER model, on the whole, was considered better. The fact that the AMBER simulation provides an adequate model for the Lα-DPPC bilayer is established by comparing this model against the MD model of the Lβ' system, and against other MD models and experimental observations.

The calculated electron density profile (Figure 3.2.2(b)) for the Lα-AMBER is characteristic of that of the liquid crystalline phase with a more rounded low density trough (Figure 3.2.1 (McKintosh, 1980)) than seen in Lβ' model indicating a more broad distribution of the terminal methyl groups of the hydrocarbon chain. The same rounded low density trough is seen in other MD studies of DPPC bilayers in the liquid crystalline state (Tu *et al.*, 1996; Egbert *et al.* 1994, Huang *et al.*, 1994). The profile of electron density in Lβ'-DPPC model shows a plateau in the region occupied by methylene groups and a sharp, distinct trough in the region of the methyl groups which is consistent with the electron density profile found from X-ray diffraction studies of the DLPE in the gel state (McKintosh, 1980), and consistent also with the profiles observed in other MD simulations of DPPC bilayers in the gel state (Tu *et al.*, 1995).

Additional confirmation that the Lα-AMBER model has the DPPC molecules in the liquid crystalline state is provided by the calculated distributions of the various atoms and fragments of the DPPC molecule. The calculated positions of the alkyl chain carbon atoms in all models (Lα-AMBER, Lα-CHARMm and Lβ') compare well with

those determined by experiment (Büldt *et al.*, 1979, Zacchai *et al.*, 1979). The calculated atomic positions in the carbon atoms for the Lα-AMBER model are different from those in the Lβ' model. The headgroup ammonium methyl (Cγ) and choline methylene carbons (Cβ and Cα) are closer to the bilayer centre and more widely distributed in the Lα-DPPC bilayer than in the Lβ' DPPC bilayer. The glycerol methylene carbons in both models (Lα-AMBER and Lβ'), surprisingly have the same mean distances from the bilayer centre, even though the Lα-DPPC has a broader distribution half-width. With the exception of the carbon C4, all other alkyl chain methylene carbons in the Lα-AMBER model are closer to the bilayer centre and are more widely distributed than in the Lβ' bilayer. It is also observed that in the Lα-AMBER model, the choline and phosphate groups have wider distributions than in the Lβ' bilayer. The fact that these atoms lie closer to the bilayer centre, and have broader distributions is a reflection of the higher incidence of *gauche* defects formed in the Lα-AMBER, and also indicates a greater fluidity of this model compared with the Lβ'. The states of fluidity of the two models are also evident in the two 'snapshots' in Figure 4.1 and 4.2.

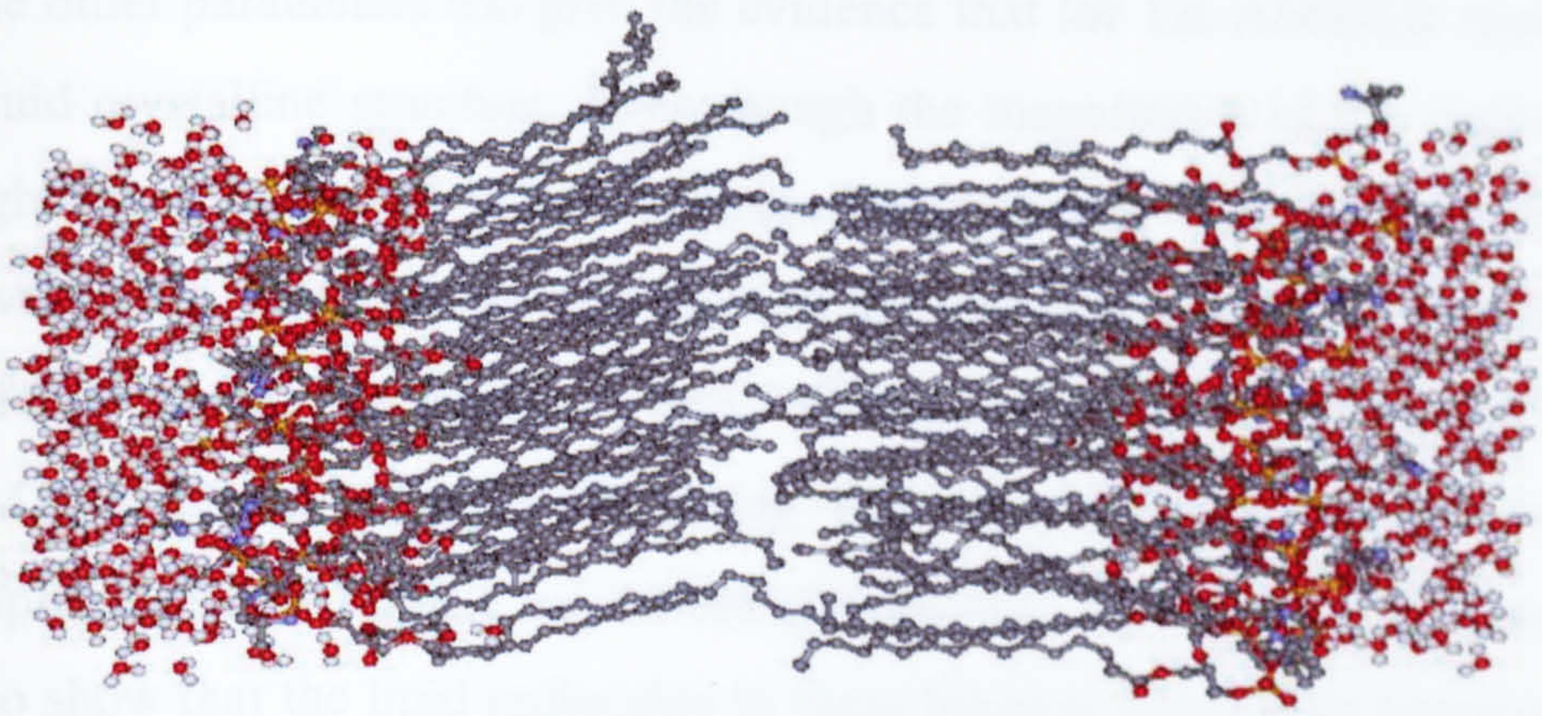

Figure 4.1: A typical snapshot of the Lβ' DPPC bilayer model during the production phase. Note the tilting of molecules (about 30° from the bilayer normal).

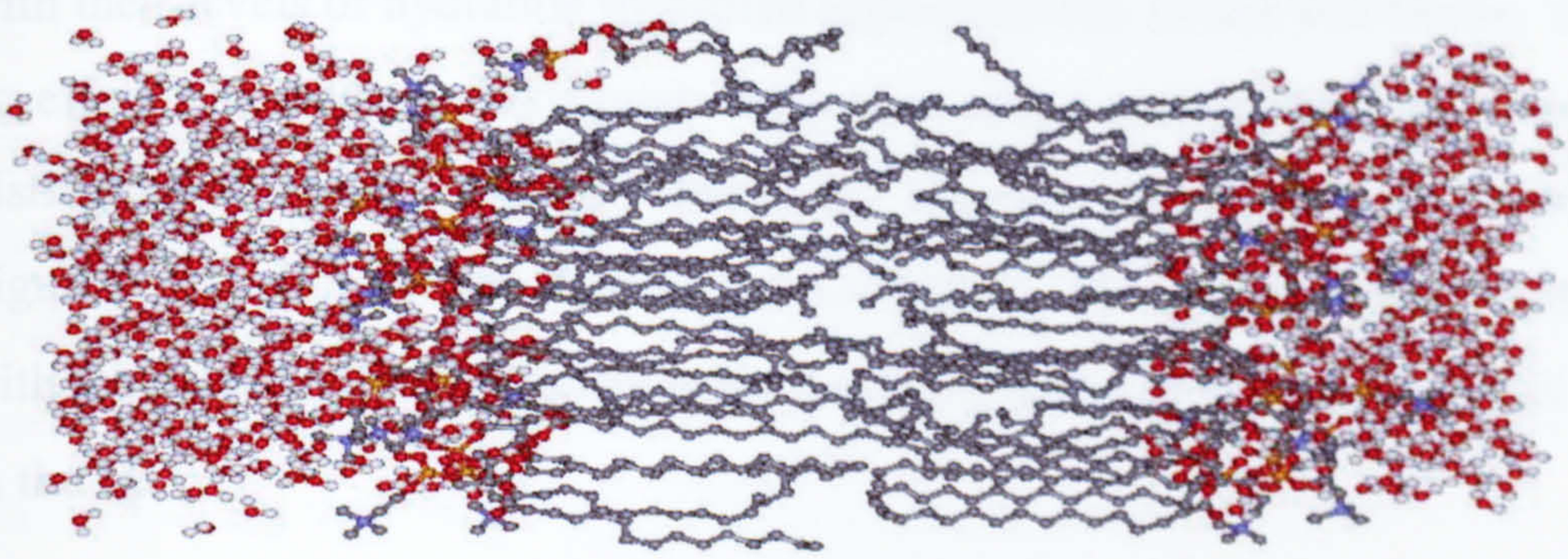

Figure 4.2 : A typical snapshot of the Lα-AMBER model during the production phase. Hydrogen atoms on the lipid molecules were omitted for clarity. Note that the structure is more disordered than that of Lβ' DPPC bilayer (Figure 4.1).

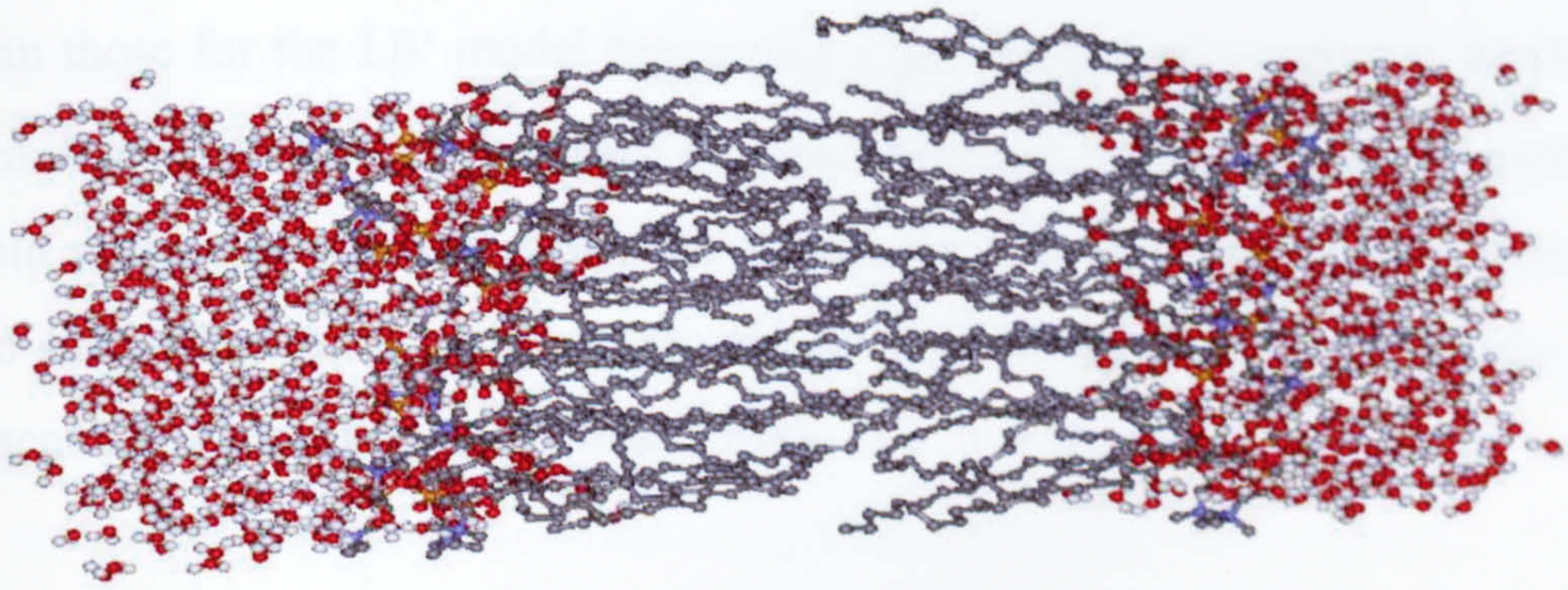

Figure 4.3 : Typical snapshot of the Lα-CHARMm model during the production phase. Hydrogen atoms on the lipid molecules were omitted for clarity. Note that the structure is more disordered than that of the Lβ' DPPC bilayer (Figure 4.1).

The order parameters too give the evidence that the Lα-AMBER model behaves as a liquid crystalline structure. Even though the magnitudes of the order parameters are higher than those determined by experiment (Seelig & Seelig, 1974), Figure 3.1.10 nevertheless demonstrates that most of the values are lower than those calculated for the Lβ' model, indicating a more disordered structure of the DPPC in the Lα-AMBER model. It is worth noting that other MD simulations of lipid bilayers employing the AMBER force-field (Damodaran & Merz, 1992; Essex *et al.*, 1994) also show that the lipid molecules in these bilayers have order parameters higher than those found by experiment.

It is quite difficult to compare the calculated levels of hydration of the DPPC bilayers with their levels of hydration measured experimentally (Finer and Drake, 1974), since no effort was made to distinguish between strongly and loosely bound water, nor to distinguish the water trapped between the bilayers. However, from Table 3.2.3 and Figure 3.2.11, it is evident that the Lα-AMBER model is more hydrated than the Lβ', with the calculated bound water in the Lα-AMBER model being about 2% more than in the Lβ'.

As final justification for the use of the Lα-AMBER model for studying the effects of Azone incorporation in DPPC bilayers, it is noted that the calculated diffusion constants for the DPPC and water molecules in the Lα-AMBER model are higher than those for the Lβ' model suggesting a greater fluidity in the Lα-AMBER model compared with the Lβ'. It should be noted however, that the diffusion coefficients for lipid molecules obtained from MD simulations are not particularly reliable because the simulation times are generally too short to obtain a reliable estimate of what is essentially a slow process (Essex, 1994).

In summary, therefore, it is seen that all the calculated properties of the Lα-AMBER are consistent with the conclusion that it provides an appropriate representation of a liquid crystalline lipid bilayer and is thus adequate for modelling the effects of Azone incorporation.

4.2 The Effect of Azone on the DPPC/Water Bilayer Model

Barry (1987) first proposed the mechanism of action of Azone in the intercellular lipids, based on various experimental observations, in particular from DSC experiments. Azone has been shown to eliminate the peaks attributed to lipid melting in the DSC thermogram (Figure 4.4) (Goodman & Barry, 1986; 1989). From these observations, it was suggested that these enhancer molecules were incorporated in the hydrocarbon region of the lamellar lipid bilayers, thereby increasing the alkyl chain mobility and hence reducing the resistance to the translational diffusion of dissolved molecules.

The present studies, not only support this theory but are also in fact able to explain the mechanism of action of Azone on the lipid membrane in a more detailed manner.

Several experiments have confirmed that Azone causes increased disorder in the lipid regions thus suggesting that Azone intercalates into the stratum corneum lipid (Quan & Maibach, 1994, Ogisho *et al.*, 1992, Bouwstra *et al.*, 1992). Previously how Azone causes the disorder and where exactly it is located in the lipid bilayer, however is not established. On the basis of the MD simulation reported here, it is found that Azone molecules reside within the alkyl chain's region of the DPPC bilayer, with their headgroups located in around 10-20Å from the bilayer centre (Figure3.3.2(a) & 3.3.3(a)). The Azone molecules are thus positioned slightly deeper inside the bilayer than the DPPC ester groups, diffusing to this position from their starting positions over the course of the MD simulations. These observations are confirmed by visual inspection of the snapshots sampled after minimisation (Figure 2.8 & 2.9) with that taken during the simulations (Figure 4.6 & 4.7).

It is also observed that the presence of Azone increases the widths of the distributions of the DPPC choline and phosphate, glycerol and acyl ester groups, as well as the hydrocarbon regions. This suggests that there is a general increase in the disorder in the polar and hydrocarbon regions of the bilayer. This disordering effect is greater for the 4Azones-DPPC bilayer than for the 2Azone-DPPC bilayer, which indicates that the disordering is concentration dependent.

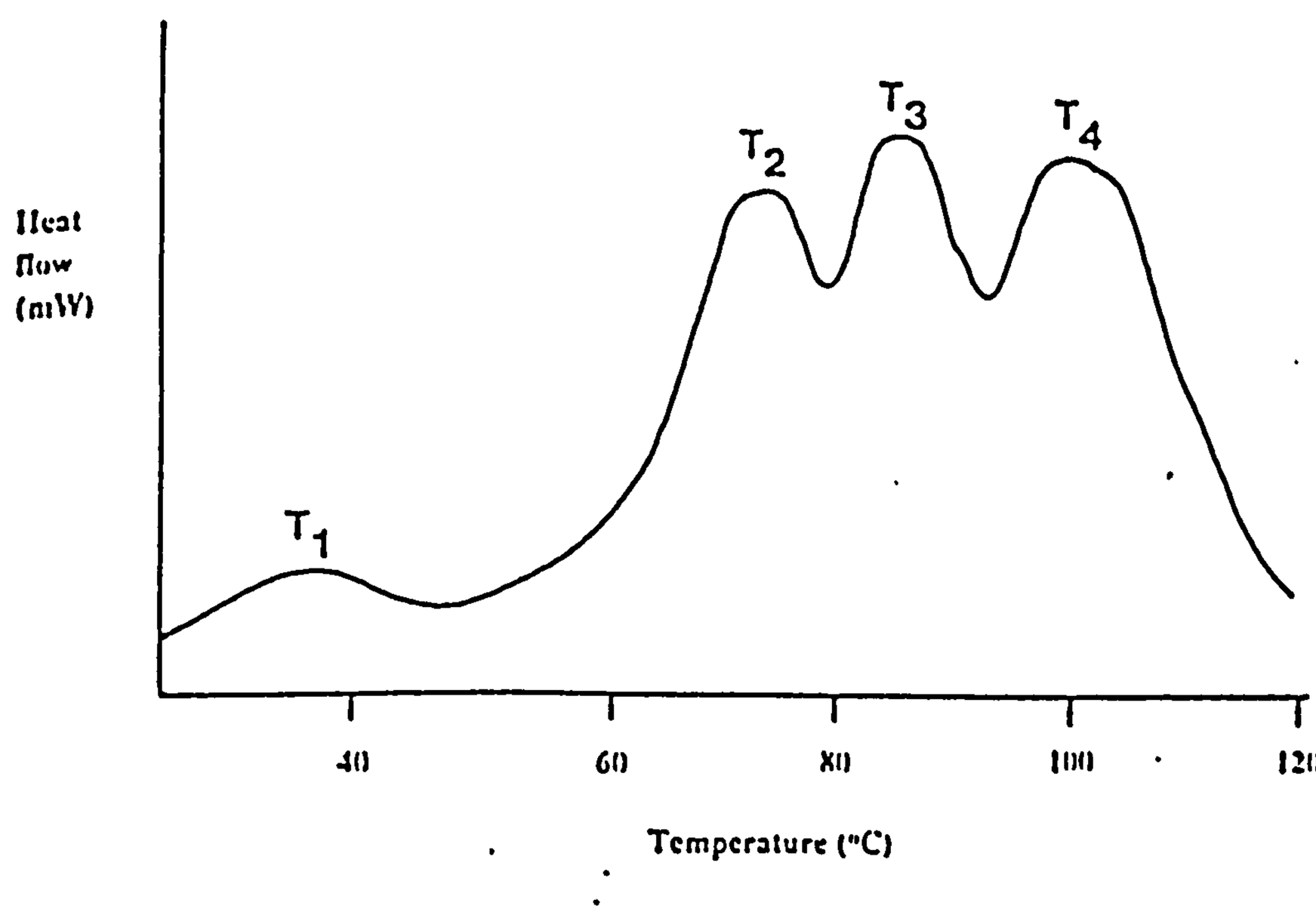

Figure 4.4: Typical differential scanning calorimetry (DSC) trace of hydrated human stratum corneum (taken from Goodman and Barry, 1989).

The disordering effect of the Azone on the DPPC hydrocarbon chain packing was also more evident by the changes in the molecular order parameters (S_{CD}). The calculated S_{CD} values for the carbon atoms in the alkyl chains of DPPC were found to be markedly reduced in the presence of Azone (Figure 3.3.4). The increased disorder in the middle area of the hydrocarbon regions was shown by a marked decrease in the S_{CD} for carbons 4-9 in the 2Azone-DPPC bilayer model. These results were also supported by the calculation of *gauche* defects in the system which showed an increase in the *gauche* population for all alkyl chain bonds (particularly torsions 2-8) in the 2Azone-DPPC bilayer model. The number density profiles indicate that the Azone molecules in this system are located either around or slightly below the DPPC acyl-ester groups. While the large headgroup of Azone reduces (or does not alter) the movement of the atoms next to the first two atoms of the alkyl chains of its neighbouring lipid, the freedom of movement of the lower part of the alkyl chains is increased due to the increase in space created by the Azone's headgroup.

The effect of Azone on the individual monolayers in the 2Azone-DPPC bilayer model were also investigated. The results showed that there was no significant difference between the order parameter profiles for the two monolayers which demonstrates the co-operative nature of this lipid membrane.

The S_{CD} values for all carbon atoms in the DPPC hydrocarbon chains in the 4Azone-DPPC bilayer were also seen to be decreased by the incorporation of Azone molecules. Unlike the 2Azone-DPPC bilayer model, however, it was found that there is a general decrease in the S_{CD} values for all the carbons along the alkyl chain compared with the pure DPPC bilayer and also a marked increased in the *gauche* population in all torsions calculated along the hydrocarbon chains in the 4Azone-DPPC bilayer model. These calculations in fact shows that there are slightly higher *gauche* populations in the 4Azone-DPPC bilayer model (35.39%) compared to the 2Azone-DPPC bilayer model (34.97%) suggesting more disorder of the former model compared with the latter. Both of these models showed an increase of about 12% in the fraction of *gauche* defects compared with the pure DPPC bilayer model (23.9%). Potts and Francouer (1990) have correlated the increase in the number of alkyl chain *gauche* conformers with an increase in the water permeability in the stratum corneum lipid. The increase in *gauche* conformers as a results of the incorporation of Azone

molecules has also been observed by Harrison *et al.* (1996) in human stratum corneum. In this later study, the greater incidence of *gauche* defects was demonstrated through an examination of the frequency shifts and variations in the rates and amplitudes of the translational and rotational motions of individual CH_2 groups. There were no quantitative data obtained on the numbers of *gauche* conformers determined in this experiment however, the authors were only able to make qualitative judgements as to the increase in the *gauche* conformers based on their observations of the spectral peak bandwidths.

The observation that Azone decreases the order parameters of the DPPC qualitatively consistent with the data obtained by Quan and Maibach (1994). These authors found that Azone reduced the order parameter of (5-doxyl stearic acid) 5-DSA used as a spin label in the stratum corneum by 54-80% at different concentrations of Azone and this was taken to indicate that Azone affected the spin label binding to the lipid bilayers, by causing an increase in the flexibility and polarity of the local bilayers surrounding the 5-DSA.

Other studies that have demonstrated the increase in fluidity of the hydrocarbon chains of the *stratum corneum* lipid model as a result of Azone incorporation include DTA (Bouwstra et al., 1989), X-ray (Bouwstra et al., 1990) and ESR studies (Ogisho et al., 1992). The latter work shows that Azone increased the molecular motion of the lipid probe by 1.6-2 times. Using fluorescent probe spectroscopy and differential scanning calorimetry Beastall et al. (1988) have shown that Azone increases the phase transition of DPPC with the suggestion, therefore, that it increases the fluidity of the lipid bilayer.

The increased disorder in the hydrocarbon chains in the lipid bilayer usually results in an increase in the lateral diffusion of dissolved molecules into the lamellar structure. The lateral diffusion of lipids and integral protein for example are strongly dependent not only on the thermodynamic phase of the lipid bilayer but also upon fluctuations and the structural organisation of the bilayer (Mouritsen & Kinnunen, 1996). In the previous MD simulations of lipid bilayers, it is established that an increase in the disorder of the lipid membrane also increases the lateral diffusion constants of DPPC and water molecules. The diffusion constants of DPPC for example, increases by a

factor of two in the Lα-CHARMm model which has been shown to have higher disorder than the Lα-AMBER model.

In the present studies, it is noted that the diffusion constants for DPPC and water are higher in the bilayers containing Azone molecules than in the pure lipid membrane. There is about a three fold increase in the diffusion constant for DPPC when two Azone molecules are incorporated in the bilayer, and a surprising 20 fold increase in the constant calculated for the 4Azone-DPPC bilayer, which again indicates that there is greater disorder as the Azone concentration is increased. The higher disorder in the 4Azone-DPPC bilayer compared to the 2Azone-DPPC bilayer is also shown by the increase in the diffusion constants for water and Azone molecules. The enhanced diffusion of water is explained by the fact that the increased disorder of the lipid bilayer increases the mobility of the hydrated lipid headgroups and thereby increases the diffusivity of the hydrophilic interlamellar layers.

These results are in agreement with the order parameter results obtained here which show that increasing the amount of Azone in the lipid membrane increases the disorder of the lipid bilayer. They also agree with the observations made in the fluorescence polarisation and diffusion cell experiments, which show that the stronger the increment effect of the enhancer on the fluidity of the lipid model, the larger the diffusion coefficients for drugs in the skin (Kai et al., 1993). On the basis of the same experiments, it was also established that the effect of Azone is more pronounced for hydrophilic drugs and lipophilic drugs. Other workers have shown similar increases in the permeability of drugs across skin treated with Azone, Hoogstraate *et al.*(1991) for example, showing that the permeability of desgly-cinamide arginine vasopressin is increased by 1.9-fold after pretreatment with Azone and Sugibayashi *et al.*, (1990) finding that Azone effectively altered the skin permeation of methanol, butanol, glucose and sucrose by fluidizing the skin lipids.

Hydration of the stratum corneum has been proposed as one of the mechanisms responsible for drug penetration enhancement. It is reported that hydration can enhance the permeability of the skin by as much as 80 fold (Scheuplein & Ross, 1970). The effect of the degree of hydration on thermal transitions of human stratum

corneum has been studied by Knutson *et al.*, (1985) who found (from DSC and infrared spectroscopic studies), that increasing the hydration of both porcine and human stratum corneum resulted in increased fluidity of the intercellular lipids. Although there are no studies yet reported which measure the effect of Azone on the hydration of skin lipid, Sugibiyashi *et al.* (1992) have shown that Azone increases the water-holding capacity of keratin tablets and also increases in the *in vivo* skin conductance.

The hydration of the various lipid models was quantified by calculating the numbers of bound and bulk waters, and the pair correlation functions of water oxygen with respect to various atoms on the DPPC headgroup. The water involved in the hydration of the lipid bilayer is usually associated with bound water and it should be noted here that, in this study, the water content of the system corresponds to 28 waters per lipid/Azone molecule, and that X-ray diffraction data show that for the Lα bilayer the maximum water content after which the bilayer properties remain unaffected by water level is 25 molecules per DPPC molecule (Ruocco & Shipley, 1982).

The incorporation of Azone surprisingly did not significantly affect the hydration of the lipids as shown from the calculations of bound water in the three models. The fractions of bound water for the pure DPPC bilayer and the bilayers incorporating 2 Azones and 4 Azones were 37.75%, 37.09% and 36.53%, respectively. The calculated pair distribution functions confirmed these observations but showed that more water penetrates into the bilayer interior as shown by the values of the co-ordination numbers for the acyl ester groups (i.e. the ester's oxygen and the carbonyl carbon, Table 3.3.1). Interestingly, for the 2Azone-DPPC bilayer there is no significant difference in the extent of hydration of the headgroup atoms between the monolayer with Azone and the one without.

The number density profiles calculated for the Azone-containing bilayer also show that water penetrates deeper into these bilayers than the pure DPPC bilayer. It is interesting to note that for the 2Azone-DPPC bilayer, the water penetrates about 3Å deeper into the Azone-containing monolayer than the pure DPPC monolayer. In fact, there is no significant change in the depth of water penetration in the pure DPPC monolayer in the 2Azone-DPPC as compared with the pure DPPC bilayer. In the

4Azone-DPPC bilayer there is also a slight increase in the depth of water penetration into the bilayer compared with the pure DPPC bilayer. Thus, while there is no significant change in the hydration of the lipid head's group caused by Azone, the presence of this molecule does allow more water to penetrate deeper into the bilayer interior. This effect is important as it makes the environment of the bilayer where water penetrates more hydrophilic thus reducing the diffusional resistance to hydrophilic molecules entering the bilayer.

Other important bilayer features affected by changes in the lipid disordering include the lamellar repeat distance (d-spacing), bilayer thickness and area per lipid headgroup. These parameters as well as the electron density profiles of the lipid bilayer are usually derived from X-ray diffraction studies (Chapman, 1983).

The average d-spacings in these simulations were determined form the electron density profiles (Figure 3.3.1) and also from the mean length of the simulation box measured in the X-direction (BoxX- Appendix 4). The two sets of results were in good agreement, and showed that there is an increase in d-spacing in the bilayer containing Azone compared with the pure DPPC bilayer. The d-spacing for the 2Azone-DPPC bilayer system determined from the average BoxX fluctuation during the production phase is 81.5Å, which represents an increase of about 8.5Å when compared with the pure DPPC bilayer. Rather surprisingly, however, when the number of Azone molecules was increased from two to four, this value dropped to about 76Å, an increase of only 3Å when compared with the pure DPPC bilayer.

The increase d-spacing is accompanied by a reduction in the surface area per DPPC/Azone molecule in the bilayers containing Azone. The values of the surface area per DPPC/Azone molecule in the 2Azone and 4Azone-DPPC bilayer models are 55.83$Å^2$ and 60.02 $Å^2$, respectively, to be compared with an area of 62$Å^2$ for the pure DPPC bilayer. The decrease in surface area per DPPC/Azone molecule is attributed to the fact that as the Azone diffuses into the bilayer hydrocarbon region it causes the DPPC headgroups to move closer together.

The observation that Azone increases the d-spacing of the DPPC bilayer is consistent with the experimental findings by Ward & Tallon (1990). In their X-ray diffraction

studies of an Azone-$C_{12}EO_5$/water bilayer (in the Lα-phase) these workers showed that the incorporation of Azone initially leads to an increase in d-spacing which is in proportion with the concentration added (Figure 4.5) and that further increases in Azone concentration lead to decrease in the d-spacing. These data and the results from the present simulations, however, are contradicted by the results from X-ray diffraction studies on an Azone-*stratum corneum* lipid model (Schuckler *et al.*, 1993). In these studies, the researchers examined the influence of Azone on a liquid crystalline lipid system composed of 6 fatty acids (stearic, palmitic, myristic, oleic, linoleic and palmitoleic acid) and also on another system containing the same fatty acids but with added cholesterol and ceramides. Incorporation of Azone in the former model, apparently did not reduce the bilayer d-spacing but did cause a slight reduction in the d-spacing in the latter model. The authors also observed that the X-ray diffraction pattern for the former system (Figure 4.6) was consistent with a mixed two-dimensional hexagonal with spacings of 58.5Å, 33.9Åand 29.3Å, and a one-dimensional array with spacing, 46.5 Å. The addition of Azone to this system did not alter the d-spacing of the hexagonal array, but at 30% w/w Azone, this character disappears leaving only the Lα's. Schuckler *et al.* (1993) explained these changes by reasoning that since Azone has a large headgroup surface area in comparison with its alkyl chain volume (implying a small critical packing parameter), the interpolation of the Azone molecules between the alkyl chains of the H_{II} structure would, therefore increase the average interfacial area per lipid/Azone molecule and induce the observed H_{II}-Lα transition.

An exact contradictory effect of Azone has been observed by Engblom and Ebgstrom (1993). In their X-ray diffraction study of the liquid crystalline model of soya lecithin incorporating Azone, these workers found that on addition of >20%w/w Azone caused an Lα-H_{II} transition in the system which was evidenced by changes in the phase diagram (Figure 4.6). On the basis of these results, it was deduced that Azone is not only anchored in the interfacial region but also distributed within the hydrocarbon core. The results from the present simulations agree with the latter observation showing that Azone distributes in the hydrocarbon regions of the DPPC (as seen in Figures 4.7 and 4.8) presumably because of its high lipophilicity (with the calculated logPoct/water, 6.21).

Another structural parameter which was monitored over the course of the MD simulations was the bilayer thickness. The bilayer thickness was determined as peak-to-peak distance in the electron density profile. (From the pure DPPC bilayer simulations, it was found that the peak of the density profile corresponds to that of the phosphorus distribution, and so can be used to estimate the bilayer thickness based on the definition of phosphorus-phosphorus separation). It was found that the bilayer thickness was reduced by the incorporation of Azone which is much as expected because of the significant increase in *gauche* defects in the hydrocarbon chains in the bilayers containing Azone molecules, which leads to a decrease in the length of the hydrocarbon chains of the lipid. As more *gauche* conformations are present in the 4Azone-DPPC bilayer than in the 2Azone-DPPC bilayer, it is thus not surprising that the former model has a lower bilayer thickness compared with the latter model. (An increased in the number of water molecules penetrating into the bilayer can also results in the decrease in the thickness of the bilayer, this was discussed earlier.)

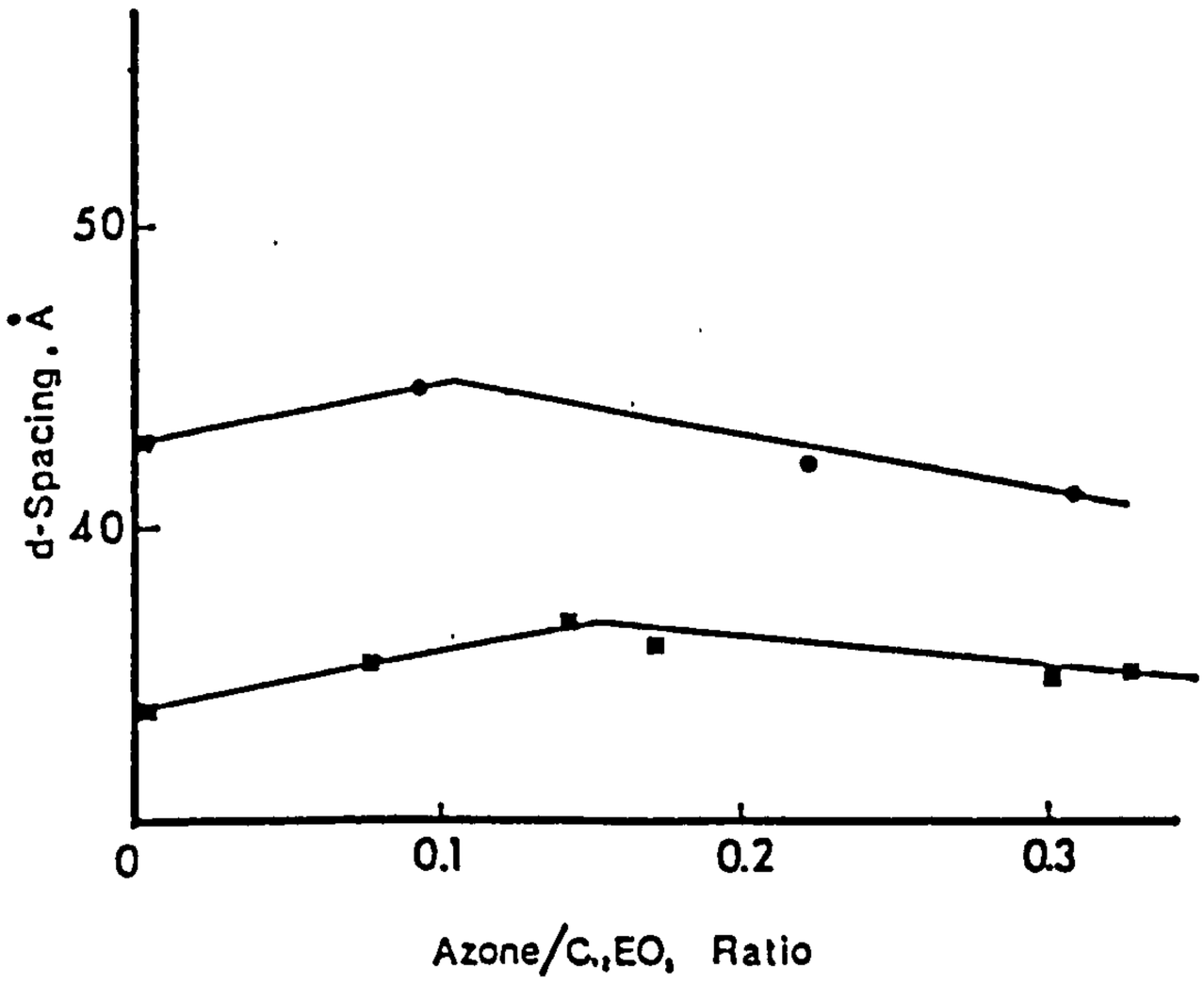

Figure 4.5 Lamellar repeat distance of the system n-dodecyl pentaoxythelene glycol ether/water as a function of Azone content. ■ 30%w/w water; ● 45% w/w water (Ward & Tallon, 1990).

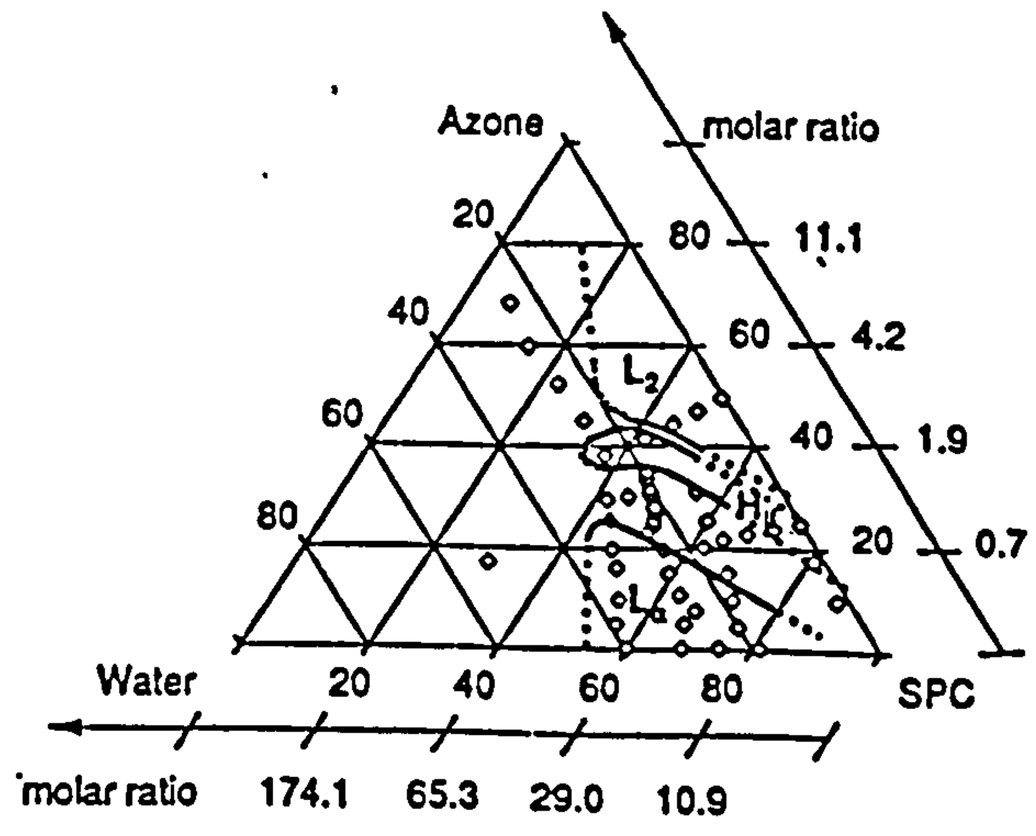

Figure 4.6 : Phase diagram for lecithin/water/Azone (Engblom & Engstrom, 1993)

All of the above observations not only describe the disordering effect of Azone on the lipid bilayer but can also be used to explain the mechanism of drug penetration enhancement of Azone on the lipid membrane. However, before describing this mechanism, it is important that the mechanism of solute diffusion into the lipid bilayer is understood. There are many theories available to explain this mechanism. The four-region model proposed by Marrink & Berendsen, (1996) is particularly pertinent to the discussions here. In this model, the membrane is divided into four regions;

Region 1: Bulk water or low head group density region. This region behaves essentially as bulk water, and so for most hydrophilic penetrants, the total permeation resistance is probably negligible. However, in the case of hydrophobic penetrants e.g. benzene, this water layer presents the largest resistance.

Region 2: The inter-phase or high head group density region. This region is said to have permeability resistance of a medium with a high dielectric constant and a high viscosity. Candidates for molecules whose permeation will be affected by this region include carbon dioxide and certain benzene derivatives which have hydrocarbon/water partition coefficients close to 1.

Region 3: Soft polymer or high tail density region. This region starts at the edges of the penetrating water interface and proceeds until the density of the membrane has dropped to a value close to that of liquid hexadecane. In most cases, this region will present barrrier to the diffusion of hydrophilic molecule because of its low solubilising capacity for this type of molecule and its low charge density. However, the formation of voids in this region will allow the small penetrants to diffuse in this region via a hopping mechanism.

Region 4: Fluid decane or low tail density region. This region has a lipid tail density much lower than that of the Region 3. Diffusion through this region is assumed to be characteristic of diffusion in liquids with low viscosity, and therefore does not provide any significant resistance to the penetrant molecules compared with the Region 3.

Relating the results of our MD simulations to this Four Region Model, it is noticed that the Azone molecules traverse very rapidly from the headgroup region (Zones 1 and 2, see Figure 2.8 & Figure 2.9) to the acyl-ester region Zone 3 where the diffusion of the molecules is slowed down for a long time (see Figures 4.7 and 4.8). This transition occurs within 30ps, and shows that Zone 1 and Zone 2 are relatively unimportant with respect to the permeation or diffusion of Azone. Even though Azone is highly lipophilic, the presence of its hydrophilic headgroup probably facilitates its diffusion into Zone 3. However, the number density profiles (Figures 3.3.2 and 3.3.3) indicate that there is an increase in the disorder and the mobility of the hydrophilic headgroup and acyl-ester regions (i.e. Zones 1 and 2). This is probably due to the voids created by Azone as it moves down into the bilayer interior. Zone 2 is said to be the rate limiting barrier for hydrophobic permeants (Marrink & Berendsen, 1996). Thus, the fact that Azone increases the disorder in this region indicate that this penetration enhancer is useful in enhancing the penetration of the hydrophobic drugs.

From considerations of the calculated number density profiles, order parameters, percentage of *gauche* defects, it was observed that Azone has its maximum disordering effect on the carbon atoms C2-C9 (See Figure 3.3.6 & Figure 3.3.7). These carbons are located in Zone 3. The results from the study of *gauche* defects show that there is a high fraction of *gauche* conformers in this zone, especially at low Azone concentration (2Azone-DPPC bilayer). Since this region is said to be region most critical to the permeation process, any perturbation of this region will reduce the diffusional resistance of other penetrating molecules, especially those that are highly hydrophilic. This thus supports the view that Azone penetration will enhance the permeation of hydrophilic molecules (Kai *et al.*, 1993).

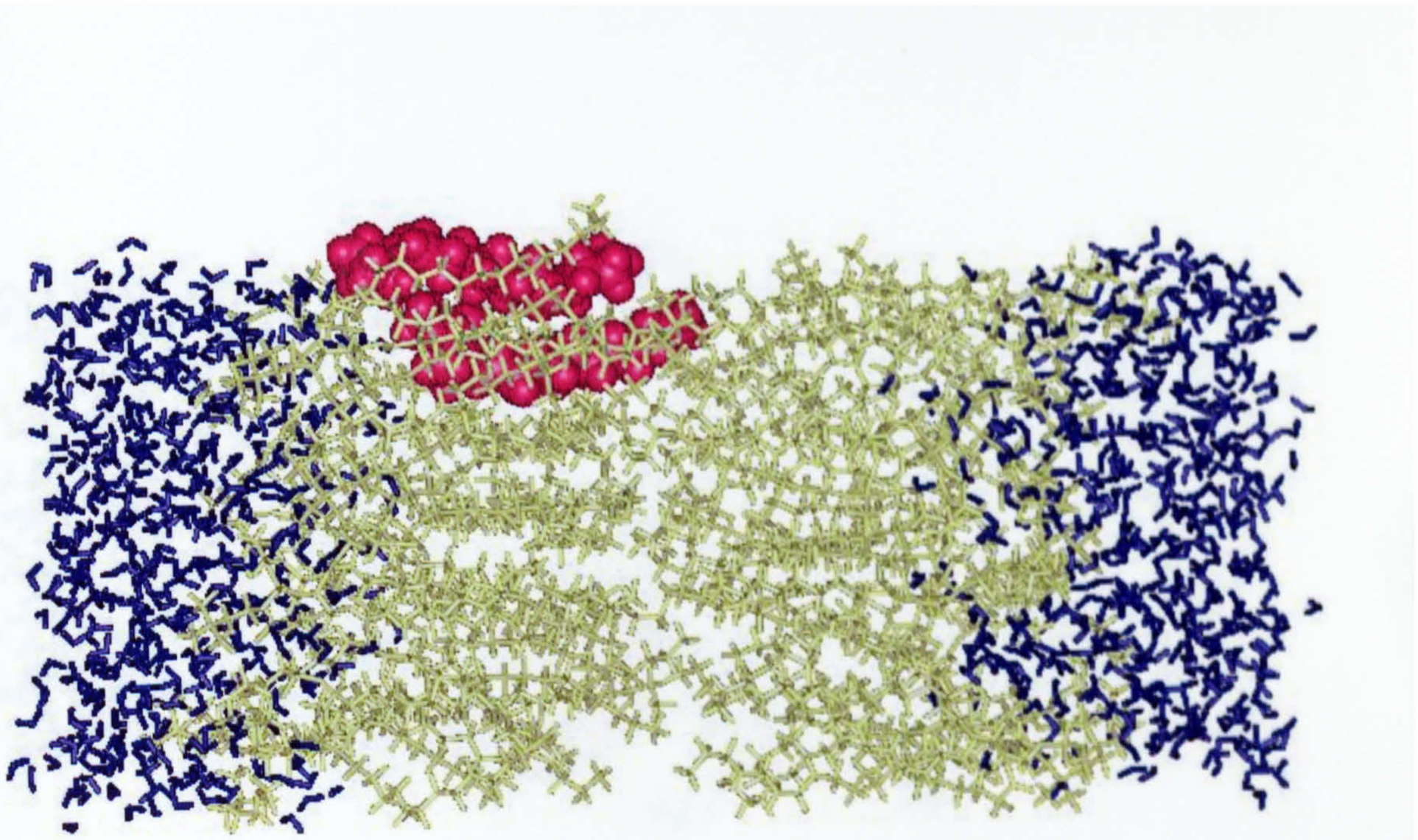

(a) at 30ps

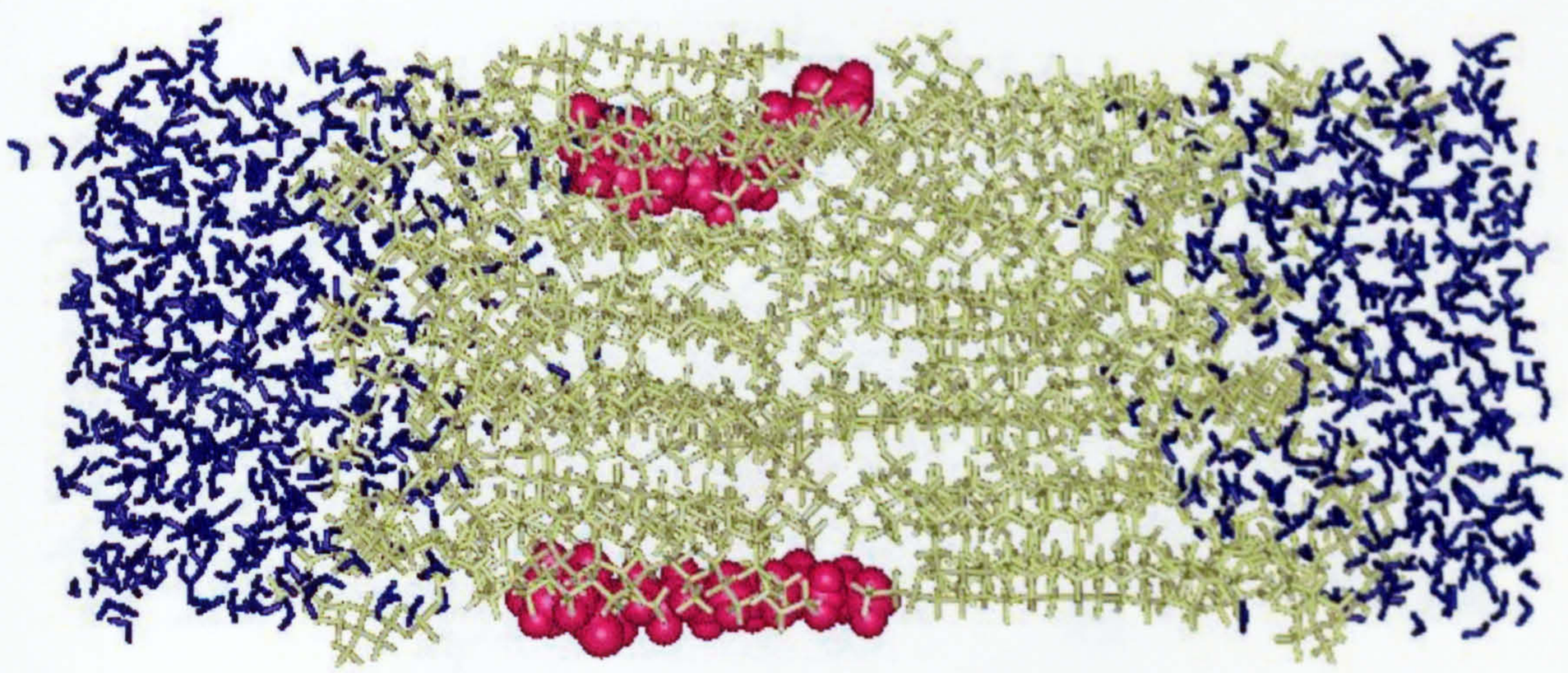

(b) at 321ps

Figure 4.7 The structure of the 2Azone-DPPC bilayer during the MD simulation.

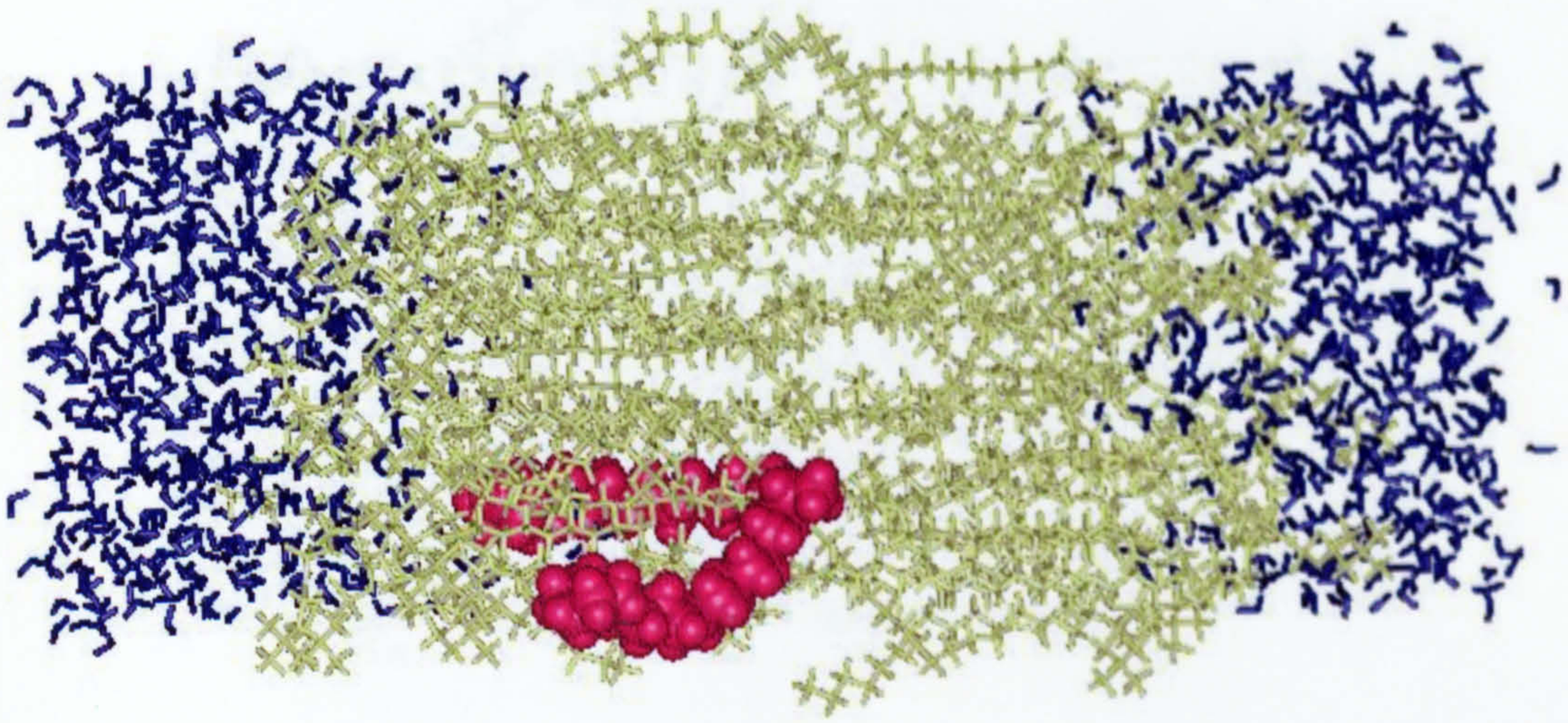

(c) at 760ps

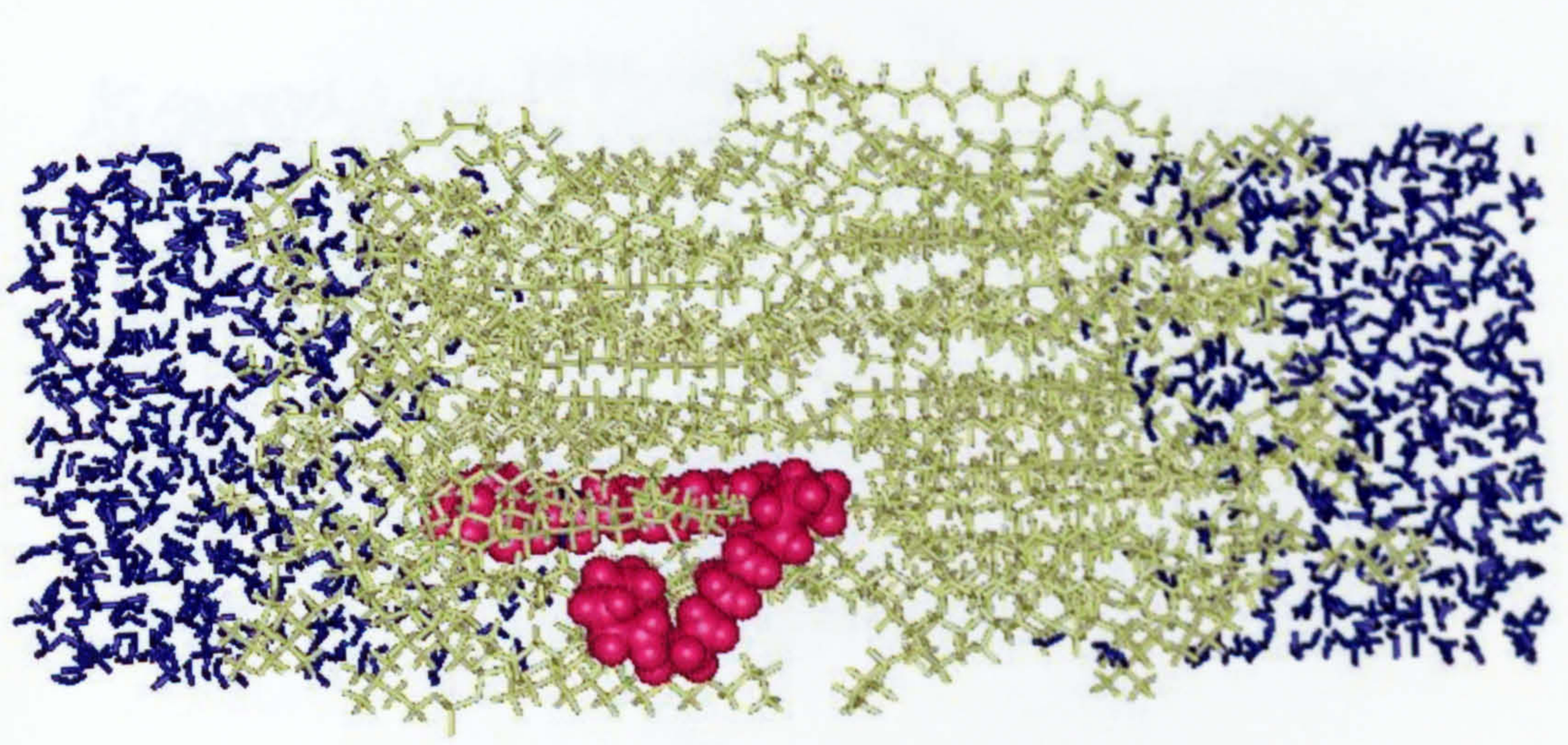

(d) at 1000ps

Figure 4.7 (ctd.) The structure of the 2Azone-DPPC bilayer during the MD simulation.

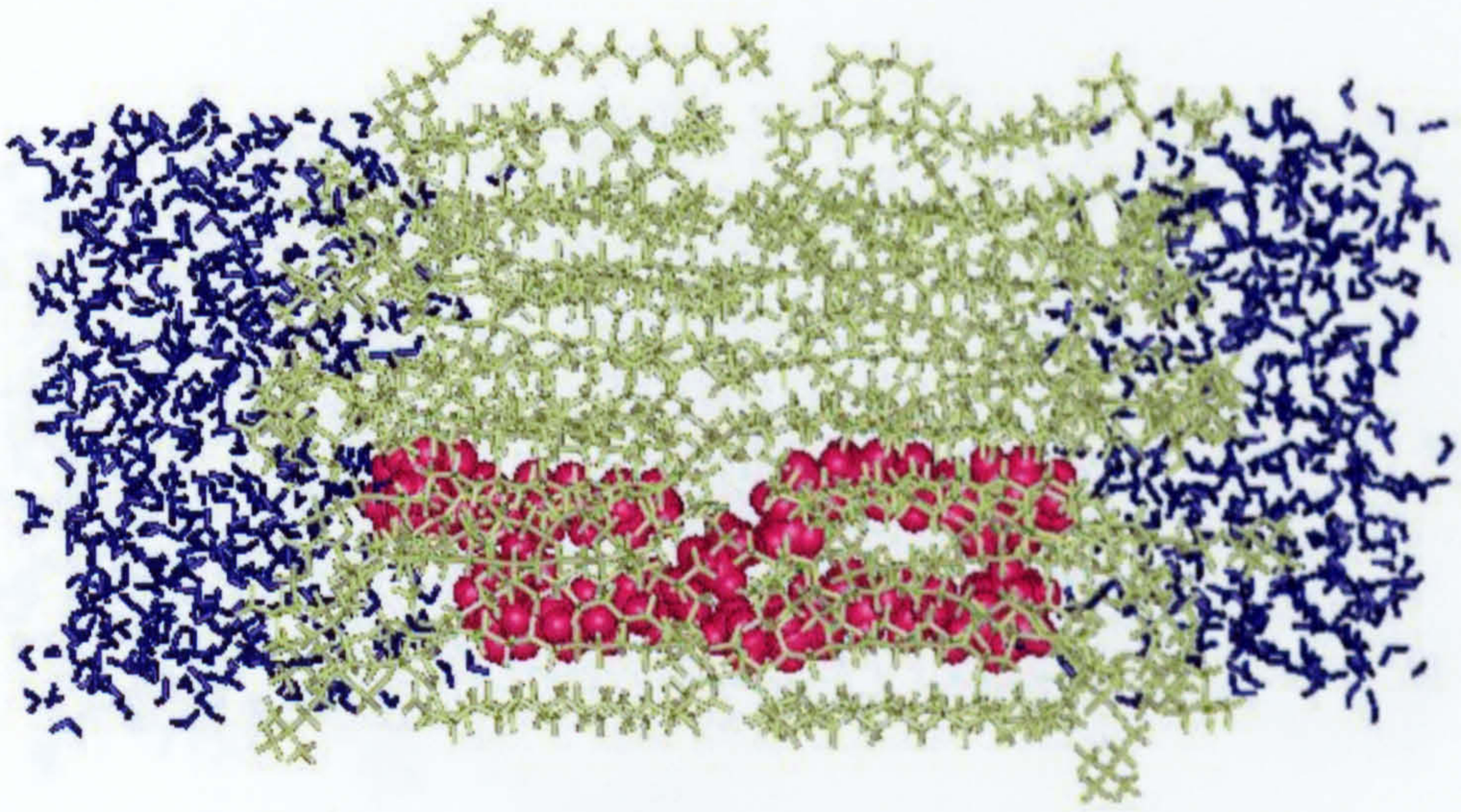

(a) at 30ps

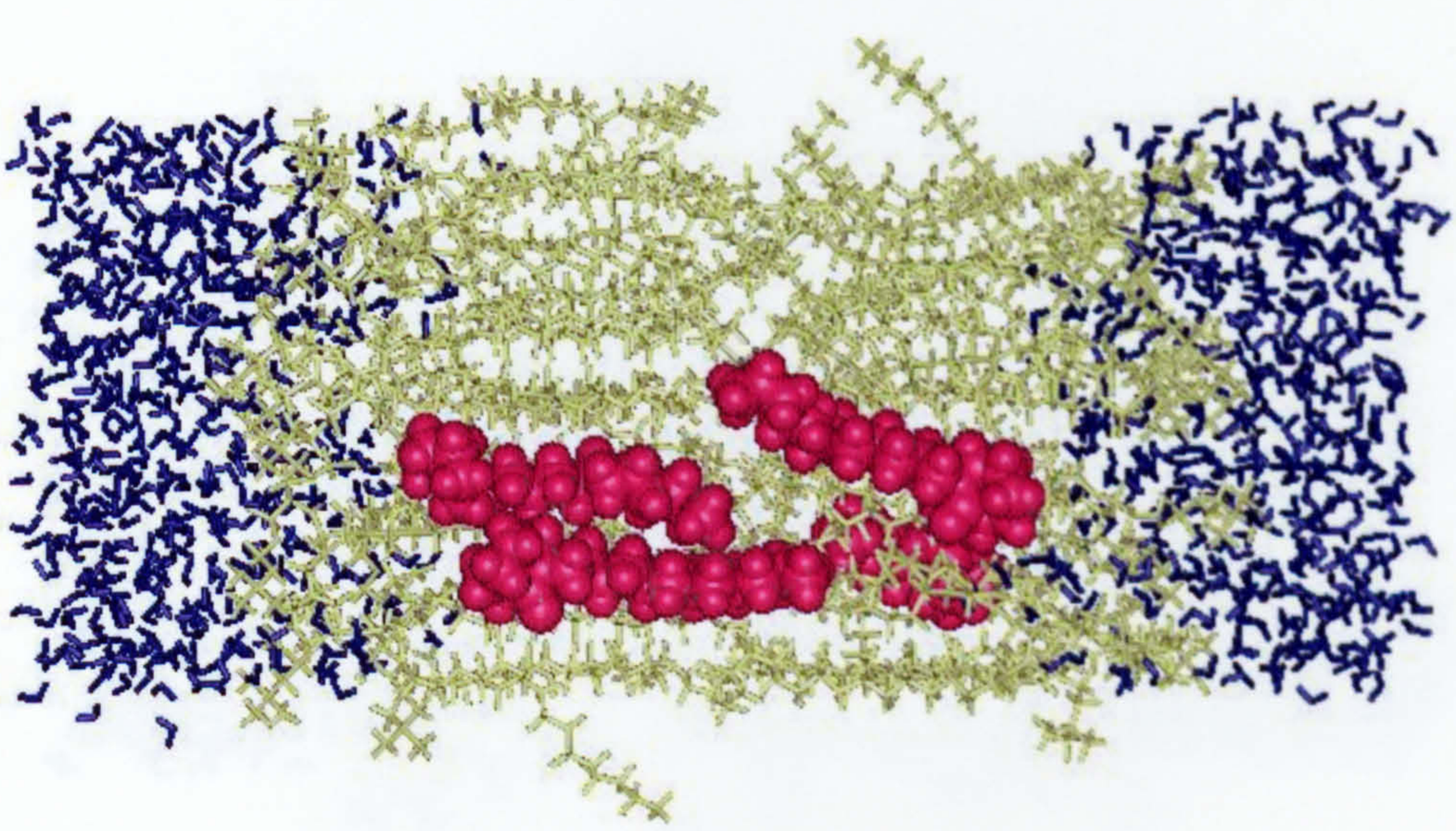

(b) at 318ps

Figure 4.8 The structure of the 4Azone-DPPC bilayer during the MD simulation.

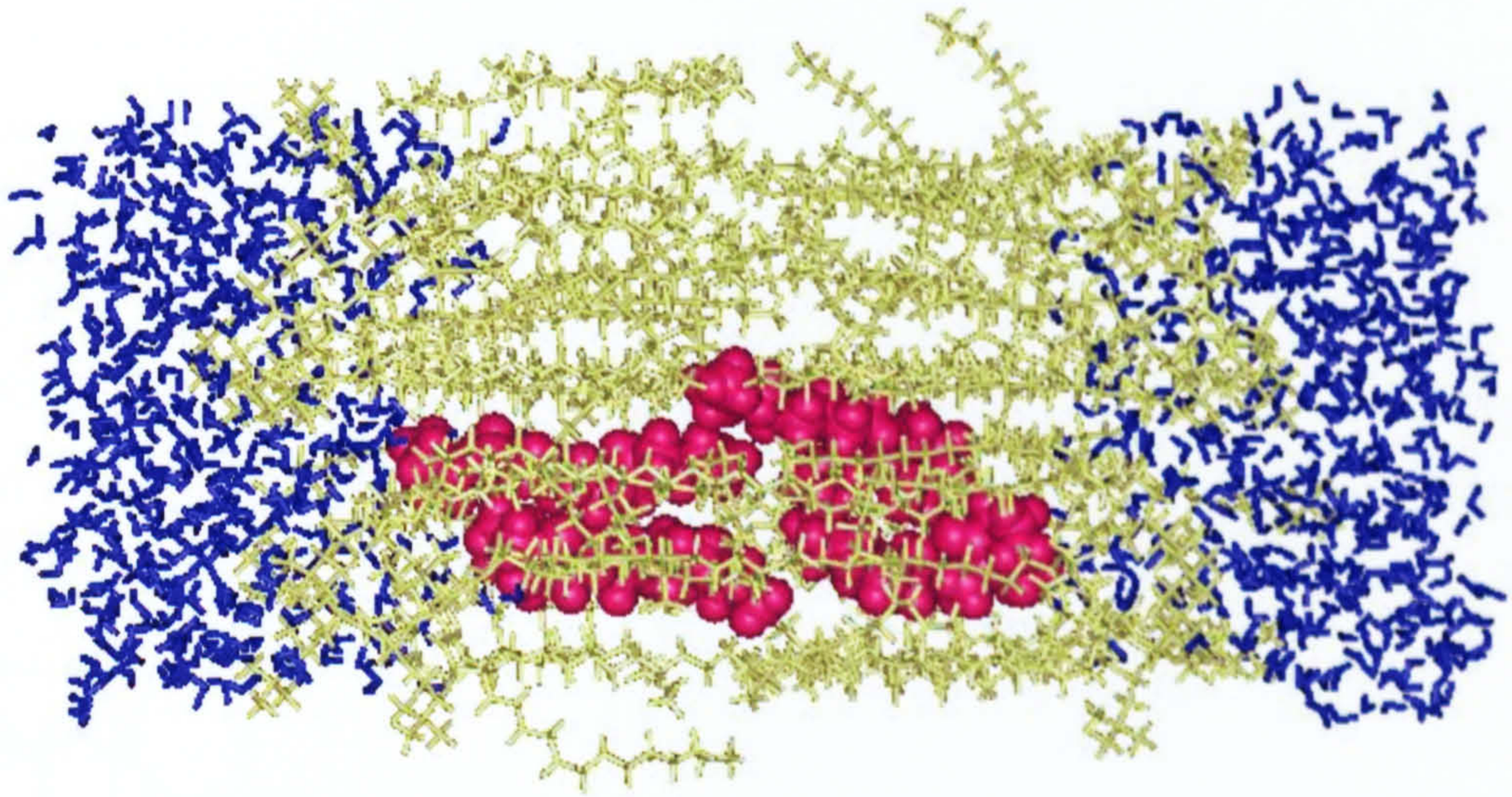

(c) at 738ps

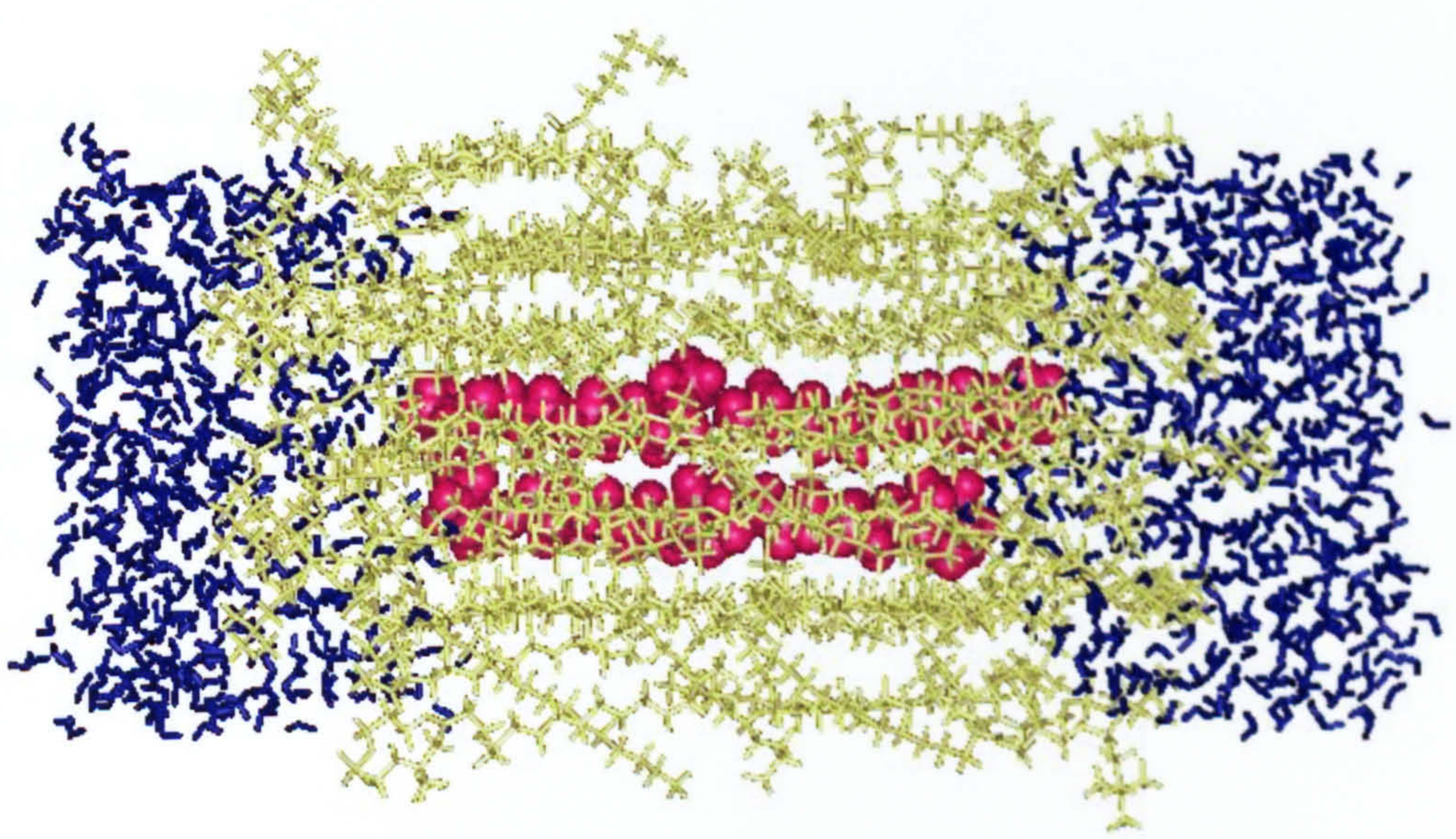

(d) at 997ps

Figure 4.8 (ctd.) The structure of the 4Azone-DPPC bilayer during the simulation.

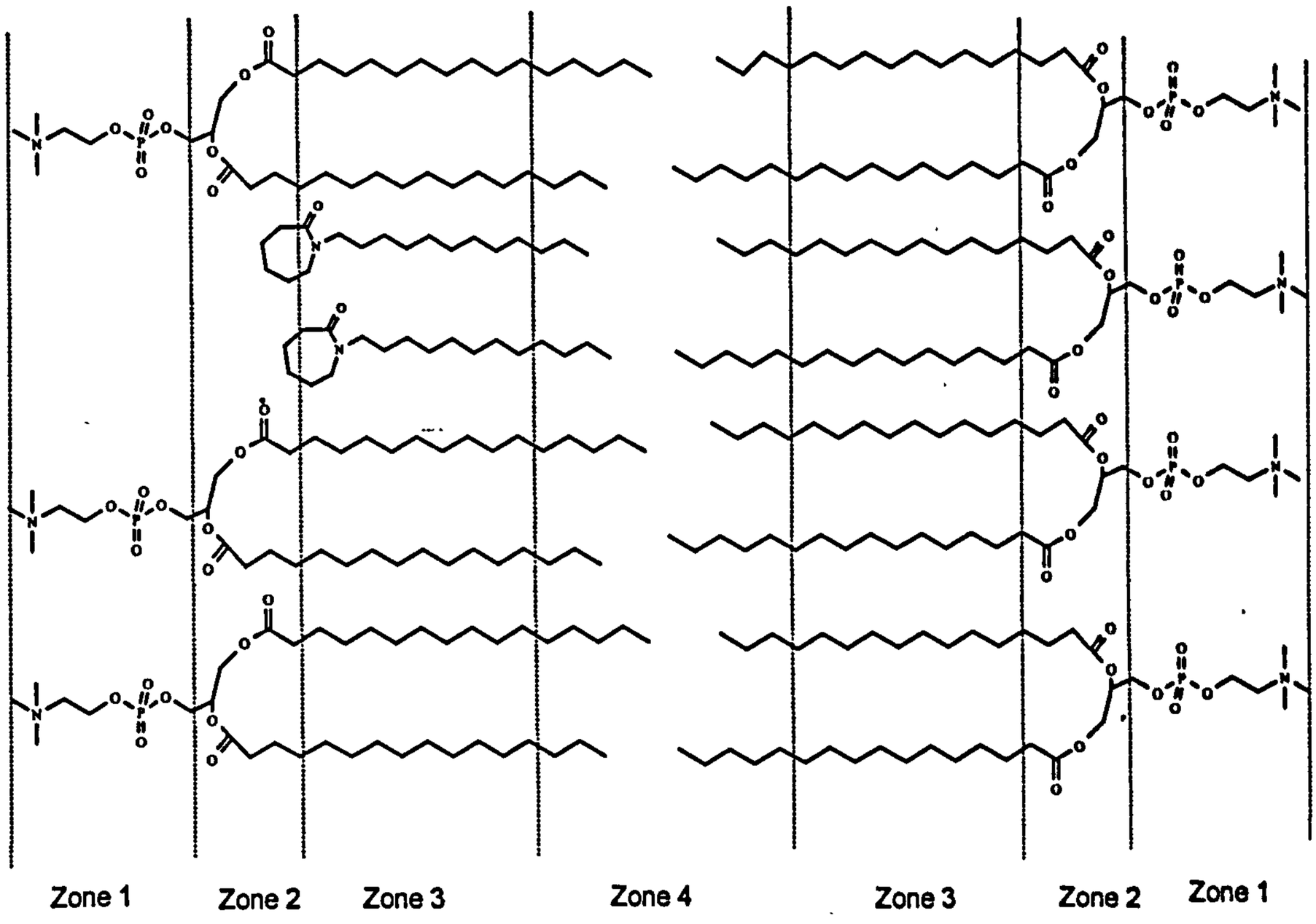

Figure 4.9: The proposed Azone Enhancement Model based on the Four Region Model (Marrink & Berendsen, 1996). Zone 1 provides the rate limiting barrier to absorption of lipophilic drugs while Zone 3 provides the main barrier to absorption of hydrophilic drugs. Intercalation of Azone in the bilayer membrane affects (i.e. disorders) both the hydrophilic regions (Zone 1 and Zone 2) as well as the hydrocarbon regions (Zone 3 & Zone 4), thus reducing the diffusional resistance of both hydrophilic and lipophilic drug molecules.

4.3 Azone Conformation

Several investigators have suggested that the conformation of Azone is an important factor accounting for its disordering effects on the lipid membranes (Lewis and Hadgraft, 1990; and Hoogstraate *et al.*, 1990). Bodde first proposed a 'spoon-shaped' model for Azone to explain its ability to disrupt the bilayer membrane (Hoogstraate et al., 1990). The evidence to support this hypothesis was presented by Lewis and Hadgraft (1990), who examined the effect of Azone on the compressibility of DPPC monolayers using a Langmuir trough. They found that Azone caused a large expansion in the mean area per molecule. Based on this result, they proposed that the Azone headgroup's conformation is important to its activity. Using a molecular modelling technique, they calculated that the energy required to produce the spoon-shaped structure (by rotating the N-C-C-C bonds adjacent to the headgroup is only 5 kcal/mol (calculated using MOPAC) above the global minimum energy conformation, which they suggested to be readily accessible at 25°C.

Hoogstraate *et al.* (1991) also supported the theory that a spoon-shaped model of Azone accounts for its lipid disordering capability. They calculated the energy of formation of this structure and the global minimum energy's structure using the same program. They found that the spoon-shaped conformer is within 1kcal/mol of the lowest energy conformer. It is argued that the formation of the spoon-shaped structure is caused by the fact that the carbonyl moiety in the molecules' headgroup (being a strong hydrogen bond acceptor) will orient itself away from the lipid bilayer and into the polar region as much as possible. With this structure, the amide oxygen becomes exposed for hydrogen bonding with the polar lipid headgroups or with the interstitial water.

In our quest to confirm this speculation, we carried out a cluster analysis of the conformations of Azone adopted in our MD simulations. The results show that the majority of the Azone conformers the headgroup ring oriented linearly with respect to the alkyl chain (Figure 3.3.10). The differences in energy of these structures were within 7kcal/mol the lowest energy structure. (Note that our calculation is based on a classical mechanical force-field and not the semi-empirical calculation, as was used by the previous workers). The fact that the spoon-shaped structure was not found

among the major cluster representatives, may be because either it does not occur or because it is not formed within the simulation time frame.

In favour of the former conclusion, it is noted that the energy minimum calculated for the spoon-shaped model (with the alkyl chain all trans) is only 0.8kcal/mol higher than the global energy minimum and so under normal circumstances, this structure should be formed easily.

From these MD studies, therefore, it seems that the carbonyl group is perfectly capable of satisfying its hydrogen bond potential without adopting the 'spoon-shaped' structure. In considering whether the spoon-shaped structure is important to account for the ability of Azone to induce disorder in the bilayer membrane therefore, the results from the present studies would indicate that it is not and that even without the formation of the spoon-shaped conformation Azone can still induce a large disorder in the membrane.

5.CONCLUSION

5.1 Objectives accomplishment and opportunities for future work

The goal of the present molecular dynamics was to study the effects of a penetration enhancer, Azone, on the physical state of a lipid membrane. A penetration enhancer is said to be effective if it is able to perturb the barrier properties of the skin membrane, which is commonly thought to be provided by the intercellular lipid. The perturbation usually results in the disorder of the membrane, thus affecting the fluidity of the membrane. Increasing the fluidity of the membrane consequently results in decreasing the permeability resistance to the penetrating molecules in the membrane.

An appropriate model and the MD methodology for studying the effects of Azone on lipid membranes have been developed. The DPPC bilayer model in the liquid crystalline state has been used in the past as a model for the stratum corneum lipid (Beastall *et al.*, 1988), and the results showed that this model is an adequate representation of the liquid crystalline lipid model. This model was consequently used as a control and also to study the effects of the incorporation of Azone molecules where the disorder (hence the fluidity) of the membrane was quantified. The disorder in the systems was monitored by measuring the distributions of the lipid components in the system, the order parameters of the carbons along the hydrocarbon chains, the number of *gauche* defects in the hydrocarbon chains and the diffusion of the molecules in the system. All of these results consistently show that Azone increases the disorder of the bilayer, and are summarised in Figure 5.1.

Figure 5.1 illustrates the effect of Azone incorporation into the bilayer membrane based on the present simulations' observations. Azone molecules are found to

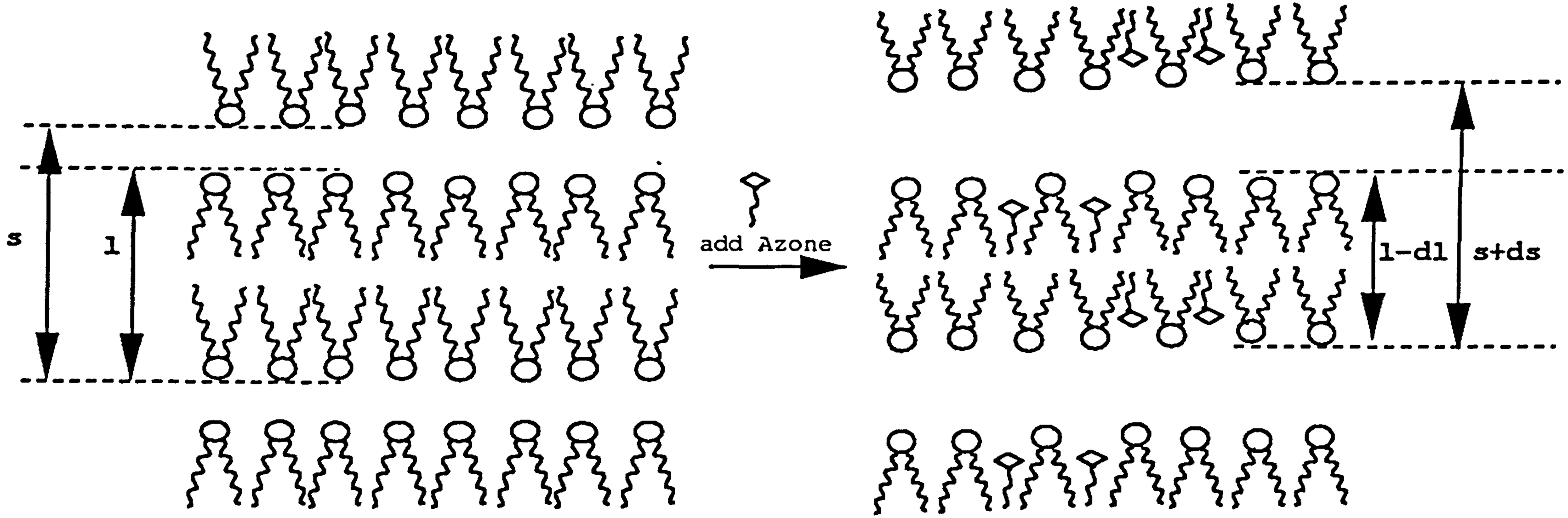

Figure 5.1 : Intercalation of Azone into the lipid bilayer . Azone increases the disorder of the headgroup and hydrocabon regions of the bilayer as well as decreasing the bilayer thickness. The lamellar repeat distance is also increased as a result of increase in the water layer.

intercalate into the hydrocarbon region of the bilayer. Due to its large headgroup, as the molecule diffuses into the hydrocarbon region of the bilayer, it creates spaces or voids above and below its ring which allow more freedom of the lipids atoms in the headgroup as well as the hydrocarbon region to move (the results are seen from the increased in the width of the distribution of the lipid's atoms in this region and increase in the *gauche* fraction in the hydrocarbon region). The increase in the disorder of the system due to the creation of voids in the system that leads to the increase in *gauche* defects in the lipid hydrocarbon chains and consequently results in a decrease in the thickness of the membrane. The simulations successfully quantified the disordering effect of Azone on the lipid membrane, although the mechanism by which it increases the permeation of hydrophilic and lipophilic drugs into the bilayer membrane remains speculative. The Azone-Enhancement model (Figure 4.9) based on the Four Region Diffusion model (Marrink & Berendsen, 1996) is an attempt to explain the ability of Azone to increase the permeation of both types of drugs and has been confirmed by a number of experiments. Based on the Four Region Model, it is clear that the lipid bilayer not only provides the rate limiting barrier to hydrophilic permeants but lipophilic permeants as well. The present simulations' results showed that Azone perturbs all the diffusion zones, reducing the permeability resistance in these regions thus explaining the ability of Azone to enhance the permeation of a wide spectrum of drug molecules.

The present study only probes the perturbation effect of Azone into the lipid membrane, and does not give the full answer as to what is happening in the *stratum corneum* environment. The heterogeneity of the *stratum corneum* undoubtedly provides different diffusional pathways to different drug molecules. However, as the intercellular lipid of the stratum corneum is said to provide the rate limiting barrier to percutaneous penetration, the results of the present study should be adequate as a basis for understanding the mechanism of action of Azone in the *stratum corneum*.

The areas of transdermal drug delivery and molecular dynamic simulations are two newly emerging areas that offer a lot of opportunity for further research. The present MD results, although agreeing with the experimental observations qualitatively, would be more useful if compared quantitatively and this would require the acquisition of further experimental data. For examples, the position of Azone in the membrane could be determined using neutron diffraction (employing deuterated Azone). In addition, it would be useful if one could derive the electron density profile of a bilayer containing Azone using X-ray diffraction. Bond order parameters for the lipid alkyl chains in the presence of Azone could also be determined using $^{II}_{2}$NMR and it would be useful to determine the diffusion coefficients of the Azone and DPPC molecules experimentally. If all of these parameters when determined experimentally were found to agree with those obtained from MD calculations, it would give greater confidence to extend the application of MD simulations to other studies.

Another important extension of the present work would be to determine the molecular features of an ideal penetration enhancer. For example, one might modify the structure of Azone (by increasing or decreasing the length of the alkyl chain, or by modifying the headgroup of the molecule so as to increase or decrease the lipophilicity of these parts of the molecule) and measure its interaction with the membrane. Such MD studies would save time and money in the rational development of improved penetration enhancers.

Concluding Remark

The results from these studies have shown that the MD simulations not only agree with the experimental observations but are also able to generate insight as to how a chemical penetration enhancer might works at an atomic level. The present study provides a clear view as to how the penetration enhancer, Azone interacts with the lipid membrane. This suggests that MD simulation may provide a powerful research tool in the area of transdermal drug delivery, enabling the study not only of penetration enhancer-lipid interactions but also drug-lipid as well as drug-penetration enhancer-lipid interactions. With the increased understanding of the mechanism of action of penetration enhancers, so provided it could be hoped that more drugs might be formulated for administration via this attractive route.

6.REFERENCES AND BIBLIOGRAPHY

Alder, B.J. & Wainwright, T.E. *J. Chem. Phys.* **27**, 1208-1209, (1957).

Allen & Tildesley, Computer Simulation of Liquids, Oxford University Press, Oxford (1987).

Alper, H. Bassolino, D., and Stouch, T., *J. Chem. Phys.* **98**, 9798, (1993)

Alper, H & Stouch, T., *J. Phys. Chem.*, **99**, 5724-5731 (1995).

Barry, B.W., Dermatological Formulations:Percutaneous Absorption, Marcel Dekker, New York, (1983).

Barry, B.W., *J. Control. Rel.*, **6**, 85, (1987).

Barry , B.W. *J. Control. Rel.*, **15**, 237(1991).

Bassolino-Klimas, D., Alper, H., & Stouch, T., *Biochem.*, **32**, 12624-12637 (1993).

Bassolino-Klimas, D., Alper, H.E., & Stouch, T. R., *J. Am. Chem. Soc.*, **117**, 4118-4129 (1995).

Bassolino, D., Alper, D., Stouch, T.R., *Drug Design Discov.*, **13**(3-4), (1996).

Beastall, J.C., Hadgraft, J., Washington, C., *Int. J. Pharm*, **43**, 207-213, (1988).

Beeman, D. *J. Comp. Phys.* **20**, 130-139 (1976).

Behl, C. R., Flynn, G. L., Linn, E.E. and Smith, W. M., J. *Pharm. Sci*, **71**, 229-234, 1982.

Behl, C.R., Flynn, G.L., Linn, E.E. & Smith, W.M., *J. Pharm. Sci*, **73**, 1287-1290 (1984).

Belohorcova, K., Davis, J.H., Woolf, T. B. & Roux, B., *Biophys. J.*, **73**, 3039-3055 (1997).

Berendsen, H.J.C., Postma, J.P.M., van Gunsteren, W.F., DiNola, A.D. & Hack, J.R. *J. Chem. Phys.* **81**, 3684 (1984).

Berendsen, H.J.C. and Egbert, E., in Structure, Dynamis and Functions of Biomolecules : First EBSA Workshop, Saltsjobadan, Enrenberg, A., Rigler, R., Grasland, A., and Nilson, L. Eds., Berlin, Springer, 1986

Blank, I.H., in Dermatology in General medicine, 3rd ed., Fitzpatrick, T.B., Eisen, A.Z., Wolff, K., Freedberg, I.M., and Austin, K.R., Eds, McGraw Hill, chap. 28. 1987

Bodde, H.E, Kruithof, M.A.M., Brusse, J., and Koerten, H.K., *Int. J. Pharm.*, **53**, 13-24, 1989

Bouwstra, J. A., Peschier, L.J.C., Brussee, J., Bodde, H. E., *Int. J. Pharm.*, **52**, 47-54, 1989

Bodde, H. E., Ponec, M., Ijzerman, A.P., Hoogstraate, A.J., Solomons, M.A.I. & Bouwstra, J, in "Pharmaceutical Skin Penetration Enhancement", eds, Walters, K.A. & Hadgradft, J., Marcel Dekker, Inc., (1993).

Bouwstra, J.A., Gooris, G.S., Brussee, J., Solomon-de Vries, M.A. & Bras, W. *Int. J. Pharm.*, **79**, 141-148 (1992).

Bouwstra, J.A., de Vries, M.A., Bras, W., Brussee, J., & Gooris, G.S., *Proceed. Intern. Symp. Control. Rel. Bioact. Mater.*, **17**, 22-25, (1990).

Bouwstra, J. A., Gooris, G.S., van der Spek, & Bras, W, *J. Invest. Dermatol.*, **97**, 1005-1012, (1991).

Bouwstra, J.A., Gooris, G. S., Brussee, J., Solomon-de Vries, M.A., & Bras, W., *Int. J. Pharm.*,**79**, 141-148, (1992).

Bouwastra, J.A., Gooris, G.S., Solomon-de Vries, M.A., van der Speck, J.A., & Bras, W, *Int. J. Pharm.*, **84**, 205-216, (1992).

Bouwstra, J.A., Gooris, G.S., & Cheng,, K., Weerheim, A., Bras, W., & Ponec, M., *J. Lipid Res.*,**37**, 999-1011, (1996).

Braganza, L.F. & Worcester, D.L., *Biochem.*, **25**, 2581 (1986).

Brain, K.R. & Walters, K.A. in. Pharmaceutical Skin Penetration Enhancement, eds. Walters, K.A. & Hadgraft, J., Marcel Dekker Inc., (1993).

Brooks, B.R., Bruccoleri, R.E., Olafson, B.D., States, D.J., Swaminathan, S., & Karplus, M., J. Comp. Chem. , 4(2), 187-217 (1983).

Buldt, G., Gally, H.U., Seelig, A., Seelig, G. & Zacchai, G., *Nature*, **271**, 182 (1978).

Buldt, G., Seelig, G. & Zacchai, G., *J. Mol. Biol.*, **134**, 673-691 (1979).

Chapman, D., Williams, R.M. & Ladbrooke, B.D. *Chem. Phys. Lipids*, **1**, 445 (1967).

Chapman, D. and Wallach, D.F.H., in *Biological Membrane*, Vol 1, Chapman, D. ed., London, Academic Press, 1968.

van Duzee, B. F. *J. Invest. Dermatol.*, **65**, 404-408, 1975.

Chapman, D. "Biomembrane Structure and Function", Macmillan Press, London, 1982.

Charifson, P.S., Hiskey, R.G., & Pederson, L.G., *J. Comp. Chem.*, **11**, 1181-1186, (1990).

Chiu, S-W., Clark, M., Balaji, V., Subramaniam, S., Scott, H.L., & Jakobsson, E., *Biophys J.*, **69**, 1230-1245, (1995).

Damodaran, K.V., Gaber, B. & Merz, K.M. Jr., *Biochem.*, **31**(33), 7657 - 7664 (1992)

Damodaran, K.V., & Merz, K.M. Jr, *Langmuir*, **9**, 1179-1183, (1993).

Damodaran, K.V., & Merz, K.M. Jr., *Biophys. J.*, **66**, 1076-1087 (1994).

Damodaran, K.V. & Merz, K.M. Jr., *J. Am.Chem.Soc.*,**117**, 6561-6571, (1995).

Downing, D.T., Wertz, P.W. & Stewart, M.E., *Int. J. Cos. Sci.*, **8**, 115-123 (1986).

Devani, S., in "Molecular dynamics simulation of pressure-induced phase transformations." PhD Thesis, University of London, (1998).

Duzee, B. F. van, J. Invest. Dermatol., 65, 404-408 (1975). Edholm , O., & Nyberg, A.M., *Biophysical J.*, **63**, 1081-1089, (1992).

Edholm, O. and Nyberg, A. M. *Biophys. J.*, **63**, 1081-1089, 1992

Egberts, E. & Berendsen, H.J.C., *J. Chem. Phys.*, **89**(6), 3718-3731 (1988).

Egbert , E., Marrink SJ, & Berendsen, H, *Eur. Biophys. J*, **22**, 423-436 (1994).

Egbert, E., *PhD. Thesis*, University of Gronigen, The Netherlands, 1988

Elias, P.M.. *Arch. Dermatol. Res.* **270**, 95(1981).

Elias, P.M., J. Inv. Derm., **80**(SS), *S44-S49*, (1983)

Elder, M., Hitchcok, P., Mason, R. & Shipley, G.G. *Proc. R. Soc. London*, **354A**, 157 (1977).

Elias, P.M., Eugene, R., Cooper, R., Korc, A. & Brown, B. *J. Inv. Dermatol.*, 76, 297-301 (1981).

Engblom, J. and Engstrom, S., *Int. J. Pharm.*, **98**, 173-179, 1993

Epand, R.M. *Biochem. Cell. Biol.*, **68**, 17-23, (1989).

Essex, J.W., Hann, M.M., & Richards, W.G., *Phil. Trans. R. Soc. Lond. B*, **344**, 239-260, (1994).

Feller, S.E. Venable, R. M., and Pastor, R.W., *Langmuir,* **13**, 6555-6561, 1997

Feingold, K.R., Crit. Rev. Ther. Drug Carrier Syst., 8(3), 193-210 (1991).

Feller, S.E. & Pastor, R.W., *Biophys. J.*, **71**, 1350-1355, (1996).

Feller, S.E., Zhang, Y., & Pastor, R.W., *J. Phys. Chem.*, **103**, 10267-10276, (1995).

Finer, E.G. & Drake, A. *Chem. Phys. Lipids*, **12**, 1 (1974).

Flynn G. L., Yalkowsky, S.H., Roseman, T., *J. Pharm. Sci*, **63**, 470-510, 19743.

Friberg, S.E. & Osborne, D.W., *J. Disp. Sci. Technol.*, **6**, 485-495, (1985).

Frisch, F.M.J., Head-Gordon, M., Trucks, G.W., Foresman, J.B., Schlegel, H.B., Raghavachari, K., Robb, M., Binkley, J.S., Gonzales, C., Defrees, D.J., Fox, D.J., Whiteside, R.A., Seeger, R., Melius, C.F., Baker, J., Martin, R.L., Kahn, L.R., Stewart, J.J.P., Topiol, S. & Pople, J.A. "Gaussian90. Revision". Gaussian Inc, Pittsburgh, PA (1990).

Fukada, T., Okazaki, S., & Okada, I., *Biophys. J.*, **64**, 1344-1353 (1993).

Gabdoulline, R.R., Vanderkooi, G. & Zheng, C. *J. Phys. Chem*, **100**, 15942-15946, (1996).

Gear, C.W. "Numerical Initial Value Problems In Ordinary Differential Equations". Prentice Hall, Englewood Cliffs, NJ. (1971).

Gennis, R.B. "Biomembrane: Molecular Structure and Function" Springer-Verlag, New York, (1989).

Gilson, M.K., *Curr Opinion in Struct. Biol.*, 5(2), 216-213, (1995).

Golden, G.M., Guzek, D.B., Kennedy, A.H., McKie, J.E. & Potts, *Biochem.*, **26**, 2382-2388 (1987).

Goodman, M., and Barry, B.W., J. Pharm. Pharmacol., **77**, 80, 1985

Goodman, M., and Barry, B.W., *Anal. Proc.* **23**, 397, (1986).

Goodman, M., and Barry, B.W., in *Percutaneous Absorption*, 2nd ed., Bronaugh, R.L. and Maibach, H.I., Eds., Marcel and Dekker, New York, (1989).

Gunsteren, W.F. van & Berendsen, H.J.C. *Mol. Phys.*, **34**, 1311-1327 (1977).

Gunsteren, W.F. van, *Mol. Sim.*, **3**, 187-200 (1989).

Gunsteren, W. F. van & Karplus, M. *Macromolecules*, **15**, 1528-44, 1982

Guy, R.H., Hadgraft, J. & Bucks, D.A.W. *Xenobiotica*, **17**(3), 325-343 (1987).

Guy, R.H. & Hadgraft, *J. Pharm. Res*, **5**, 753-8 (1988).

Hadgigeorgiou, C., in "Molecular Modelling Studies on Bidentate Iron Chelators." PhD Thesis, University of London (1997).

Hadgraft, J., *Int. J. Pharm.*, **16**, 225, (1983).

Hadgraft, J., & Ridout, G., *Int. J. Pharm*, **42**, 97-104, (1988).

Hadgraft, J., William, D.G. & Allan, G. in "Pharmaceutical Skin Penetration Enhancement". Walters, K.A. & Hadgraft, J. Eds., Marcel Dekker Inc, New York (1993).

Haile, J.M. "Molecular Dynamics Simulation: Elementary Methods", John Wiley & Sons, New York (1997).

Harrison, J.E., Groundwater, P.W., Brain, K.R., & Hadgraft, J., *J. Controlled Release*,**41**, 283-290, (1996).

Hauser, H., Pascher, I., Pearson, R.H., & Sundell, *Biochim. Biohys. Acta*, **650**, 21-51, (1981).

Heller, H., Schaefer, M., Svhulten, K., *J. Phys.Chem*, **97**, 8343-8360, (1993).

Hockney, R.W. *Methods Comput. Phys.* **9**, 136-211, (1970).

Hoogstraate, A.J., Verhoef, J., Brussee, J., Ijzerman, A.P., & Bodde, H.E., *Int. J. Pharm.*, **76**, 37-47 (1991).

Hsieh, CH, & Wu, W., *Biophys. J.*, **69**, 4-12, (1995).

Huang, P., Perez, J.J., & Leow, G.H., *J. Biomol. Struc. & Dynamics*, **11**(5), 927-956, (1994).

Huang, P., Bataccini, E. & Leow, G.H., *J. Biomol. Struc.& Dynamics*, **12**(4), 725-754, (1995).

Hypercube Inc., Hyperchem version 4.5 (1996).

Israelachvili , *Quart. Rev. Biophys.* (1980)

Jahnig, F. *Biophys. J.*, **71**, 1348-1349 (1996).

Jakobsson, E., Subramaniam, S. & Scott, H.L., in "Biological Membrane - A Molecular Perspective from Computation and Experiment" Merz, K.M., Jr., & Roux, B., eds, Birkhauser, Boston, (1996).

Jorgensen, W.L., & Triado-Rives, J., *J. Am. Chem. Soc.*, **110**, 1657, (1988).

Jorgensen W. L., Chandrasekhar, J., Madura, J.D., Impey, R.W., & Klein, M.L. *J. Chem. Phys.*, **79**, 926-935 (1983).

Huang, P., & Leow, G., *J. Biomol. Struc. & Dynamics*, **12**(5), 937-956, (1995).

Kai, T., Nakazono, M., Kurosaki, Y., Nakayama, T. & Kimura, T. *Biol.Pharm. Bull.*, 16(8), 801-805 (1993).

Karplus , M & Petsko, G.A. *Nature*, **347**, 631-639 (1990).

Katsu, T., Kurozo, M., Sanchika, K, Morikawa, T, Kurosaki, Y, Nakayama, T., Kimura, T, & Fujita, Y., *Int. J. Pharm.*, **53**, 61-66, (1989).

Knutson, M., Potts, R.O., Guzek, D.B., Golden, G.M., McKie, J.E. Lambers, W.J. & Higuchi, W.I., *J. Controlled Release*, **2**, 67-87, (1985).

Kothekar, V., *J. Biomol. Str. & Dynamics*, **13**(4), 601-613, (1996).

Landmann, L. *Anat. Embryol.*, **178**, 1-13 (1988).

Leach, A.R. "Molecular Modelling: Principles And Applications", Longman, Singapore (1996).

Lesslauer, W., Cain, J.E. & Blassie, J.K. *Proc. Nat. Acad. Sci. USA*, **69**, 1499-1503 (1972).

Lewis, D., & Hadgraft, J., *Int. J. Pharm.*, **65**, 211-218, (1990)

Liang, C., Ewig, C.S., Stouch, T. & Hagler, A.T. *J. Am. Chem. Soc.*, **115**, 1537-1545 (1993).

Luzzatti, V., Mustacchi, H., Skoulios, and Husson, F, *Acta Cryt.* **13**, 660-667 (1960).

Luzzatti, V. in *Biological membranes*, Chapman.D., Eds., Vol. *1*, 71-123, London, Academic Press, 1968

Marrink and Berendsen, *J. Phys. Chem.*, **100**, 16729-16738,1996

McKintosh, T. J. *Biophys. J.* **29**, 237-246, 1980

MacKerrel, A.D. Jr, Wiorkiewicz-Kuzera, J., & Karplus, M., *J. Am. Chem. Soc.*, **117**, 11946-11975 (1995).

MacKerrel, A.D. Jr., *J. Phys. Chem.*, **99**, 1846-1855 (1995).

Marrink S.J., Berkowitz, M. & Berendsen, H., *Langmuir*, **9**, 3122-3131, (1993).

Marrink, S.J., & Berendsen, H., *J. Phys. Chem.*, **98**, 4155-4168, (1994).

Merz, K Jr., *J. Comp. Chem.* **13**(6), 749-767 (1992).

Merz, K.M. Jr. & Roux, B. Biological Membranes: A Molecular Perspective from Computation and Experiment, Birkhauser, Boston, (1996).

Merz, K Jr. & Damodaran, K.V. Personal Communication, (1997).

Merz, K. Jr., *Curr. Opin. Struct. Biol.*, **7**, 512-517, (1997).

Mouritsen, O.G. & Kinnunen, P. K. J, in "Biological Membranes - A Molecular Perspective from Computation and Experiment " Merz, K.M., Jr. & Roux, B., eds., Birkhauser, Boston (1996).

Muranishi, S., *Crit. Rev. Ther. Drug Carrier Syst.*, **7**(1), 1-35, (1990).

Nagle, J.F. and Weiner, M.C. *Biochim. Biophys. Acta*, **942**, 1-10 (1988).

Nagle, J.F. *Biophys. J.*, **64**,1476-1481 (1993).

Ongpipattanakul, B., Francoeur, M.L., & Potts, R.O., *Biochim. Biophys. Acta,* **1190**, 115-122, (1994).

Ogiso, T., Iwaki, M., Kazuiko, B. & Yoko, T., *J. Pharm. Sci.*, **81**(8), 762-766 (1992).

Pastor, R.W., *Curr. Opin. Struct. Biol.*, **4**, 486-492, (1994).

Pearlman, DA, , Case, D. A., Caldwell, J.C., Seibel G.L., Singh, U.C., Weiner, P., Kollman, P.AMBER41, Univeristy of California, San Francisco (1995).

Pearson, R. H., & Pascher, I., *Nature*, **281**, 499 (1979).

Perkins, T.D.J. and Barlow, D.J. *J. Mol. Graphics*, **8**, 156-162 (1990).

van der Ploeg & Berendsen, H.J.C., *J. Chem. Phys.*, **76**, 3271 (1982).

van der Ploeg & Berendsen, H.J.C., *Mol. Phys.*, **11**, 1 (1983).

Pohorille, A., & Wilson, M. A., *Origins of Life & Evolution of the Biosphere,* **25**(1-3), 21-46, (1995).

Potts, R.O. & Francouer, M.L. *Natl. Acad. Sci. U.S.A.* **87**, 3871-3873 (1990).

Ogiso, T., Iwaki, M., Bechako, K. & Tsutsumi, Y. J. *Pharm. Sci.*, **81**(8), 763-766 (1992).

Quan, D. and Mailbach, H., *Int. J. Pharm.*, **104**, 61-72, (1994).

Reiss- Husson, F., *J. Mol. Biol.*, **25**, 363, 1967
Robinson, A.J., Richards, G., Thomas, P., & Hann, M.H., *Biophys. J.*, **68**, 164-170, (1995).

Ruocco, M.J. & Shipley, G. *Biochim Biophys Acta*, **691**, 309-320 (1982).

Schaefer, H. Stutten, A., Schalla, W., Gazith. J. & Bauer , *Adv. Pharmacol. Ther.*, 9, 223-235 (1978).

Scheuplein, R.J., and Blank, I. H., *Physiol. Rev.*, **51**, 702-747, (1971).

Scheuplein, R.J. and Ross, L., J. *Soc. Cosmetic Chemists*, **21**, 853 (1970).

Schlenkrich, M., Brickmann, J., MacKerrel, A. D. Jr., & Karplus, M. in "Biological Membranes - A Molecular Perspective from Computation and Experiment " Merz, K.M., Jr. & Roux, B., eds., Birkhauser, Boston (1996).

Schuckler, F., & Lee., G., *Int. J. Pharm.*, **70**, 173-186, (1991)

Schuckler, F., Bouwstra, J. A., Gooris, G. S., & Lee, G., *J. Cont. Rel.*, **23**, 27-36, (1993).

Seelig, J. & Seelig, A. *Biochemistry*, **13**(23), 4839 (1974).

Shen, L., Bassolino, D., & Stouch, T., *Biophys. J.*, **73**, 3-20 (1997).

Shinoda, W. Fukada, T., Okazaki, S., and Okada, I., *Chem. Phys. Lett.*, **232**, 308., (1995).

Silver, B. L. "The Physical Chemistry of Membranes - An Introduction to the Structure And Dynamics of Biological Membranes" Allen & Unwin, The Solomon Press, New York, (1985).

Spoel, D. van der, Maaren, P.J. & Berendsen, H.J.C. *J. Chem Phys.*, **108**(24), 10220-10230 (1998).

Stouch, T.R., Ward, K.B., Alfieri, A., Hagler. A.T., *J. Comp. Chem*, **12**(8), 1033-1046, (1991).

Stouch, T.R., *Mol. Sim.*, **10**(2-6), 335-362 (1993).

Stouch, T.R., Alper, H.E., Bassolino, D., *Supercomputer. App. & High Performance Computing.*, **8**, 6-23, (1994).

Stouch, T.R., & Bassolino, D. in "Biological Membranes- A Molecular Perspective from Computation and Experiment" Merz, K.M. Jr. & Roux, B. eds. Birkhauser, Boston, (1996).

Stoughton, R.B. & McClure, W.D. *Drug Dev. Ind. Pharm*, **9**,725-744 (1983)

Sugibiyashi, K., Nakayama, S., Seki, T. Hosaya, K. & Morimoto, Y. J. Pharm Sci., 81(1), 58-64 (1991).

Tardieu, A., Luzzatti, V. and Reman, F.C, *J. Mol. Biol.*, **75**, 711 (1973).

Tieleman, D.P., & Berendsen, H.J.C., *J. Chem., Phys.*, **105**(11), 4871-4880 (1996).

Trager, R.T "Physical Functions of Skin, Academic Press, New York, (1966).

Tu, K., Tobias, D.J., & Klien, M., *J. Phys. Chem.*, **99**, 10035-10042 (1995)

Tu, K., Tobias, D.J., & Klein, M.K. *Biophys. J.*, **69**, 2558-2562 (1995)

Tu, K., Yobias, D.J., Blasie, J. K. & Klein, M.K. *Biophys. J.*, **70**, 595-608 (1996).

Vanderkooi, G., *Biophys. J.*, **66**, 1457-1468, (1994).

Vanderkooi, G., *Biochem.*, **30**, 10760-10768 (1991).

Venable, R.M., Zhang, Y., Hardy, B.J., & Pastor, R.W., *Science*, **262**, 223-226 (1993).

Verlet, L., *Phys. Rev.*, **159**, 98 (1967).

Ward, A. & Tallon, R. In "Topical Drug Delovery Formulation". Osbourne, D. & Amman, A., Eds., Marcel Dekker, New York, (1990).

Weiner, S.J., Kollman, P.K., Case, D.A., Singh, U.C., Ghio, C., Alagona, G., Profeta, S., & Weiner, P. *J. Am. Chem. Soc.*, **106**, 765 (1984).

Weichers J. W., Jonkman, J.H.G and de Zeeuw, R.A. *Pharm. Res.* **4**, 519-523, 1987,

Weichers J. W., Drenth, B.H.F., Jonkman, J.H.G. and de Zeeuw, R.A. Int. J. Pharm., 47:43-49 (1988).

Weichers, J.W. *Pharm Weekbl [Sci]*, **11**(6),185-98 (1989).

Weichers, J.W., and de Zeeuw., RA, *Drug Design Delivery*, **6**, 87(1990).

Wertz, P.W and Downing, P.T., in Transdermal Drug Delivery, Hadgraft, J. and Guy, R.H. eds. Marcel Dekker, New York, pp. 1-22 1989.

Williams, A.C., & Barry, B.W., *Crit. Rev. Ther. Drug Carrier Syst.*, **9**(3,4), 305-353, (1992)

Woolf, T.B., & Roux, B., *J. Am. Chem. Soc.*, **116**, 5916-5926, (1994)

Woolf, T.B., & Roux, B., *Proc. Natl. Acad. Sci. USA*, **91**, 11631-11635 (1994b).

Woolf, T.B. & Roux, B. *Proteins*, **24**, 92-114, (1996).

Yardley and Summerly, *J. Pharm., Ther.*, **13**, 357, (1983)

Zacchai, G., Blasie, J.K. & Schoenborn, B.P., Proc. Nat. Acad. Sci., U.S.A., 72, 376-380, 1975

Zacchai, G., Buldt, G., Seelig, A. & Seelig, J. *J. Mol. Biol.*, **134**, 693-706 (1979).

Zacchai, G., Blasie, J.K., Schoenborn, B.P., Proc. *Nat. Acad. Sci., USA*, **72**(1), 376 (1980).

Zhou, F., & Schulten, K., *J. Phys. Chem.*, **99**, 2194-2207 (1995).

7.APPENDICES

Appendix 1: The output of the first-step in the minimisation of Hexane

a) SANDER program

```
NB-update: NPAIRS =       90  HBPAIR =        0
Urey-Bradley energy:   9.983253122123915 4E-02
Urey-Bradley energy:   2.706721066699654 6E-02

  NSTEP        ENERGY          RMS            GMAX         NAME    NUMBER
     1      6.0427E-01     1.8713E+00     4.4747E+00      C6        17

BOND   =         0.1334  ANGLE   =         0.8843  DIHED      =         0.0620
VDWAALS =       -0.6811  EEL     =         1.0345  HBOND      =         0.0000
1-4 VDW =       -0.3860  1-4 EEL =        -0.4428  CONSTRAINT =         0.0000
EPOLAR  =        0.0000  ETHREEB =         0.0000
```

b) CHARMm22 program

```
MINI MIN: Cycle       ENERgy       Delta-E         GRMS     Step-size
MINI INTERN:           BONDs       ANGLes       UREY-b     DIHEdrals     IMPRopers
MINI EXTERN:         VDWaals         ELEC       HBONds                       USER
 ----------         ---------    ---------    ---------    ---------    ---------
MINI>          0       0.62918      0.00000      1.97307      0.01000
MINI INTERN>           0.13343      0.76278      0.12635      0.06306      0.00000
MINI EXTERN>          -1.05570      0.59927      0.00000                   0.00000
```

Appendix 2 : The CHARMm22 dihedral profile

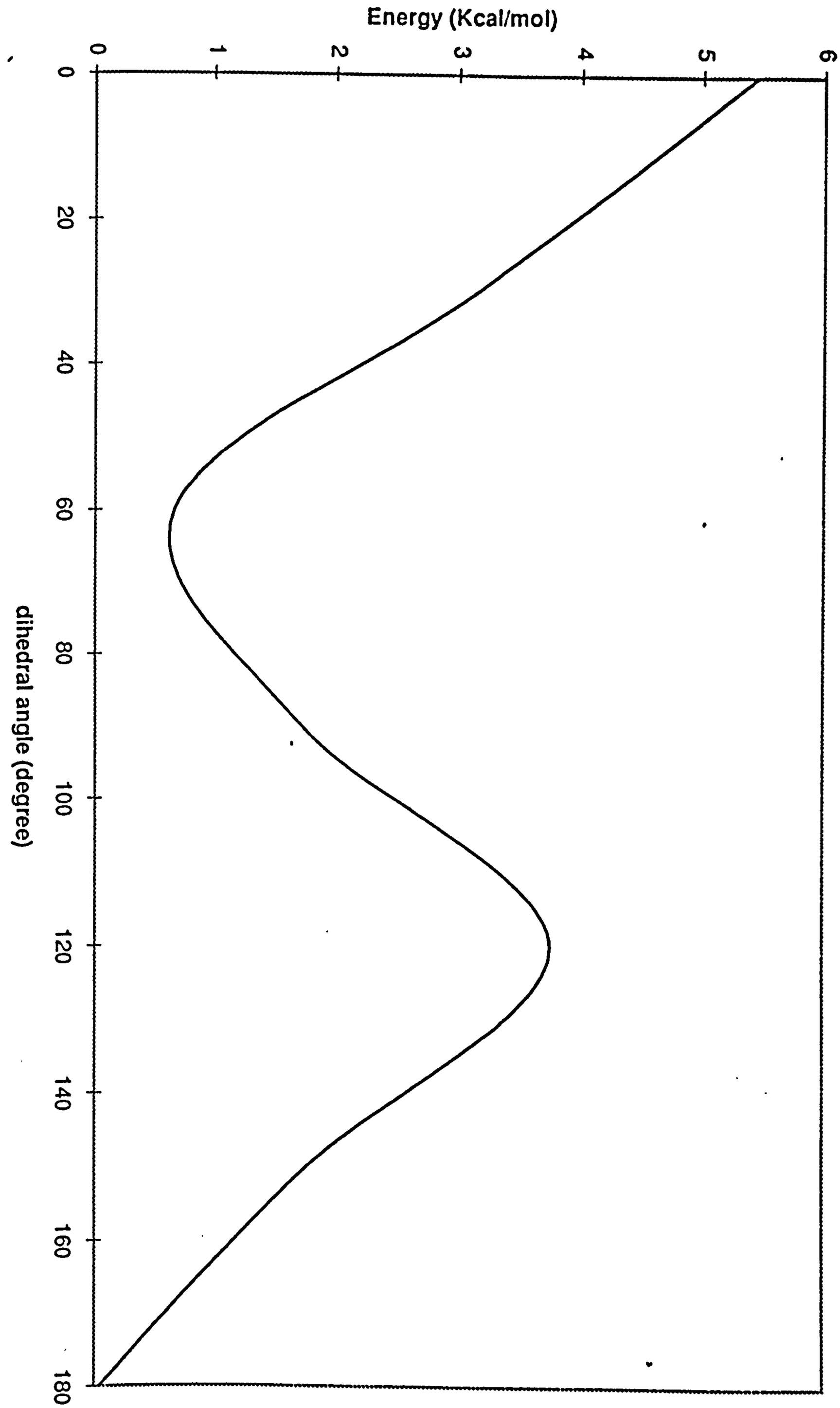

Appendix 3: The AMBER parm91.dat dihedral profile

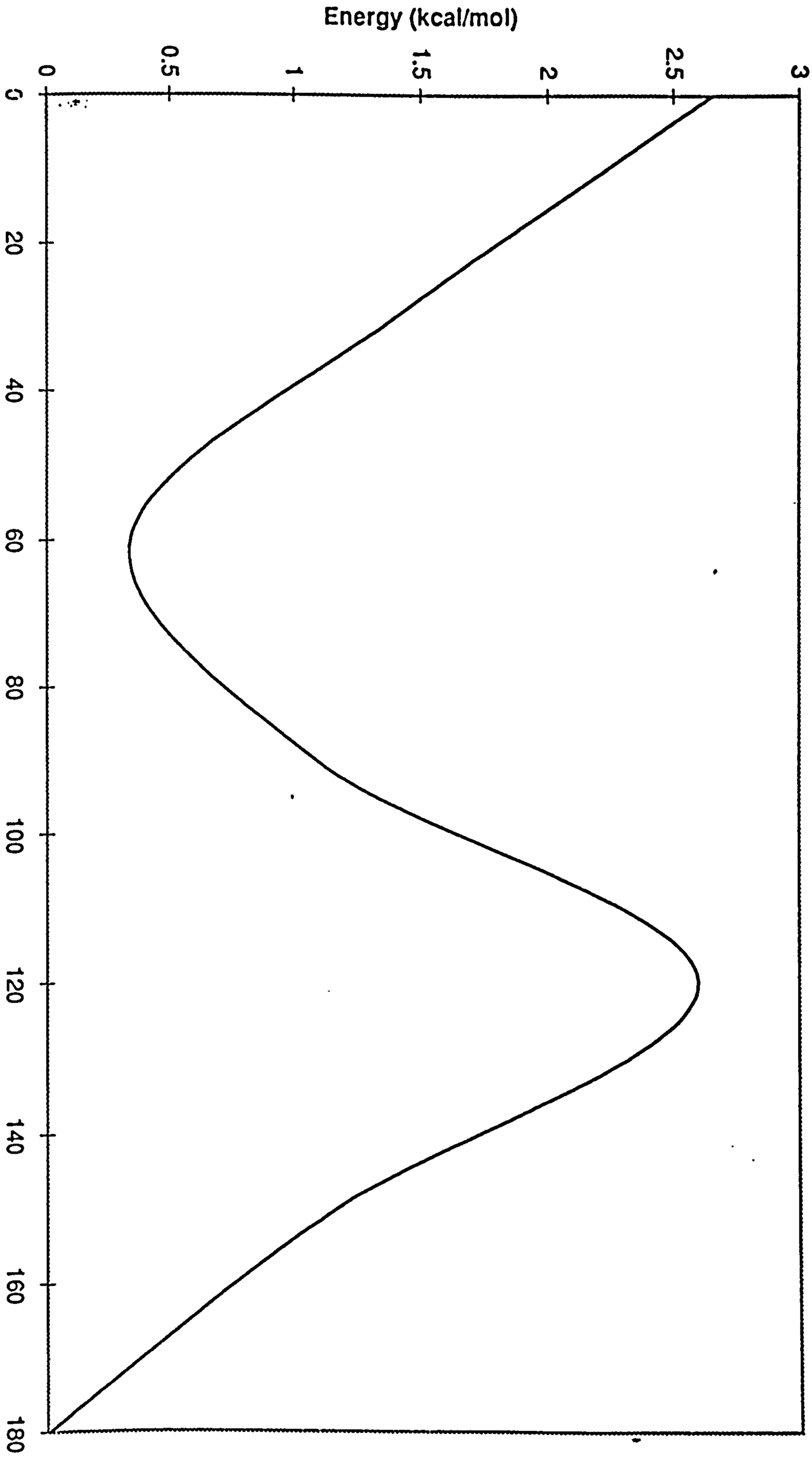

Appendix 4: The BoxX Dimension vs. time

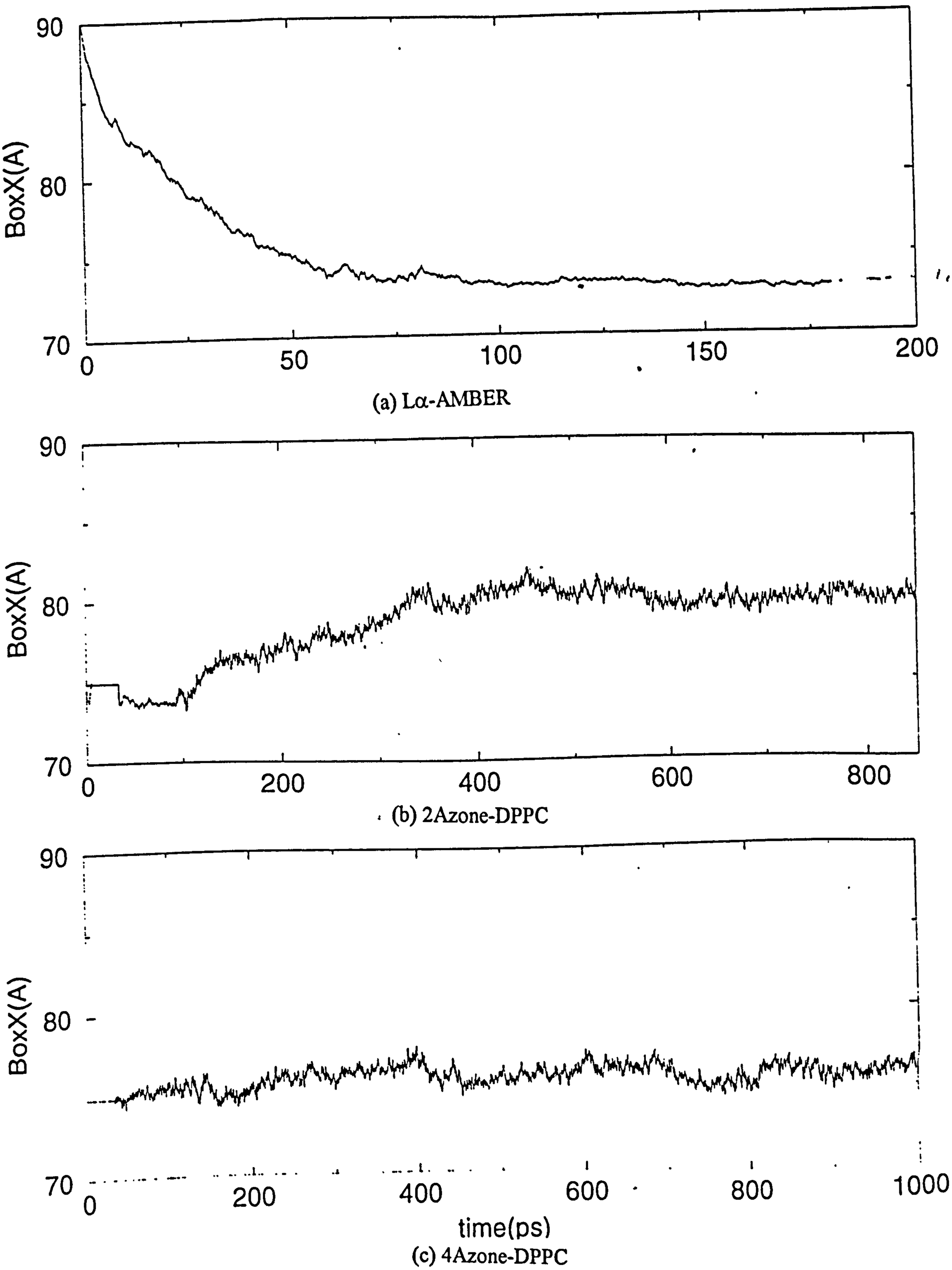

(a) Lα-AMBER

(b) 2Azone-DPPC

(c) 4Azone-DPPC

Appendix 5: The structure of the unsuccessful simulation employing CHARMm22 potentials

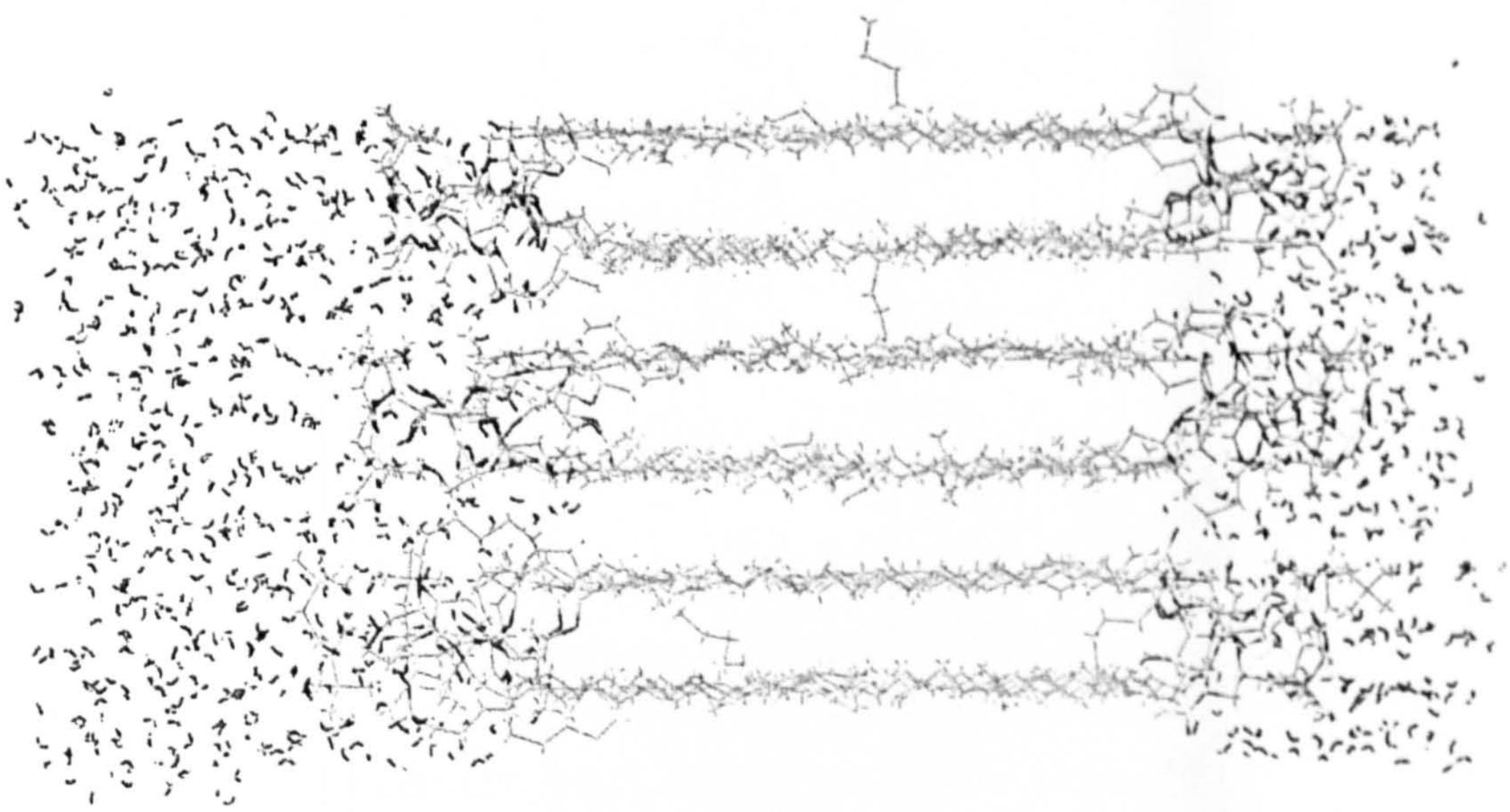

Note : the structure is highly order even after more than 180ps simulation.

Appendix 6: Equilibration of Lα-AMBER

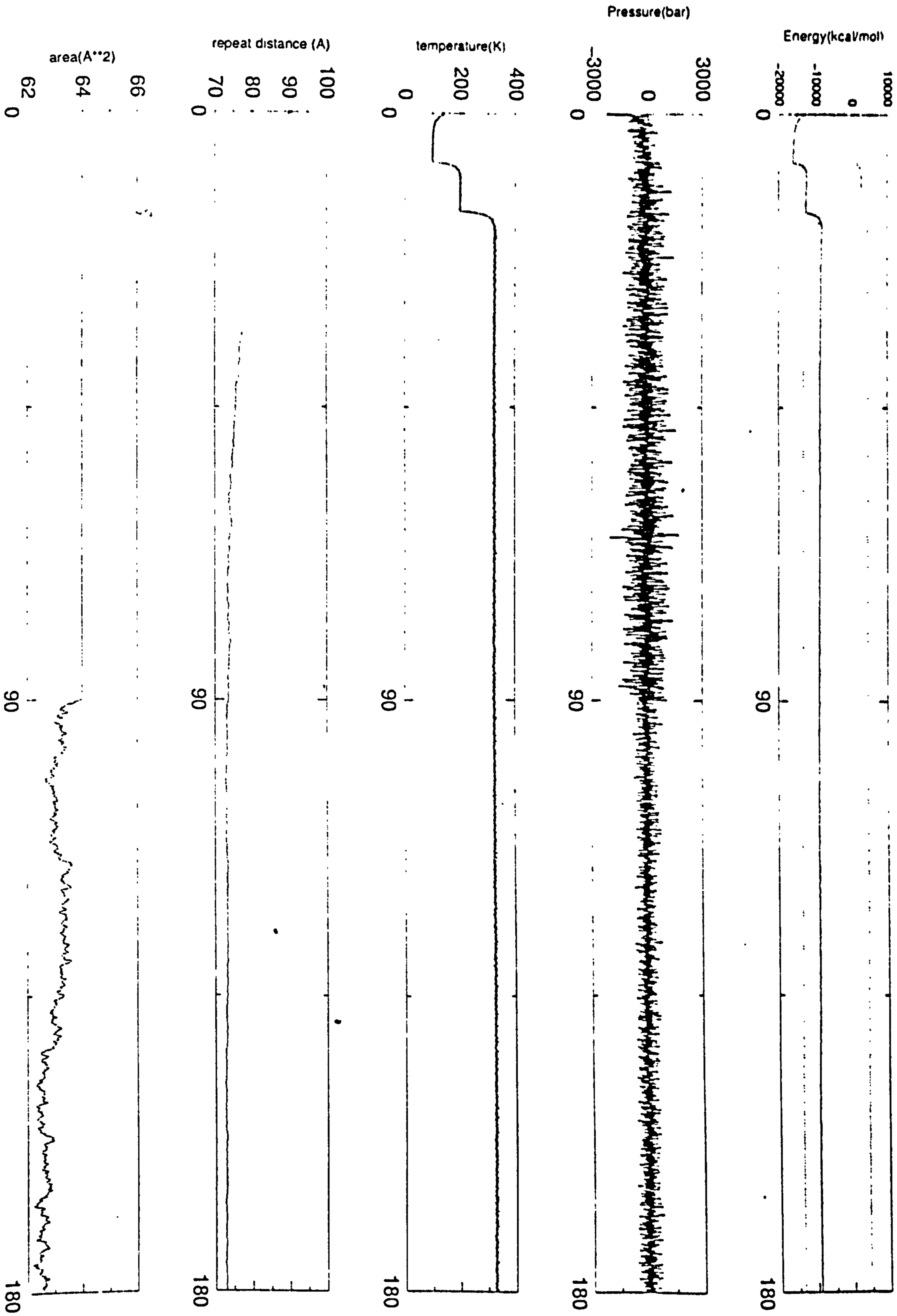

APPENDIX 7 - PROGRAM RADIAL DISTRIBUTION FUNCTION
WRITTTEN BY DR. K.V. DAMODARAN
MERZ GROUP, 152 DAVEY LABORATORY,
PENNSYLVANIA STATE UNIVERSITY,
UNITED STATE OF AMERICA

```
C Calculates the water rdfs for specific lipid atoms listed in the input
C control file. The reference atoms on the lipid around which water rdfs
are
C calculated are input in the list()... in the control file
C
C
C  The accumulated rdf data along with variables for the control file
are
C  written in the restrt.file. So, a restrt.file may be used as
control.file
C  in a subsequent run for further averaging over additional trj files..
C
C  It is assumed that the model is set up as lipids' coords. first and
then
C  water coords.
C
      IMPLICIT none
      INTEGER maxatm, maxspec, maxbin, maxrefs
      parameter (maxatm=7100, maxspec=30, maxbin=200, maxrefs=30)

      INTEGER  ittl(20), list(maxrefs), nrdfo(maxspec, maxbin)
     1        ,nrdfh(maxspec, maxbin), iarg, nlip, nlipat
     2        ,nwater, natom, nrefs, nlrdf,nsrdf,irdf
     3        ,maxint,nframe,iread,ilip,iref,ialip,iwat,nh1,nh2
     4        ,natlip,nwatst,nwat,nx,i,j,ij,ibox,icc,intx,nwrite
c
      DOUBLE PRECISION x(maxatm),y(maxatm),z(maxatm)
     1                 ,boxx,boxy,boxz,boxhx,boxhy,boxhz,cutoff,cutsqr
     2                 ,pi,resol,rho,rhoinv,dxo,dxh1,dxh2,dyo,dyh1
     3                 ,dyh2,dzo,dzh1,dzh2,rsqo,rsqh1,rsqh2,ro,rh1
     4                 ,rh2,crdo,crdh,rr,rdf,gofro,gofrh,bx,by,bz
      CHARACTER*80 ctrfil, crdfil, restfil
C
      iarg=0
      pi = 3.14159257d0
C
      iarg=iarg+1
      call getarg(iarg,ctrfil)
      iarg=iarg+1
      call getarg(iarg,restfil)
      open (unit=3,file=ctrfil,status='old',form='formatted')
C
      read(3,'(5i5)') nlip,nlipat,nwater,natom
C nlip: number of lipids, nlipat:number of atoms on each lipid
      read(3,'(5i5)') nrefs
C nrefs:number of reference atoms on the lipid
C
      read(3,'(5i5)') (list(j),j=1,nrefs)
      read(3,'(3f12.6)') cutoff,resol
      read(3,'(3f12.6)') boxx,boxy,boxz
      read(3,'(i5)')nlrdf
C nlrdf: set to zero, when starting a fresh data averaging. This is set
to
C 1 in the restart file. When nlrdf=1, the accumulated data are read in.
C
```

```
      if(natom.gt.maxatm) then
        write(6,*)'REDEFINE X Y Z & natmx, recompile the code'
      stop
      end if
      if(nrefs.gt.maxspec) then
      write(6,*)'  REDEFINE nrdfs & nrefmx, recompile the code'
      write(6,*)' MAX. no. of ref atoms exeeds the limit'
        write(6,*)nrefs, maxspec
      stop
      end if
      nwatst = nlip * nlipat + 1
C
      boxhx = boxx*0.5000d0
      boxhy = boxy*0.5000d0
      boxhz = boxz*0.5000d0
      cutsqr=cutoff*cutoff
      maxint = int(cutoff/resol + 0.50d0)
      write(6,'(5i5)') (list(j),j=1,nrefs)
C
      if(maxint.gt.maxbin) then
        write(6,*)'REDEFINE nrdf & maxbin, recompile the code'
      stop
      end if
C
      if(nlrdf .eq. 1) then
        write(6,*)' RESTART RUN'
      read(3,*)nsrdf
      do irdf=1,maxint
        read(3,'(5i8)')(nrdfo(ij,irdf),ij=1,nrefs)
        end do
      do irdf=1,maxint
        read(3,'(5i8)')(nrdfh(ij,irdf),ij=1,nrefs)
        end do
      else
      nlrdf = 1
            nsrdf=0
      do irdf=1,maxint
        do icc=1,nrefs
          nrdfo(icc,irdf)=0
          nrdfh(icc,irdf)=0
        end do
      end do
      end if
      open(unit=14,file=restfil,status='new',form='formatted')
      write(14,'(5i5)') nlip,nlipat,nwater,natom
      write(14,'(5i5)') nrefs
      write(14,'(5i5)') (list(j),j=1,nrefs)
      write(14,'(3f12.6)') cutoff,resol
      write(14,'(3f12.6)') boxx,boxy,boxz
      write(14,'(5i5)')nlrdf
C
C     rhoinv = (boxx*boxy*boxz)/float(nwater)
C     rho = 1.00e0/rhoinv
      rho = 0.033431394e00
      rhoinv = 1.000e0/rho
      nframe=0
      iread=7
C
 9753 continue
      iarg = iarg + 1
      call getarg(iarg,crdfil)
```

```
      if(crdfil.eq.'endinp') then
      write(6,*)'  + + +  END of COORDINATE INPUT  + + + + '
      write(6,*)'  Total of ',nframe,'  frames read in this run'
      write(6,*)' RDFs Accumulated over ',nsrdf,'  frames'
      goto 9754
      else
        write(6,*)' READING FILE  NFRAME IS ', nframe
      write(6,*)crdfil
      endif
      open(unit=iread,file=crdfil,status='old',form='formatted')
      read(iread,'(20a4)')(ittl(j),j=1,20)
100   continue
      read(iread,'(10f8.3)',end=102)(x(i),y(i),z(i),i=1,natom)
      read(iread,'(10f8.3)',end=102)bx,by,bz
      nframe=nframe+1
      nsrdf=nsrdf+1
      do ilip = 1, nlip
         do iref   = 1, nrefs
            natlip = list(iref)
            ialip  = (ilip - 1)*nlipat + natlip
            do iwat = nwatst,natom, 3
               nh1  = iwat + 1
               nh2  = iwat + 2
               dxo  = x(ialip) - x(iwat)
               dyo  = y(ialip) - y(iwat)
               dzo  = z(ialip) - z(iwat)
               if(abs(dxo).gt.boxhx) dxo = dxo - sign(boxx,dxo)
               if(abs(dyo).gt.boxhy) dyo = dyo - sign(boxy,dyo)
               if(abs(dzo).gt.boxhz) dzo = dzo - sign(boxz,dzo)
               dxh1 = x(ialip) - x(nh1)
               dyh1 = y(ialip) - y(nh1)
               dzh1 = z(ialip) - z(nh1)
               if(abs(dxh1).gt.boxhx) dxh1 = dxh1 - sign(boxx,dxh1)
               if(abs(dyh1).gt.boxhy) dyh1 = dyh1 - sign(boxy,dyh1)
               if(abs(dzh1).gt.boxhz) dzh1 = dzh1 - sign(boxz,dzh1)
               dxh2 = x(ialip) - x(nh2)
               dyh2 = y(ialip) - y(nh2)
               dzh2 = z(ialip) - z(nh2)
               if(abs(dxh2).gt.boxhx) dxh2 = dxh2 - sign(boxx,dxh2)
               if(abs(dyh2).gt.boxhy) dyh2 = dyh2 - sign(boxy,dyh2)
               if(abs(dzh2).gt.boxhz) dzh2 = dzh2 - sign(boxz,dzh2)
               rsqo = dxo*dxo + dyo*dyo + dzo*dzo
               if (rsqo.le.cutsqr) then
                  ro   = sqrt(rsqo)
                  ibox = 1 + int(ro/resol + 0.50d0)
                  nrdfo(iref,ibox) = nrdfo(iref,ibox) + 1
               end if
               rsqh1 = dxh1*dxh1 + dyh1*dyh1 + dzh1*dzh1
               if (rsqh1.le.cutsqr) then
                  rh1  = sqrt(rsqh1)
                  ibox = 1 + int(rh1/resol + 0.50d0)
                  nrdfh(iref,ibox) = nrdfh(iref,ibox) + 1
               end if
               rsqh2 = dxh2*dxh2 + dyh2*dyh2 + dzh2*dzh2
               if (rsqh2.le.cutsqr) then
                  rh2  = sqrt(rsqh2)
                  ibox = 1 + int(rh2/resol + 0.50d0)
                  nrdfh(iref,ibox) = nrdfh(iref,ibox) + 1
               end if
            end do
         end do
      end do
```

```
      end do
      goto 100
 102  continue
      goto 9753
9754  continue
      write(14,'(5i5)')nsrdf
      do irdf=1,maxint
        write(14,'(5i8)')(nrdfo(ij,irdf),ij=1,nrefs)
      end do
      do irdf=1,maxint
        write(14,'(5i8)')(nrdfh(ij,irdf),ij=1,nrefs)
      end do
      close(unit=14)
      do nx  = 1, nrefs
        crdo = 0.0000e0
        crdh = 0.0000e0
      do intx  = 2, maxint
          rr     = resol*float(intx-1)
        rdf    = float(nrdfo(nx,intx))/float(nlip*nsrdf)
          gofro  = rhoinv * rdf/(4.0d0*pi*rr*rr*resol)
          crdo   = crdo + rdf
        rdf    = float(nrdfh(nx,intx))/float(nlip*nsrdf)
          gofrh  = rhoinv * rdf/(4.0d0*pi*rr*rr*resol)
          crdh   = crdh + rdf
          nwrite = nx+20
          write(nwrite,'(6f10.4)')rr,gofro,crdo,gofrh,crdh
        end do
      end do
      stop
      end
```

APPENDIX 8 - MEAN SQUARED DISPLACEMENT PLOTS VS. TIME

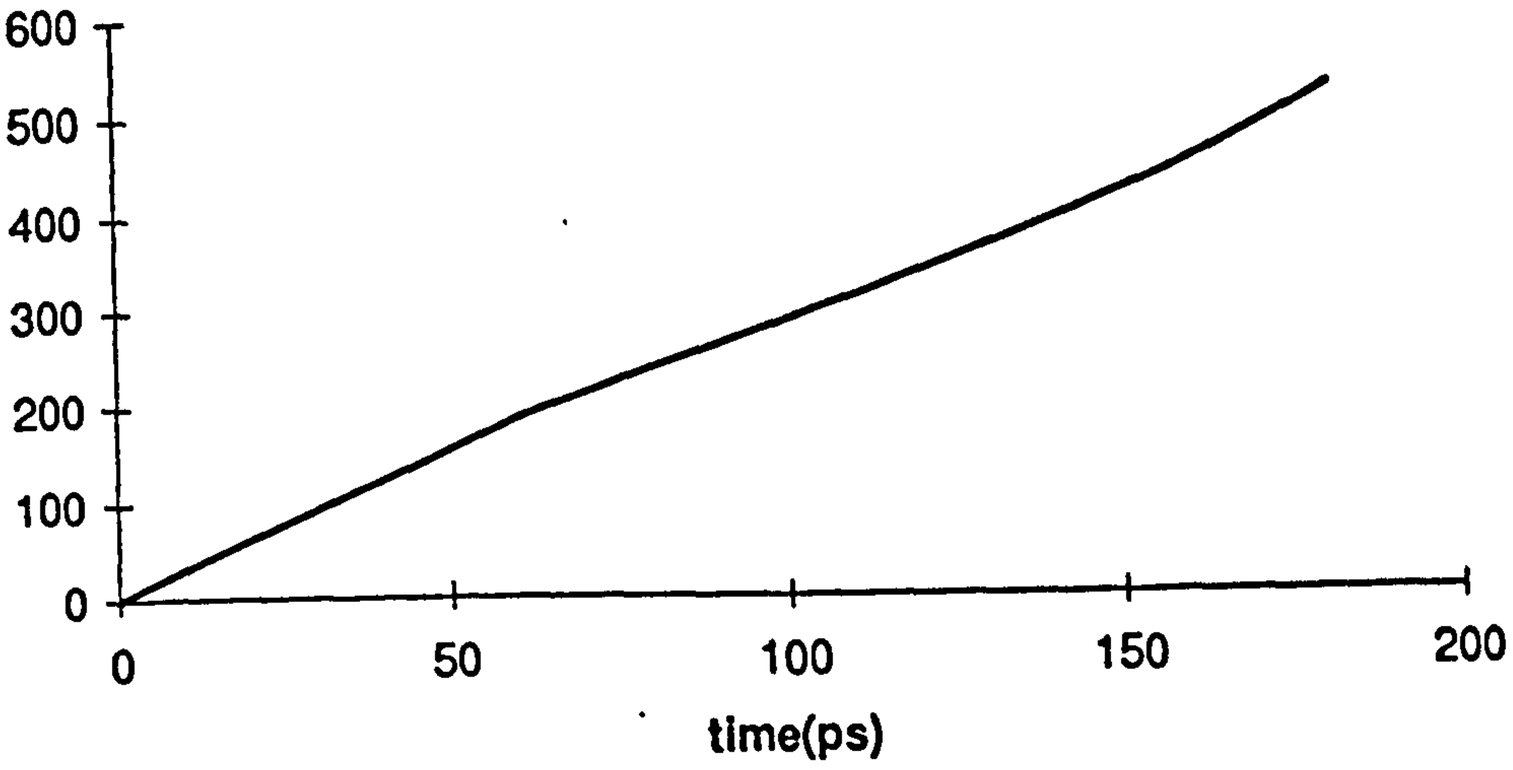

(a) water (Lα-AMBER)

a) lα-AMBER

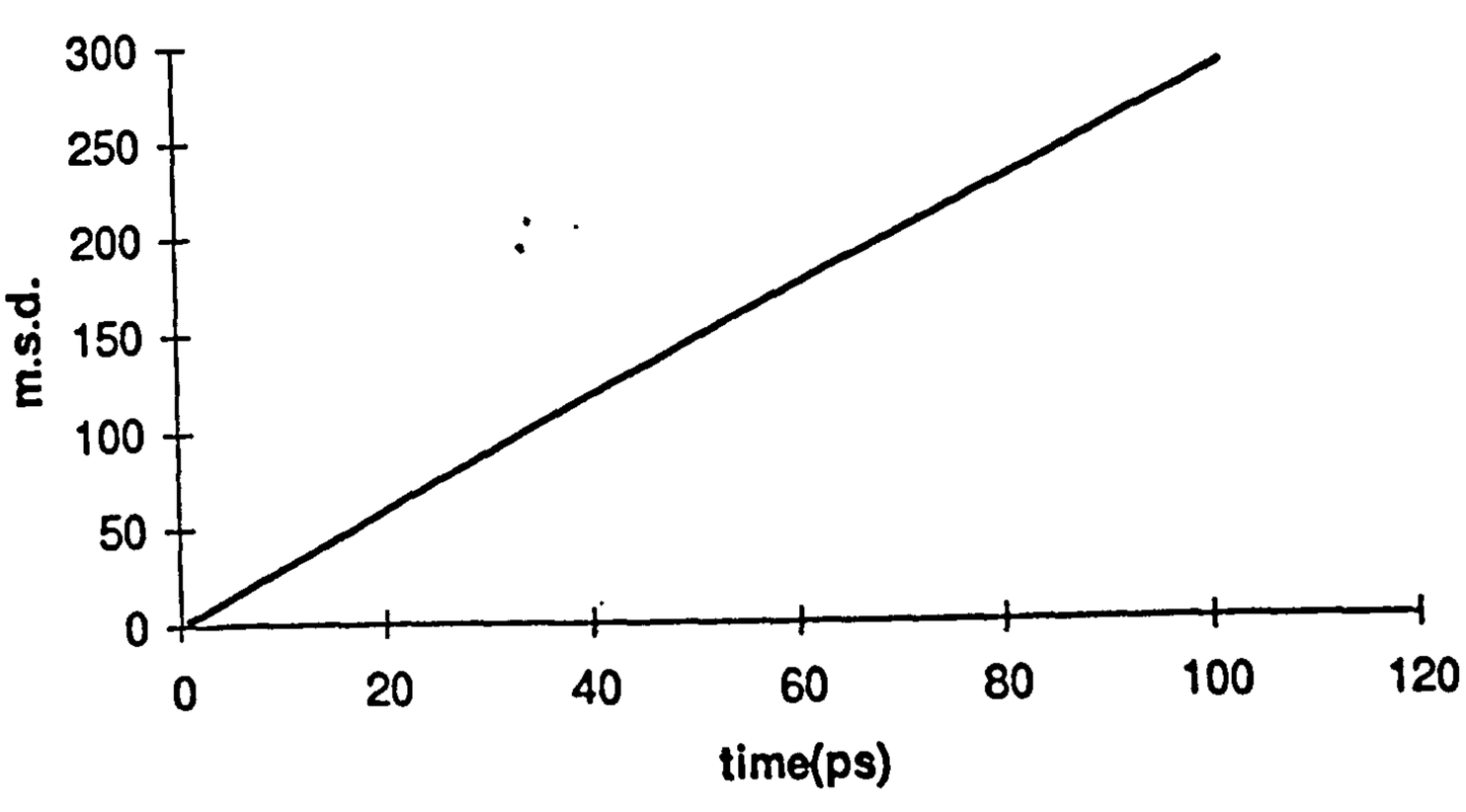

(b) water (Lα-CHARMm)

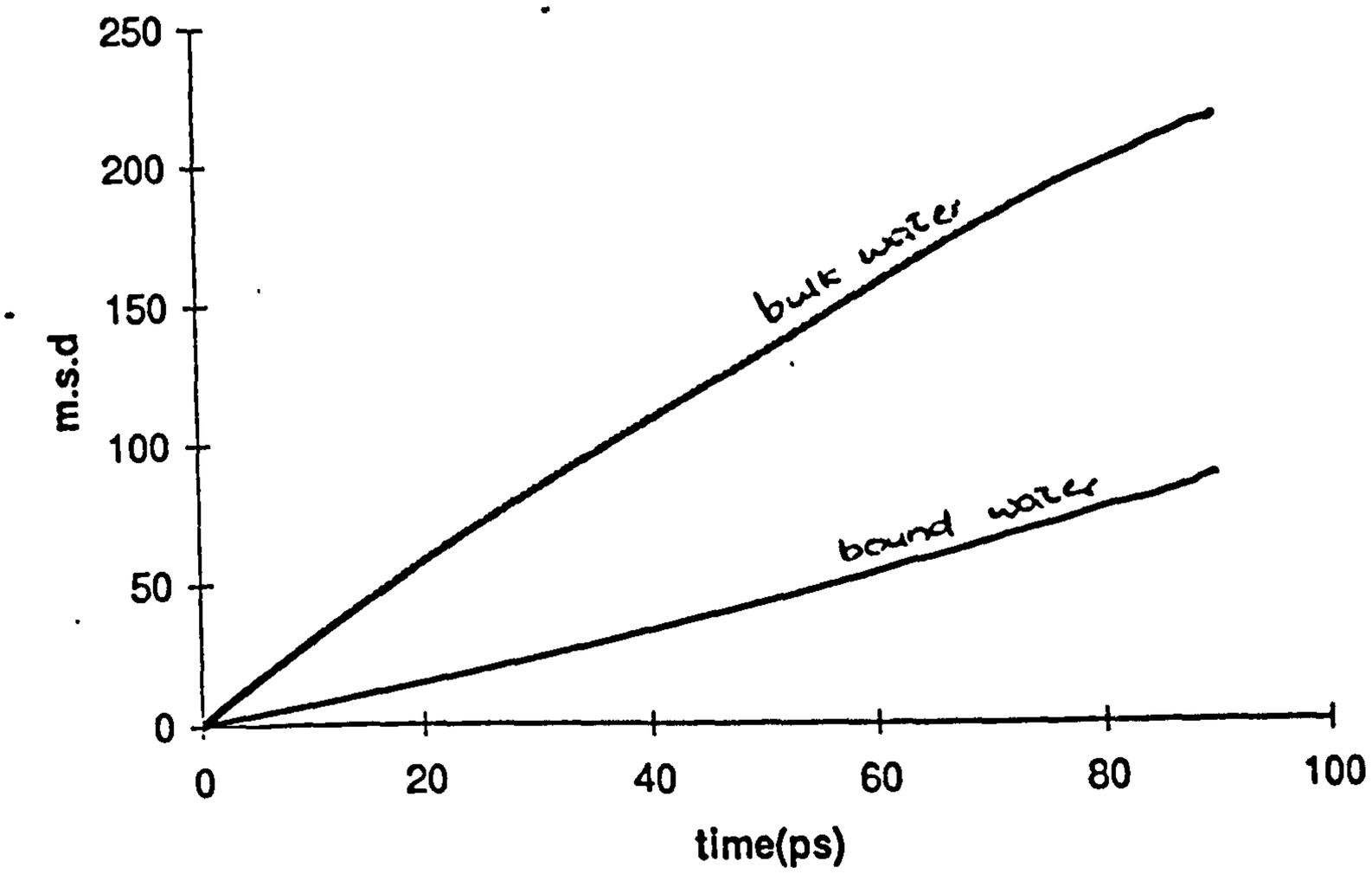

(c) water (2Azone-DPPC)

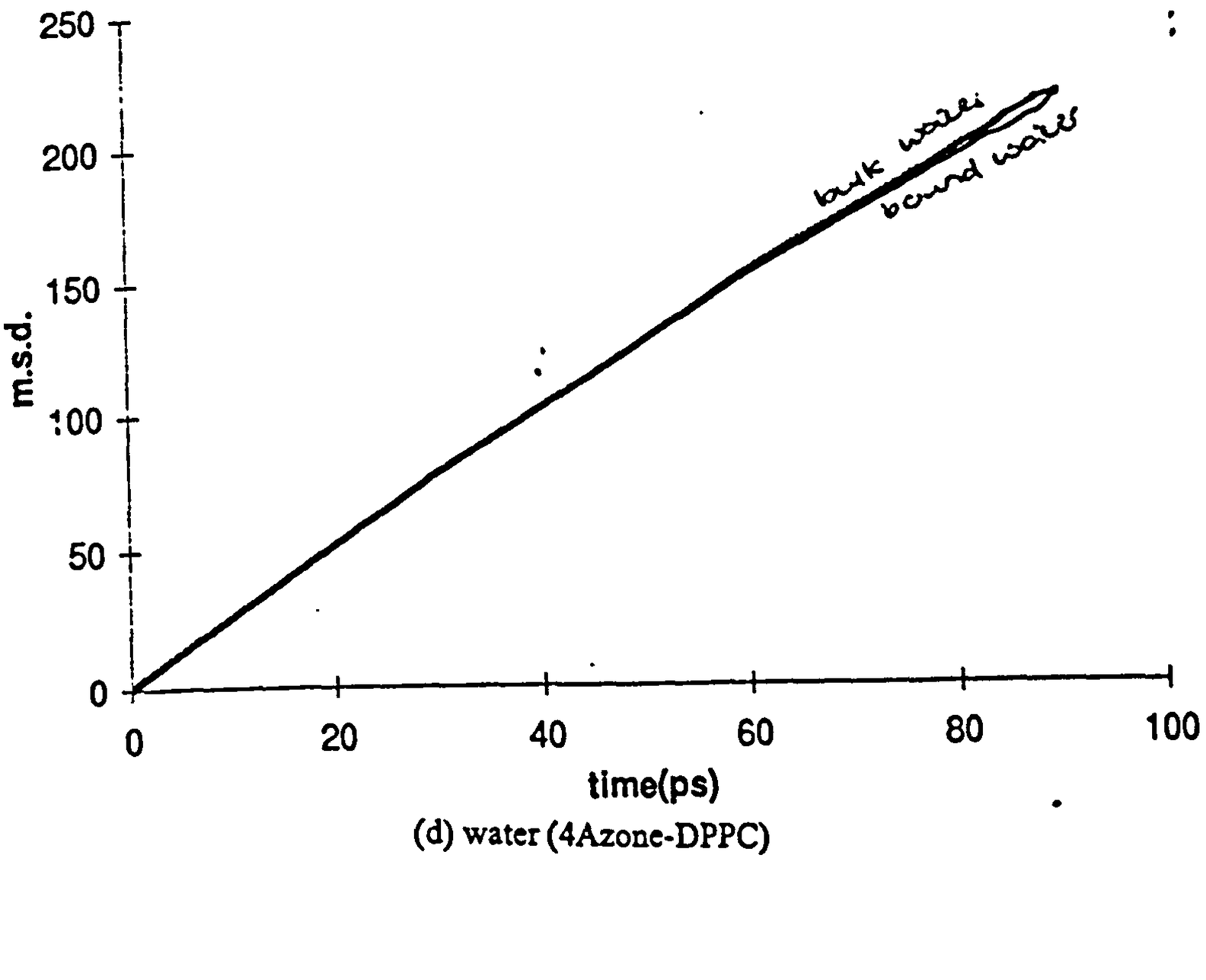

(d) water (4Azone-DPPC)

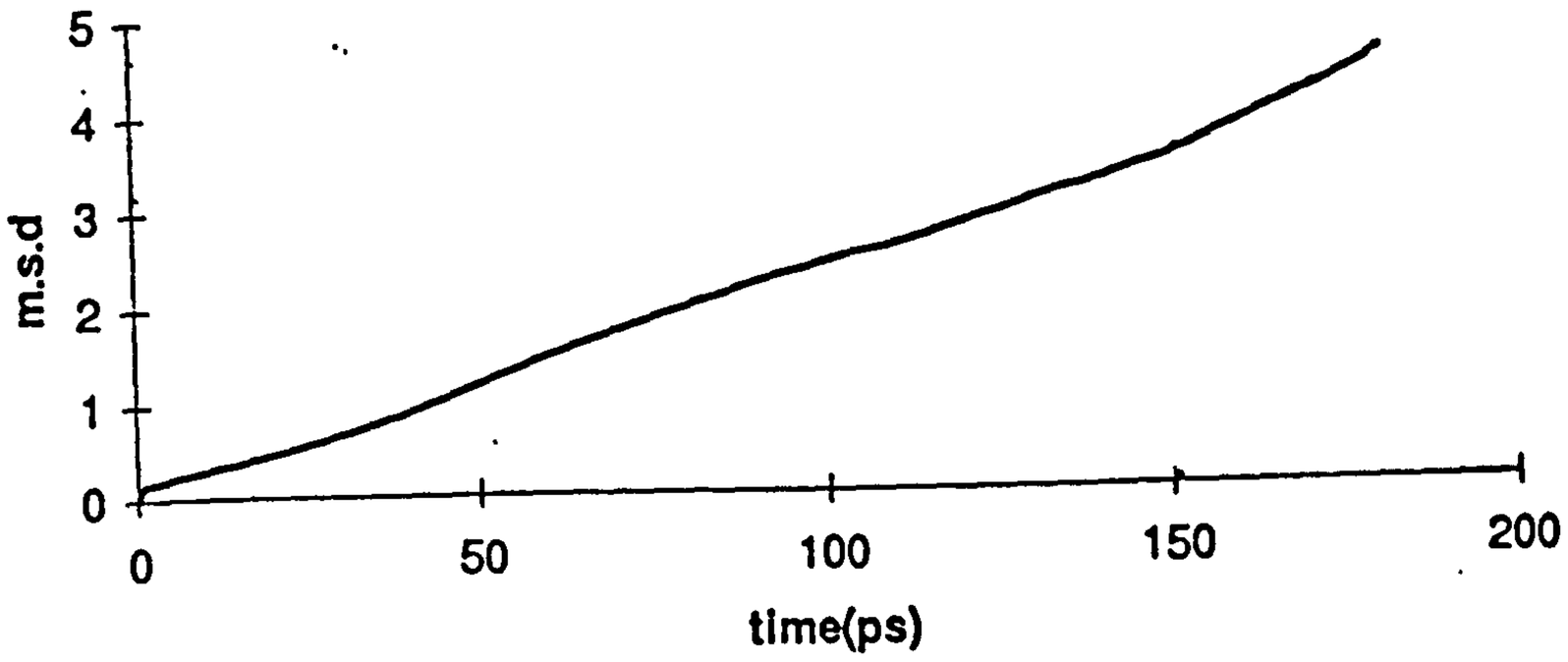

(e) lipid (Lα-AMBER)

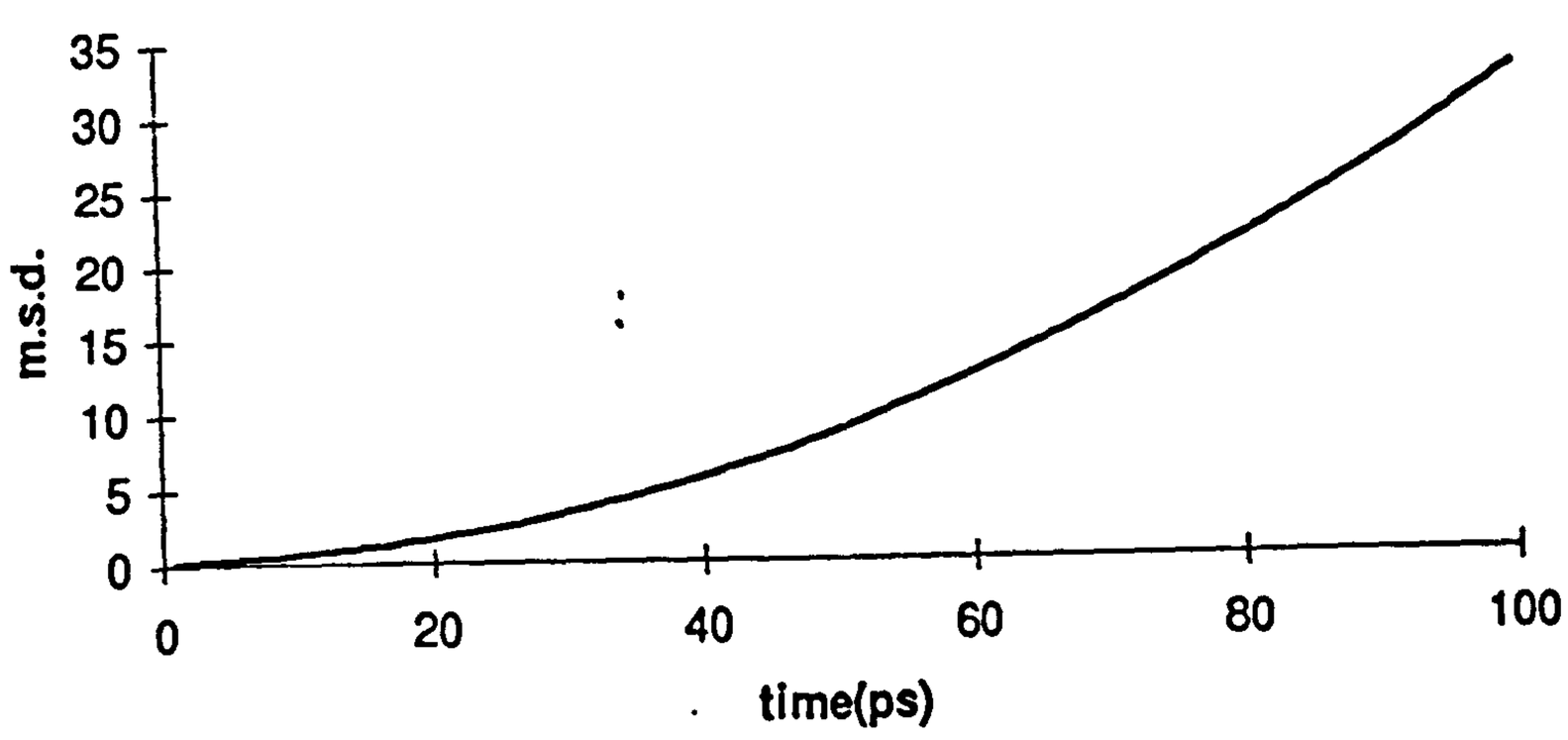

(f) lipid (Lα-CHARMm)

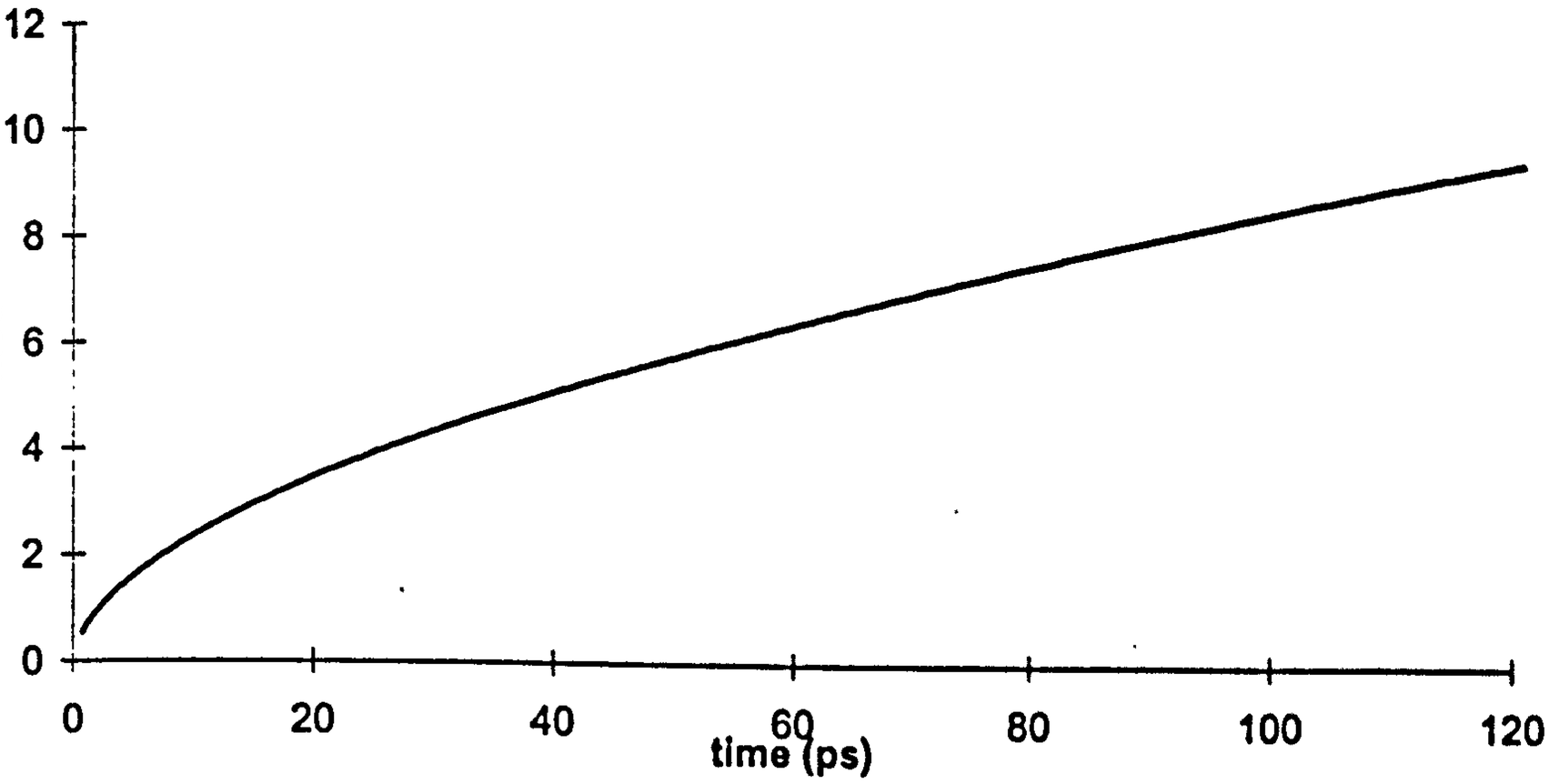

(g) azone (2Azone-DPPC)

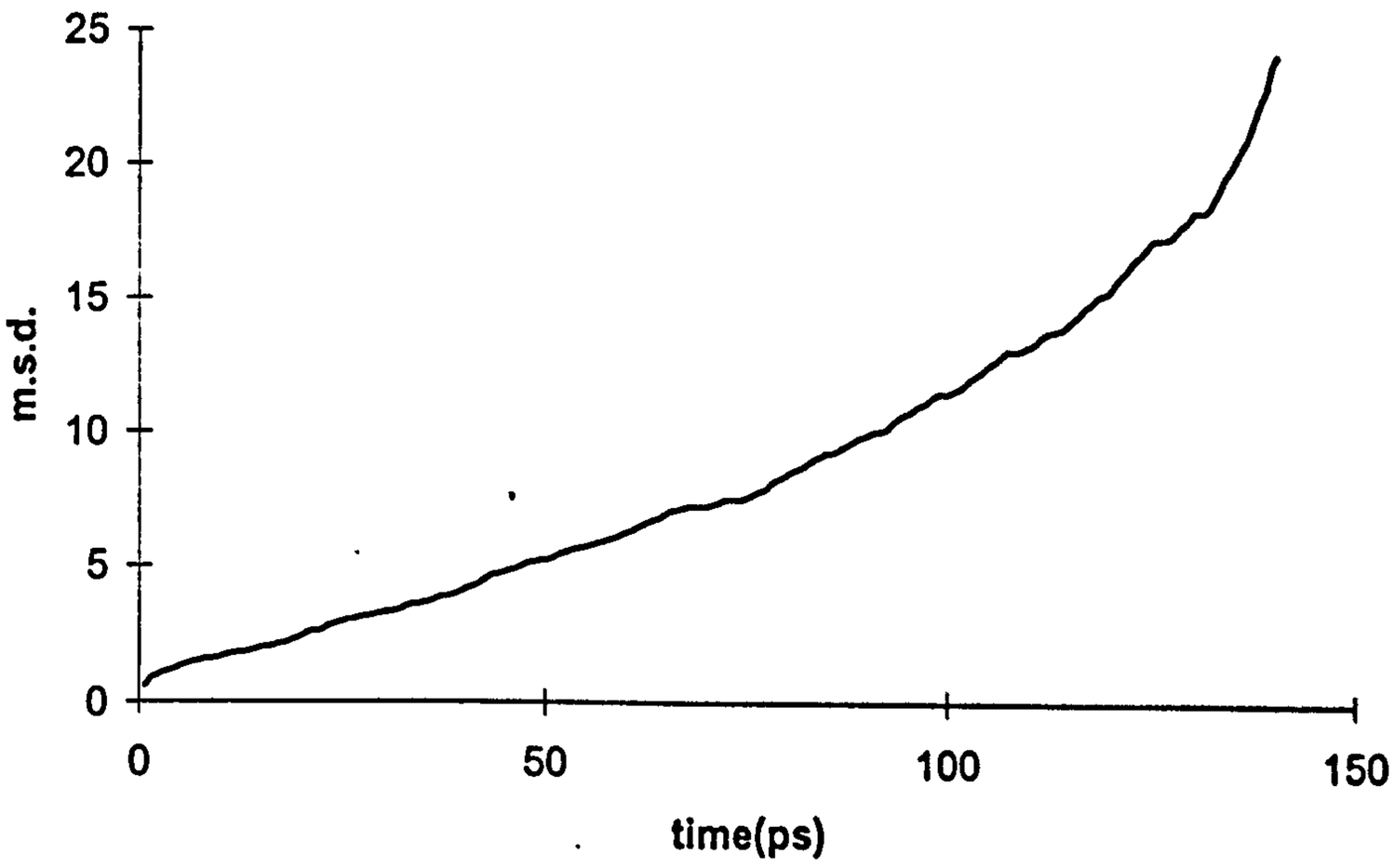

(h) azone (4Azone-DPPC)

Note :

Time t=0, refers to the time after equilibrium is achieved